INFORMATION TO USERS

This manuscript has been reproduced from the microfilm master. UMI films the text directly from the original or copy submitted. Thus, some thesis and dissertation copies are in typewriter face, while others may be from any type of computer printer.

The quality of this reproduction is dependent upon the quality of the copy submitted. Broken or indistinct print, colored or poor quality illustrations and photographs, print bleedthrough, substandard margins, and improper alignment can adversely affect reproduction.

In the unlikely event that the author did not send UMI a complete manuscript and there are missing pages, these will be noted. Also, if unauthorized copyright material had to be removed, a note will indicate the deletion.

Oversize materials (e.g., maps, drawings, charts) are reproduced by sectioning the original, beginning at the upper left-hand corner and continuing from left to right in equal sections with small overlaps. Each original is also photographed in one exposure and is included in reduced form at the back of the book.

Photographs included in the original manuscript have been reproduced xerographically in this copy. Higher quality 6" x 9" black and white photographic prints are available for any photographs or illustrations appearing in this copy for an additional charge. Contact UMI directly to order.

U·M·I

University Microfilms International
A Bell & Howell Information Company
300 North Zeeb Road, Ann Arbor, MI 48106-1346 USA
313/761-4700 800/521-0600

Order Number 9307651

The galactic center stellar population in the near infrared

Haller, Joseph William, Ph.D.

The University of Arizona, 1992

U·M·I

300 N. Zeeb Rd.
Ann Arbor, MI 48106

THE GALACTIC CENTER STELLAR POPULATION IN THE NEAR INFRARED

by

Joseph William Haller

A Dissertation Submitted to the Faculty of the

DEPARTMENT OF ASTRONOMY

In Partial Fulfillment of the Requirements
For the Degree of

DOCTOR OF PHILOSOPHY

In the Graduate College

THE UNIVERSITY OF ARIZONA

1 9 9 2

THE UNIVERSITY OF ARIZONA
GRADUATE COLLEGE

As members of the Final Examination Committee, we certify that we have read the dissertation prepared by Joseph William Haller

entitled THE GALACTIC CENTER STELLAR POPULATION IN THE NEAR INFRARED

and recommend that it be accepted as fulfilling the dissertation requirement for the Degree of Doctor of Philosophy

Marcia J. Rieke	8/17/92 Date
John H. Black	8/17/92 Date
Robert C. Kennicutt	8/17/92 Date
Edward W. Olszewski	8/17/92 Date
	Date

Final approval and acceptance of this dissertation is contingent upon the candidate's submission of the final copy of the dissertation to the Graduate College.

I hereby certify that I have read this dissertation prepared under my direction and recommend that it be accepted as fulfilling the dissertation requirement.

Dissertation Director Marcia J. Rieke — 8/17/92 Date

STATEMENT BY AUTHOR

This dissertation has been submitted in partial fulfillment of requirements for an advanced degree at the University of Arizona and is deposited in the University Library to be made available to borrowers under the rules of the Library.

Brief quotations from this dissertation are allowable without special permission, provided that accurate acknowledgement of source is made. Requests for permission for extended quotation from or reproduction of this manuscript in whole or part may be granted by the head of the major department or the Dean of the Graduate College when in his or her judgement the proposed use of the material is in the interests of scholarship. In all other instances, however, permission must be obtained by the author.

SIGNED: Joseph W. Haller

ACKNOWLEDGEMENTS

I would first like to thank Marcia Rieke for introducing me to Galactic Center research and her continuing support through resources, conferences, encouragement, and many opportunities working with the near-infrared cameras. She had already begun the LPV study when I signed on with her. George Rieke provided numerous useful comments and suggestions in the development of this project as well as some timely words of encouragement. The both of them of course must receive a large measure of credit and gratitude for suggesting the CO study, travelling to Chile in June, 1989 and interrupting their excursion to Machu Picchu to obtain the data presented in chapter 5. Jay Frogel is to be thanked as well for obtaining the L data at CTIO.

The committee composed of Marcia Rieke, Rob Kennicutt, John Black, and Ed Olszewski offered many useful comments and criticisms that sharpened my understanding of the Galactic Center. Any remaining errors or omissions are, of course, entirely my own.

Thanks go to Adam Burrows who taught me a great deal of foundational astrophysics; R. Elston, B. Jannuzi and others for introducing me to IRAF; E. Olszewski and R. Schoemer for help with DAOPHOT and I. Barg for installing and supporting it on the IRCAMERA computer; L. Paley for helping to reduce the H data; many praises to Jim Speer for doing the L photometry and learning database reductions; Robin Catchpole and M. Feast of the SAAO for their expertise in Mira variables, and additional thanks to Robin for many good times during his stay at Steward; Fulvio Melia for offering his comments on the work and giving me more opportunities in Galactic Center research.

My gratitude also goes to Scott Grossman, Todd Henry, Davy Kirkpatrick, Hans Walter Rix, Dennis Zaritsky, and Diana Foss who were the classmates that helped make graduate school enjoyable. Bill and Diane Latter, Doug Kelly, Kim and Brian McLeod, Karen Visnovsky, Jim Bollinger, Barry Meyers-Rice, Tom Green, Rex Safford, Pat Hall, Laird Close, Crystal Martin, and Milagros Ruiz - who have been good friends and/or Steward office mates and have provided uncountable occasions of learning while I have been in Tucson; Jill Kirby for her valuable military insights while my father was on duty in the Gulf War. Thank you James Lowenthal for your friendship and being a groomsman at our wedding. Karen and I enjoyed many barbecues with Joe and Penny Hora, and Joe planted the seed for the "cell" matching procedure in chapter 2...

To some special Tucson friends: Mark, Teresa, and Kathleen Aronson, Alexis Stanton and "Little" Alexis; Fr. Michael Sherwin, O.P., Prof. A. Pacholczyk, Prof. M. Hewlett and others at the St. Albert Forum....

To Bishop Joseph Hart, my mentor in life; my lifelong friends Joe Swiatek, Bill O'Donnel, James Schumaker, Sheryl and Aaron Van Pelt; Karen's parents, Spike and Margaret Ann Hladky - for all you have given me and your support...

To Mom, Dad, Jim, Tom, Bob, Karen, and Janet - a part of each of you is in me and this would not have happened without any of you, for countless reasons...

... and most of all to you Karen, for your love, patience, and support through the many ups and downs we have had in the last few years. Your faith in me (and occasional prodding) was indispensible.

To

Karen, my wife

and

Mark, our son

As the geometer who tries so hard
to square the circle, but cannot discover,
think as he may, the principle involved,

so did I strive with this new mystery:
I yearned to know how our image fit
into that circle, how could it conform;

but my own wings could not take me so high -
then a great flash of understanding struck
my mind, and suddenly its wish was granted.

At this point power failed high fantasy
but, like a wheel in perfect balance turning,
I felt my will and my desire impelled

by the Love that moves the sun and the other stars.

Dante Alighieri, *The Divine Comedy: Paradise,* Canto XXXIII
Translated by Mark Musa

TABLE OF CONTENTS

LIST OF ILLUSTRATIONS 8

LIST OF TABLES 10

ABSTRACT 11

CHAPTER 1 : INTRODUCTION TO THE GALACTIC CENTER 12

- Overview 12
- The Galactic Center Environment 13
- The Galactic Center Stellar Population - In General 16
- The Galactic Center Stellar Population - Particular Objects 18
- Interstellar Dust and Gas Within 10 pc of the Galactic Center 21
- Sgr A* – A Massive Black Hole at the Galactic Center? 24
- Starbursts at the Galactic Center 26
- The Galactic Center and the Nucleus of M31 30
- Summary 31

CHAPTER 2 : HKL PHOTOMETRY OF GALACTIC CENTER STARS 33

- Background 33
- Observations 33
- Data Reductions : Photometry 35
- Data Reductions : Database Construction 36
- Summary 44

CHAPTER 3 : HIGH LUMINOSITY LATE-TYPE STARS IN THE GALACTIC CENTER STELLAR POPULATION 45

- Foreground Extinction 45
- Bolometric Corrections 50
- Discussion 51
- Conclusions 57

CHAPTER 4 : A SEARCH FOR LONG PERIOD VARIABLE STARS AT THE GALACTIC CENTER USING HKL PHOTOMETRY 58

- Background 58
- Variable Star Dataset 61
- Variability Analysis 62
- Indications of Variability from HKL Photometry 75
- Discussion 81
- Conclusions 87

TABLE OF CONTENTS (CONTINUED)

CHAPTER 5 : THE UNRESOLVED LATE–TYPE STELLAR POPULATION WITHIN 30″ OF SGR A* AND KINEMATIC EVIDENCE FOR A 1.7×10^6 $M_\odot$ BLACK HOLE 90

Background 90
Previous Studies of the CO 2.3μm Absorption Feature 90
Theoretical Relations for the Enclosed Mass vs. Radius of Spherically Symmetric Systems 91
The Galactic Center Stellar Kinematics 93
Observations and Data Reductions 96
The CO Absorption Feature 106
The Line-of-Sight Radial Velocity and Velocity Dispersion 109
The Enclosed Mass vs. Radius 119
Discussion 121
Interpretations of the CO Feature 121
The Galactic Center Rotation Curve 128
The Central Mass Distribution 134
Conclusions 136

CHAPTER 6 : SUMMARY AND PROSPECTS FOR FUTURE RESEARCH 137

APPENDIX 1 : ESTIMATION OF STELLAR FOREGROUND CONTAMINATION 140

Estimate of Disk Contamination 140
Estimate of Bulge Contamination 143

APPENDIX 2 : HK PHOTOMETRY OF GALACTIC CENTER STARS 148

APPENDIX 3 : HKL PHOTOMETRY OF GALACTIC CENTER STARS 165

LIST OF REFERENCES 172

LIST OF ILLUSTRATIONS

1-1 : Detection sensitivity at 2.2μm for stars at the Galactic Center 20

2-1 : Fraction of multiply detected sources at each 2.2μm epoch 40

2-2 : Positional map of the HK Sources in the sample to $m_K = 11.0$ 42

2-3 : The apparent luminosity function for the HK sample and the sources detected at L 43

3-1 : The observed H-K color distribution in the final database before the removal of suspected foreground stars 46

3-2 : Bolometric corrections at K as a function of $(H-K)_0$ for different samples of late-type stars 52

3-3 : The derived bolometric luminosity function for the complete sample of Galactic Center stars compared to Baade's Window 53

4-1 : The raw K magnitude residuals between September, 1987 and May 1988 for each star 63

4-2 : The average K magnitude residual between September, 1987 and May 1988 in the immediate vicinity of each star 64

4-3 : The K magnitude residuals between September, 1987 and May, 1988 for each star corrected for the average residual 65

4-4 : The amplitude parameter, Δm_K, vs. the average magnitude residuals $\langle m_K(3)-m_K(1)\rangle$ and $\langle m_K(3)-m_K(2)\rangle$ 68

4-5 : The observed number distribution of Δm_K compared to a theoretical distribution of nonvariables 69

4-6 : The amplitude parameter, Δm_K, vs. apparent K magnitude, $m_K(3)$ 70

4-7 : The total probability that a LPV of a given period and amplitude will have $\Delta m_K > 0.274$ mag 72

4-8 : The total amplitude integrated probability that a variable of a given period will have $\Delta m_K > 0.274$ for various amplitude distributions 73

4-9 : The average $(H-K)_{OBS}$ vs. M_{BOL} for LPVs and the total sample HK sample 74

4-10 : The dereddened (K-L) vs. (H-K) diagram for the "nonvariable" sample of stars detected at H,K, and L 77

4-11 : The dereddened (K-L) vs. (H-K) diagram for the LPV sample of stars detected at H, K, and L 78

4-12 : The dereddened (H-K) vs. Δm_K diagram for the HKL sample of stars 79

LIST OF ILLUSTRATIONS (CONTINUED)

4-13 : The dereddened (K-L) vs. Δm_K diagram for the HKL sample of stars 80

4-14 : The bolometric luminosity distribution of the HK sample along with the distribution of LPVs 82

4-15 : The fractional distribution of LPVs in the bolometric luminosity distribution at the Galactic Center and in Baade's Window 84

5-1 : Slit Positions for 2.3μm CO Spectra 97

5-2 : Long Slit 2.3μm CO Absorption Spectra 99

5-3 : Estimated Continuum Signal-to-Noise 102

5-4 : CO Band Strength vs. Projected Angle From Sgr A* 105

5-5 : $\chi^2(r)$ vs. V_{OFFSET} for Slit Position 1 Spectra 107

5-6 : Spectra that could not be cross correlated 108

5-7 : Results of Cross Correlation Technique Systematic Error Analysis 111

5-8 : σv and V_{LSR} vs. r_{SgrA*} 116

5-9 : The Galactic Center Rotation Curve 117

5-10 : Velocity Broadening Effects on the CO Band Strength 118

5-11 : CO Absorption vs. r_{SgrA*} compared to Sellgren *et al.* (1990) models 124

5-12 : Generalized Models for CO absorption vs. r_{SgrA*} 125

5-13 : V_{LSR} and σ_v vs. CO Band Strength 129

5-14 : Relative Intensity and CO Absorption Profiles for Slit P1 130

5-15 : The Systematic Effects of CO Band Strength on V_{LSR} and σ_v 131

5-16 : Kinematic Enclosed Mass vs. r_{SgrA*} Estimates Compared to 2.2μm Mass Estimates . 132

A1-1 : Estimated $(H-K)_{OBS}$ color distribution of foreground disk contaminants 145

A1-2 : The distribution of disk stars along the line-of-sight to the Galactic Center 146

A1-3 : The estimated percentage of stars in the Galactic Center sample within a distance $|x - R_0|$ of the nucleus along the line-of-sight 147

LIST OF TABLES

1-1 : Projected Radii From Sgr A* For Galactic Center Objects 16

1-2 : Apparent K Magnitudes of Luminous Stars at the Galactic Center 19

1-3 : Galactic Center Luminous Late-Type Stars 27

1-4 : Lower Limits on the Galactic Center Star Formation Rate 28

3-1 : Effect On Derived Bolometric Magnitude From Assumed Extinction and Color 55

4-1 : Variability Effects Due to Changing Extinction 60

4-2 : OH/IR Star Identifications 81

5-1 : List of 2.3μm Spectra Slit Positions 98

5-2 : Raw Velocity Dispersions and Relative Velocities From IRS 7 110

5-3 : Velocity Dispersions and Relative Velocities Corrected For Systematic Errors 115

5-4 : Enclosed Mass vs. Radius Estimates 121

5-5 : 2.2μm Enclosed Mass Estimates 135

5-6 : Enclosed Mass to Light Ratio vs. Radius 135

A2-1 : Galactic Center HK Photometry 148

A2-2 : Stars with Optically Determined Positions 164

A3-1 : Galactic Center HKL Photometry 165

ABSTRACT

Near infrared photometry is presented for 659 stars within 2.5′ of the Galactic Center from three epochs of 2.2μm and one epoch of 1.6μm observations. The data were taken with a Rockwell 64×64 HgCdTe IR array at the Steward Observatory 1.6m telescope and are complete to $m_K = 11.0$. Additional photometry at 3.4μm for a subsample of 258 stars taken with a 58×62 InSb array at CTIO is also included. The sample has an average $(H-K)_{OBS}$, which is consistent with a late-type population with $(H-K)_0 = 0.3$ and $A_V = 31.8$ mag, and luminosities several magnitudes brighter than the Baade's Window AGB. A variability analysis shows 59 stars are long period variable candidates at the 3σ level. These stars show correlations in $(H-K)_0$ vs. $(K-L)_0$ and $(K-L)_0$ vs. Δm_K consistent with Mira variables on the AGB. The LPV luminosities are consistent with a population few×10^8 yr old which is older than the Galactic Center central cluster stars and younger than bulge stars in Baade's Window, implying the Galactic Center has repeating episodes of star formation. Observations of the CO(v=2←0) 2.3μm absorption feature taken at the CTIO 4m with the IR Spectrometer Array of the unresolved stellar emission at 9 positions within 30″ of Sgr A* are presented. It is shown that the CO band strength is highly correlated with r_{SgrA^*} for radii less than $R_{CO} \approx 8.5''$ (0.28 pc). The Galactic rotation curve has a radial gradient of −16 km s^{-1} $arcsec^{-1}$ inside $r_{SgrA^*} \approx 10''$ (0.33 pc) where it reaches a minimum. Estimates of the enclosed mass vs. radius show there is $(1.7 \pm 0.3)\times10^6 M_\odot$ inside $r_{SgrA^*} = 5.2''$ (0.17 pc) with a mass-to-light ratio on the order of 10. Assuming the CO absorption samples stellar emission at each projected radius, these results are strong evidence for a massive black hole at the Galactic Center.

CHAPTER 1 :

INTRODUCTION TO THE GALACTIC CENTER

Overview

The work presented here focuses on the stellar population within 5 pc of the Galactic Center. The ability to study these stars with greatly improved detail has recently been made possible by advances in near-infrared detector array technology during the 1980's. For the first time, properties of the individual stars can now be studied in this wavelength region using methods that are common in optical astronomy. Instead of laborious scans made from single element detectors with poor spatial resolution, whole arcminute fields can be imaged at subarcsecond pixel scales. Because of the high density of objects in the central arcminutes, small amounts of observing time produce large amounts of photometric information. The large stellar survey presented here, among the first to be done with the new arrays, necessitated the development of numerous data reduction techniques and database procedures that were innovative to near infrared astronomy.

This chapter gives the motivations for the experiments presented in later chapters through a brief overview of the Galactic Center region and the important objects known to reside there. The observations can then be placed within a broader perspective. Chapters 2, 3, and 4 are collectively a detailed photometric investigation of the brightest stars within the central 5′ × 5′ (10pc × 10pc) of the Galactic Center. Data are presented from observations at 1.6μm (H), 2.2μm (K), and 3.4μm (L) that show the luminosity function, the color characteristics, and variability for a sample of 659 stars which are then compared to a well studied stellar population in the Galactic bulge to test for the presence of late-type supergiants. A small subset are demonstrated to be long period variables on the asymptotic giant branch (AGB) using photometric techniques. Their presence supports the hypothesis that several episodes of star

formation have occurred at the Galactic Center. Chapter 5 presents spectroscopic data of the 2.3μm CO absorption feature due to the late-type stars within 30″ of Sgr A* (a bright radio point source commonly thought to be the dynamical center of the Galaxy), which are among the highest spatial and spectral resolutions attained for this region. A deficit of CO absorption at the center previously observed by other workers is confirmed and is shown to have a highly correlated spatial distribution. An analysis of the enclosed mass vs. radius from Sgr A* is then performed using the velocity dispersion and rotational velocities at six positions from 5.2″ to 10.4″ from Sgr A*. The results, which are in agreement with several other determinations, support the hypothesis that a massive compact object resides at the Galactic Center. Chapter 6 offers some concluding remarks and outlines prospects for further research.

The Galactic Center Environment

Twenty five years ago the study of the Galactic Center was sedate compared to current research. In the late 1960's two important discoveries by Becklin and Neugebauer (1968) and Low *et al.* (1969) showed that large amounts of radiation, on the order of 10^6-10^7 $L_\odot$, were being emitted in the near- and far-infrared from a region that was only a few parsecs in size. These observations established the significant nature of the Galactic Center and laid the foundations for subsequent studies at progressively higher spatial and spectral resolutions which characterize current research. Unusual ejection phenomena observed in HI gas several hundred parsecs from the center characterized Galactic Center research during the 1960's and 1970's (e.g. Oort 1977) and motivated much scrutiny at smaller length scales. The 1970's and early 1980's saw great progress with the discovery of various gaseous and dust components (i.e. the "molecular ring" and the "minispiral") and demonstrated the very high mass density within the central parsec. However, the massive amount of data accumulated on the central few parsecs during the 1980's and early 1990's (e.g. Genzel and Townes 1987; Morris 1989) as yet gives no

clear connection to these larger scale features. Can a 10^6 $M_\odot$ black hole or massive star formation at the very center explain structures at radii of 1 kpc? A unified theory is currently lacking.

Recent review articles on this subject can be found in Genzel and Townes (1987) and Morris (1989). More synoptic but dated accounts can be found in Oort (1977), Brown and Liszt (1984), and Riegler and Blandford (1982) as well as Backer (1986). The outline of the Galactic Center given below is not comprehensive but does try to emphasize the important properties of those objects generally regarded as significant contributors to the overall structure, dynamics, and energetics as well as the important constraints on models that attempt to explain this highly complex region.

A distance modulus to the Galactic Center of 14.2 will be adopted which corresponds to a true distance, R_0, of 6.9 kpc. This value will be assumed unless otherwise noted. It was chosen to agree with Frogel and Whitford (1987) in their study of the late-type stellar population in Baade's Window and is based on the distribution of RR Lyrae variables along the line-of-sight to the Galactic Center (Blanco and Blanco 1985), estimates of the distance to the centroid of the Galactic globular cluster distribution (Frenk and White 1982), and H_2O maser proper motions in newly formed massive stars near the Galactic Center (Reid *et al.* 1986). It is lower than the values derived in recent reviews of this subject (R_0 = 8.5 kpc, Kerr and Lynden-Bell 1986; R_0 = 7.7 kpc, Reid 1989). The next three chapters deal with photometry of Galactic Center stars and this value of R_0 allows direct comparison with the Frogel and Whitford (1987) data. Since it may be underestimated by 10 to 20%, the corresponding absolute magnitudes will be systematically too faint by 0.2 - 0.4 mag.

The first thing to note about the Galactic Center is its close proximity in comparison with other galactic centers. At a distance of 6.9 kpc (23,000 light years) 1 parsec has a projected angle of 30″ when viewed from the solar system. The typical seeing limit of ground based near-infrared work is around 1″ which corresponds to 0.03 pc (6900 a.u.) at the Galactic Center. In

contrast, 1 parsec at the distance of M31, the closest spiral galaxy most similar to our own, will have a projected angle of only 0.4″ and the smallest visible structures will be on the order of 2.5 pc in size. Thus, comparable structures seen in the center of our own Galaxy cannot be resolved by ground based instruments in even the closest spiral galaxy. The problem only becomes worse for even more remote galaxies.

The term "Galactic Center" itself has a variety of meanings for observational techniques that consider different concentric solid angles in the constellation of Sagittarius. For gamma and X-ray astronomy the Galactic Center can include a solid angle of width 5 to 10°, with a projected size of 600-1200 pc! Infrared observers tend to concentrate on a solid angle with a projected size of only 5 pc or less. Such vastly different length scales lead to very distinct topics that has occasionally caused confusion from observational limitations. For instance, the object E1740.7-2942 was recently discovered to be the source of e+e- annihilation line radiation at 511 kev but it is significantly displaced from the dynamical center of the Galaxy by a projected angle of 0.5° (Sunyaev *et al.* 1991). The annihilation line radiation was viewed as strong evidence for a massive black hole at the Galactic Center (e.g. Brown and Liszt 1984). But such a large separation between E1740.7-2942 and the dynamical center means that the annihilation line source is irrelevant to the energetics within the central 10 pc (5″) of the Galaxy.

The photometric study in chapters 2 through 4 examines the Galactic Center stellar population within a solid angle of approximately 5′×5′ with a projected radius of 5 pc. The CO absorption study discussed in chapter 5 examines the unresolved stellar emission from within 30″ (1 pc) of the Galactic Center. The projected radii for some significant objects discussed below are listed in table 1-1 for comparison (R_0 = 6.9 kpc).

The main physical components within the center are observed or inferred from a wide variety of observational techniques spanning nearly the entire electromagnetic spectrum with the exception of the visible and UV bands. These include a stellar population, a multi-phase interstellar medium of gas and dust, a peculiar radio point source commonly presumed to be

a massive black hole, and magnetic fields. Many of the present efforts in Galactic Center research center on the details of these components and their relative importance.

TABLE 1-1 : Projected Radii From Sgr A* For Galactic Center Objects

Object	Angular Radius (″)	Projected Radius (cm)
Schwartzschild Radius of 2×10^6 $M_\odot$ Black Hole	5.8×10^{-6}	5.9×10^{11}
IRS 16 C	1.5	1.5×10^{17}
IRS 7	6.5	6.7×10^{17}
Mini-spiral	1-38	$1.0\text{-}39.\times10^{17}$
Molecular Ring	35-206	$3.6\text{-}21.2\times10^{18}$
Stellar Survey of Chapters 2-4	< 150	1.5×10^{19}
E1740.7-2942	1800	1.85×10^{20}
Baade's Window	13700	1.41×10^{21}

The Galactic Center Stellar Population — In General

The stars at the Galactic Center seen in the near-infrared (1-3 μm) are the dominant mass component (Genzel and Townes 1987) in the region for R > 1 pc. When stellar emission was first observed by Becklin and Neugebauer (1968), several fundamental characteristics were established that remained important in subsequent investigations (e.g. Lebofsky *et al.* 1982; Allen, Hyland and Jones 1983; Rieke and Lebofsky 1987; Sellgren *et al.* 1987). There is a central peak in the surface brightness of 2.2μm emission that is proportional to $\theta^{-0.8}$, where θ is the projected angle away from the central emission peak. This emission was identified with the Galactic Center from its coincidence with the bright radio source Sgr A (Downes and Maxwell 1966) and the dynamical center as determined by observations of HI in the Galactic plane (Oort and Rougoor 1960). For a stellar population at the Galactic Center with a spherically symmetric luminosity density of the form $\rho_* \times R_{GC}^{-\alpha}$, no significant occultation effects from crowding, a constant mass-to-light ratio and uniform foreground extinction, the surface brightness μ at

projected radius R along the z-axis line-of-sight will be given by

$$\mu = \rho_* \int_{-\infty}^{\infty} R_{GC}^{-\alpha}\, dz \propto R^{-\alpha+1}.$$

This will reproduce the observed surface brightness profile for $\alpha = -1.8$. The assumption of uniform extinction is consistent with the relatively constant (H-K) color observed with large apertures across the central few arcminutes (Becklin and Neugebauer 1968). If the intrinsic colors of these stars are typical for late-type stars then the foreground visual extinction to the Galactic Center is on the order of $A_V = 30$. It is also notable that the flux density of 2.2μm radiation implies a total luminosity of few$\times 10^6$ $L_\odot$ radiating from within the central few parsecs and translates into a stellar density that is 10^6 times greater than in the solar neighborhood if the mass to light ratio is similar to M31 (Becklin and Neugebauer 1968).

There is a dominant central cluster of stars ($\theta < 30''$) which has been intensively studied (e.g. Becklin and Neugebauer 1975; Lebofsky *et al.* 1982; Allen, Hyland and Jones 1983; Rieke, Rieke and Paul 1989; Depoy and Sharp 1991). Near-infrared spectra show that many of these stars have strong CO absorption at 2.3μm (Neugebauer *et al.* 1976; Treffers *et al.* 1976; Lebofsky *et al.* 1982; Wollman, Smith and Larson 1982) which is characteristic of high-luminosity late-type stars. It increases in strength with increasing luminosity and decreasing temperature (e.g. Kleinmann and Hall 1986). The strength of the CO feature in the central cluster stars shows they are supergiant stars. The 2.2μm luminosity of the central cluster is dominated by the point source "IRS 7" which also has the strong CO absorption (Neugebauer *et al.* 1976; Treffers *et al.* 1976; Lebofsky *et al.* 1982; Wollman *et al.* 1982; Sellgren *et al.* 1987). Along with IRS 7, Lebofsky *et al.* (1982) listed 6 other sources (sources 11, 12, 19, 22, 23, and 24) with late-type supergiant spectra. This strong concentration of supergiants within such a small region ($R < 4$ pc) implies considerable recent star formation activity which will be more extensively discussed below.

The enclosed mass versus radius from the Galactic Center has been determined using radial velocities of individual sources (Sellgren *et al.* 1987; Rieke and Rieke 1988) and the velocity dispersion of the unresolved background stellar emission (McGinn *et al.* 1989; Sellgren *et al.* 1990). These efforts will be discussed in more detail in chapter 5 and an extension of the latter method will be made in this work.

The Galactic Center Stellar Population — Particular Objects

The objects within 30″ of Sgr A* have many unusual features and there is no clear consensus on the relative importance for many of them. The more important objects are discussed here.

• **IRS 7** - The bright source IRS 7 has an apparent K magnitude of 6.7; its bolometric magnitude is approximately −8.0 (1.3×10^5 $L_\odot$). Near infrared spectra show it has a luminosity class of M2Ia (Lebofsky *et al.* 1982) which implies an age < 10^7 yr. The brightness of this supergiant star is so outstanding (~1/10 the total 2.2μm luminosity in the central parsec) that it was detectable in the initial near-infrared aperture scans of Becklin and Neugebauer (1968). Several features have clearly established that IRS 7 is located near the Galactic Center. An excess of Brα emission was interpreted by Rieke and Rieke (1988) as the ionization of a stellar wind from IRS 7 by ambient UV photons. They placed an upper limit on its distance from the center < 0.6 pc . Recently, radio continuum observations (Yusef-Zadeh and Morris 1991) have revealed a cometary "tail" of ionized gas streaming from the location of IRS 7 in a direction away from the IRS 16 complex and the dynamical center. A theoretical analysis of these observations by Yusef-Zadeh and Melia (1991) modeled the tail as the interaction between the stellar wind of IRS 7 and a much more powerful wind from IRS 16 C or Sgr A*.

• **The IRS 16 Complex and Evidence for Massive Blue Stars** - The resolved sources known as the IRS 16 complex lie within 1-5″ of Sgr A*. The dereddened colors of these stars

are notable because they are much bluer than those of late-type stars (Becklin and Neugebauer 1975; Allen, Hyland and Jones 1983; Rieke, Rieke and Paul 1989). This compact cluster has four main components (IRS 16 NE, IRS 16 C , IRS 16 NW and IRS 16 SW) with numerous fainter point sources and related unresolved emission. Initially IRS 16 C and Sgr A* were not clearly distinguishable, but astrometric comparisons between radio, mid- and near- infrared positions have shown a separation by about 1″ (Allen and Sanders 1986; Becklin *et al.* 1987; Forrest *et al.* 1987). The vicinity of IRS 16 shows strong HeI (2.06μm) emission lines (e.g. Hall, Klienmann and Scoville 1982; Geballe *et al.* 1991; Krabbe *et al.* 1991) with velocity components that correlate with the 2 μm continuum of the IRS 16 cluster and are very broad with a velocity width ~ 1500 km s^{-1} indicative of high velocity mass-loss winds from early-type stars (Krabbe *et al.* 1991). The late-type supergiants and the enigmatic nature of the bluer IRS 16 sources suggest that a considerable population of progenitor blue main-sequence stars is present as well. Imaging such sources is impossible however given severe crowding in the central 20″ and the spatial resolutions that are currently available. This is illustrated in table 1-1 that shows the estimated K magnitudes for a progenitor blue main-sequence O star (Maeder 1991) and a red supergiant (Lebofsky *et al.* 1982). Figure 1-1 shows an H-R diagram with sensitivity curves at various 2.2μm detection thresholds for stars at the Galactic Center assuming they have black body spectra.

TABLE 1-2 : Apparent K Magnitudes of Luminous Stars at the Galactic Center

Spectral Type	Luminosity	Effective Temperature	2.2μm Flux	K
O7V	2.5×10^5 $L_\odot$	35,000 K	2.57 mJy	13.6
M2I	1.0×10^5 $L_\odot$	3,000 K	500 mJy	7.8

The observations presented in chapters 2 – 4 were made with a Rockwell 64×64 array at

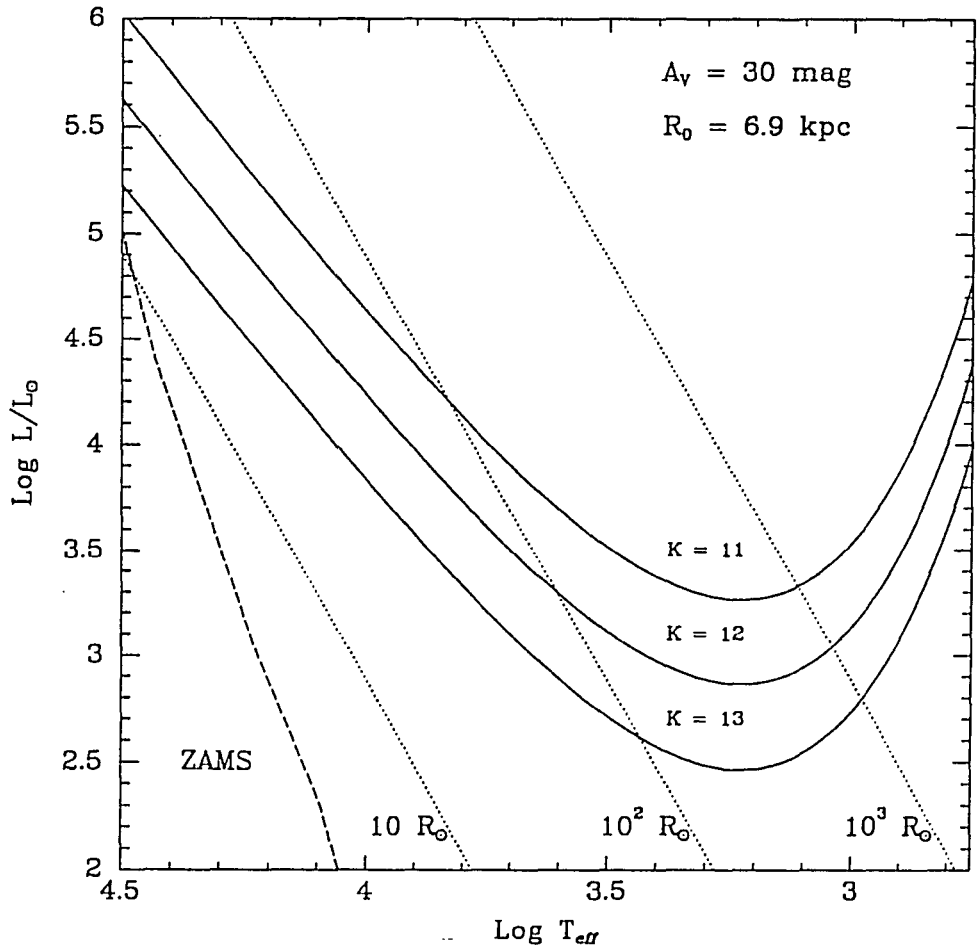

Figure 1-1: The figure shows the region in the L vs. T_{eff} diagram accessible by the corresponding sensitivity limits at 2.2μm of K = 11, 12, and 13 mag for Galactic Center stars, assuming they have black body spectra. Values of R_0 = 6.9 kpc and foreground extinction A_V = 30 mag are assumed and the position of the zero age main sequence (ZAMS) comes from Mihalas and Binney (1981).

1.2″/pixel resolution. The images were confusion limited for sources fainter than K ≈ 12.0 mag but stars could not be reliably detected from overlapping frames for K > 11.0 mag. Thus significant improvements in spatial resolution are needed to detect massive blue main-sequence stars. Such stars may perhaps be inferred by effects on surrounding material or by line emission processes that substantially exceed continuum emission.

There are indications that massive blue stars may be present. Within the thermal gas and dust structure known as the "minispiral" (see below) is a collection of point sources visible at 10μm. The interpretation of these sources had been controversial, either attributed to dust density enhancements (Gatley 1982, 1987) illuminated by Lyα photons, or to embedded stars that locally heat the dust (Rieke, Telesco, and Harper 1978). Shorter wavelength observations (Rieke, Rieke, and Paul 1989) show significant J-band emission from at least three of these sources (1, 9, and 13) with two-component infrared spectra consistent with hot stars, of spectral type G or earlier (from the lack of 2.3μm CO absorption), and *locally* heated dust. These sources also show the strong HeI emission lines (Krabbe *et al.* 1991).

Interstellar Dust and Gas Within 10 pc of the Galactic Center

Far infrared observations show that considerable amounts of reprocessed energy (few × 10^6 $L_\odot$) are radiated by dust in the Galactic Center (e.g. Gatley *et al.* 1977; Becklin, Gatley and Werner 1982). This radiation is comparable to the observed near infrared emission from the late-type stars (Becklin and Neugebauer 1968). The 30 μm dust emission is peaked at the same location as the 2.2μm radiation as well as the 50-100 μm color temperature. The emission seen at 50μm and 100μm is double lobed on either side of the temperature and luminosity peaks indicating a ring structure for the dust which is depleted in the central parsec. The normalized emission radial profiles broaden with increasing wavelength which shows the dust color temperature and luminosity decrease with increasing radius from the Galactic Center. Such a

configuration raises the possibility of a compact central source dominating the energetics of the inner few parsecs. Early models for the dust heating (Gatley *et al.* 1977) included a hot luminous central source, identified with Sgr A*, and the local population of late-type stars. An upper limit for the total luminosity of the region assuming thermal equilibrium for the dust grains and a dust absorption coefficient that varies as λ^{-1} (e.g. Spitzer 1978) gives $L_{TOTAL} \leq$ 1-3×10^7 $L_\odot$ (Becklin *et al.* 1982). The dust thermal equilibrium relation, which has the form $T_{dust}^5 \propto LR^{-2}$, was calibrated from known Galactic HII regions and was applied to the Galactic Center using a grain temperature of 70K from the highest color temperature at 50-100μm and a characteristic dust radius given by the lobes at 100μm. Producing this 1-3×10^7 $L_\odot$ of radiation from a volume only several parsecs in size is one of the important constraints to be satisfied by models for the Galactic Center region.

The Circum-Nuclear Disk - The dust seen at mid- and far-infrared wavelengths is associated with a ring of atomic and molecular gas with a sharp inner edge 35″ from the IRS 16 complex. Molecular hydrogen (2.12μm) at the inner edge of the disk shows evidence of being shocked by an outward flowing wind with an implied mass loss rate of 10^{-3} $M_\odot$ yr^{-1} (e.g. Gatley *et al.* 1984; Gatley *et al.* 1986). Atomic lines of hydrogen (21cm) (Liszt *et al.* 1983), and oxygen (63μm) (Lester *et al.* 1981; Genzel *et al.* 1985), as well as molecular lines of CO(2.6mm) (Liszt *et al.* 1983) and HCN (3mm) (Wright *et al.* 1987) collectively show a disk that extends to at least 3′ from the dynamical center. It rotates in the sense of Galactic Rotation at ~110 km s^{-1} from the inner edge of the disk out to 1.4′ with turbulent velocity widths of 50 km s^{-1}. It is inclined with respect to the Galactic Plane by approximately 60° at the inner edge and shows evidence of being warped (e.g. Güsten 1987). The disk material has a filling factor of only 5-10% allowing exciting UV radiation from the central 1.5 pc to penetrate nearly 8pc from the center and thus heat the dust seen in the far-infrared. Comparisons of CO (Lugten *et al.* 1987) and atomic (Genzel *et al.* 1985) line ratios with collisional excitation calculations show gas temperatures of few×10^2 K and densities of few×10^4 cm^{-3} at the inner disk edge and there is

decreasing excitation, energy density, and gas pressure with increasing distance from the center (e.g. Genzel 1989).

Ionized Gas and the "Minispiral" - Within the molecular ring is the ionized gas distribution known as the SGR A West complex, which is confined to several discrete filamentary structures known as the "mini-spiral" (Lo and Claussen 1983). It has been observed both in the radio continuum (e.g. Ekers *et al.* 1983; Pedlar *et al.* 1990) and in the [NeII] 12.8μm line (e.g. Lacy *et al.* 1980; Lacy *et al.* 1982; Serabyn *et al.* 1988; Lacy, Achtermann and Serabyn 1992). Hot dust is intermixed with the ionized gas and is observable at near infrared wavelengths (e.g. Rieke, Telesco and Harper 1978; Gezari and Yusef-Zadeh 1991). The filaments show systematic velocity changes along their lengths that indicate predominantly orbital motion rather than outflow or inflow. The velocities give an inferred enclosed mass of 1.6×10^6 $M_\odot$ inside a radius of 10″ (Serabyn *et al.* 1988). It is most likely that the "Western Arc" is the inner ionized edge of the molecular ring and the other filaments are probably infalling clumps that have been tidally elongated. Complicating the analysis of the motions of the filaments is the contribution of the local magnetic field. Only a lower limit of 10 mgauss is known for the field strength (Aitken *et al.* 1986). The excitation of the [NeII] implies a Ly continuum flux of 10^{51} photons s^{-1} emerging from the central parsec. This Ly continuum luminosity is among the largest for Galactic HII regions (e.g. Wynn-Williams and Becklin 1974) yet the implied ionizing spectrum is among the coolest (Lacy *et al.* 1980). The ratio of $N(Ar^{+2})/N(Ar) < 0.5$ for the ionized cloud closest to the center implies that Ar^{+2} photons (and thus He^+ photons) ionize less than half its material. This places an upper limit to the HeII ionizing flux which in conjunction with the estimated Ly continuum flux gives an upper limit for the temperature of the ionizing UV radiation field. If it arises from distributed sources in the central parsec then the temperature is less than 35,000 K and less than 31,000 K if it is from a dominant central source (Lacy *et al.* 1980).

Unusual line emission centered about 3″ to the south west of Sgr A* at 2.217μm has

recently been seen by several workers (Allen, Hyland and Hillier 1990; Eckart *et al.* 1992). Eckart *et al.* (1992) showed the gas is spatially extended with a velocity FWHM of 500 km s^{-1} and offset from Sgr A* forming an arc around a particular feature in the "mini-spiral" known as the "mini-cavity" which is opposite the IRS 16 complex from Sgr A*. They suggested it was either an [Fe XII] transition observed in the solar corona or an [Fe III] transition at 2.2178(20) μm. Wardle and Yusef-Zadeh (1992) model the emission as the collisional excitation of stellar wind material originating from IRS 16 that is gravitationally focused around Sgr A* and then shocked by its impacting on the "mini-spiral" feature. This interpretation favors an [Fe XII] identification for the line emission since it is likely that the post-shock gas temperature would too hot for significant [Fe III] emission.

Sgr A* — A Massive Black Hole at the Galactic Center?

Lynden-Bell and Rees (1971) first postulated that a massive black hole was present at the Galactic Center and a strong nonthermal radio point source was subsequently discovered by Balick and Brown (1974) and became known as Sgr A*. The above discussion has shown that there are several indications from the dust and gas emissions for a centralized energy source with a characteristic temperature ~ 35,000 degrees, a total luminosity on the order of 10^7 $L_\odot$ within a region which has a mass density on the order of 10^6 $M_\odot$ pc^{-3}. Much research has attempted to establish the presence of a central engine (see Genzel and Townes 1987; Gatley 1989) and the unique properties of Sgr A* have made it a frequent candidate. The motivations for such an hypothesis are obvious. If we can understand the activities at the center of our own Galaxy through processes involving a massive black hole then perhaps it can serve as a scaled-down version of active galactic nuclei in distant galaxies and quasars.

The observational status of Sgr A* has been summarized by Lo (1982, 1987, 1989). If any object can be identified as a massive black hole, as suggested by gas dynamics and stellar

velocities, it is likely to be Sgr A* because it has a number of features that are unique within the Galaxy. Pulsar interpretations for this object are ruled out because its low variability amplitude, ~20%, and radio spectral index (v^{α}) of α = 0.2 are outside typical pulsar values. It is also more radio luminous than the brightest known pulsar by a factor of 10^3. The radio spectrum is similar to objects found in the nuclei of M81 and M101. The angular size of Sgr A* varies as λ^2 for wavelengths longer than 1mm, consistent with thermal scattering by interstellar electrons.

As mentioned above, the early conjectures that Sgr A* and IRS 16 were coincident proved incorrect by the demonstration that these objects are separated by at least 1″ (Allen *et al.* 1986; Becklin *et al.* 1987; Rieke, Rieke, and Paul 1989). This left a somewhat confusing picture for proponents of a central engine because there was no detectable near-infrared source at the location of Sgr A* consistent with the luminosity and temperature constraints for a central source. Recently there have been several efforts to identify Sgr A* with high resolution near-infrared imaging. Depoy and Sharp (1991) reported observations from a 100×1″ image at 0.3″/pixel resolution giving a 3σ upper limit on Sgr A* of K $\geq$ 13.5 and Eckart *et al.* (1992) reported a detection of Sgr A* at K = 13.7 ± 0.6 using a 2000×(0.5″ or 1″) image at 0.05″/pixel resolution. If the Galactic Center is to be a "mini-AGN" then it seems the central engine is in a relatively inactive state and the source of the 10^7 $L_{\odot}$ must lie elsewhere, most likely the IRS 16 complex.

The presence of a central black hole in the Galactic Center is also suggested by dynamical evidence that shows central masses on the order of 10^7 $M_{\odot}$ in the nuclei of M31 and M32 (Tonry 1987; Kormendy 1988; Dressler and Richstone 1988). It is notable that if such an object were within our Galactic Center is would already have been detected by a 250 km s^{-1}

velocity dispersion for stars in its proximity. This has been ruled out by near-infrared stellar radial velocities (Sellgren *et al.* 1987; Rieke and Rieke 1988; McGinn *et al.* 1989) but a compact object with a mass an order of magnitude less can still be accommodated (see chapter 5).

Starbursts at the Galactic Center

Lebofsky, Rieke, and Tokunaga (1982) found 7 supergiant stars in the central 1.5′ from near-infrared spectroscopy and the results of Lebofsky, Rieke, Deshpande, and Kemp (1982) suggested five other stars with similar photometric and polarization properties could also be supergiants. The fact that the Galactic Center contained numerous late-type supergiants led to the consideration that starburst-like phenomena in the Galactic Center could explain the overall energetics and characteristics of the ionizing radiation without resorting to explanations involving a central engine. The spectral type of IRS 7 implies a progenitor of ~20 ± 2.5 $M_\odot$ (e.g. Maeder and Maynet 1989) which has formed within the last 10^7 yr.

It is useful to present the calculation of Lebofsky *et al.* (1982), using revised values of the Galactic Center distance and the stellar evolution tracks of Maeder and Maynet (1989), to demonstrate the significance of massive star formation within the Galactic Center environment. When the spectral types and estimated bolometric luminosities are compared to stellar evolution tracks to find the appropriate progenitor mass, an upper limit to the age of the population is given by the age of the most massive star. These mass estimates show a minimum of ≈ 60-70 $M_\odot$ was consumed in the formation of this group of stars. The time scale for the starburst can be taken as the age of IRS 7 at 10^7 yr.

TABLE 1-3 : Galactic Center Luminous Late-Type Stars

Source	Spectral Type[a]	m_K[a]	$(H-K)_o$[a]	M_K[b]	Progenitor Mass[c] ($M_\odot$)
IRS 7	M1.3Ia	6.7	0.29	-11.5	20
IRS 12	M4Ib	8.1	0.35	-9.5	7-9
IRS 19	M4Ib	8.1	0.49	-9.7	9-12
IRS 11	M0Ib	9.5	0.22	-5.0	3-4
IRS 22	M6II	7.8	0.50	-9.0	5-7
IRS 23	M6II	7.9	0.51	-9.4	7-9
IRS 24	M6II	7.9	0.49	-9.8	9-12

[a]Lebofsky, Rieke and Tukanaga (1982), [b]R_0 = 6.9kpc,BC_K = 3.0 [c]Maeder and Maynet (1989)

A lower limit to the star-formation rate can be made by considering an initial mass function (IMF) for star formation of the form $f(m) \propto m^{-2.35}$, which is the Salpeter form. The mass contribution from stars of masses between m and m+dm will be given by $dm = m \times f(m)\, dm \propto m^{-1}\, dm$. For a starburst event with an upper cutoff mass of m_2 and a lower cutoff mass of m_1, the fractional mass contribution, F, for stars with progenitor masses greater than m_3 will be equal to

$$F = \frac{\int_{m_3}^{m_2} m\, f\,(m) dm}{\int_{m_1}^{m_2} m\, f\,(m) dm} = \frac{m_2^{-0.35} - m_3^{-0.35}}{m_2^{-0.35} - m_1^{-0.35}} \quad .$$

Using numbers derived from the observed supergiants (and knowing the resulting stars must have $T_{eff} < 35{,}000$ K), we may take $m_2 = 20\ M_\odot$, with a minimum amount of 70 $M_\odot$ of stars with $m > 7\ M_\odot$, the resulting lower limits on the star formation rate follow for the assumed lower mass cutoffs listed:

TABLE 1-4 : Lower Limits on the Galactic Center Star Formation Rate

m_l ($M_\odot$)	F	M_1 ($m > 7M_\odot$)	M_{TOTAL} ($M_\odot$)	SFR ($M_\odot$ yr^{-1})	SFR ($M_\odot$ yr^{-1} pc^{-2})
0.1	0.08	70	875	8.8×10^{-5}	3.1×10^{-7}
1.0	0.24	70	291	2.9×10^{-5}	1.0×10^{-7}

So the approximate star formation rate in this burst was on the order of 2×10^{-7} $M_\odot$ yr^{-1} pc^{-2}. This is two orders of magnitude greater than the Galaxy wide average rate of $3\text{-}7\times10^{-9}$ $M_\odot$ yr^{-1} pc^{-2} (Miller and Scalo 1979; R_0 = 10 kpc), but comparable to the rate within the central 800 pc of the bulge of $\approx 4\times10^{-7}$ $M_\odot$ yr^{-1} pc^{-2} (Smith, Biermann, and Mezger 1978; R_0 = 10 kpc). The amount of mass inferred to be involved in the starburst and the rate of star formation are rather modest compared to the theoretical results of Loose, Krügel and Tutukov (1982) that are discussed below (0.01%). Nevertheless, the presence of large numbers of late-type supergiants is evidence that starburst episodes might occur and could account for the high luminosity within the region.

There is abundant raw material for starbursts within 1 kpc of the Galactic Center in giant molecular clouds that have been mapped in ^{12}CO, ^{13}CO, and CS (e.g. Bally *et al.* 1987, 1988; Stacy, Dame, and Thaddeus 1989). Stark *et al.* (1991) estimated the masses for the six largest clouds to be on the order of a few $\times$ 10^6 $M_\odot$ from tidal limitations by the bulge, the Virial theorem, and CO and CS column densities. The perturbed orbits of bulge stars enhance the density of material behind each cloud resulting in dynamical friction that eventually causes the cloud to spiral into the center within only a few hundred million years. Unless the rate of star formation within a cloud is sufficiently high to consume it during its fall, it will cause a starburst upon collapsing to the center. The number of clouds and the time scale for infall suggest a steady state recurrence of starbursts every 100 Myr.

A theoretical study by Loose, Krügel and Tutukov (1982) examined the relevance of massive star formation in the Galactic Center environment. They pointed out that unlike the

disk of the Galaxy, gaseous material collecting at the Galactic Center cannot escape because it is at the bottom of a potential well thus leading to large amounts of raw material to form stars. The mass density distribution of stars, ρ^*, that determines the gravitational potential varies as $R^{-1.8}$. For a gaseous cloud's internal gravity to overcome tidal forces its density must be $\rho > \rho^* \propto R^{-1.8}$, so clouds must be increasingly dense with decreasing radii from the center to undergo Jeans instability. Because of the increased effects of rotation, gas temperature, turbulence, magnetic fields, and coalescence of fragments after collisions, the stars that form near the center are likely to have higher masses than stars formed in the disk. They described two models that assumed an IMF of the form $dN \propto M^{-2.35}dM$ with an upper cutoff of 60 $M_\odot$. Their "Case A" had a lower IMF cutoff at 1.0 $M_\odot$ and exhibited a 10^8 yr periodic cycle of gas accumulation which led to bursts of high mass star formation. Each burst, lasting a few $\times$ 10^7 yr converted approximately 10^7 $M_\odot$ into ~ 10^5 OB stars. These OB stars would each in turn expel 10^{51} erg of energy back into the gaseous material via supernova explosions. All of the star formation occurred within 10 pc of the center with a peak luminosity of 10^9 $L_\odot$. The other model discussed, "Case B", had a lower IMF cutoff at 0.1 $M_\odot$ producing a smaller fraction of supernova progenitors. This model showed an initial buildup of gas and a subsequent burst of star formation. However, the amount of energy returned by supernovae was insufficient to disrupt the accumulated gas and led to the formation of a quasi-hydrostatic core in the central few parsecs. Both models show that accumulated material from mass loss by late-type stars and ambient gas at the bottom of the deep gravitational potential of the Galactic Center may lead to unusual star formation conditions unlike anywhere else in the Galaxy.

The claim that star formation is important for understanding the Galactic Center was contested (e.g. Gatley 1987) by the assertion that knot structures observed in the 10 μm emission and associated with thermal emission seen in the radio (which later became known as the "mini-spiral") should show up in the color temperature distribution of the far-infrared emission if they are internally heated by hot stars. Also it was suggested that a star-formation event should

produce a more chaotic configuration in the gas and dust structures seen at the center. The far-infrared observations indicated that the dust distribution has a central cavity and the symmetric luminosity and temperature profiles about the center meant the energetics could well be dominated by a strong central ionizing source. Subsequent continuum and line measurements of the K sources at the positions of these 10 μm knots show they are likely to be massive blue stars (Rieke, Rieke, and Paul 1989; Allen, Hyland and Hillier 1990; Krabbe *et al.* 1991). Even so, the picture of star-formation at the Galactic Center does not contend that formation is currently ongoing, merely that it occurred in the recent past and its effects are still felt from the high-mass stars that were produced. The variability study presented here was initiated mainly to find further evidence of recent star-formation (chapter 4).

The Galactic Center and the Nucleus of M31

Despite being ~10^2 times further away, there are several features in the center of our Galaxy that are also present in the nucleus of M31. The center of the M31 normalized 2.2μm light profile is similar to the 2.2μm light distribution of the Galactic Center when the Galactic observations are degraded to comparable resolution (Becklin and Neugebauer 1968; Rieke and Lebofsky 1987). There is a nucleus with a radius on the order of 2″ (0.6pc) that is distinct from the bulge (Light, Danielson and Schwarzschild 1974; King *et al.* 1992). King *et al.* also reported the detection of ~150 UV point sources in the central 44″ which they interpreted as post-asymptotic giant branch stars. These PAGB stars only contributed less than 20% of the total UV light emerging from the M31 nucleus indicating that some fainter and more distributed population is responsible. One possibility they suggested was a high-metallicity AGB population but they add that the characteristic ages and masses of these stars are yet to be determined from stellar evolutionary tracks.

There is the kinematic evidence for a central mass concentration on the order of 10^7 $M_\odot$

from the optical and near-infrared velocity dispersion and rotation curves as mentioned above (Kormendy 1988; Dressler and Richstone 1988) with a mass to light ration in excess of 10^2 $M_\odot/L_\odot$. Recently Crane, Dickel, and Cowan (1992) recently reported the 5σ detection of a radio point source at 3.6 cm coincident with the dynamical nucleus with a flux density of 28 ± 5 μJy which is intrinsically 1/5 as bright as Sgr A* at the same wavelength. Further information as to its nature requires future observations but its proximity to the nucleus and the evidence for a compact mass concentration suggests it may be analogous to Sgr A*.

Unlike the Galactic Center, M31 does not show significant emission in the mid- and far-infrared from dust emission at 10 μm (Rieke and Lebofsky 1978) or 100 μm (Telesco 1977) and there is a low density of gas (Brinks 1984; Soifer *et al.* 1986) which may account for the low luminosity of the radio point source if it is similar to Sgr A* (Crane *et al.* 1992). M31 shows many features that are similar to the Galactic Center but there is not a complete one-to-one correspondence. Nevertheless, its is likely that a more comprehensive understanding of either nucleus will help in understanding the other because the larger distance to M31 is compensated to some extent by its lower central extinction (Sandage, Becklin and Neugebauer 1969).

Summary

The inner 10pc of the Galactic nucleus is an extremely complex region. There is a central cluster of stars with a density on the order of a few×10^6 stars pc^{-3} that shows evidence of recent star formation and a hot blue population of unknown extent. There is a ring of molecular and atomic material, in roughly circular orbit about the center, intermixed with dust which absorbs a significant amount of UV radiation and reradiates in the far infrared. Within the inner edge of the molecular ring is a cavity largely devoid of gas except for a few very striking ionized filaments with motions that suggest orbital trajectories. Finally there is the

mysterious Sgr A* which has unique radio properties and is well placed spatially and dynamically to be identified with a massive black hole of approximately 1-2×$10^6 M_\odot$, although energetically it is difficult to view it as an active central engine. Two competing hypotheses to explain the energetics have invoked recent massive star formation or an active central engine analogous to what is thought to be in other galaxies. This is the broad background in which the following observations are to be placed.

CHAPTER 2 :

HKL PHOTOMETRY OF GALACTIC CENTER STARS

Background

The central peak of the Galactic Center 2.2μm emission was initially attributed to older Population II stars within the core of the Galactic Bulge (Becklin and Neugebauer 1968), similar to the population seen in the center of M31 (Sandage, Becklin and Neugebauer 1969). Subsequent spectroscopic studies showed the brightest point sources to be younger late-type supergiants (Neugebauer et al. 1976, Lebofsky et al. 1982, Wollman, Smith, and Larson 1982). Whatever older bulge-like stars may be present are intermixed with at least a few recently formed massive stars. The first large-scale high resolution imaging of the center (Rieke, 1987) revealed nearly 1000 stars detectable at K(2.2μm) in a 5'x5' area to a limit of K=12. The Galactic Center luminosity function suggested there is an excess of high-luminosity stars compared to the population in Baade's Window at Galactic latitude l=-3.8° (Frogel and Whitford 1987). Since the only information available came from photometry in two wavebands at a single epoch, remaining questions about the nature of the constituent stars (e.g. their predominant luminosity class and evolutionary state) could not be fully answered using these data. The present chapter describes new observations at K (2.2μm), H (1.6μm), and L(3.4μm) that form an extended investigation of the general traits of the luminous Galactic Center stars seen in the near IR.

Observations

The K observations were made at three epochs: 1987, May 5; 1987, September 2; 1988 May 26. The first two epochs were taken by M. Rieke and the third by M. Rieke and J. Haller.

Each night was photometric, and the data were acquired close to the local meridian to minimize problems associated with the relatively high air mass of the Galactic Center when observed from Tucson, Arizona ($z \geq 2.06$). The Steward Observatory 1.54-m telescope was used at f/45 with a 64×64 HgCdTe infrared detector array with a CCD readout fabricated by Rockwell International. The camera is described in Rieke *et al.* (1986). The camera's reimaging optics provided a plate scale of 1.2"/pixel and a field of view of 77". The repeated imaging was done at K(2.2μm) since shorter wavelengths are more severely attenuated by interstellar extinction ($A_V \approx 30$; Becklin and Neugebauer 1968; Rieke *et al.* 1978; Becklin *et al.* 1978; Lebofsky *et al.* 1982; Rieke, Rieke, and Paul 1989), and would have required much longer exposures. Exposure times were limited to 20 seconds because source confusion was becoming apparent. The read noise of 600 electrons was adequate for the images to be background-limited. An additional map was made during the May 1988 observing run at H (1.6μm) with 90-second exposures, providing color information.

At each epoch the region was mapped in a series of seven columns of constant right ascension stepped by 4 sec of time, with 4"-10" of overlap between rows to ensure that every star was imaged at least twice. The area of the observed region was approximately 5′ × 5′ (the south eastern corner was not mapped because of its high extinction from a foreground molecular cloud) and was centered on IRS 7 ($K \approx 7.0$). Frames of blank sky were also taken at a position an hour east of the Galactic Center for flat fielding. The flux calibration was based on observations of standards from Elias *et al.* (1982).

The L data were taken by J. Frogel in May 1988 at the CTIO 1.5m telescope using a Santa Barbara 58×62 InSb infrared detector array with 60^s integration times. There were 60 individual readouts of 1 sec each, coadded to produce the total integration time. The angular resolution was 0.9″/pixel. The central 5′×5′ of the Galactic Center centered on IRS 7 was mapped as seven rows of constant declination in eighteen steps. Frame overlapping ensured that most of the detected sources were imaged at least twice for confirmation. Since the

background at L due to thermal sky emission is considerable and rapidly changing, flatfields were constructed for each row by median averaging all of the frames within each row.

Data Reductions : Photometry

The data frames were reduced first by the replacement of data in bad pixels with the average value of surrounding pixels and were then flat-fielded using an averaged sky frame. Because this field is severely crowded, the repeatability of aperture photometry and point spread function fitting (PSF) methods were tested. Photometry was extracted for 40 stars in a region overlapped by two data frames with an aperture diameter ~ FWHM of the PSF and it was found that the dispersion of the magnitudes using PSF fitting was approximately half that for aperture photometry. Consequently, the package DAOPHOT (Stetson, 1987) was used to fit PSFs to measure the stellar fluxes.

The detection threshold for the images was determined from the standard error per pixel that includes contributions from the read noise of the detector, the Poisson noise from the thermal sky background, and the variations of the intrinsic stellar background caused by the unresolved stars in the Galactic Center (see Appendix 1 for a discussion of the likely distribution of these stars along the line-of-sight). Empirical standard error estimates were derived by calculating the dispersion of 50 to 250 pixel values in regions where no resolved sources were apparent. The contributions due to the read noise were negligible while the thermal background accounted for only about 10% of the total, thus the 3-σ detection threshold of the images was dominated by the confusion of faint stellar sources. For the K-maps the 3-σ detection limit was between K = 12 to 12.5, while for the H map the 3-σ detection limit was H = 15. These magnitude limits imply a foreground extinction limit of $A_V < 43$ mag for stars with an intrinsic H-K = 0.3, the observed average in Baade's Window (Frogel and Whitford 1987).

Candidate objects were located by convolving each image with a Gaussian PSF with the

observed FWHM and preliminary magnitudes were derived using aperture photometry. The PSF was constructed empirically using stars selected from a pool of the 20 brightest sources on an image. Groups of stars with overlapping PSFs were iteratively reduced to find the best fitting profile using the DAOPHOT routines GROUP and NSTAR. Because of the severe crowding by faint sources, some of the data frames had groups exceeding 100 stars. These frames had to be regrouped with a smaller fitting radius of the Gaussian core of the PSF until the group sizes were reduced below the maximum of 60 stars per group allowed by DAOPHOT.

The surface density of sources at L was surprisingly lower relative to K, even with 60s exposures because the high thermal emission still dominated the background. The density of sources was sufficiently low that stellar magnitudes could be measured using aperture photometry. This was also advantageous because poor tracking during some of the exposures caused the images to have very elongated stellar profiles. The IRAF package APPHOT was used instead of DAOPHOT. In the central 20" the source crowding was considerable so smaller aperture sizes were used with corrections applied from photometry on stars in less crowded areas. These problematic stars are not included in the data presented in this analysis, however.

Data Reductions : Database Construction

A total of 155 K data frames was processed, which yielded 11,777 stellar measurements. A typical star was likely to have been observed two to three times at each of the three epochs and at each wavelength. Thus a procedure was required to reduce the multiplicity of measurements. An initial database was generated for each epoch from the results of NSTAR. Each record in this database contained a listing of the original data frame, epoch, magnitude, pixel coordinates, and so forth. Each star was measured from two to six times per epoch

because of frame overlapping. All of the frames were placed on a standard coordinate system by measuring relative offsets from brighter stars. The multiple measurements of each star were then combined to produce a final database for each epoch.

The algorithm to produce the compiled databases went through several stages of development to accommodate computational limitations. An initial approach centered on frame-to-frame comparisons that treated each epoch on an equal footing. Records were sorted by data frame and each data frame was was given an index number specifying the epoch and relative position within the map. For instance, the frame labelled "236" was taken during the second epoch, September 1987, and was located in the third column, sixth row. To find matches for stars in frame 236, a search would be made in frames *j*25, *j*26, *j*27, *j*35, *j*36, *j*37, *j*45, *j*46, *j*47 for $j = 1, 2, 3$ with the provision that frame 236 not be searched against itself. For an average number density of stars per frame, ρ, the time for each frame-to-frame search is proportional to ρ^2. Restricting the search to particular data frames is a significant improvement over a direct star-to-star search throughout the entire database but with the computer facilities available this was still too unwieldy. It was also more difficult to implement uniqueness criteria that would prevent unwanted duplicate records in the resultant database.

The next phase of development incorporated two important changes. It was realized that significant residual positional errors occurred when comparing maps between two epochs and this caused a significant number of unmatched records. So a fiducial epoch in K was selected (May 1988) in which the frame offsets were measured with great care. Subsequent data frames from other epochs were then to be compared directly to the May 1988 K map to determine their global position rather than to other adjacent frames within the same epoch. The global offsets were then applied to the stars within that frame. This greatly improved the record matching between the epochs without compromising significantly the positional accuracy of the other maps. Also because the crowding in this field was so great it was deemed best not to combine the epochs into a final database until each epoch had its own compiled database.

This again prevented unwanted record duplications.

The problem of time consuming frame-to-frame matching was solved by extending the very same method to smaller length scales. The map was divided up into square cells of uniform size and each cell was given a character string label 8 letters in length such that the cell centered on the coordinate system origin was designated " 0 0". The 80^{th} cell along the x-axis and -167^{th} cell along the y-axis would then be designated " 80-167". Each star was then labelled by the character string label appropriate for the cell in which it resided. The cell size is chosen to be slightly larger than the expected positional errors but smaller than the average separation between stars. This procedure is more advantageous because adjacent cells can be addressed easily by computation and are relatively close within the database when it is sorted by cell position. Since it is still possible for a star to reside near the cell edge, it is still necessary for adjacent cells to be searched. However, the average number of stars per cell is on the order of unity and this results in a substantial increase in computational speed. Also there was little computational time spent addressing potentially matching stars because discrete character string cell labels eliminate the need to calculate positional tests of the form $\delta r > [(x_1 - x_2)^2 + (y_1 - y_2)^2]$ in most cases.

When searching adjacent cells for a given test star, two important criteria apply to reject duplications and spurious matches. If two stars happen to lie within the same cell that is tested, then the star to be matched is the one with the minimum spatial separation. Secondly, stars which are within the same data frame as the test star must be rejected since this will produce a spurious match. Using the cell algorithm, stars in each epoch were matched by searching for positional coincidences with cell sizes of 0.75". The final list of K detections was then collated with the database containing H magnitudes, resulting in a final database containing magnitudes and colors of over 1400 stars. The photometric errors estimated from the repeated measurements of stars were 0.088, 0.070, and 0.095 mag for May 1987, September 1987, and May 1988 respectively.

After the three K observations were compiled into a single list, an additional correction to the photometry was applied because of systematic magnitude differences between epochs. The systematic errors were spatially variable across the map, often correlated with particular data frames or columns of data frames. The fact that the standard stars were observed at slightly different air masses than the Galactic Center, as well as extinction variations, both in time and airmass, contributed to these errors. (The procedure is discussed more in detail in chapter 4 where it is most relevant to the search for variable stars.) All data were normalized to the May, 1988 map because this epoch included the H measurements. The final H-K colors for a star were derived from the H data and only the K data from May, 1988. In 15 instances there was no K detection in May 1988 to match with the H measurement because the H map is slightly deeper than the K map relative to typical obscured stellar colors. In these cases the H-K color was computed from the May 1988 H magnitude and the average K magnitude from the other epochs in May 1987 and September 1987.

Finally, it was necessary to extract from this compiled database a sample that was complete for each epoch. The 3-σ detection limits listed above were used by DAOPHOT to locate sources on the data frames, but the data are not complete to those limits. At each epoch, a large percentage of all sources should have been detected at least twice because of the overlapping of the data frames. Figure 2-1 shows the actual fraction of sources detected at least twice for each epoch as a function of K magnitude. The dashed horizontal line on each plot indicates the fraction of the map covered multiple times by the mosaic of frames. To first order, the fraction of the map covered multiple times by image frames is equal to the expected fraction of stars in the database

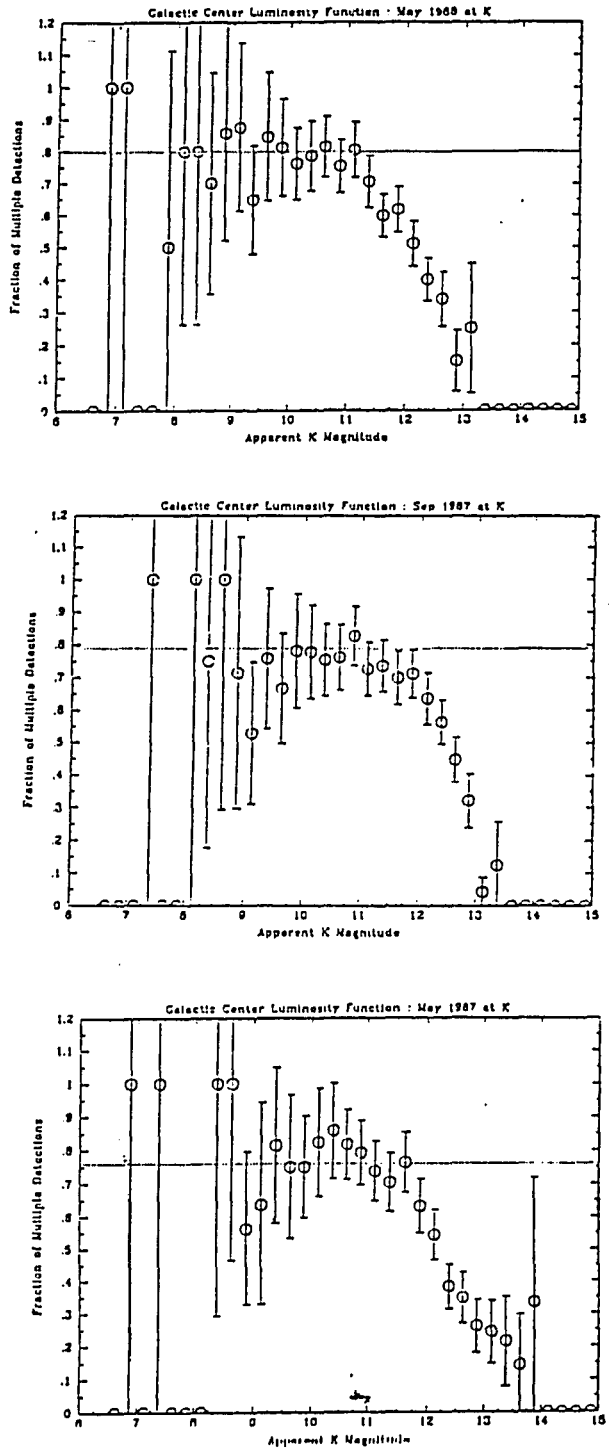

Figure 2-1: Fraction of multiply detected sources at each 2.2μm epoch. The dashed lines indicate the expected fraction of multiple detections based on overlapping of images. Every epoch clearly shows a sharp deviation indicating a magnitude limit in multiple detections. The completeness limits of K = 11.00 and H = 13.00 thus set by the the magnitude limit for multiple detections.

that are detected multiple times, assuming a constant source density in the 5′×5′ survey field. If the FIND routine in DAOPHOT worked perfectly, and all the data parameters were set correctly, one would expect a higher fraction of multiple detections down to the 3-σ detection limit. Based on these diagrams, completeness limits of K=11.50 for May, 1987, K=11.25 for September, 1987, K=11.00 and H=13.0 for May, 1988, were determined by the magnitude where the fraction of multiple detections begins to deviate from the appropriate fraction for each map. The database discussed here is composed of all the sources brighter than these limits and thus preserves much of the measurement redundancy in each epoch. A positional map showing the region surveyed is shown in figure 2-2.

An additional database was constructed for the L photometry that produced approximately 1300 stellar magnitude and position measurements. Global coordinates within the 5′×5′ field were again measured for each L image to a precision of ± 0.5″ against the stellar positions of the previous HK database to minimize residual positional errors between wavelengths. The L frame coordinates were then applied to the individual stars to agree with the global K system. The multiple measurements of each star were then matched using the "cell" procedure using a cell size of 0.75″ and matched records were collated into a final L database. The estimated completeness limit was empirically determined in the same way as the HK database. The fractional distribution of multiple detections vs. m_L shows a strong roll over in the data at $m_L > 8.5$, so only those stars brighter than this limit were compiled with the H and K data. The L magnitudes for sources in regions of low density have an internal error of ±0.25 mag, based on the repeatability of the measurements from frame overlapping. The final L database was then combined with the previous HK database, again by the "cell" searching technique, to produce a three color sample of 278 stars. The apparent K luminosity function from the HK database as well as the K stars detected at L in the HKL database is shown in figure 2-3.

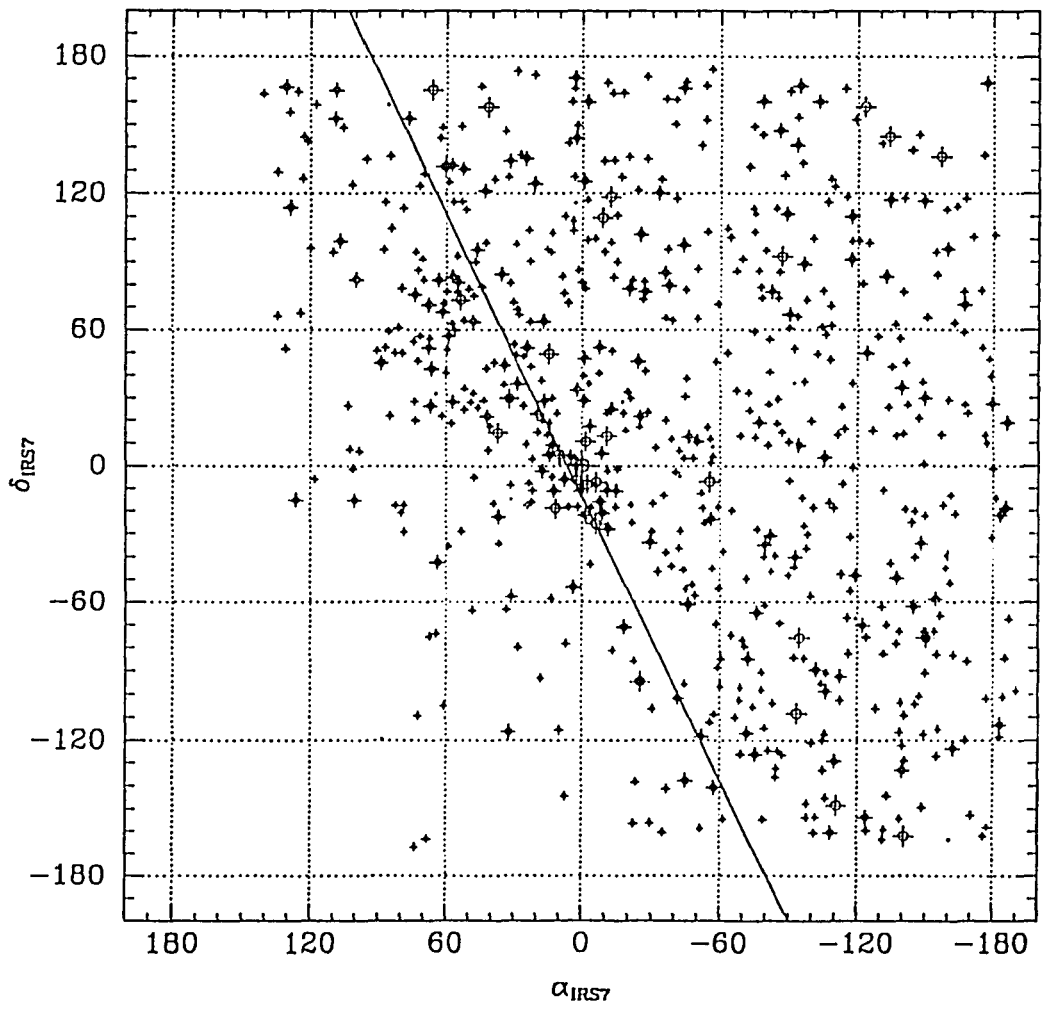

Figure 2-2: A positional map of the stars used in the *HK* database complete to $m_K = 11.0$ and $(H\text{-}K)_0 > 1.5$. The bordered outline shows the extent of the overlapping data frames taken at H and K.

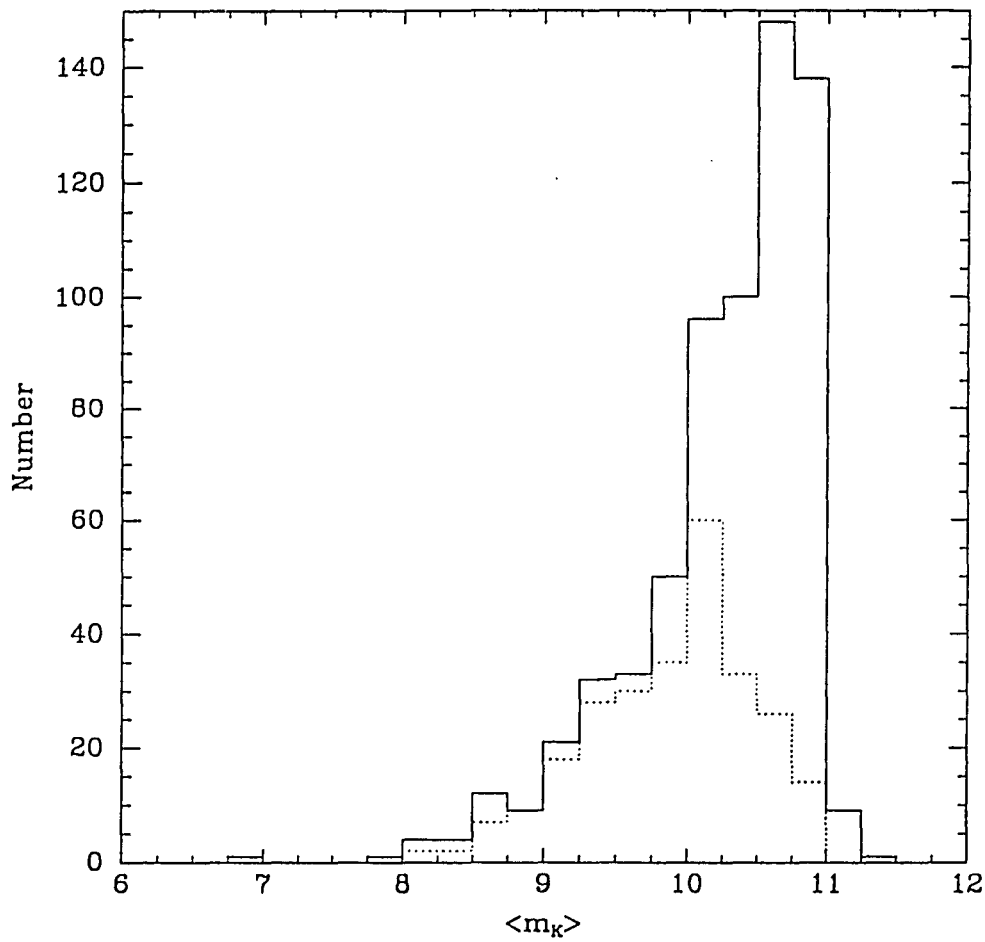

Figure 2-3 : The apparent K magnitude luminosity function showing the complete sample of H and K stars. The dashed histogram is the subsample comprising the HKL database.

Summary

The final products of the observations were the sample of 688 H and K stars complete to m_K = 11.0 and another sample of 278 H,K, and L stars complete to L = 8.5. Chapter 3 will examine the H and K sample in detail and show that the Galactic Center stellar population is composed of high luminosity stars that are substantially different from stars in the nearby bulge. Chapter 4 undertakes a search for variability using both the HK and HKL databases and shows that luminous late-type AGB stars reside in the central few parsecs of the Galaxy.

CHAPTER 3 :

HIGH LUMINOSITY LATE-TYPE STARS IN THE GALACTIC CENTER STELLAR POPULATION

The basic properties of the Galactic Center stellar population derived from the H(1.6μm) and K(2.2μm) photometry (Appendix 2) will be examined in this chapter by a careful analysis of the foreground extinction, expected intrinsic colors, and bolometric corrections that are needed to compare this population with stars in Baade's Window. A cursory examination of the images reveals an extraordinarily high star density of around 80 stars arcmin^{-2} which was noted in Rieke (1987). Her older data were taken with a 32x32 array, with poorer performance, and with barely adequate integration time at H. In spite of these shortcomings, these older data can still be used to compare the newer data of higher quality with the extinction properties derived from the old data being close to the values derived from the newer data.

Foreground Extinction

The interstellar extinction law has been measured toward the Galactic Center (Rieke and Lebofsky 1985; Rieke, Rieke, and Paul 1989) from 1-13 μm observations which showed no evidence for any significant variations between the A5 star oSco and several stars in the Galactic Center. A known constant extinction law then allows an accurate dereddening of the stars in our images. Figure 3-1 shows the distribution of observed H-K colors for the sources in the original complete sample. Because only one color is available it is not possible to assign uniquely the

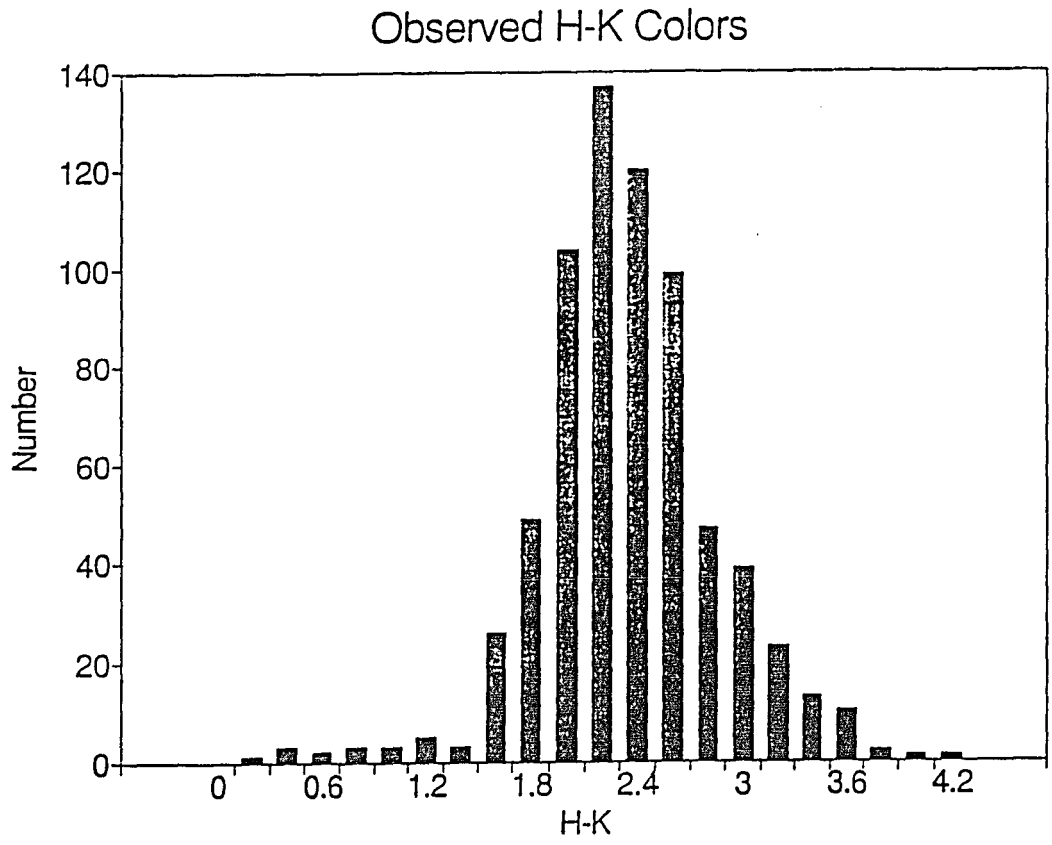

Figure 3-1 : The observed H-K color distribution in the final database before removal of suspected foreground stars.

extinction and intrinsic color for each star. However, several pieces of evidence can be used as a guide to estimate the averages of these quantities. First, there is spectroscopy that shows strong 2.3μm CO absorption for approximately 100 of these stars (Rieke and Rieke unpublished data; Rieke 1988; Rieke and Rieke 1988). Other studies of both resolved sources and unresolved stellar emission confirm that the CO feature is common in this population (McGinn et al. 1989, Sellgren at al. 1990; see also chapter 5). This feature is most pronounced in M giants and supergiants (Klienmann and Hall 1988). Therefore it can be assumed stars are predominately late-type stars and have relatively narrow range of intrinsic H-K color (the H-K color ranges from 0.0 to 0.5 from spectral type A0 to M9). Secondly, an empirical estimate of the average H-K color can be derived from the closest comparison population in Baade's Window (Frogel and Whitford 1987) where the average intrinsic H-K $\approx$ 0.3 and there is a relatively narrow spread in the intrinsic H-K colors. The extinction can be separated from the intrinsic color to acceptable accuracy given the limited data. For the complete sample of Galactic Center stars, the average observed H-K of 2.24 is in good agreement with an extinction of about 30 magnitudes (Becklin and Neugebauer 1968) for an assumed average H-K color of 0.3 mag.

The relative number of stars with H-K redder than 0.5 in at late-type population is small so the redward spread in Figure 2 is most easily attributed to some stars having higher than average extinction. The relative lack of stars on the southeast side of the Galactic Center as compared to the northwest side seen in large scale images supports the suggestion of some regions having higher extinction than the average (Catchpole, Glass, and Whitelock 1989).

Although no independent distance estimates exist for this group of stars, the amount of reddening corresponds somewhat to the relative locations of these stars. Those stars with the least amount of intervening material are the bluest and therefore the nearest and so are likely to be foreground stars. The foreground star reddening limit was chosen to be an observed $(H-K)_{obs} < 1.5$. There were 29 such stars, comparable to the expected number of foreground stars observed along this line-of-sight from a calculation that assumes a solar

neighborhood stellar luminosity function and a relatively uniform distribution of foreground dust. Appendix 1 describes this calculation in detail using a simple model of the Galactic stellar disk and dust distributions as well as an estimate of the line-of-sight dispersion for stars in the central bulge. The disk calculations shows that about 20-35 stars with H-K <= 1.5 would be detected, depending largely on the value of the disk scale length. The values used in the calculation ranged from 3 to 5 kpc (de Vaucouleurs and Pence 1978). The agreement between this simple model and the observed number of blue stars supports the identification of these stars as foreground objects. Sources with H-K significantly less than 1.5 may have a sufficiently low level of extinction that they may be observable at visible wavelengths and ten of the 29 foreground stars have been found on the Palomar red plate. Positions with accuracies of 0.5" in each coordinate were determined for these stars using the NOAO Grant machine. Table A2-2 in appendix 2 lists the optical and infrared positions and photometry of these stars. The disk calculation also predicts that 3 to 9 foreground stars would have H-K > 1.5. This amount of contamination is at the 1% level and is certainly acceptable considering the accuracy of the data and cannot affect the conclusions presented later in this chapter. Thus both on the basis of the Galactic structure calculation and optical identifications, sources with $(H-K)_{obs} < 1.5$ were removed from the complete sample.

The remaining group of 659 stars lie essentially at the Galactic Center. The distance to the Galactic Center is here taken to be 6.9 kpc ($(m-M)_0 = 14.2$; see chapter 1) so that direct comparisons can be made with studies of Baade's Window by Frogel and Whitford (1987). This will be regarded as the distance to the majority of the stars in our sample. The Galactic bulge density calculation described in Appendix 1 shows that 80% of these stars lie within 20pc of the Galactic Center; 90% are within 50pc. The intrinsic spatial depth of this group of stars will produce a photometric dispersion on the order of ~0.006 mag is much smaller than the typical photometric error which is on the order of 0.1 mag.

The reddest stars in the sample may lie beyond the Galactic Center, suffer greater

extinction from intervening dust clouds of greater than average density, or have circumstellar dust shells. Background contaminants beyond the Galactic Center would be much less numerous than foreground contaminants. Given that $A_V \approx 30$ mag has been confirmed for many stars with spectroscopic data, and that the underlying unresolved stellar distribution has a brightness of around 13th magnitude per square arc sec, the probability of detecting many background sources at a limit of K=11 is low. Their inferred luminosities would be underestimated and therefore would not change the conclusions of this work. Therefore, with a very high level of confidence, we may treat this sample of stars as representative of the brightest late-type stars *at* the Galactic Center.

In the final sample of stars, excised of foreground contaminants, the average extinction implied by the observed H-K color distribution is $A_V = 31.8$ mag, for an intrinsic <H-K> = 0.3. It would be possible to estimate the individual extinction for every star with the observed H-K color and carefully chosen intrinsic color. But the H-K colors in this sample are not accurate enough ($\approx \pm 0.15$ mag) for this procedure to be implemented effectively. Instead, a uniform extinction estimate based on the above average value was applied to the data to avoid a spurious bright tail in the derived luminosity function. Significant local variations in the extinction exist at the level of $\pm$ 6 mag in A_V from foreground molecular clouds (Glass, Catchpole, and Whitelock 1987) as well as individual clouds in the molecular ring (Genzel 1989) but the resulting *average* intrinsic H-K color is quite sensitive to the choice of the extinction correction. Decreasing the assumed average extinction by 5 magnitudes will shift the average intrinsic H-K to 0.6 which would be implausibly large. Increasing the average extinction by 5 magnitudes will shift the intrinsic H-K to -0.02 and imply a very hot stellar population, but this is ruled out on spectroscopic grounds by the large number of stars with strong CO absorption. So the dispersion within a given luminosity bin may be increased but there should not be a bias in the average luminosity levels from spuriously bright stars.

Bolometric Corrections

A bolometric luminosity function is the most useful for direct comparisons with other populations. Thus an appropriate estimate of the bolometric correction must be made to apply to the dereddened K magnitudes. In general these corrections would be derived from spectral types or the J-H and H-K colors of each star. Since our data are limited to H and K information, the bolometric corrections were estimated from the expected values for late-type stars. Figure 3-2 shows the K bolometric correction as a function of H-K for several different samples of late-type stars. The bolometric correction depends on metallicity and luminosity class, as evidenced by the differences seen between the correction for SMC supergiants, LMC supergiants, Milky Way supergiants (Elias et al. 1985), and Baade's Window giants and long period variables (Frogel and Whitford 1987).

Currently, there are no metallicity determinations for the stars at the Galactic Center. The K giants in Baade's Window, which again are the closest comparison population, appear to be super metal rich (SMR) (Rich 1988) as is the case for the M stars (Terndrup et al. 1991). Blanco (1988) has observed a steep gradient in the relative numbers of early- and late-type M giants with decreasing distance from the center. This was interpreted as evidence for a steep metallicity gradient that drives the observed spectral types to cooler temperatures due to line blanketing effects. Some indirect evidence on the metallicity of the stars at the center (Lester *et al.* 1981) comes from the argon emission lines of ionized gas in the central 14″×28″ which shows an abundance 2-3 times solar. Solar abundances at the center cannot be ruled out, and although SMR abundances were not explicitly examined, the Lester *et al.* (1981) data appear to rule out abundances as high as 10 times solar for the gas. These results, as well as the metallicity gradient in the bulge, suggest stars in the Galactic Center are likely to have higher than solar metallicities but less than 10 times solar.

Since Baade's Window has the most metal rich population with known bolometric

corrections, these are the most suitable to apply to the Galactic Center. A uniform bolometric correction K_{BC} of 3 magnitudes was applied to the stars in the complete sample, corresponding to an intrinsic H-K color of 0.3. From the trends in figure 3-2, if the metallicity is higher, K_{BC} should be larger. If the stars have higher luminosities than giants, K_{BC} should be smaller. Since these two effects change K_{BC} in opposite directions, the choice of K_{BC} = 3.0 for the Galactic Center population appears justified.

Discussion

The result of the above analysis is the derived luminosity function shown in figure 3-3 as well as the luminosity function for Baade's Window (Frogel and Whitford 1987). The assumptions used in converting from K to bolometric magnitudes are a distance modulus of 14.2 (6.9 kpc; see chapter 1) in agreement with the value of Frogel and Whitford (1987), a uniform foreground extinction of A_V = 31.8, and a uniform bolometric correction of 3.0. The most prominent result of Figure 3-3 is the large number of high luminosity Galactic Center stars significantly brighter than the luminosity cutoff in Baade's Window.

The luminosity function for Baade's Window in figure 3-3 has been normalized relative to the Galactic Center following the same procedure as used in Rieke (1988). This normalization is based on the relative surface brightness at 2.4μm of Baade's Window and the center

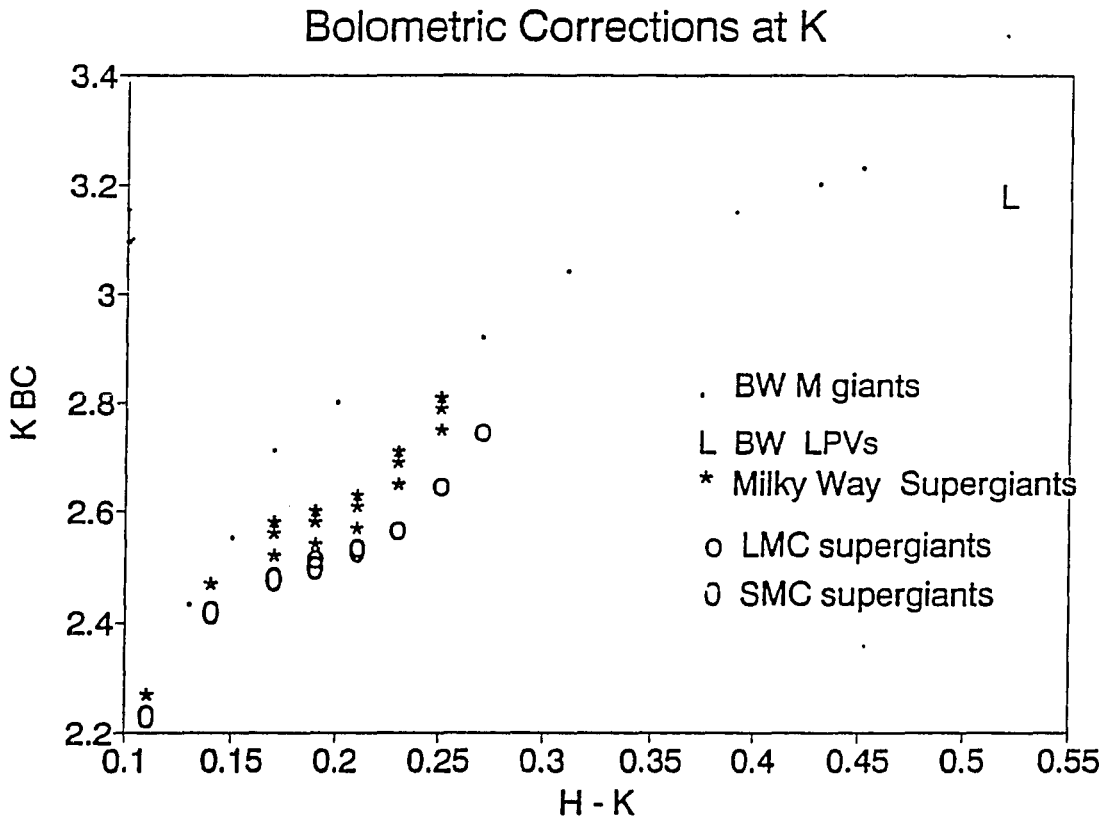

Figure 3-2: Bolometric corrections at K(2.2μm) as a function of H-K color for different stellar populations. The Baade's Window corrections are from Frogel and Whitford (1987) and the others are from Elias et al. 1985.

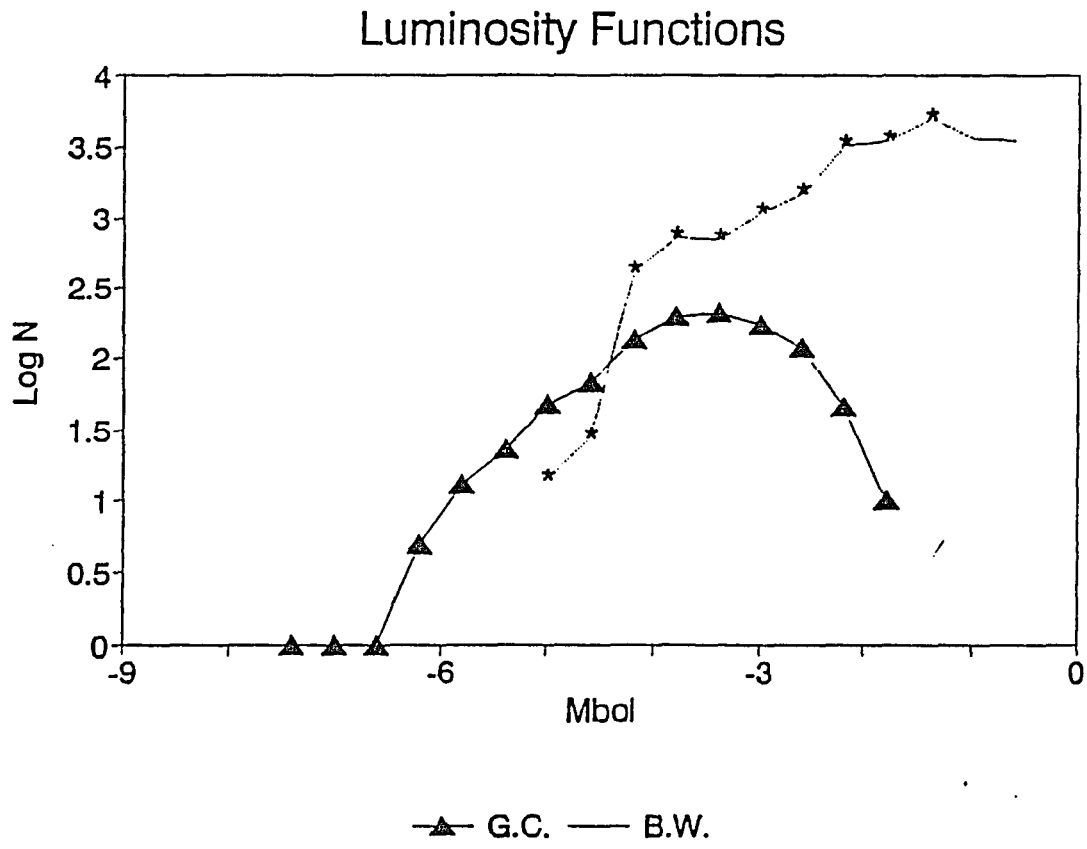

Figure 3-3: The luminosity function for the Galactic Center compared to Baade's Window (Frogel and Whitford 1987). The normalization between the two regions is discussed in the text.

(Matsumoto *et al.* 1982). The correction factor from this method is 14; i.e., our survey contains 14 times as many stars as the Frogel and Whitford (1987) survey of Baade's Window. Another method of normalizing the counts is based on normalizing only the actual observed counts in each region at the same luminosity. If the normalization is based on equalizing the number of stars seen at $M_{bol} = -4$, a correction of 5 is found.

The Galactic Center luminosity function appears to have an excess of high luminosity stars in comparison to Baade's Window. The important question to ask is whether the high luminosity stars at the Galactic Center are a distinct population from Baade's Window or are they similar stars but the high density of stars has allowed better sampling of the bright end of the luminosity function. If a normalization factor of 14 is applied to the Baade's Window luminosity function then there will be 9 stars with $M_{bol} \leq -5$. If the factor is 5, then 24 such stars should be found. There is only one star brighter than this limit in Baade's Window (Frogel and Whitford 1987). The luminosity functions for fields at b^{II} ranging from -3° to -12° in Frogel et al. (1990) show a slight trend for the higher latitude (and hence presumably less metal-rich) fields to have luminosity functions extending to brighter magnitudes. The -12° field includes stars as bright as $M_{bol} = -5.8$. Yet, none of these fields has stars as bright as the bright tail at the Galactic Center. So the high luminosity tail at the Galactic Center cannot easily be discounted as a better statistical sample of a generic bulge luminosity function.

It also does not appear likely that the high luminosity tail is an artifact from the analysis of the data. Since the distance modulus to the center was the same as adopted by Frogel and Whitford (1987), this cannot account for the difference between the populations. The effect on the Galactic Center luminosity function for choices of A_V and K_{BC} is shown in Table 3-1. The derived spread in M_{BOL} is shown for a range of intrinsic H-K between 0.1 to 0.5. Changes in the extinction drive M_{BOL} in an opposite direction from the effects of the K_{BC} changes and the maximum change in M_{BOL} which could result from changing these assumptions is only 0.11 magnitudes. This is negligible in comparison to the differences between the Galactic Center and

Baade's Window luminosity functions. Given that JHK colors are driven towards bluer values at higher metellicities (eg. Terndrup et al. 1991), it would seem most likely that the average H-K color for the Galactic Center stars might be less than 0.3 rather than larger than 0.3; the changes to M_{BOL} from this cause would be very small.

TABLE 3-1 : Effect On Derived Bolometric Magnitude From Assumed Color and Extinction

$(H-K)_0$	A_V	ΔBC_K	ΔA_K	ΔM_{BOL}
0.1	34.9	0.75	-0.71	0.04
0.2	33.3	0.20	-0.17	0.03
0.3	31.8	0.00	0.00	0.00
0.4	30.2	-0.15	0.18	0.03
0.5	28.6	-0.25	0.36	0.11

On all accounts the high luminosity tail at the Galactic Center must be regarded as real. It is best explained by a population which is much younger than the typical bulge population in Baade's Window. The supergiants in the central cluster show this is at least partially true. The progenitor mass of IRS 7 is at least 20 $M_\odot$ and so has a maximum age of about 10 million years. But aside from the stars in the inner 1.5' there are no confirmed supergiants from spectroscopic evidence. It could also be that these stars have a variety of ages. Many of the high luminosity stars would then be on asymptotic giant branch (AGB). For this explanation to be correct, the high luminosity stars would have masses of at least 3 $M_\odot$ and an age of no more than about 500 million years. The stars brighter than $M_{BOL} \approx -6$ require at least 5 $M_\odot$ progenitors and ages around 125 million years (Maeder and Meynet 1989). If many of the high luminosity stars are on the AGB, they should be variable. This is the topic of the following chapter. In either case, the Galactic Center stellar population has a younger component than seen in Baade's Window which confirms the earlier suggestions (Lebofsky *et al.* 1982) of recent star formation at the Galactic Center. Whether this younger population represents a form of the

starburst phenomenon seen in other galaxies awaits further work.

High luminosity stars up to 1 magnitude brighter in M_{BOL} than the Baade's Window population have also been discovered using near-infrared JHK photometry in the central bulge of M31 (Davies, Frogel and Terndrup 1992; Rich and Mould 1991) and in M32 (Freedman 1992; Elston and Silva 1992). While Davies *et al.* (1992) contend that the luminous population is due to contamination from the disk of M31, the other workers interpret these populations as luminous AGB stars that have an age less than the Baade's Window population. The Galactic Center population discussed here is yet again another magnitude brighter than the M31 and M32 populations, indicating an even younger age. While the *known* spatial extent of the luminous Galactic Center population is much smaller by comparison, future survey work will investigate if these populations have further degrees of similarity.

Conclusions

Two-color near-infrared photometry for a complete sample of 659 stars to an apparent K magnitude of 11.0 from the central 5′×5′ of the Galactic Center shows that a significant luminous stellar population lies within 6 parsec of the Galactic Center. Self-consistent solutions to the colors of this population lead to an average A_V of 31.8 magnitudes and an intrinsic H-K of 0.3. The luminosity function of the Galactic Center stars contains a substantial number of stars brighter than the brightest stars at M_{bol} = -4.6 seen in Baade's Window. The Galactic Center population includes younger components than are present in the Galactic bulge. The inferred bolometric luminosities of these stars indicate an age of 100-500 million years if they are on the AGB or 10 million years if they are supergiants but from these data alone it is not possible to decide what type of population is predominant.

CHAPTER 4 :

A SEARCH FOR LONG PERIOD VARIABLE STARS AT THE GALACTIC CENTER USING HKL PHOTOMETRY

Background

Near infrared spectra of bright sources within the central parsec of the Galactic Center showed the large concentration of young supergiant stars having an estimated age of 10^7 yr (e.g. Neugebauer *et al.* 1976; Lebofsky *et al.*, 1982; Wollman *et al.*. 1982). Lebofsky *et al.* (1982) suggested these stars were the result of a recent starburst episode in the Galactic Center and could explain the overall energetics of the region in an alternative way to interpretations that invoke a central massive black hole. The data analyzed in chapter 3 showed further evidence of a population that is younger than the AGB stars in Baade's Window from the excess number of high-luminosity stars brighter than the AGB stars in the bulge.

The Galactic Bulge population has been studied extensively in the area known as Baade's Window (Frogel and Whitford 1987) and has an estimated age of 11-14 Gyr (Terndrup 1988). The near-infrared light is dominated by late-type M giant stars on the AGB and a large fraction of the brightest stars are Mira long period variables (LPVs) (Frogel and Whitford, 1987). These stars have been extensively studied using near-infrared techniques and their characteristics are well known. Miras are thought to be a terminal phase of AGB evolution during which the star loses mass at an increasing rate through a wind driven by radial stellar pulsations. The light variations caused by pulsation have a range of periods from 150 to 700 days and amplitudes at K (2.2μm) from 0.1 to 1.0 mag (Feast et al., 1982; Whitelock, Feast and Catchpole 1991). There is also a Period-M_{BOL} relation that is similar in many respects to that of Cepheid variables and is insensitive to metallicity differences as shown by a comparison

between the Galactic bulge and the LMC (Feast and Whitelock 1987). There has been a claim for an period-age relation (e.g. Wood and Bessell 1983) but this has been disputed (e.g. Feast 1986) since the P-L relation between the LMC and the bulge are indistinguishable within the errors. While Miras in the bulge are among the brightest members of that population there are also nonvariables at the top of the AGB which are just as bright (e.g. Frogel and Whitford, 1987; figure 17). In contrast, globular cluster Miras typically exceed the luminosity of all the AGB nonvariables (e.g. Frogel and Elias 1988). In LMC clusters, the brightness of stars at the AGB tip (where LPVs are predominantly found) is a decreasing function of time (Mould and Aaronson 1980). Therefore knowledge of the bolometric magnitudes of the LPVs gives an estimate for the age of an AGB population.

In sharp contrast to an AGB population, a stellar population of predominantly younger, high mass, late-type supergiant stars, will not show the Mira-like variability. High mass supergiants can be variable but the amplitudes are typically 0.1 mag or less at 2.2μm and the luminosity changes are not periodic since they do not have the structural instability to excite the acoustic oscillations that characterize Miras.

This distinction between an older, low-mass population and a younger high-mass population is the basis for the variability experiment presented here. The goal is to determine if either of these two population types can predominantly characterize the high luminosity late-type stars in the central few parsecs of the Galactic Center. This is done using repeated imaging taken during the course of one year to reveal light variations with amplitudes characteristic of Miras. If there are few LPVs above the brightest characteristic luminosity of the bulge luminosity function then the brighter nonvariables are likely to be young supergiants and this would strengthen the starburst hypothesis. If the brightest stars in the luminosity function are predominantly LPVs then this argues for an older population and limits the extent of a recent starburst.

The data used in this experiment were previously introduced in chapter 2. Since these

observations are limited to only three epochs there are no complete light curves. The measurements for variability may also be complicated by the severe crowding. It is desirable to test the reliability of detecting LPVs through light variations and to verify that stars with high amplitude variations can be identified with Miras. The colors derived from the HKL data set, a subset of the complete HK sample, are compared with the properties of Miras in the nearby bulge and Baade's Window.

A possible mimicking of intrinsic variability for a given star at the Galactic Center could perhaps occur because of changes in the foreground extinction from the motions of intervening dust. Given the correlation of foreground extinction with the column density of hydrogen gas (e.g. Spitzer 1978) and the Galactic Center extinction law of Rieke and Lebofsky (1985), then table 4-1 shows the changes in K magnitude and H-K color corresponding to the total fractional changes in the column density of foreground material:

TABLE 4-1 : Variability Effects Due To Changing Extinction

ΔK	Δ(H-K)	ΔN(H)/N(H)
0.1	0.056	0.03
0.2	0.112	0.06
0.3	0.168	0.09
0.4	0.224	0.12
0.5	0.280	0.15

Individual clouds in the molecular ring have sizes on the order of 0.2 pc (6″), rotation speeds of ~110 km s^{-1} and average densities of ~3×10^4 cm^{-3} with corresponding extinctions of $A_V \approx$ 30 mag (Genzel 1989). The *total* fractional column density changes required to show significant effects in the variability analysis discussed below would have to be in excess of 10%. Changes in the fractional column density for a molecular ring cloud would have to be even more extreme, by at least a factor of 2, since the column density of a cloud is comparable to all other foreground material. The timescale for such an effect can be estimated by the time for a clump

to cross in front of a given star: ~2×10^3 yr. The characteristic length scale that could probed by this experiment is approximately 20 a.u. during one year of observations. Thus the gas would have to be significantly clumped or shocked on length scales 5×10^{-4} times smaller than the size of the cloud. It seems unlikely that this would make a significant contribution to the variability of the stars in the HK sample. In any case, a star with time-variable extinction could in principle be identified from a shift parallel to the reddening line which has a slope of 1.78 in the K vs. (H-K) diagram. However, this set of data only has color information from one epoch and would thus not be able to discriminate this effect from intrinsic variability. The extent of its influence on the data will be evaluated by light curves derived from future observations.

Variable Star Data Set

The details of the of H and K database were discussed in chapter 2 but for completeness some of the important parameters are restated here. The photometric errors estimated from the overlapping of single frames were ±0.088, ±0.070, and ±0.095 mag for May 1987, September 1987, and May 1988 respectively. The stars have a positional accuracy of ±0.5". The database is a magnitude and color sample of 659 stars empirically determined to be complete to $m_K = 11$. Estimates of the foreground contamination due to disk stars show only ≈ 10 stars would be in our final sample with an observed H-K > 1.5. Also given the compactness of the Galactic Center stellar density distribution inferred from the 2.2μm surface brightness profile, 90% of the observed stars within our field will lie within 50 pc of the Galactic Center and 60% will lie within 6.4pc (0.5 × 5′ × 6.9pc).

Variability Analysis

To determine the intrinsic variability of these stars, residual systematic errors between

the three epochs of data had to be minimized. Our observations were taken at high air mass ($z > 2.00$) so there are expected to be significant variations in the sky thermal background. Also the data frames were very crowded and the PSF was nearly critically sampled. This resulted in variations of the PSF across the map on the order of arcminute length scales corresponding to the size of each data frame. This in turn reflects the maximum extent of a group of stars reduced in DAOPHOT. In some cases the group size exceeded the maximum allowed for DAOPHOT (60 stars), so the fitting radius of the PSF had to be reduced. To eliminate the systematic errors from the photometry, the average magnitude difference $\langle m_K(i) - m_K(j) \rangle$ between each pair of epochs i and j was calculated for each star within a box of size 20″, 40″, or 60″ such that it contained at least 20 stars. If the stellar magnitudes were free from any systematic errors, it would be expected that the average of the distribution of magnitude residuals would be near zero. The observed raw residual magnitudes between the September 1987, $m_K(2)$, and May 1988, $m_K(3)$, observations are shown in figure 4-1. A noticeable constant offset is present as well as scatter that was most likely introduced from PSF and background variations across the map. The average residual in the immediate vicinity of each star, described above, is shown in figure 4-2. It is clear that systematic errors between epochs are not corrected by a simple constant, but that spatial variations in the systematic errors are present. Visual inspection of the spatial distribution of the average magnitude residual shows correlations with the placement of the data frame columns on the sky. Since the size of the systematic errors is comparable to the size of the amplitude variations to be investigated, they were removed by a simple subtraction. The improvement in the data by subtracting off the local average residual can be seen in figure 4-2. The average residual for each

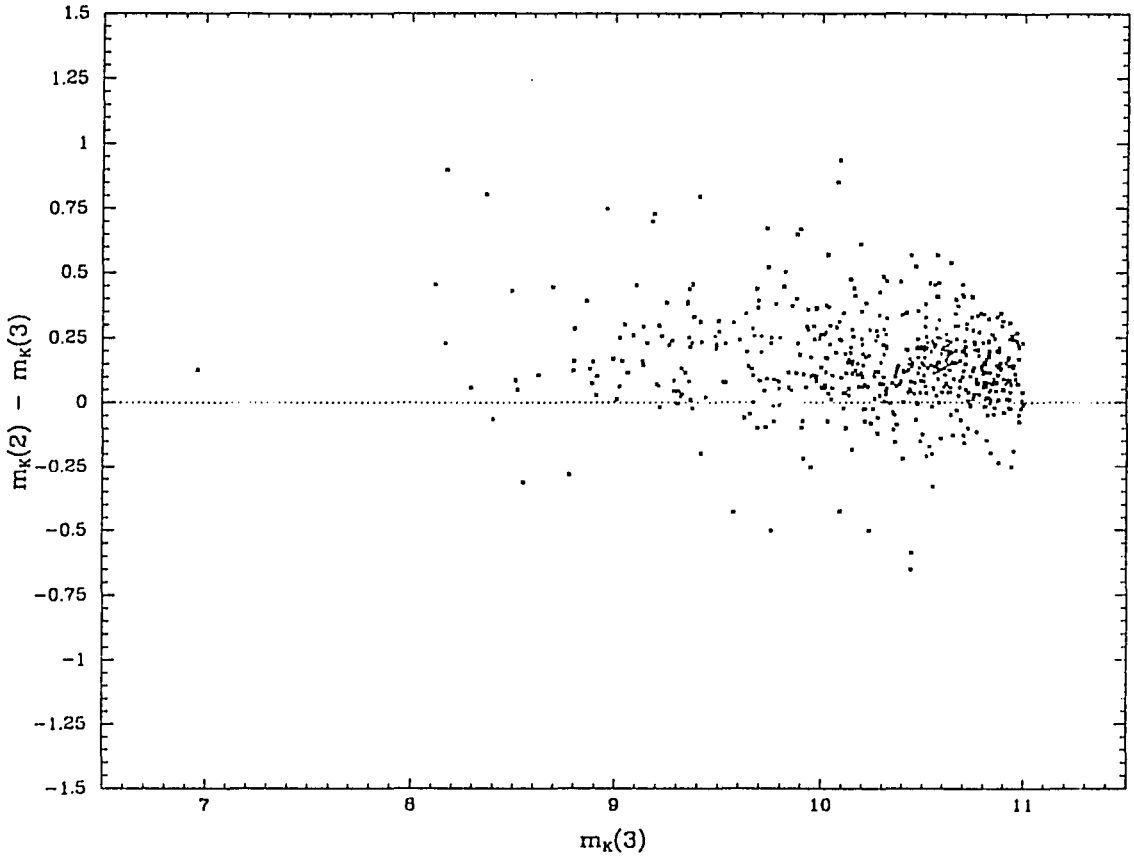

Figure 4-1. - The observed raw magnitude residuals between the September 1987, $m_K(2)$, and May 1988, $m_K(3)$.

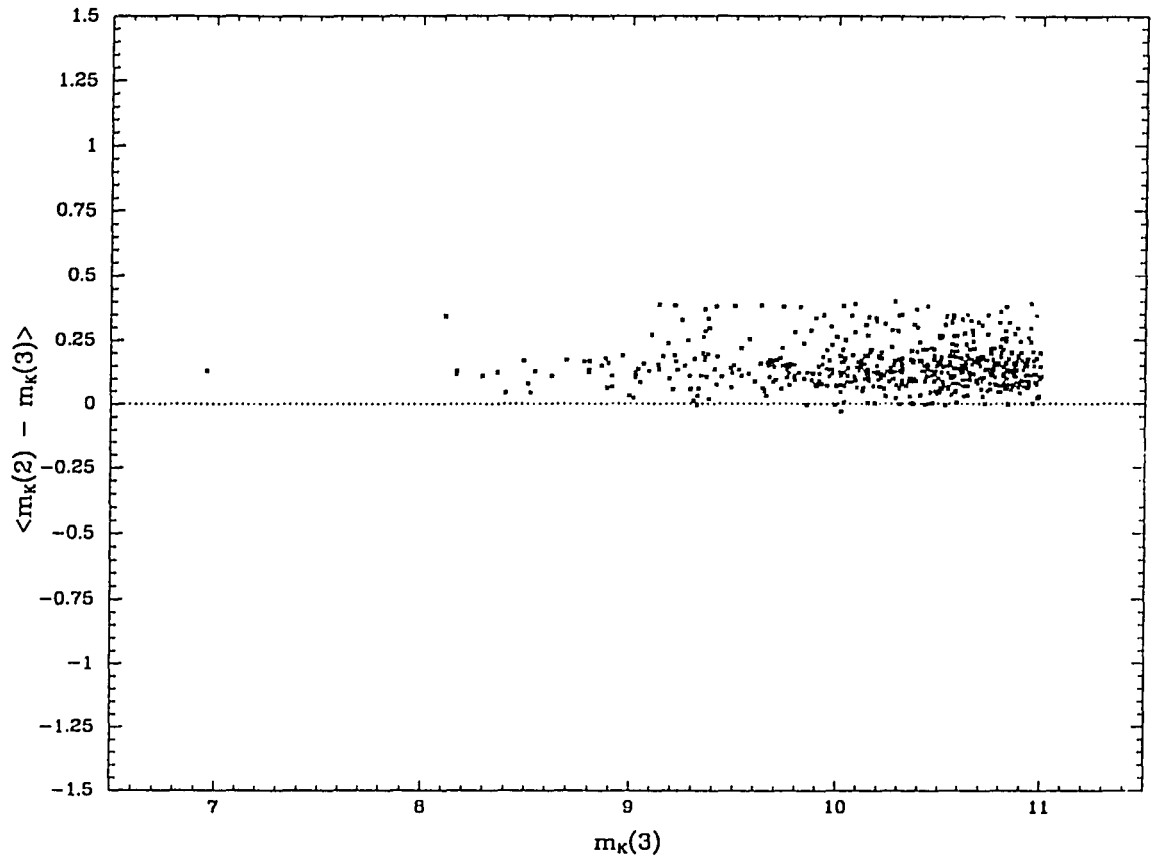

Figure 4-2 - The average magnitude residual $<m_K(2) - m_K(3)>$ between September 1987 and May 1988. The residual included all stars within a box around a given star of size MIN(20″,40′,60″) such that at least 20 stars were included in the average.

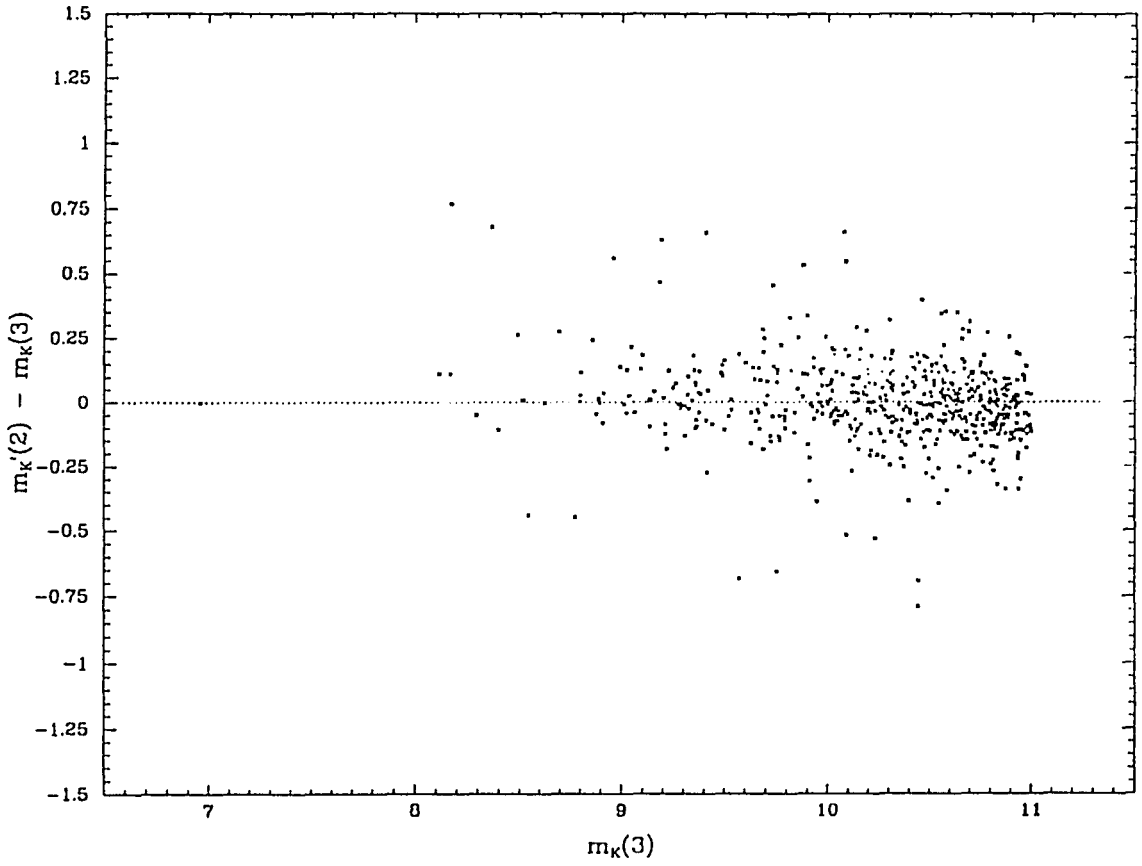

Figure 4-3. - The observed magnitude residual between September 1987 and May 1988 corrected by the average magnitude residual for each star. The average of the residuals is now 0.0 mag and the dispersion is reduced.

star is nearly zero and the dispersion is also reduced.

The data sample the stars at only three epochs and this is inadequate to reliably fit the amplitudes, periods, and phases for potential variable star candidates. Harmon and Gilmore (1988) attempted to estimate statistically the period distribution of Mira stars detected by IRAS using only three epochs of data. Subsequent work on bulge Miras (Whitelock, Feast, and Catchpole 1991) with greatly improved phase sampling showed that the statistical methods overestimated the periods of the Miras and so led to spurious underestimates to their ages. Thus, it was not deemed desirable to proceed with such an analysis on the Galactic Center stellar population. However, the inadequate phase coverage of the data presented here is offset by the ability to detect large amplitude variations that are characteristic of LPVs. The more modest approach applied here uses the amplitude variations to identify potential LPV stars and then evaluates their relative numbers and positions within the bolometric luminosity function.

The RMS magnitude residual between epoch pairs, Δm_K was chosen as the parameter to identify the variable candidates (e.g. Reid, Glass, and Catchpole, 1988). The Δm_K parameter is defined by the following general expression for N discrete observations:

$$\Delta m_K^2 = \frac{1}{N(N-1)} \sum_{i=1}^{N} \sum_{j=1}^{N} (m_K(i) - m_K(j))^2$$

For this particular data set, N = 3 and the expression reduces simply to:

$$\Delta m_K = \sqrt{\frac{1}{3} \left[(m_K(1) - m_K(2))^2 + (m_K(1) - m_K(3))^2 + (m_K(2) - m_K(3))^2 \right]}$$

Confirmation of the intrinsic character of Δm_K is shown in figure 4-4 which plots Δm_K vs. $\langle m_K(3) - m_K(1) \rangle$ and $\langle m_K(3) - m_K(2) \rangle$. The amplitude parameter values are not functions of the

corrections to the magnitude residuals, which implies that the effects of variability, apparent by high values of Δm_K, are intrinsic and not an artifact of corrected systematic errors. Variable candidates were identified by values of Δm_K at least 3σ above the expected average for a nonvariable star with the same photometric errors as the stars in this sample. The expected distribution of Δm_K for nonvariable stars was estimated using a Monte Carlo calculation with 10^7 trials. The average nonvariable residual, $<\Delta m_K>$, was 0.106 ± 0.056 mag; thus the imposed minimum Δm_K for a LPV star to be identified at the 3σ level was 0.274 mag. From this calculation we can also reconstruct the nonvariable distribution of Δm_K values expected from the time sampling intervals of our data set, averaged over phase. This distribution is shown in figure 4-5 along with the observed distribution of Δm_K. The estimated nonvariable distribution is fitted to have the same number of stars that occur in the first six bins of the observed distribution (78% of the total sample). The widths of the two distributions match very closely in this part of the diagram, giving confidence that we have reasonably estimated the photometric errors. It is very important to note that, while most of our stars are indistinguishable from nonvariables, there is an *excess* of stars with high values of Δm_K. In figure 4-6 the RMS residuals Δm_K vs. $m_K(3)$ show that there is no significant trend of LPV amplitude with magnitude so we cannot attribute the effect to incompleteness effects. The 59 stars with $\Delta m_K > 0.274$ will be regarded as LPV candidates.

The efficiency of this method in detecting LPVs was estimated by a further extension of the above Monte Carlo calculation. The LPV light curves were modelled as sinusoidal functions of period and amplitude with randomized phase, ϕ, sampled at times t_i of 0^d, 120^d, and 387^d corresponding to the time intervals of our observations:

$$m_K(i) = A \sin\left[2\pi\left(\frac{t_i}{P}\right) + \phi \right] + e_i$$

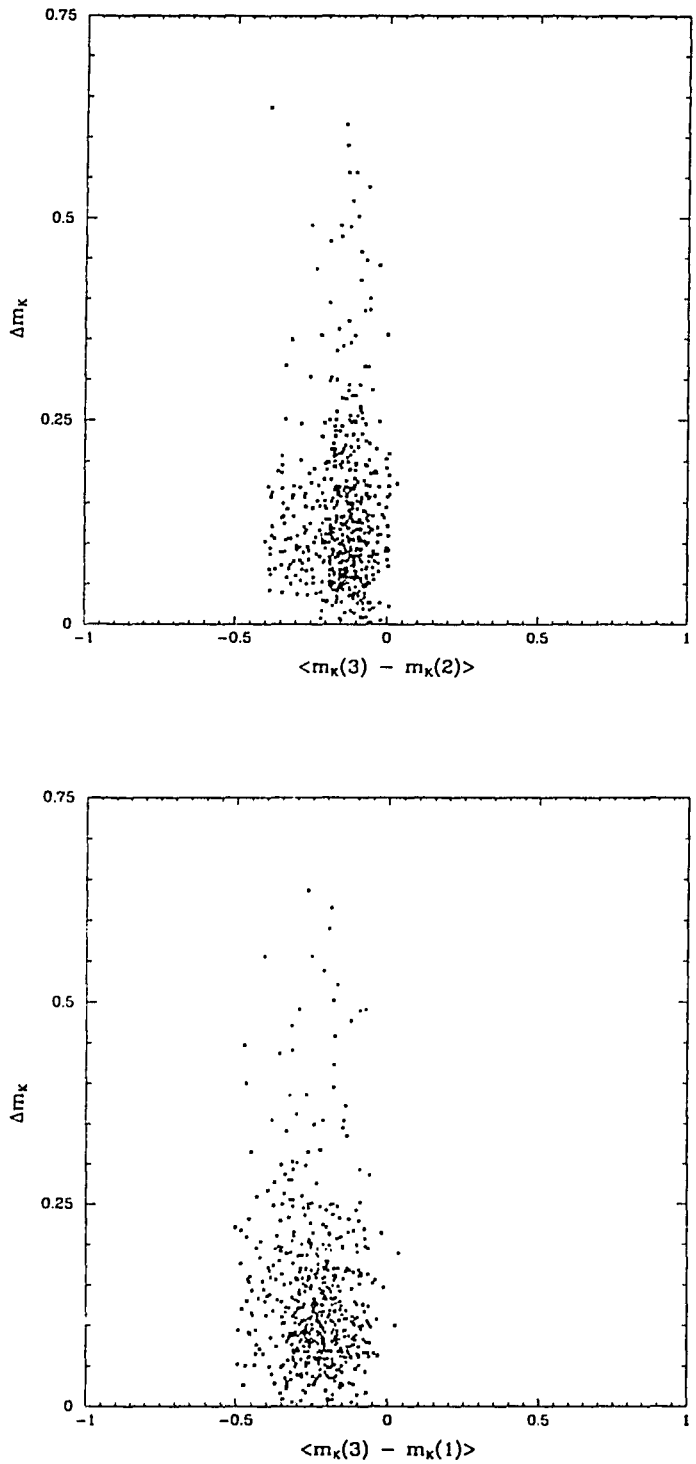

Figure 4-4. - The average magnitude residual correction vs. Δm_K. This shows the derived values of Δm_K are not functions of the corrections for systematic errors.

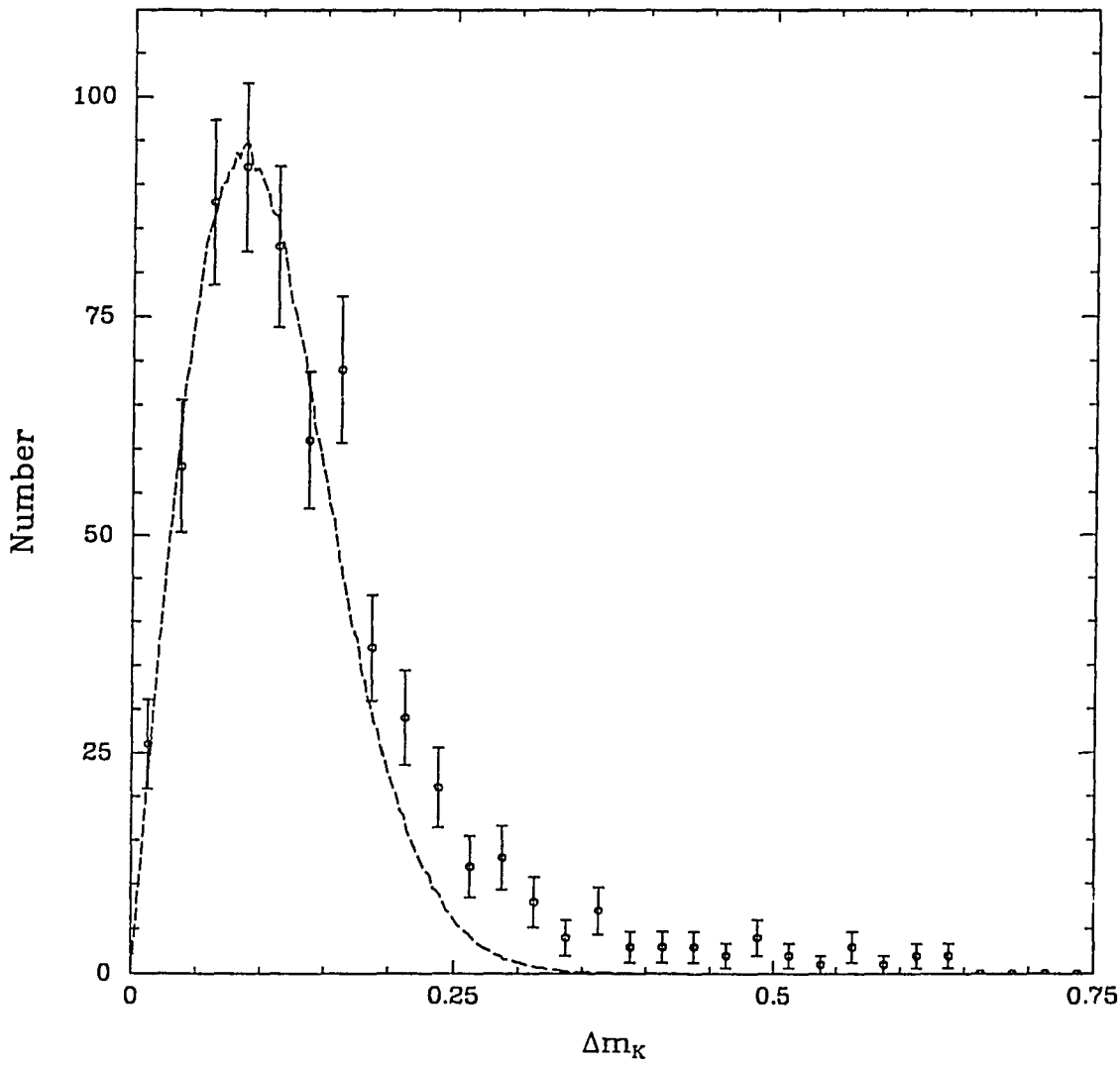

Figure 4-5 - The observed distribution of Δm_K binned to 0.025 mag. The expected Δm_K distribution for nonvariable stars with the same photometric errors calculated by a Monte Carlo simulation is shown by the dashed line. The simulated nonvariable distribution is normalized to have the same number of stars as the observed distribution for $\Delta m_K < 0.15$ mag (78% of our observed sample). The excess number of stars at high values of Δm_K is due to LPVs. Nonvariable stars can be excluded from our LPV sample at the 3σ level for $\Delta m_K > 0.274$.

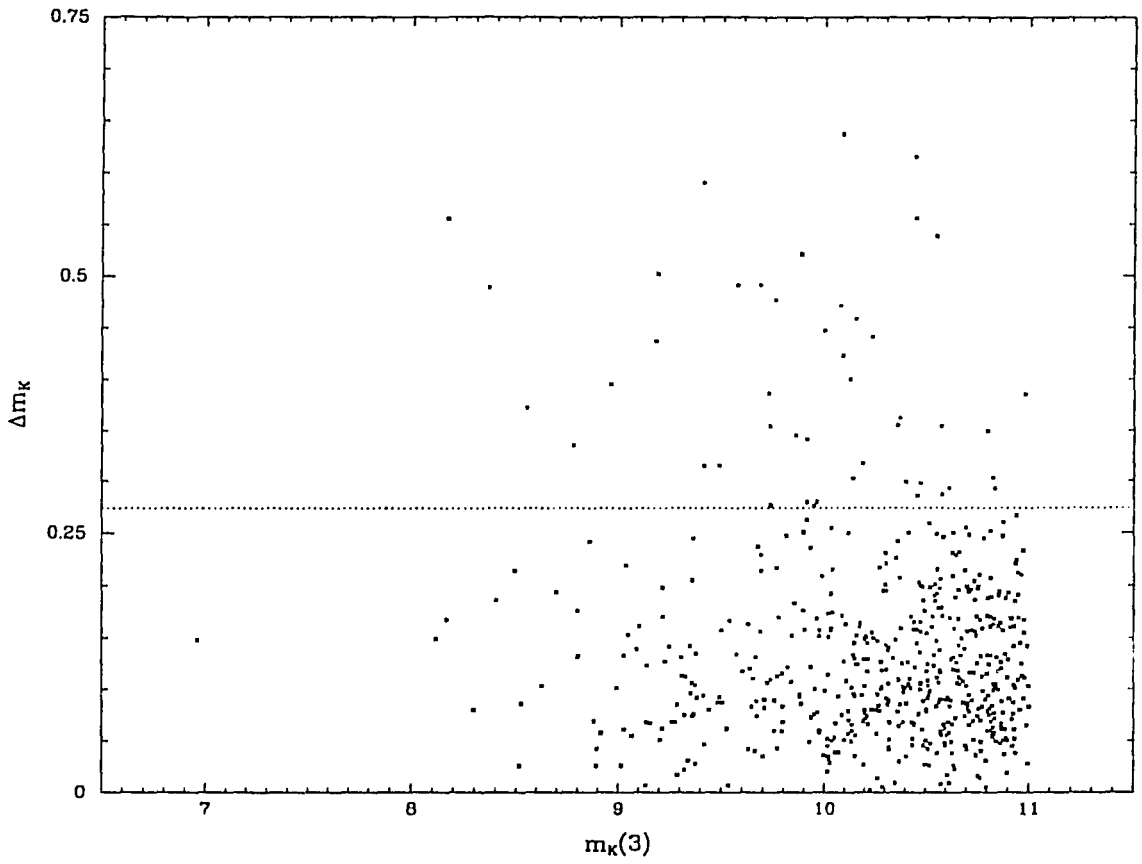

Figure 4-6 - The Δm_K vs. $m_K(3)$ diagram. The stars above the horizontal line at $\Delta m_K = 0.274$ are the variable candidates; stars below the line cannot be distinguished from nonvariables. The diagram also shows there is no strong correlation of LPV amplitude with magnitude.

At each epoch a random photometric error, ε_i, was added that was drawn from a Gaussian distribution with a dispersion corresponding to the photometric error of that epoch. A variety of periods, P, and amplitudes, A, were chosen to encompass the observed characteristics of Galactic Miras with periods ranging from 50 to 800 days and half amplitudes from 0.0 to 0.5 magnitudes (Feast et al., 1982). A large number of trial observations ($\approx 10^6$) with randomized phase was then made at each period and amplitude and the normalized distribution of Δm_K values was calculated. For nearly the whole range of input amplitude and period values, the Δm_K distributions were approximately Gaussian so the fraction of stars with $\Delta m_K > 0.274$ could be easily estimated.

Thus for each period and amplitude, the average magnitude residual, $<\Delta m_K>$, and its dispersion were used as the input parameters of a normalized Gaussian distribution. The resulting total, phase-averaged detection probability, for LPVs with $\Delta m_K > 0.274$ mag, as a function of period and amplitude, is shown in figure 4-7. For periods greater than 160 days there is a general trend of increasing detectability with increasing amplitude and a nearly constant level of detectability at a given amplitude with approximately 10% variations with increasing period. There is rapidly fluctuating sensitivity for periods below 140 days, but in this region of the A-P plane the total detection probability never greatly exceed 50%.

To determine the variable detection efficiency at a given period some form of amplitude distribution must be assumed. From what is known of the Galactic neighborhood Miras (Feast et al., 1982) there is a relatively uniform distribution of amplitudes with $0.2 < A < 1.0$ K mag for the 100 to 300 day periods. The amplitudes at longer periods have large average values because there are few with $A < 0.5$ mag. Figure 4-8 shows the average detection probability at a given period for various assumptions of the amplitude distribution. All assume a uniform distribution of variable amplitudes between $A_{Low} = 0.0, 0.1, 0.2, 0.3$ and $A_{Hi} = 0.5$ mag. The most conservative case would be for a population containing very low amplitude variables ($A_{Low} = 0.0$). Although

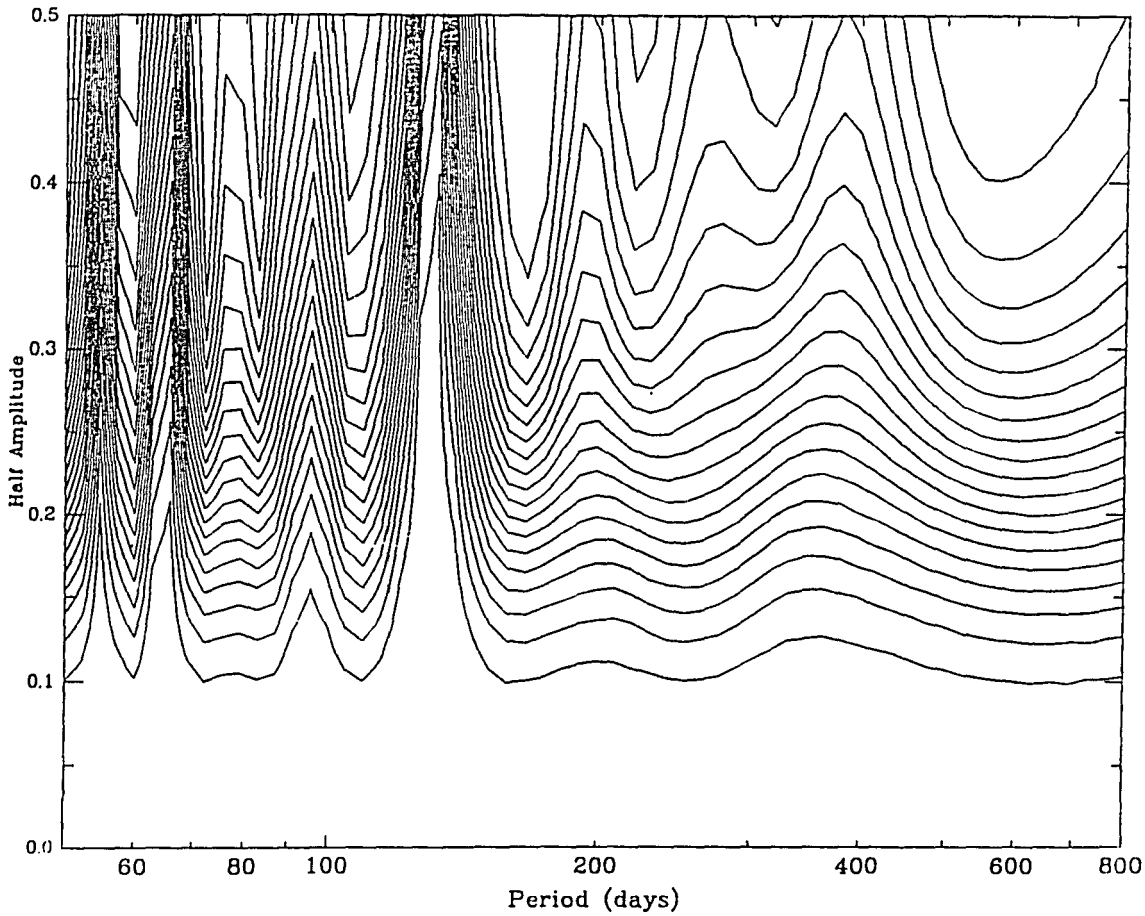

Figure 4-7. - The contours of the total probability that a LPV of a given period and amplitude will have an $\Delta m_K > 0.274$ mag. The lowest contour of 0.05 is at the lower part of the figure while the highest contour of 0.95 is in the upper right. Contour intervals are in steps of 0.05.

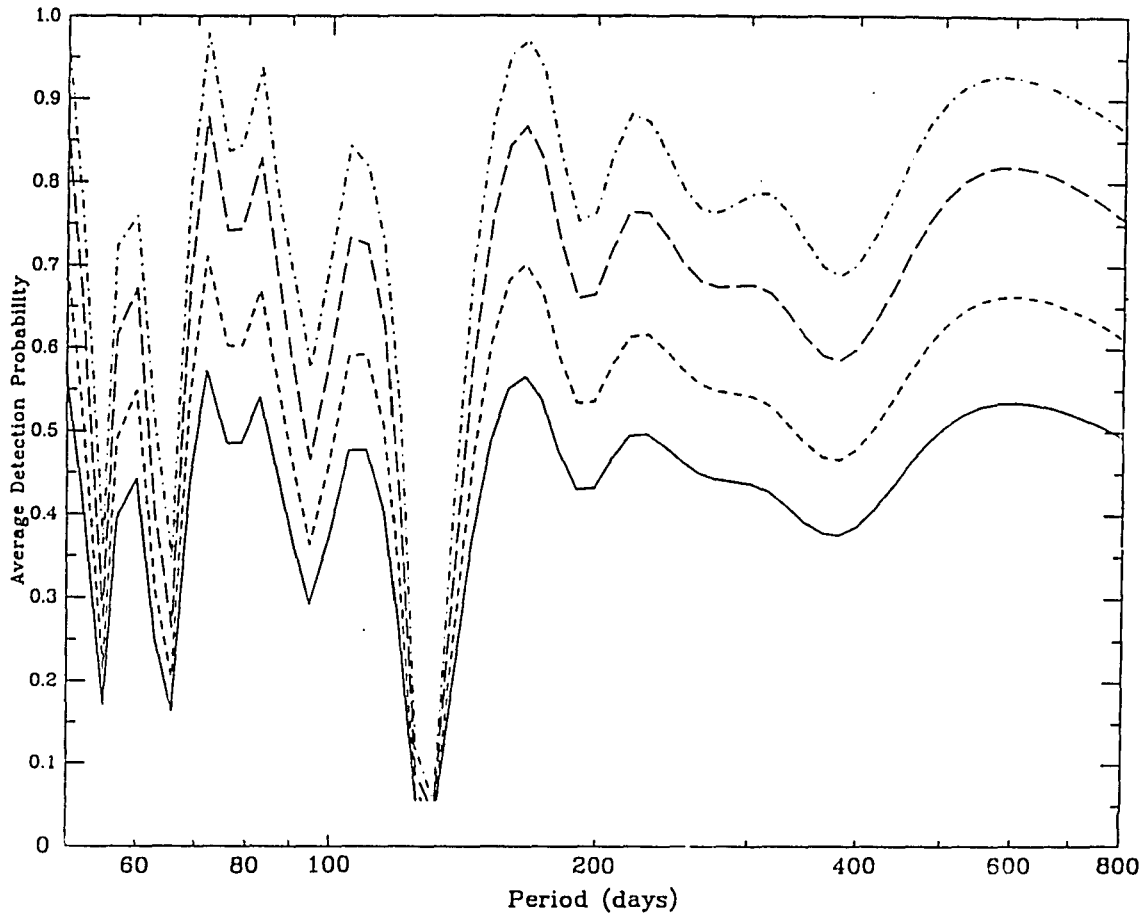

Figure 4-8. - The total amplitude-integrated probability that a variable of a given period will have $\Delta m_K > 0.274$ mag for various amplitude distributions. The solid line assumes amplitudes uniformly distributed between 0.0 and 0.5 mag. Subsequent lines also assume a uniform distribution with the same upper bound but with lower bounds of 0.1, 0.2, and 0.3 mag.

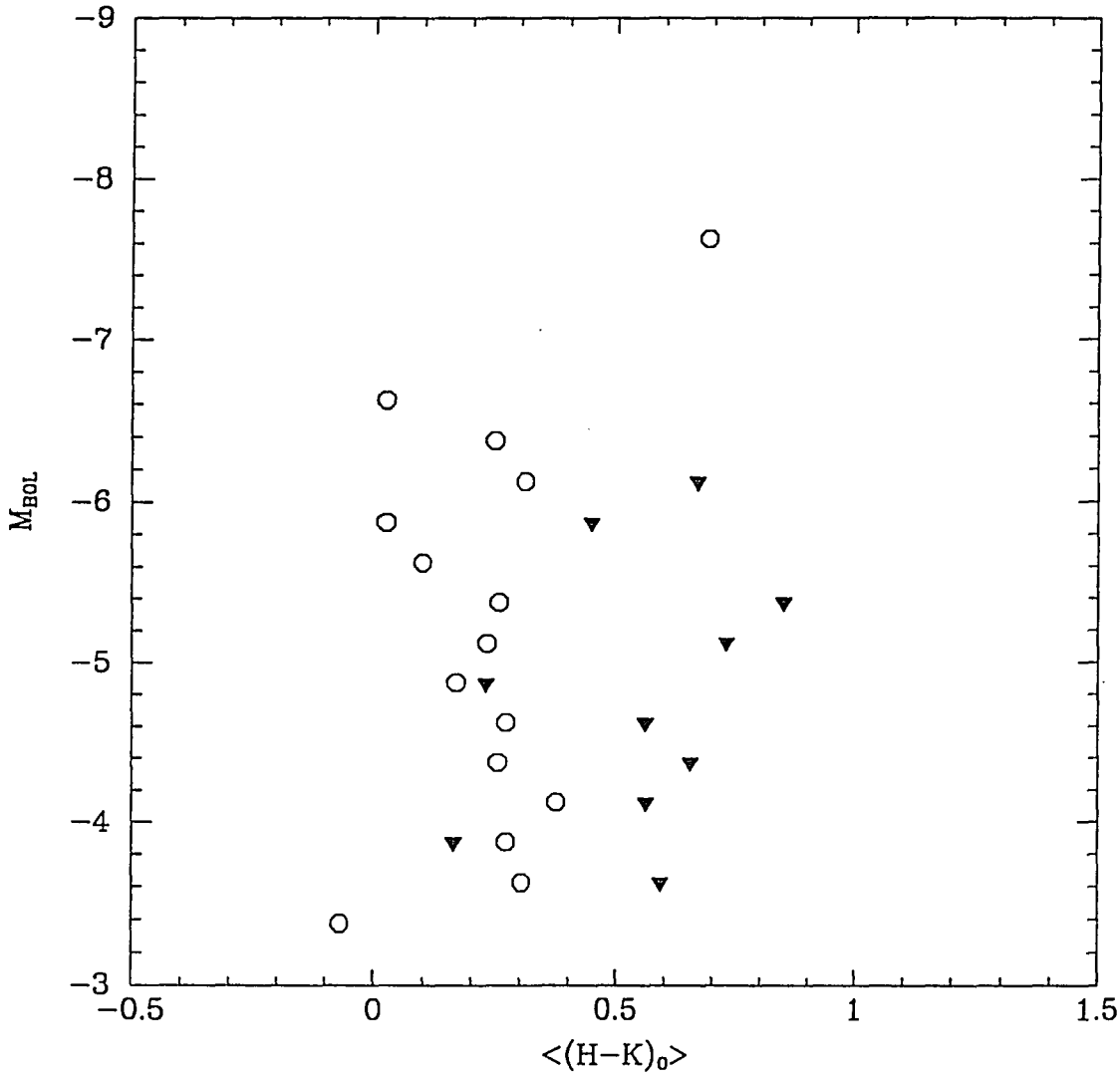

Figure 4-9. - The average M_{BOL} vs. $(H-K)_{obs}$ for LPVs and the total distribution. The bin size is 0.25 mag. The LPVs on average are systematically redder while the non-LPVs tend to be bluer at the bright end relative to fainter non-LPVs and LPV samples respectively.

the resulting observed amplitude distribution would not well represent the intrinsic distribution, the calculations shows there is a 45% chance of detecting variables above 200 days, while there is a slightly lower average value for shorter periods. For those distributions that have preferentially higher amplitudes, the detection efficiency increases considerably. If the amplitude distribution of LPVs at the Galactic Center is similar to Miras in the Solar neighborhood, approximately 75% of the longer period ($P > 300^d$) variables in this sample have been distinguished from nonvariables.

Indications of Variability From HKL Photometry

Having selected LPV candidates from high values of Δm_K, they are further distinguishable by higher values of the average dereddened H-K (figure 4-9). The LPV sample is redder in $(H-K)_{obs}$ by approximately 0.3 mag from the total sample of stars within the expected range for bulge Miras. This result is consistent with the circumstellar reddening that is common with mass-losing stars on the AGB. The nonvariable stars at the bright end of the distribution are also bluer than both LPVs and non-LPVs below M_{BOL} of -4.0.

Figures 4-10 and 4-11 show the dereddened (H-K) vs. (K-L) diagrams for the nonvariables dereddened by an assumed $A_V = 31.8$ mag (see chapter 3). The nonvariable color distribution clusters near (K-L) ≈ 0.1 with a dispersion consistent with the photometric errors and with no clear correlation in the two colors. The color-color distribution for the LPV sample is quite different with a strong color correlation present and an average (K-L) ≈ 0.5. The range of the LPV (K-L) color distribution is not as great as Baade's Window (Frogel and Whitford 1987) or the sample of Miras at $l = \pm 7^\circ$ selected by IRAS colors (Whitelock *et al.* 1991) because of the completeness criteria that $m_k < 11.0$ mag for the complete K sample. In any case, the correlation in the LPV sample is clearly consistent with the expected effects of varying degrees of reddening caused by circumstellar dust shells that condense out of the stellar winds

associated with Mira pulsation (e.g. Bowen and Willson 1991).

A more interesting result comes from the comparison of the (K-L) and (H-K) colors with Δm_K, the amplitude parameter used to select LPVs. Figure 4-12 shows dereddened (H-K) vs. Δm_K, with a vertical line at $\Delta m_K = 0.274$ that separates the nonvariable stars and LPV candidates. It is apparent in the diagram that LPV candidates are redder on average than the nonvariables in (H-K) by 0.3 mag. But they never dominate any portion of the diagram at constant (H-K). They are only distinguishable from the nonvariable because there are relatively few at bluer (H-K) colors, but overall the color distributions in (H-K) overlap to such an extent that the LPV sample cannot be clearly separated. However, the corresponding diagram of dereddened (K-L) vs. Δm_K shows a detectable correlation as illustrated in figure 4-13; $(K-L)_0$ increases as Δm_K increases. Figure 14 from Whitelock *et al.* (1991) shows a similar behavior for IRAS-selected Miras in the bulge at $l = \pm 7°$. This effect can again be understood as an increase in mass loss with increasing pulsational amplitude. It is important to note that this effect is peculiar to Miras. Cepheid variables, for instance, are not subject to substantial mass-loss effects while for Miras the size of the circumstellar dust shell (and hence the amount of increased reddening) is directly related to the pulsational amplitude.

Even in the absence of complete light curves, it is clear the HKL color differences between the LPV and nonvariable samples show that the Δm_K parameter is a robust indicator of Mira variability despite the small number of observations. The Mira sample is certainly incomplete and poor phase coverage means the reddest stars in the nonvariable sample are likely to be undetected LPVs. Further confirmation comes by comparing these stars with known OH/IR stars that lie in this field. There are 4 out of 11 OH/IR stars of the Lindqvist *et al.* (1992a) sample within the central 5′×5′ that match with objects in the HK sample (table 4-2). Each has at least one color and/or amplitude consistent with the properties of OH/IR stars. The fact that all were not identified is not surprising considering the large circumstellar extinction caused by dust shells around OH/IR stars.

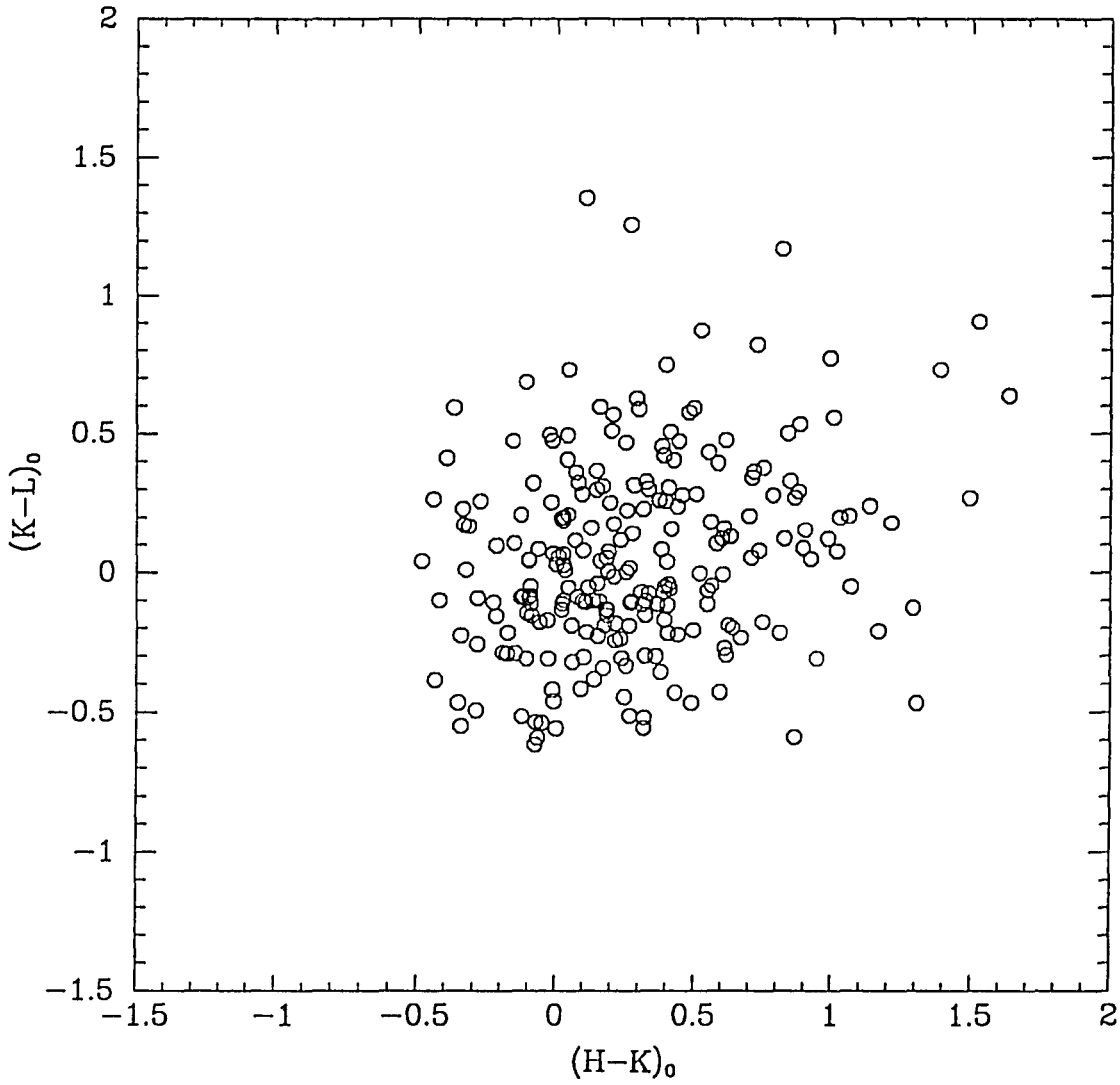

Figure 4-10. The dereddened (K-L) vs. (H-K) diagram for the "nonvariable" sample of stars detected at H, K, and L. The dispersion in the diagram is consistent with the photometric errors.

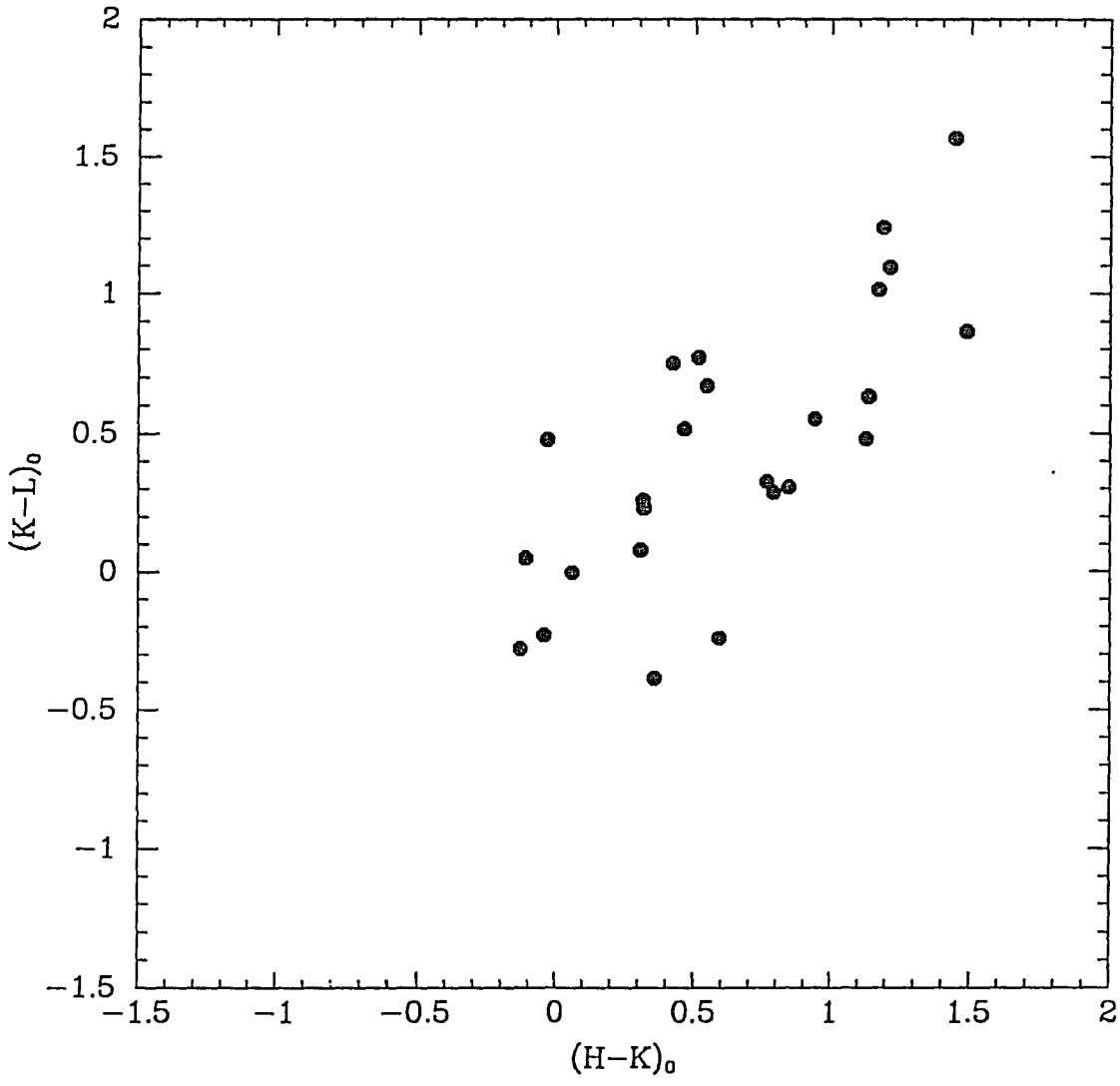

Figure 4-11. The dereddened (K-L) vs. (H-K) diagram for the LPV sample of stars detected at H, K, and L. There is a strong color-color correlation for this sample of stars selected on the basis of Δm_K.

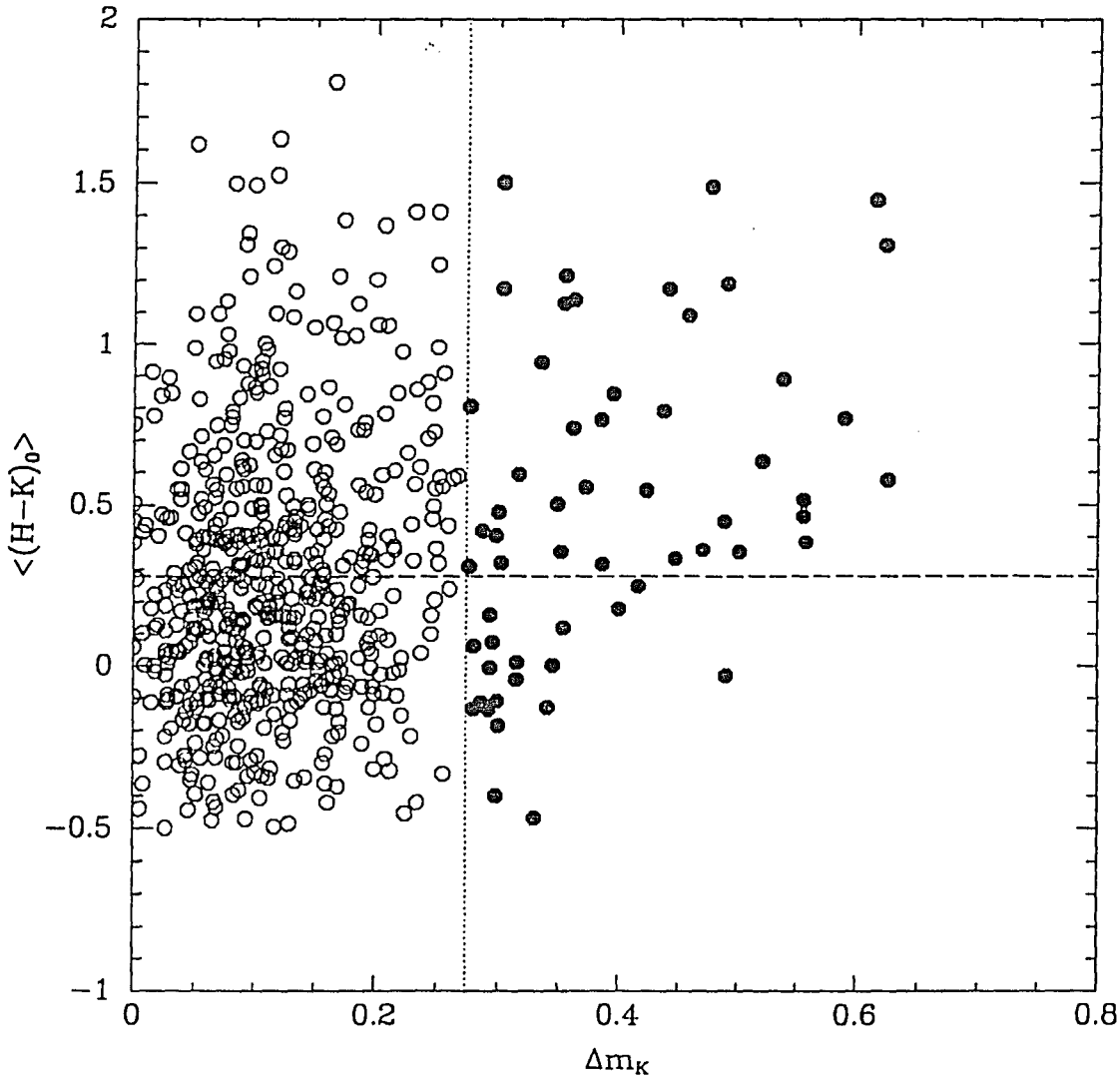

Figure 4-12 The $(H-K)_0$ vs. Δm_K diagram for the HKL sample. The vertical line shows the 3σ cutoff for nonvariables with $\Delta m_K > 0.274$. The LPV candidates are shown with filled circles and nonvariables with open circles. The horizontal line is the average $(H-K)_0$ for the nonvariable sample and emphasizes the systematically redder $(H-K)_0$ color of the LPVs, but a clear color correlation is not so apparent.

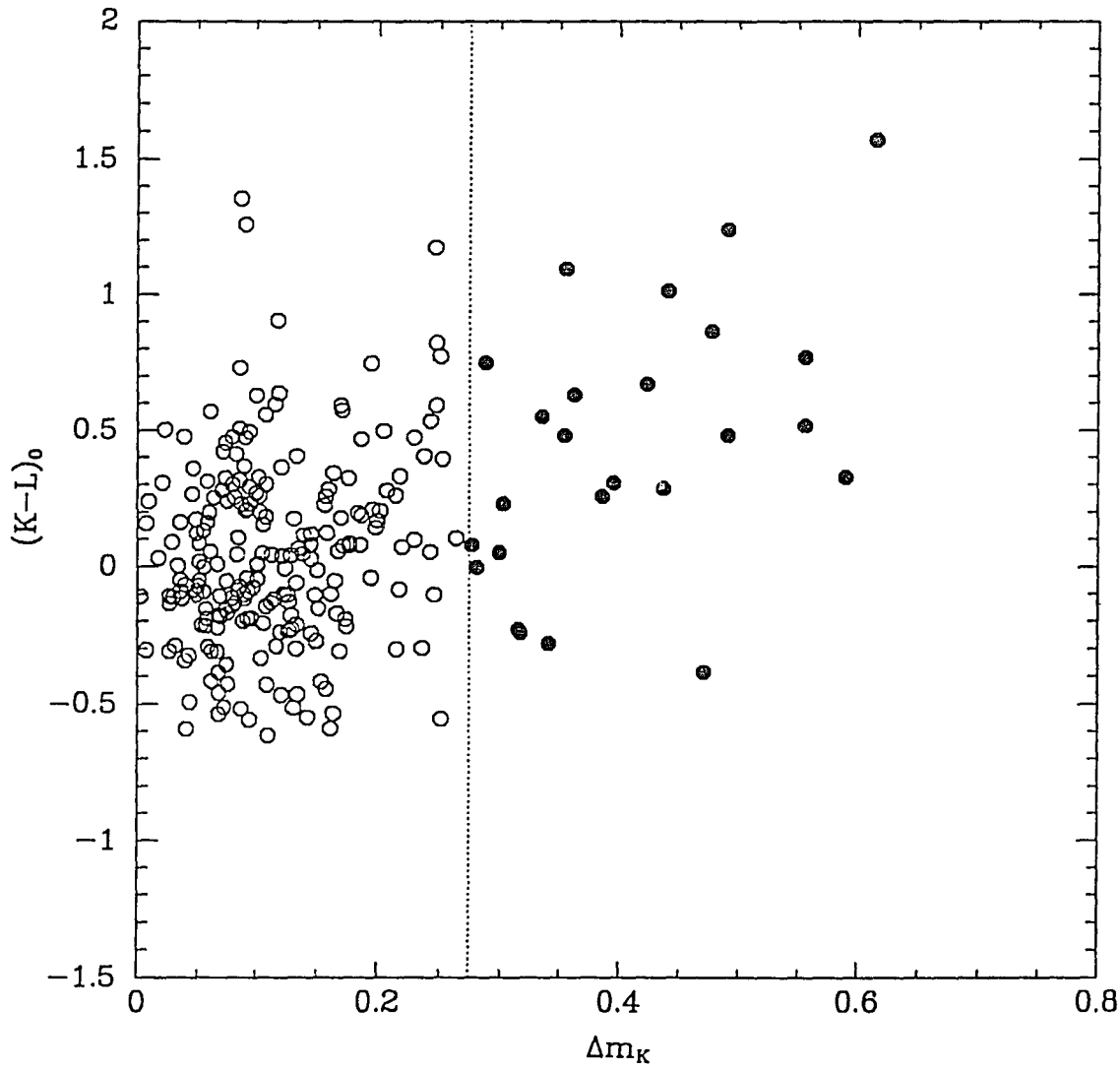

Figure 4-13: The $(K-L)_0$ vs. Δm_K diagram for the HKL sample. The vertical line shows the 3σ cutoff that excludes nonvariables for $\Delta m_K > 0.274$. The LPV candidates are shown in filled circles and nonvariables are shown with open circles. The nonvariables have an average $(K-L)_0$ near zero while the LPVs show a correlation of color with amplitude parameter. This is characteristic of Mira variables studies in the bulge (Whitelock *et al.* 1991, fig. 14).

TABLE 4-2 : OH/IR Star Identifications

Source[a]	ID[b]	m_k	Δm_K	$(H-K)_0$	$(K-L)_0$	M_{BOL}
OH359.946-0.047	455	9.17	0.63	0.58	—	−5.44
OH359.954-0.041	436	10.73	0.25	0.73	0.82	−3.88
OH359.970-0.047	562	8.22	0.15	0.61	−0.27	−6.38
OH349.986-0.061	647	10.15	0.64	2.50	2.03	−4.45

[a]Lindqvist *et al.* (1992a), [b]Appendex 2

Discussion

The bolometric luminosity function derived from the data set in chapter 2 is shown in figure 4-14 along with the distribution of the LPV candidates. The expected periods from the P-M_{BOL} relation for Miras are shown at the top of the diagram for comparison (Feast et al., 1982). Several features are to be noted in interpreting these results. First, these stars are well above the He flash luminosity of the RGB extrapolated to [Fe/H] = 1.0 by the He flash - metallicity relation of Sweigart and Gross (1978) and so they are too bright to be first-ascent giant stars. Secondly, they lie below the maximum luminosity of an AGB star of M_{BOL} = -7.1 implied by the core mass luminosity relationship (Paczynski, 1971) and so on the basis of their luminosities they are either bright AGB stars or lower luminosity supergiants. Studies in the LMC show that AGB stars characteristically have K amplitudes greater than 0.25 mag while supergiant K amplitudes are less than 0.25 amplitudes (Wood, Bessel, and Fox, 1983). The imposed cutoff of Δm_K of 0.274 mag in the Galactic Center sample selects against supergiants and favors AGB stars. For these reasons and the fact that stars in our sample with high values of Δm_K are systematically redder in $(H-K)_{obs}$ and $(K-L)_{obs}$, and the correlation between $(K-L)_0$ and Δm_K, we infer that these stars are Mira LPVs on the AGB. Applying the M_{BOL} vs. age calibration of the peak AGB luminosity and turnoff age (Mould and Aaronson 1980; Aaronson and Mould 1982) with the consideration that these stars are likely to be super-metal-rich (Blanco 1988), they have

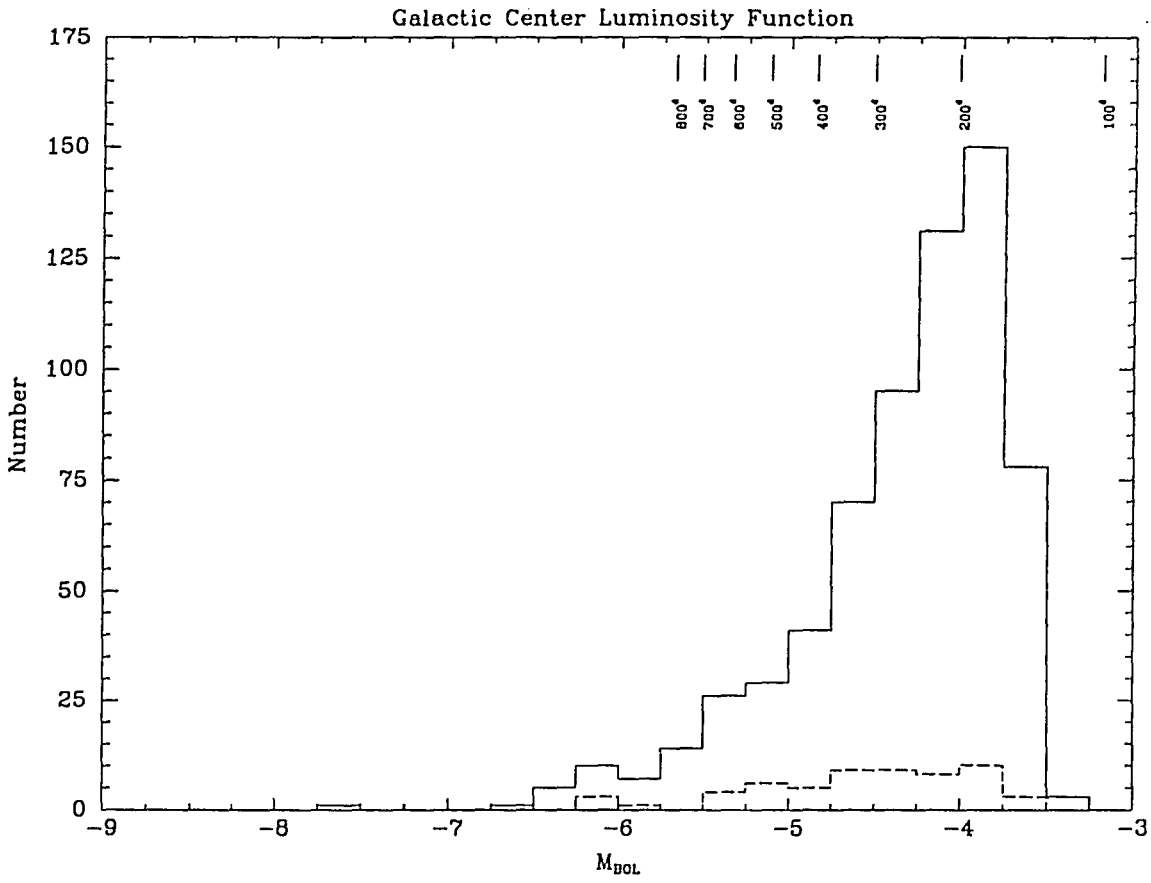

Figure 4-14. - The derived bolometric luminosity function for the 659 stars in our complete sample with $m_K < 11.0$ and H-K color > 1.50. The solid histogram shows the total distribution while the dashed histogram is for the LPV candidates with $\Delta m_K > 0.27$ mag. The expected periods for LPVs from the M_{BOL} vs. Period relation of LMC and bulge Miras is shown for comparison (Feast *et al.* 1982).

ages on the order of 2-5×10^8 yr. This is an order of magnitude younger than stars in Baade's Window but also an order of magnitude older than the young 10^7 yr supergiant population in the central cluster. Blöcker and Schönberner (1991) recently reported there may be a breakdown in the core mass-luminosity relation for AGB stars with masses of the order of 7 $M_\odot$. The brightest stars in our sample have bolometric luminosities at approximately the same level, and if this result holds true it would substantially reduce the age estimates below the values estimated by the Aaronson and Mould calibration (1982). Unfortunately, more detailed interpretations of this population are problematic because stellar evolution models are not generally available for intermediate- and high-mass stars with high metallicities and young ages. Such models would be highly desirable for interpreting the Galactic Center and other high-metallicity star-forming regions, such as starburst galaxies.

There are several other features to note when comparing the LPV distribution at the Galactic Center to the bulge population in Baade's Window at -3.8° and other outlying fields (Frogel and Whitford, 1987; Frogel et al., 1990). The greatest frequency of Galactic Center LPVs occurs in the magnitude range of the bulge LPVs ($-4.5 \leq M_{BOL} \leq -3.2$). This result should be compared to the fractional distribution of bulge LPVs shown in figure 4-15 (Frogel and Whitford 1987; Frogel *et al.* 1990). The greatest fractional contribution of LPVs in the bulge luminosity function occurs at the tip of the AGB near $M_{BOL} = -4.5$ above which there is only one LPV. Since the highest frequency of LPV candidates in our sample occurs near this bulge cutoff it is conceivable that this is due to a bulge population component. If this is true, then the bulge population has been traced in the near infrared from the halo at -12° (Frogel and Whitford, 1987; Frogel et al., 1990) all the way into the center of our Galaxy. But significantly unlike the bulge population, the Galactic Center LPV population has no cutoff above $M_{BOL} = -4.5$ as would be expected for an older AGB sample. There are significant numbers of LPVs extending to higher luminosities, by as much as 1.5 mag. Even so, the LPVs never dominate the luminosity function within any bin. Given the estimated LPV detection frequencies, this implies that most of the

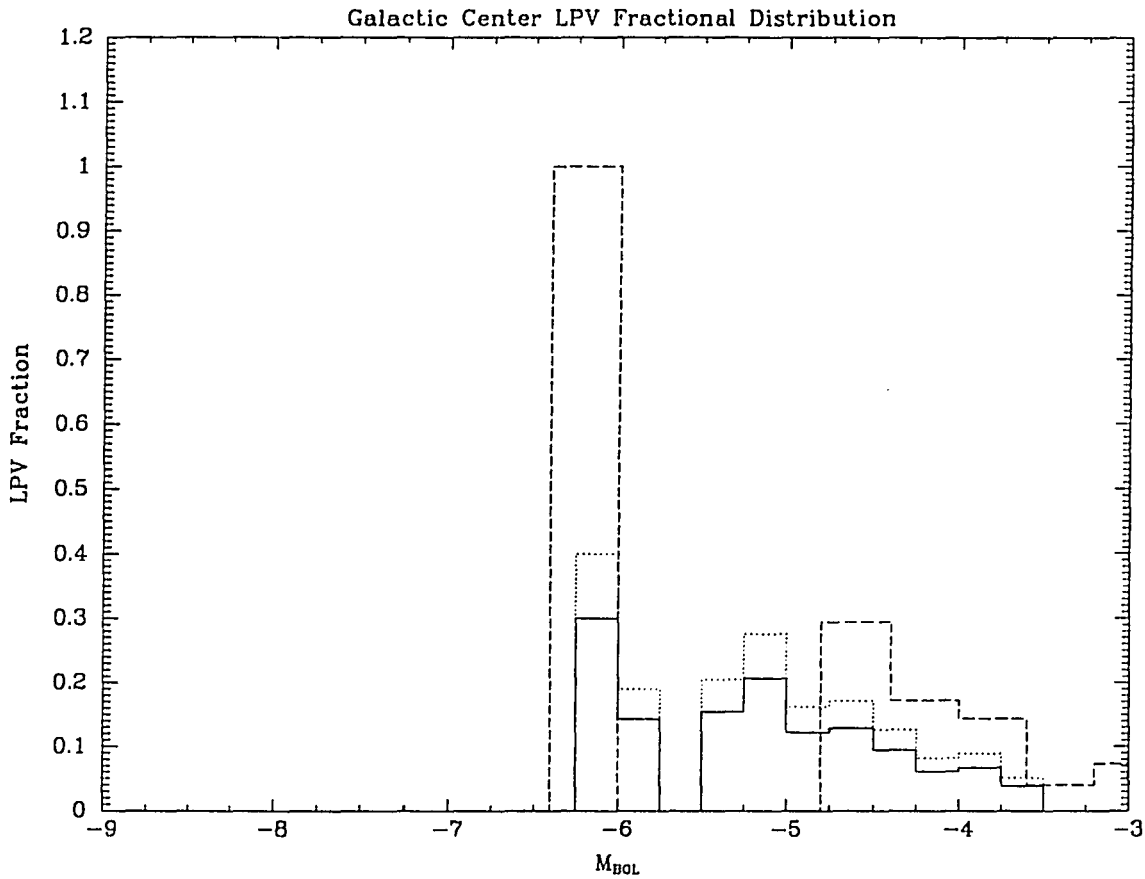

Figure 4-15. - The fractional distribution of LPVs in the bolometric luminosity function. The fractional contribution of Bulge LPVs to each bin of the Baade's Window luminosity function is represented by the dashed line (Frogel and Whitford 1987 and Frogel *et al.* 1990). The fractional contribution of LPVs to each bin in the observed Galactic Center luminosity distribution is shown by the solid line while the dotted line shows the same distribution corrected for ≈ 75% detection efficiency expected for an LPV population with preferentially high amplitudes.

stars at the bright end of the bolometric luminosity function are nonvariable.

The remaining bright nonvariables with $M_{BOL} < -4.5$ are either older AGB stars or younger supergiants. Supergiants would be distinguished by bluer (H-K) colors than AGB stars and this agrees with the observed color distribution. The presence of stars like IRS 7 in the central parsec and the low frequency of LPVs in the luminosity distribution suggest that many of these remaining stars could be supergiants as well. If this is so, then massive star formation associated with the central cluster happened over a much larger volume than the central few parsecs. The best way to confirm supergiants would be to examine the 2.3μm CO absorption feature between the LPV and nonvariable samples. If the nonvariables are supergiants they should show systematically deeper CO.

In globular clusters, LPVs derive their luminosity from H and He shell burning and are always brighter than the H shell burning stars on the first ascent of the RGB (e.g. Frogel and Elias 1988). This feature has been incorporated in semi-empirical theoretical studies of stellar evolution (e.g. Charlot and Bruzual 1991) based on stellar evolutionary tracks (Maeder and Maynet 1989). One important exception is the SMR population observed in Baade's Window (Frogel and Whitford 1987) where not all of the brightest stars on the AGB are LPVs. As mentioned in chapter 2, counts of M giants in the bulge at different Galactic latitudes (Blanco 1988) show the frequency of M giants decreases faster with increasing distance away from the Galactic Center than would be expected from an $R^{1/4}$ law. This was attributed to the effect of increasing metallicity toward the Galactic Center. Frogel and Whitford (1987) asserted that stars on the giant branch have enhanced luminosities because higher metallicity translates into a longer time spent on the main sequence. So the strong possibility of high metallicity in the Galactic Center would mean that at least some of the bright nonvariables in the luminosity function will be nonvariable giants of the same population as the Miras. The contribution of these nonvariables is presently unknown. Even so, they are still be far too bright for an old bulge population and are more similar to the young clusters in the LMC (Mould and Aaronson

1980). Those Miras with $M_{BOL} \approx -6$ (there are 4 such stars in our sample) imply a main-sequence turnoff mass of $\approx 5\ M_{\odot}$ indicating a prior episode of star formation occurring in the same region approximately 10^8 yr ago (Charlot and Bruzual A., 1991). The calculation in Appendix 1 estimating the proximity of these stars to the Galactic Center shows that 90% of the observed population is within 50pc of R_0 because of the sharply peaked stellar density distribution that is implied by the 2.2μm surface brightness profile so explanations resorting to foreground contamination are untenable.

It is significant that either choice for the nonvariables is consistent with theoretical models of periodic star formation at the Galactic Center discussed previously (e.g. Loose, Krügel, and Tutukov, 1982), where one would expect to find different temporal "strata" of stars within the region. Whether or not a central engine drives the overall dynamics or energetics of this region, star formation has occurred at least several times, within intervals much less than the age of the Galaxy.

Such a picture of continual star formation at the Galactic Center rests on the identification of the LPVs as young AGB stars. In the absence of complete light curves, one may question the strength of these conclusions. The obvious way to confirm this hypothesis would be to obtain accurate light curves by follow up observations over several years. Such an experiment is now underway but data have not been reduced to a sufficient extent to derive periods.

It is then clear that star formation has occurred in the Galactic Center at different times. An important question to ask is what is its spatial extent? It would be useful to have some way to sample easily these populations through future near-infrared surveys. This may indeed be possible for a young AGB population. Because of the strong circumstellar reddening by dust shells it is likely that those stars with a (K-L) > 1.0 are LPVs. Comparing the fractional contribution of stars with red K-L to the total luminosity function may indicate whether the remaining bright nonvariables are supergiants. If the supergiant population is confined to the

central few arcminutes of the Galactic Center, then with increasing projected distance from the center, a larger fraction of luminous stars will have $(K\text{-}L)_0 > 1.00$. This can then also be used to find LPV candidates for further study. There were approximately 2 LPVs arcmin^{-2} in the K photometry sample. With the extremely high source density ($\approx$ 25 stars arcmin^{-2}) in this region the opportunities for acquiring large samples of complete LPV light curves would be promising because variable candidates could be identified by a photometric index that avoids the tedious procedure of acquiring complete light curves for a large sample of stars to identify the variables.

Lindqvist, Habing, and Winnberg (1992b) showed their sample of OH/IR stars divided into two distinct spatial groups by the expansion velocity of the OH emission line. Those with $v_{exp} > 18$ km s^{-1} were spatially concentrated to within 16′ (32 pc) of the center and they interpreted them as a population of relatively younger AGB stars (Baud *et al.* 1981). This may be an indication of how far from the center the high luminosity AGB population extends. All of the Lindqvist *et al.* (1992a) OH/IR stars that were identified with the HK sample stars in table 4-2 belonged to this younger population.

Conclusions

We have searched for LPVs within the central 5′×5′ of the Galactic Center from a data set of three 2.2μm epochs and one 1.6μm epoch using the RMS residual magnitude differences between epochs. Monte Carlo calculations show that, with our photometric errors, nonvariable stars will have $<\Delta m_K> = 0.106 \pm 0.056$ mag. This was used to determine a 3σ cutoff in Δm_K to exclude nonvariable candidates from our LPV sample. If the amplitude distribution of the Galactic Center Miras is similar to that in the solar neighborhood, then a majority of the brightest LPV's have been detected. The number of detected variables is greatest in the range characteristic of bulge LPVs but does not show the expected cutoff at $M_{BOL} < -4.5$. Galactic Center LPVs have an average $(H-K)_{obs}$ color 0.2 - 0.3 mag greater than the sample without LPVs in nearly every magnitude bin of the luminosity distribution. From this we conclude the LPVs in our sample are Miras on the AGB.

The results of HKL photometry for 264 stars taken from the complete sample of HK stars show that stars selected with as LPV candidates have strongly correlated $(H-K)_0$ and $(K-L)_0$ as well as $(K-L)_0$ vs. Δm_K. Both correlations support the procedure used to identify the variables and their identification as Miras.

The luminosities of the LPVs and presumed high metallicity indicate the ages for these stars is on the order of 5×10^8 years. This shows that star formation has occurred over at least 6pc length scales within the Galactic Center and the importance of this process to the energetics to the region merits consideration. Given the presence of the 10^7-year-old supergiants in the central cluster, it would also appear that star formation is also recurrent. The stars at the Galactic Center region are not a simple bulge population but are a composite of at least three distinct stellar populations characterized by different periods of star formation. First, there is the expected older bulge-like population identified by the peak in the number distribution of

the Mira LPVs at the characteristic cutoff luminosity of the bulge. Secondly, there are the extremely young massive stars which reside within the central 1.5′ identified by such members as IRS 7 and the IRS 16 complex. Thirdly, there is an intermediately bright distribution of bright Mira LPVs, that are brighter than the typical bulge AGB. The nature of the intermediately bright nonvariable population remains to be determined.

CHAPTER 5 :

THE UNRESOLVED LATE-TYPE STELLAR POPULATION WITHIN 30" OF SGR A* AND KINEMATIC EVIDENCE FOR A 1.7 × 10^6 $M_\odot$ BLACK HOLE

Background

Previous chapters examined the late-type stars within 6 pc of the Galactic Center showing that a composite population was likely formed by several episodes of star formation. This chapter will focus on the unresolved stars within 1 pc of the dynamical center, provisionally identified with Sgr A*. Previous spectral studies of this central stellar cluster have clarified the general nature of the brightest resolved sources. Several attempts have been made to traced the enclosed mass distribution about the center, using the motions of the ionized and molecular gas as well as the resolved and unresolved stars, to place upper limits on the mass of a central black hole. The surest way to probe for a large compact mass would be the surrounding stars because they are not dynamically affected by ambient magnetic fields and interact only through gravitation. If such a compact object exists it could ultimately serve as the central engine driving the energetics and of surrounding phenomena. This task has been complicated because of ambigous dynamical evidence and the presence of other known sources (i.e. IRS 16) that could alternatively explain the overall features through something resembling a starburst.

Previous Studies of the CO 2.3μm Absorption Feature

The only near infrared spectral feature that has been used to measure the enclosed mass distribution by stars is the 2.3 μm CO (v=2←0) transition because the extinction in the K band (approximately 0.1 × A_V) is rather modest, it is a strong feature in the spectra of late-type stars, and the fact that no other line can be reliably used at shorter wavelengths. Neugebauer *et al.*

(1976) first classified the bright sources of the central cluster as supergiants because of strong CO absorption and the blue continuum of IRS 16 implied it was either a cluster of M dwarfs or luminous early-type stars. These results were confirmed by many subsequent workers (Hall, Kleinmann, and Scoville 1982; Wollman, Smith, and Larson 1982; Lebofsky, Rieke, and Tokunaga 1982). Lebofsky *et al.* (1982) extended the list of supergiant stars and proposed the starburst hypothesis. Wollman *et al.* (1982) measured radial velocities for sources 7, 12, and 19 and found they were all blue shifted to the local standard of rest, with a slight trend of increasing velocity with decreasing distance to IRS 16.

Four extensive CO velocity studies have been made in recent years (Sellgren *et al.* 1987; Rieke and Rieke 1988; McGinn *et al.* 1989; Sellgren *et al.* 1990), attempting to measure the enclosed mass versus radius in the vicinity of IRS 16 and Sgr A*. The first two works measured the radial velocities of resolved sources while the second pair used the velocity dispersion of the fainter unresolved emission. Because of the common theoretical basis of these studies as well as the work presented here, it is appropriate to outline the three methods used to measure the enclosed mass vs. radius using velocity dispersions.

Theoretical Relations for the Enclosed Mass vs. Radius of Spherically Symmetric Systems

For radial velocity measurements of individual sources, a minimum estimate of the enclosed mass is made by assuming a gravitational potential dominated by a single object resulting in stellar orbits that approach Keplerian (Sellgren *et al.* 1987). From conservation of energy, the minimum enclosed mass within a projected radius r will be given by

$$M(r) \geq \frac{v_{los}^{2}\, r}{G}.$$

where v_{los} is the line-of-sight radial velocity.

A more precise estimate can be made using the "projected mass" method of Bachall and Tremaine (1981). The mass estimate derived from each star is of the same form but is suitably weighted for the predominant type of stellar orbit (i.e. circular or radial) and overall mass distribution (dominant central mass or distributed mass). The general form of this mass estimator is given by

$$M(R) = \frac{C}{\pi} \frac{1}{N} \sum_{i=1}^{N} \frac{v_i^2 r_i}{G} \qquad r_i \leq R$$

where the normalization constant for a dominant central mass, C, is 32/3 for circular orbits, 16 for isotropic orbits, and 32 for radial orbits. These normalizations are doubled for a self gravitating stellar system (Heisler *et al.* 1985). The fractional error of the estimated mass is proportional $N^{-0.5}$ and depends slightly on the mass distribution and orbit type. The virial theorem is not preferred for these estimates because it does not always converge on the correct value of the mass, or does so only very slowly as $N \rightarrow \infty$. The projected mass method will give similar answers as the virial theorem (when the virial theorem works correctly) and its variance is also well behaved (unlike the variance of the virial theorem mass estimator).

A third method derives the enclosed mass from the observed velocity dispersion, $\sigma(r)$, and rotational velocity, $V_{ROT}(r)$, as well as information from the total light distribution by utilizing the first moment of the equation of stellar hydrodynamics (Hartwick and Sargent 1978):

$$M(r) = \frac{r\,\sigma(r)^2}{G} \times \left[- \frac{d \ln n(r)}{d \ln r} - \frac{d \ln \sigma(r)^2}{d \ln r} + (\lambda - 2) + \frac{V_{ROT}(r)^2}{\sigma(r)^2} \right]$$

Here $n(r)$ is the number density of test particles, and λ is the ratio of the tangential to radial

velocity dispersions. This method requires more information about the distribution of sources and their orbits but, generally, reasonable assumptions can be made to reduce the complexity of its application. For instance, the run of $n(r)$ is generally derived from the 2.2μm surface brightness distribution which implies a density law of $n \propto r^{-1.8}$ for a constant mass to light ratio (Neugebauer *et al.* 1968; Allen *et al.* 1983). There is also evidence that the stellar orbits are isotropic and so $\lambda \approx 2$ (McGinn *et al.* 1989).

The Galactic Center Stellar Kinematics

A study of OH/IR stars by Winnberg *et al.* (1985) measuring the 1612 MHz OH maser line radial velocities for 33 stars in the central 34′ × 34′ was able to determine a rotational velocity gradient of 270 ± 80 km s^{-1} per degree in this region. Several of these stars have also been used in the following studies of the enclosed mass vs. radius near the Galactic Center.

The first extensive velocity study in the central few parsecs by Sellgren *et al.* (1987) used 120 km s^{-1} resolution data on sources 7, 11, 12, 19, 22, and 23 with a 3.8″ aperture. They applied each of the above methods to their data, augmented by seven OH/IR star velocities (Winnberg *et al.* 1985). Their data showed that the motions of the gas and the stars are distinct and are not likely to be coupled. Assuming no velocity dispersion gradient, no bulk stellar rotation, and isotropic orbits they were able to apply the stellar hydrodynamic equation, which reduced to a simple linear function of radius. All three enclosed mass estimators indicated approximately 1×10^6 $M_\odot$ of mass was concentrated within 0.3 pc of IRS 16 and $2\text{-}10\times10^6$ $M_\odot$ within 1 pc (R_0 = 8.5 kpc). In general the enclosed mass vs. radius was proportional to radius, unlike the results derived from gas velocities which show a constant mass distribution inside of 10 pc (Gatley *et al.* 1984; Ekers *et al.* 1983; Geballe *et al.* 1984).

The list of radial velocities was greatly extended by Rieke and Rieke (1988) who measured CO velocities for 43 stars within 6.5 pc (R_0 = 8.5 kpc) of the Galactic Center at 277 km

s^{-1} resolution. They also included eight sources from Winnberg *et al.* (1985) and the IRS 19 and IRS 23 measurements of Sellgren *et al.* (1985) in their analysis. Significantly, the velocity dispersion of their sample was constant at 72 km s^{-1} out to a distance of 2 pc. This was much smaller than the velocities of the gas which are typically ~300 km s^{-1} within the same region which again showed that the stars and the gas have very different kinematic properties. The projected mass method also excluded a dominant central mass model because the enclosed mass was an increasing function of distance. Whatever compact object may reside at the center, it does not dominate the total mass beyond 0.5 pc, since the stellar cluster contributes a nonnegligible fraction as evidenced by the rising M(r) curve. Further, if the core radius of the stellar distribution is 0.1 pc (Allen, Hyland, and Jones 1983) then no anomalous M/L ratio results but a core radius of 0.6 pc (Rieke and Lebofsky 1987) would make their data compatible with a central compact object of 2×10^6 $M_\odot$.

McGinn *et al.* (1989) and Sellgren *et al.* (1990) examined the CO band velocities of the diffuse stellar emission within ± 90″ of Sgr A*. Using 120 km s^{-1} velocity resolution observations and a 20″ aperture that sampled positions every 10″ along the Galactic equator and meridian passing through IRS 16, they were able to measure both the rotation curve and the gradient in the velocity dispersion. The velocity dispersion peaked at ≈ 125 km s^{-1} within 20″ of IRS 16 and exceeded the rotational velocity by at least a factor of four, indicating the stellar distribution is pressure supported and the stars rotate only half as fast as the gas at a distance of 1.6 pc. Unlike the constant value of σ_v measured by Rieke and Rieke (1988), there was a monotonic decline in velocity dispersion of -0.79 ± 0.14 km s^{-1} $arcsec^{-1}$ with increasing distance as well as large fluctuations. They estimated that brighter resolved sources contributed 25% of the total average flux in their apertures, yet simulations indicated no significant effects on their results. Possibilities for the differing results from Rieke and Rieke (1988) included small number statistical problems with the earlier sample, dynamical differences between the bright and faint populations due to differing ages (a 10^7 yr population would not have time to become

dynamically relaxed with the central cluster), or perhaps significant foreground contamination in the bright star sample. They derived the *M(r)* vs. *r* relation via the stellar hydrodynamic method. It was a significant improvement over Sellgren *et al.* (1987) because the velocity dispersion gradient and the rotational velocity could be meaningfully evaluated, and assumption of an isotropic velocity dispersion could be further justified. They measured 2.5×10^6 $M_\odot$ of material within 0.6 pc of IRS 16 (R_0 = 8.5 kpc), in close agreement with Sellgren *et al.* (1987) and Rieke and Rieke (1988).

Sellgren *et al.* (1990) extended the McGinn *et al.* (1989) study to the central 1 pc, near IRS 16. They obtained two measurements with a 5.0″ aperture and five with a 7.8″ aperture at 120 km s^{-1} spectral resolution and another eight measurements using a 2.7″ aperture using the cooled grating array spectrometer on the NASA IRTF at 250 km s^{-1} resolution. Their goal was velocity dispersion measurements at locations selected to avoid the bright resolved sources to determine the enclosed mass to within 0.05 pc of IRS 16. Their data suffered from significant contamination by the bright 2.2μm sources of the central cluster and the larger apertures. They were able to confirm a rising velocity dispersion (McGinn *et al.* 1989) in the vicinity of IRS 16 to approximately 125 km s^{-1}. However, they also detected a significant decrease in the depth of the CO absorption feature within the central 20″. This prevented velocity dispersion measurements within 0.4 pc. Even with drift errors up to half the aperture size, they claimed that four of their 2.7″ aperture measurements within 15″ of IRS 16 had no contamination and showed the average CO depth was 21%, much smaller than the average value of 35% outside of 15″. Their interpretation was that stars within 15″ have diminished CO strength and hence the measured velocity dispersions are indicative of foreground and background stars. Thus the velocity dispersion does not reflect the stars at the projected distance from IRS 16 but instead this technique is limited to extracting information outside the central cluster where CO is depleted. This interpretation will be further discussed below.

Lindqvist, Habing and Winnberg (1992) recently used a sample of OH/IR stars to

measure the enclosed mass from 4-80 pc by both of the above methods. They found good agreement using the projected mass method with the enclosed mass vs. radius derived by Sellgren *et al.* (1987) and McGinn *et al.* (1989). Their OH/IR star sample also extended the enclosed mass curve, as measured by stars, to a considerably larger projected radius.

Observations and Data Reductions

The new CO spectra presented here were acquired at the CTIO 4m telescope at f/33 using the Infrared Spectrometer on the nights of June 24, 26, and 28, 1989. The detector was a SBRC 58×62 InSb array with a read noise of 380 electrons. The spatial scale along the slit was 0.81″/pixel and the grating was set for a pixel resolution of ~3000 which is half the spectral resolution, with a corresponding velocity resolution of 99.6 km s^{-1}. The slit was 15″×1.3″ in projected size on the sky, oriented in the north-south direction. Table 5-1 lists the nominal slit coordinates offset from IRS 7 and the cumulative exposure times. At each slit position spectra were taken at the nominal wavelength of 2.3μm (the "A" set of spectra) as well as another set with the grating "jogged" by ½ of a pixel element (the "B" set of spectra) so the light was sampled at twice the pixel resolution. The selection of the slit positions (figure 5-1) were determined from a high resolution K map (Rieke and Rieke, unpublished) to minimize the contamination from bright point sources that would diminish the CO absorption feature. The signal was peaked on IRS 7 with short test exposures and then the telescope was wobbled to the offset position. Sky frames at the same exposure were obtained from a position ~90″ south of the nominal slit positions in a region of very high extinction ($A_V \approx 60$ mag) due to a foreground molecular cloud (Glass, Catchpole, and Whitelock 1987). Velocity reference spectra were made from IRS 7 with 60 exposures and sky transmission frames were made from 30 sec exposures of a G dwarf star, all of which bracketed the data exposures in time. Bias frames, dome flats, and dark current frames at each exposure time were made at the end of the night.

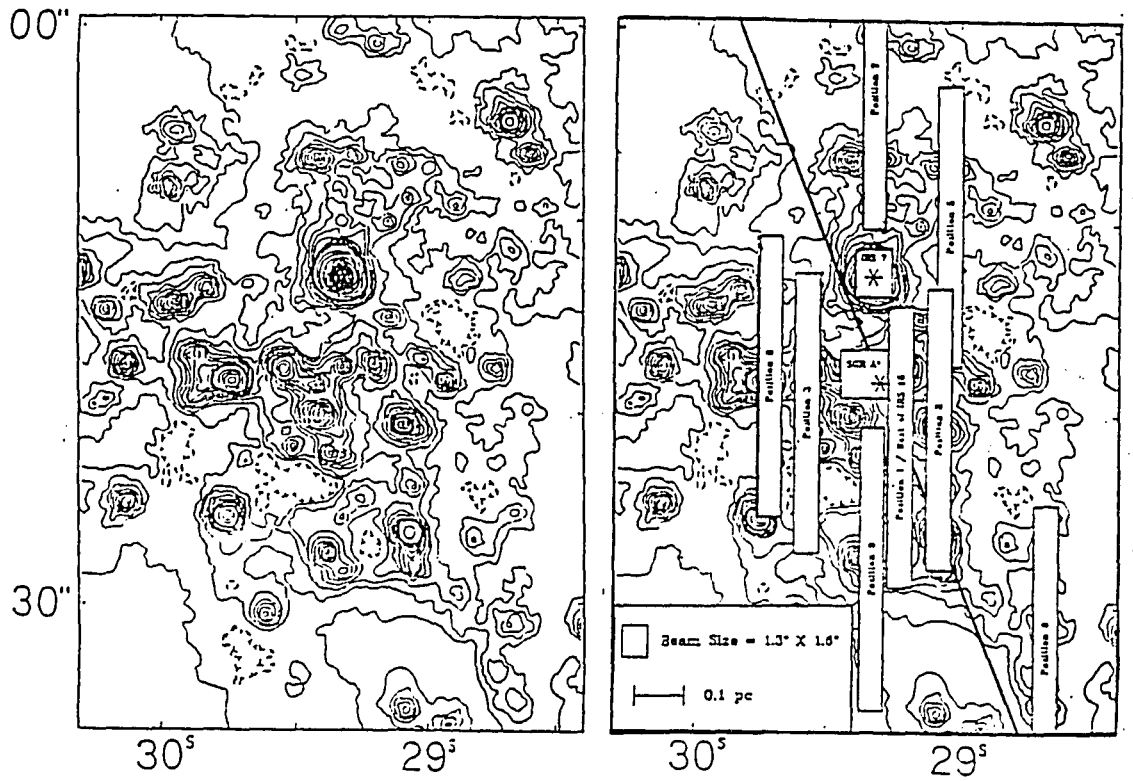

Figure 5-1: The placement of the nine slit positions with respect to a high resolution 2.2μm image (Rieke and Rieke, unpublished). The nominal positions of IRS 7 and Sgr A* are shown in boxes and the IRS 16 complex is directly to the left of Sgr A*. The diagonal line is the Galactic Equator. The slit "Position 1" is in the "valley" of emission immediately to the west of IRS 16. The slit designated "wi16" is listed in the log book with the same offset position, however the intensity profiles do not agree, indicating an error in the R.A. coordinate.

TABLE 5-1
LIST OF 2.3μm CO SPECTRA SLIT POSITIONS

Night of Observations	Slit Position	α_{IRS7} (″)	δ_{IRS7} (″)	Total Exposure Time (Sec)
	1	-1.5	-8.0	1200
June 24/25, 1989	2	-3.5	-7.0	480
	3	+3.5	-7.0	480
	5	-4.0	+3.0	480
June 26/27, 1989	6	-9.0	-18.0	480
	7	+11.0	+0.0	240
	8	+5.5	-4.5	480
June 28/29, 1989	9	+0.0	-14.5	480
	WI16	-1.5	-8.0	240

Only a small 62×19 pix^2 region of the array contained usable data. This was extracted and a small number (~ 10) of dead pixels were masked. After correction for dark current and bias levels, a flat field was made from the dome exposures and applied to the data and sky transmission frames. The sky transmission spectrum was replicated in the spatial direction of the array and divided into the flat fielded data frames to remove telluric features. Finally, those spectra with multiple exposures were coadded. Eighteen spectra were extracted from each slit position, two pixels wide in the spatial direction with an effective beam size of $\Delta\alpha \times \Delta\delta$ = 1.3″×1.6″ and sequentially spaced by one pixel from north to south . The extracted spectra were normalized to unity in the continuum blueward of the 2.29μm CO absorption feature. The "A" spectra and the "B" spectra data were then combined by interleaving the two sets. There were 162 final spectra, which after trimming of the edges had a velocity range of 4700 km s^{-1} with an inverse dispersion of 49km s^{-1} pixel^{-1} (figure 5-2).

An estimate of the signal-to-noise in each spectrum was made from the ratio of the average blueward continuum to the scatter of the "A" spectra interpolated to the shifted "B"

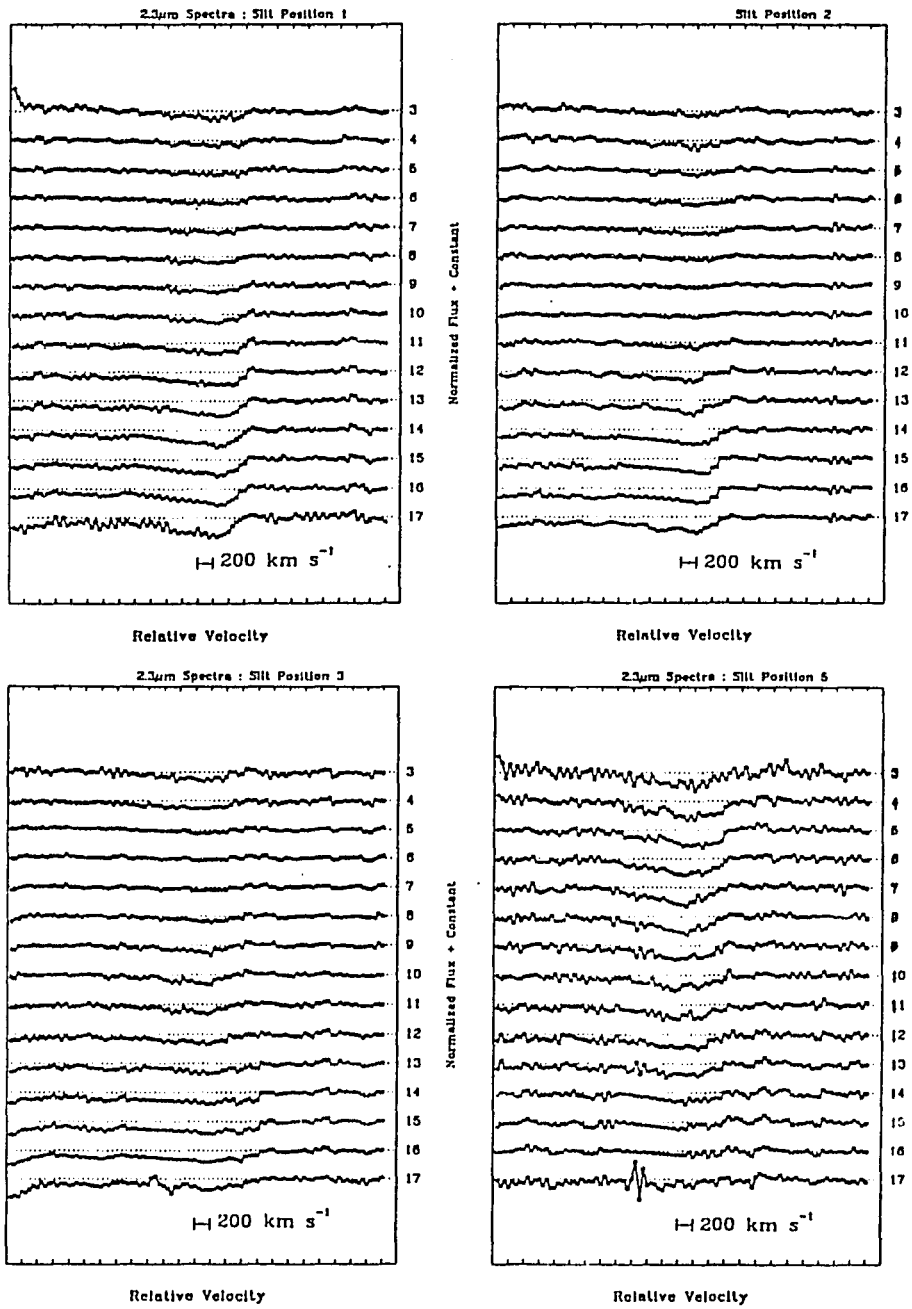

Figure 5-2: The extracted long slit spectra of the CO absorption feature at 2.3μm. North is at the top and each spectrum has been normalized to unity in the continuum level blueward of the CO feature as shown by the dotted lines. Each spectrum is coadded by 2 pixels in the spatial direction and sequentially spaced across the slit by one pixel. The effective beam size is 1.6″×1.3″. The spectra are separated by ½ of the continuum level. Shorter wavelengths are to the right.

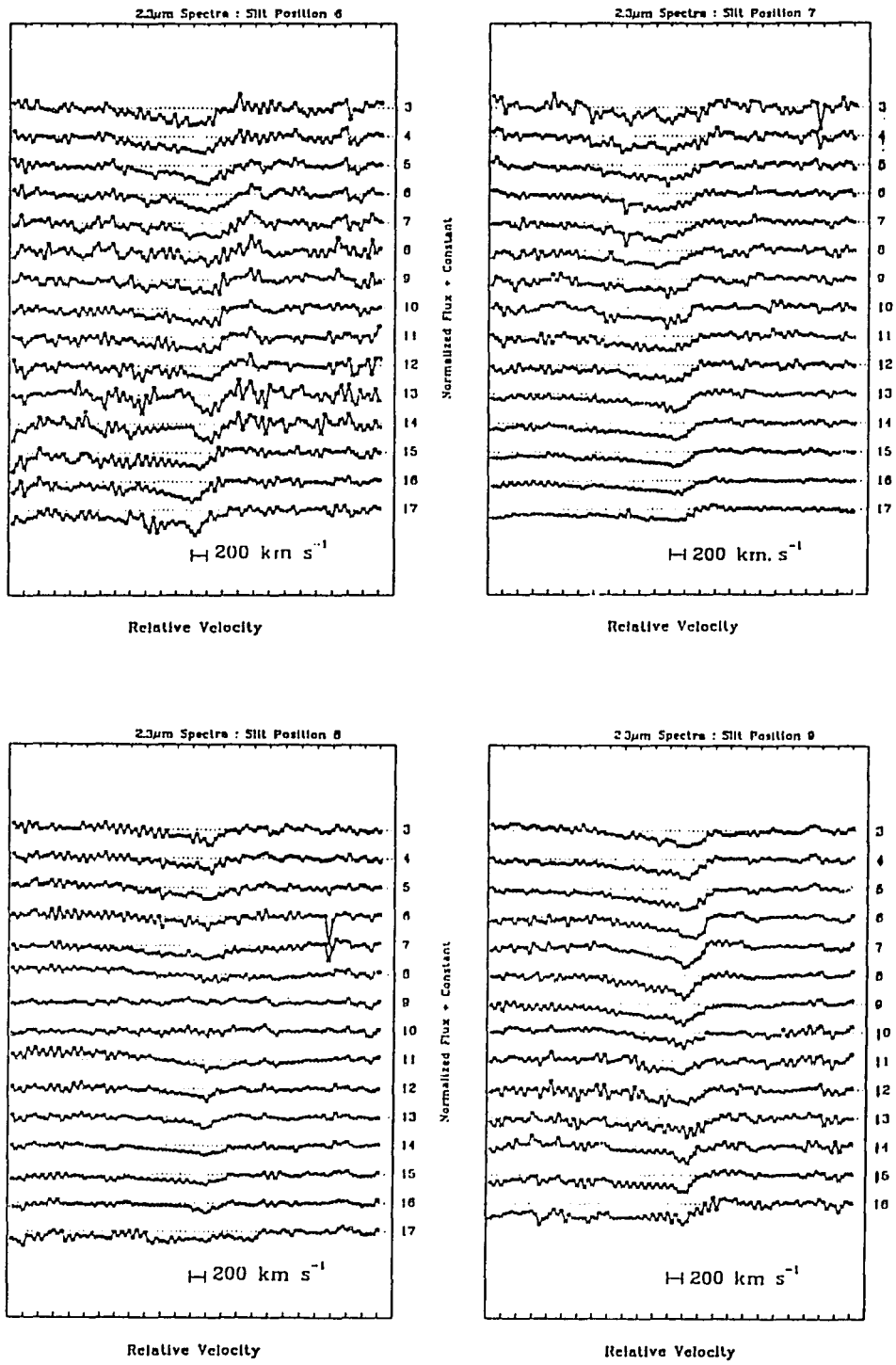

Figure 5-2: Continued

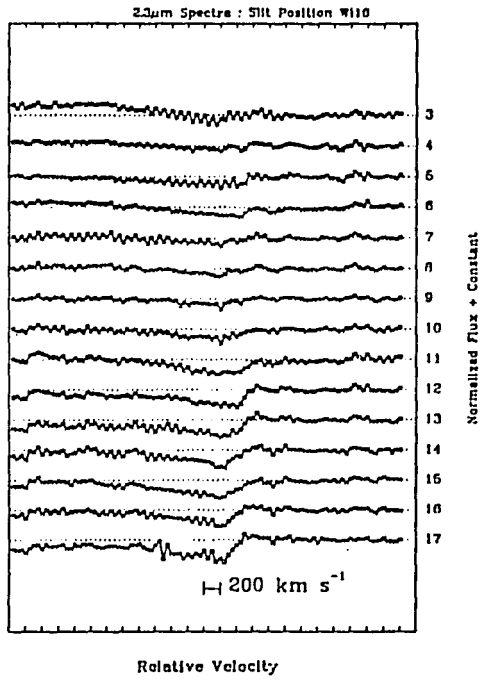

Figure 5-2: Continued.

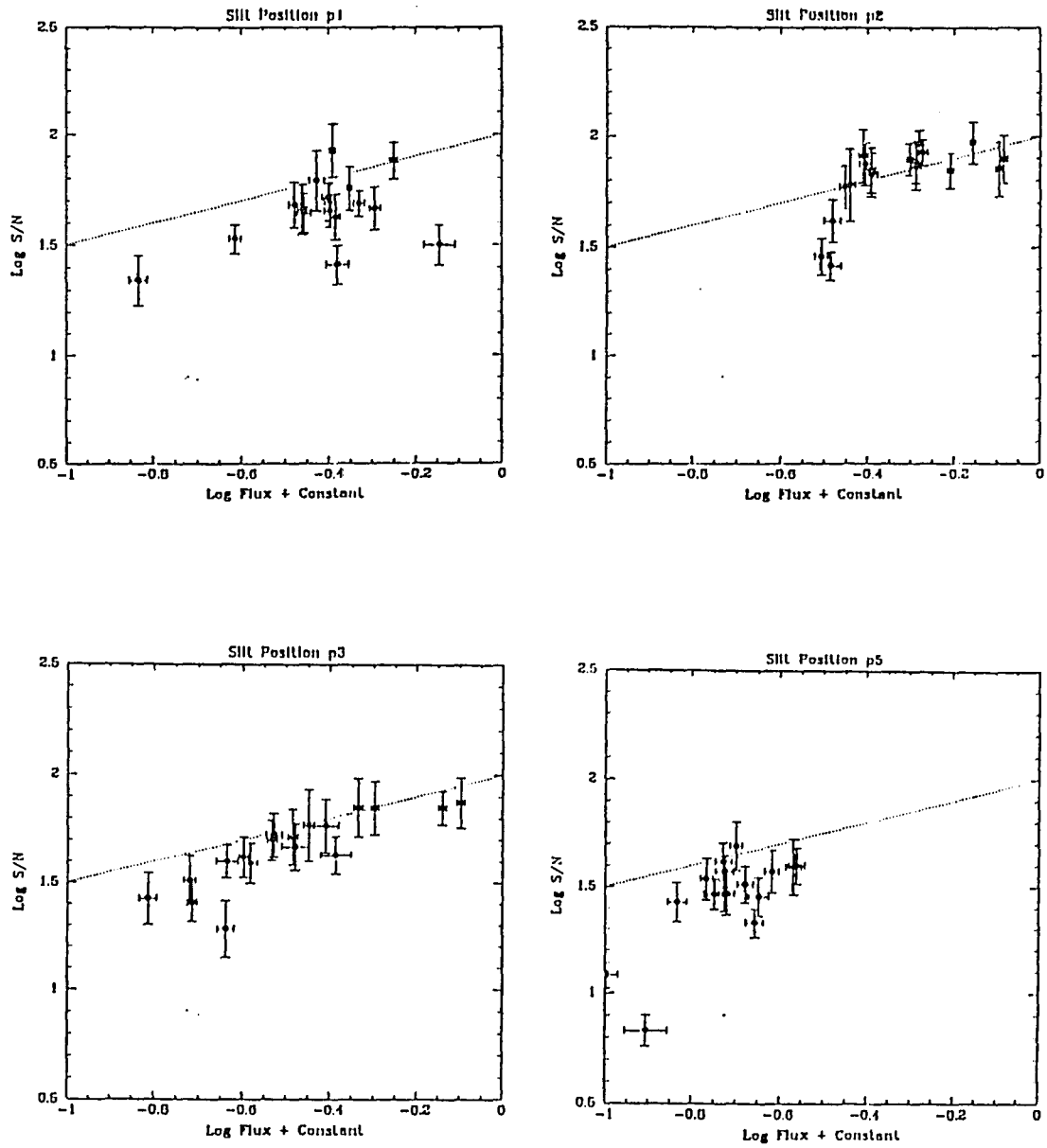

Figure 5-3: Estimated Signal-to-Noise in the CO spectra. The dotted line is the theoretical S/N relation for a slit spectrum with a peak relative flux of 1.0 at S/N = 100.

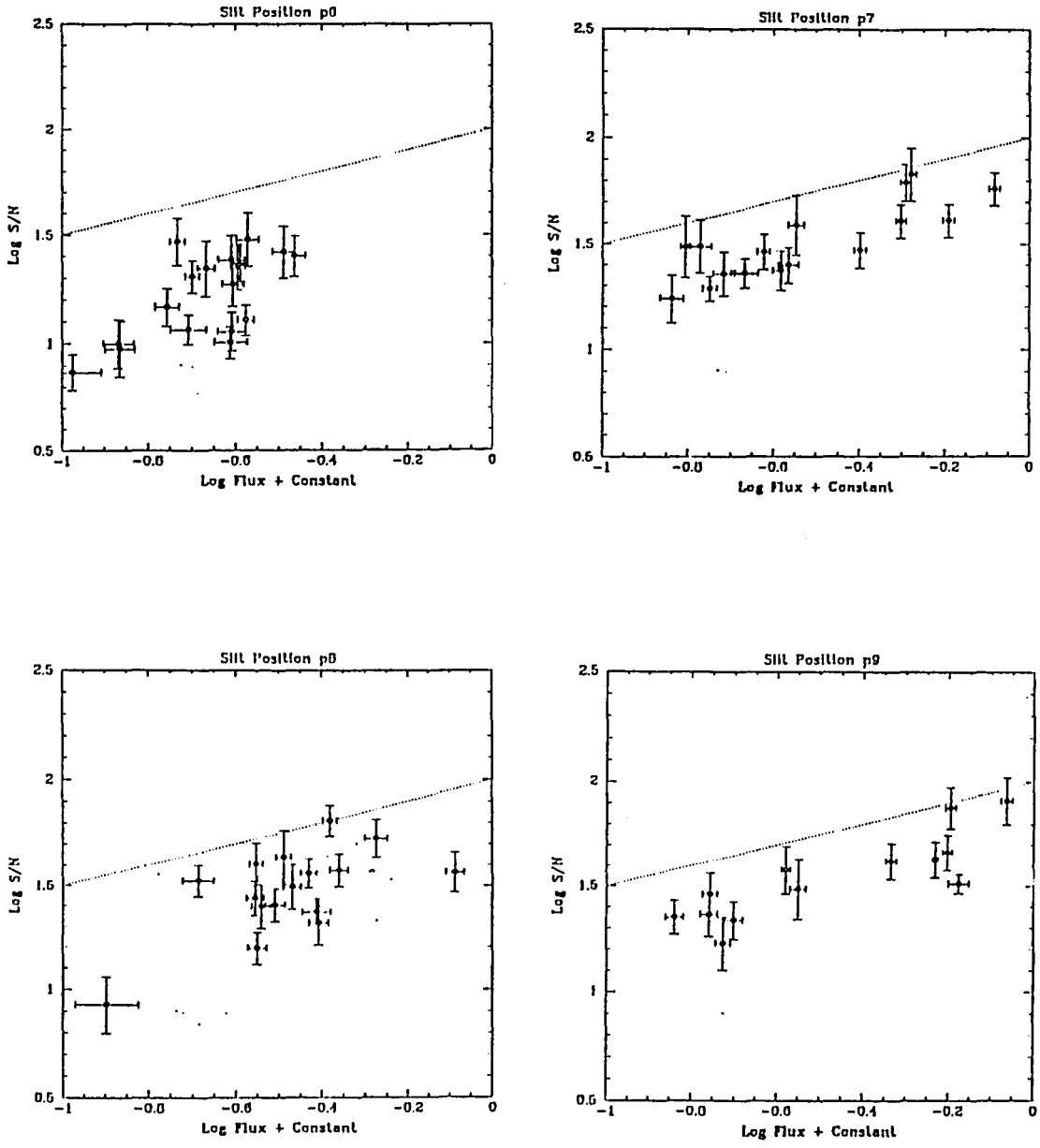

Figure 5-3: Continued.

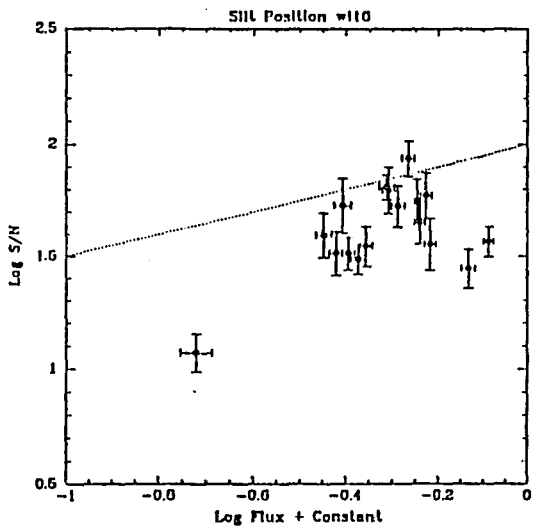

Figure 5-3: Continued.

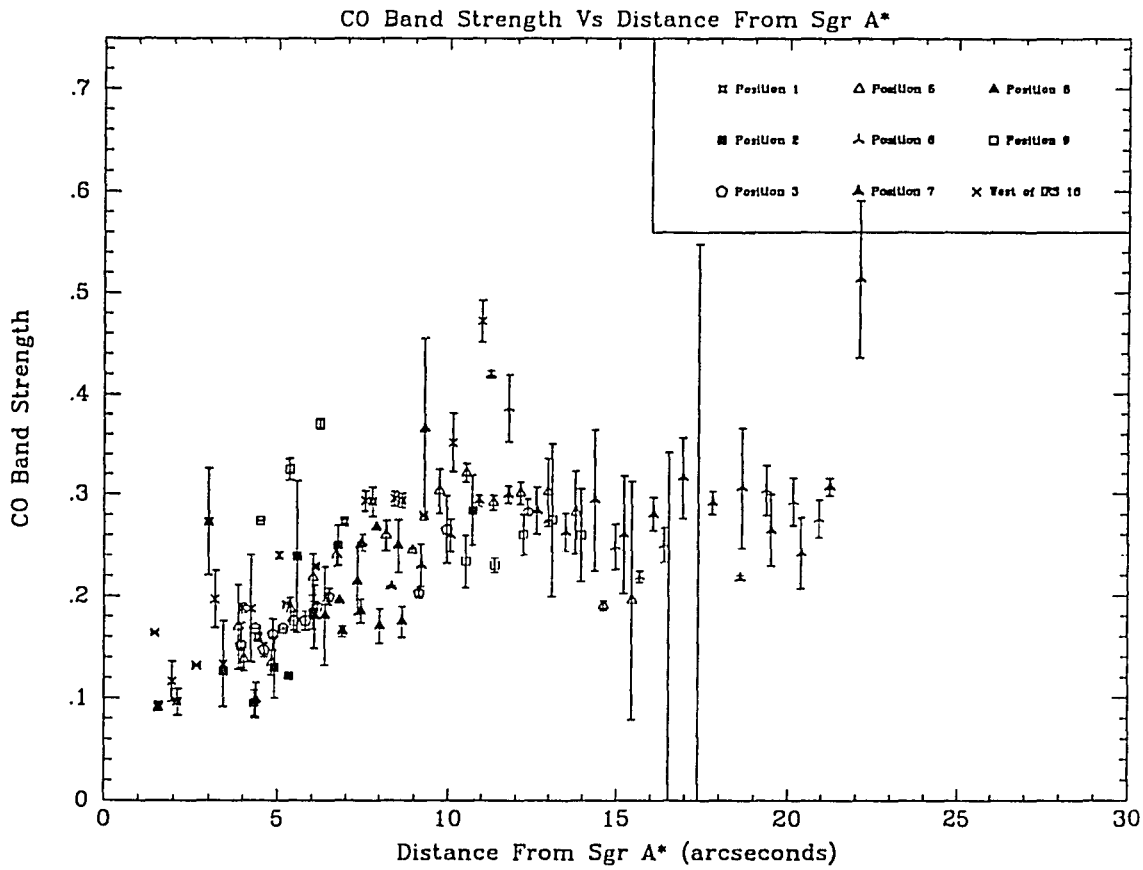

Figure 5-4: The CO Band Strength vs. Projected Angle from Sgr A*. The absorption strength has a high spatial correlation with separation from Sgr A*. The legend shows the correspondence between the markers and the slits. Obvious sources of contamination have been removed from the sample. The correlation is insensitive to recentering to within ±1″ of Sgr A*.

spectra positions. Figure 5-3 shows the estimated signal-to-noise vs. the relative continuum intensity along the spatial direction of the slit. In general, there is good agreement with the theoretical expectation that the signal to noise is proportional to the square root of the accumulated counts.

The CO Absorption Feature

The CO band strength is here defined as the depth of the absorption feature relative to the blueward continuum and this was measured for each spectrum. The intensity profile along each slit was examined for contamination from known point sources on the high resolution map and these were excluded from the CO sample. To determine the spatial position of each spectrum, a fiducial pixel position was identified by the average location of IRS 7 in the velocity standard exposures prior and subsequent to each data frame exposure. This nominal pixel position was assigned the positional offset from IRS 7 recorded in the logbook. Subsequent pixel positions were calculated in the north-south direction by the pixel angular scale.

The CO depth vs. angular distance from Sgr A* is shown in figure 5-4. We confirm the result of earlier studies (Allen *et al.* 1989; Sellgren *et al.* 1990) that CO absorption is diminished within the central 0.35 pc. The most significant result is that the CO depletion is *highly* correlated with projected distance from Sgr A*. The dispersion of the CO spatial correlation is insensitive to recentering within ±1.0″ of Sgr A*, beyond which it becomes considerable. Sellgren *et al.* (1990) showed that the CO strength is constant at a level of ~35%, as expected for a late-type stellar population, from 20″ out to at least 90″. Between 10-20″ their few data points had an average CO strength of 21%. These data in the same region have an average CO strength of 27%, but there is noticeable scatter caused by contaminating blue sources. But it is important to note that at this point the line depths have been uncorrected for the effects of the line-of-sight velocity dispersion. That will be addressed below.

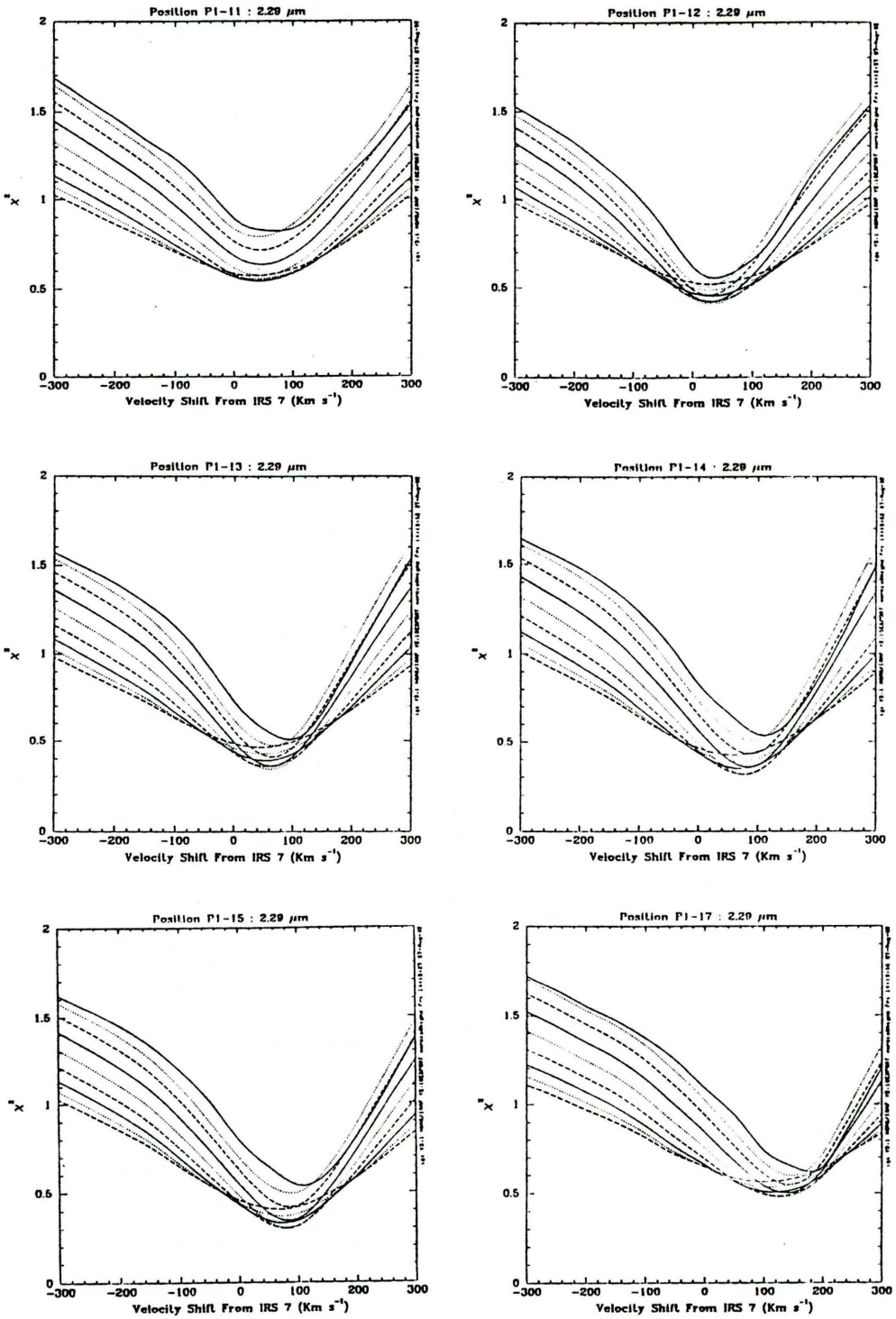

Figure 5-5: The $\chi^2(r)$ vs. V_{OFFSET} curves at velocity dispersions of 0, 25, 50, 75, 100, 125, 150, 175, 200, 250, and 300 km s^{-1} for the six spectra listed in Table 5-2. In each diagram the top curve corresponds to a velocity dispersion of 0 km s^{-1}.

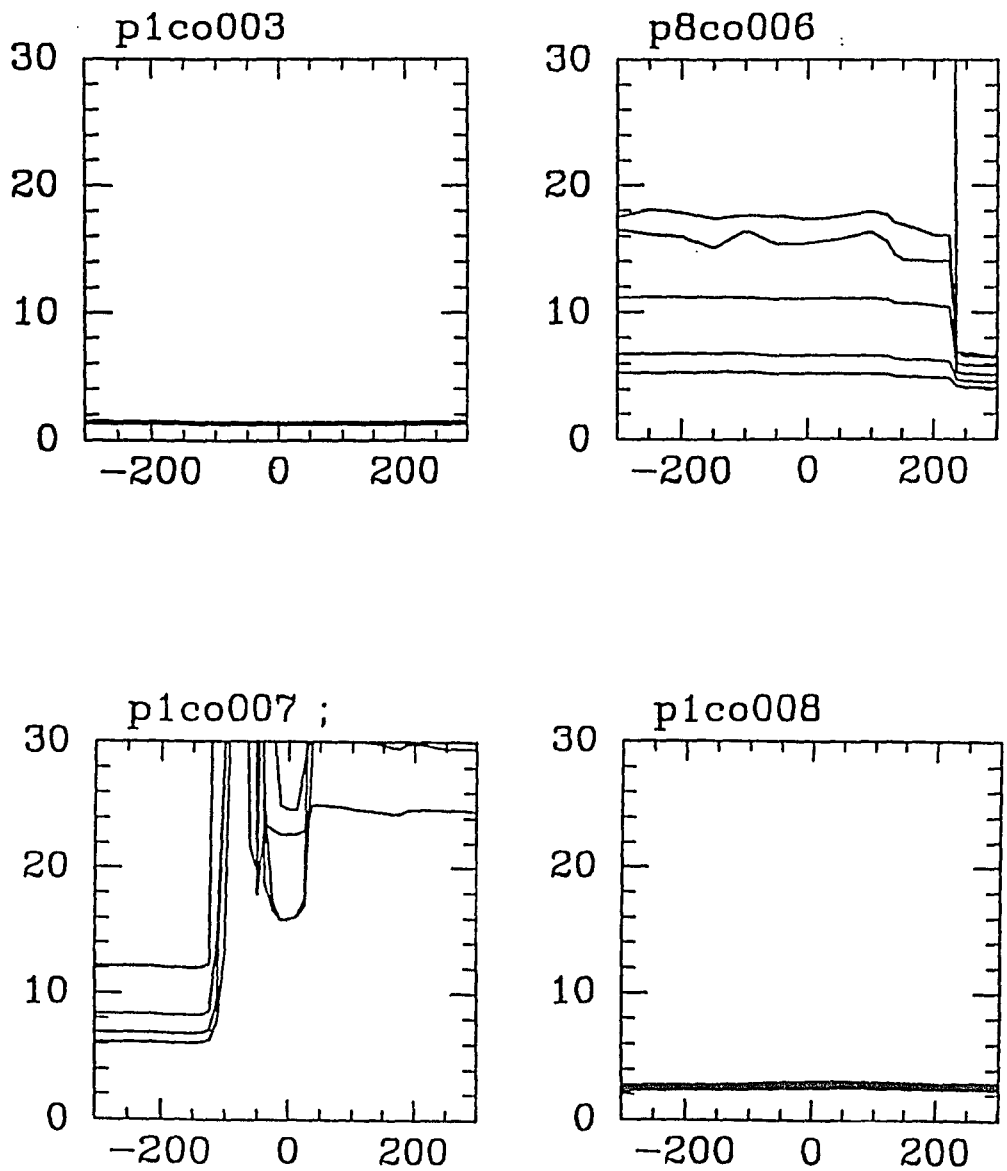

Figure 5-6: Examples of spectra that could not be cross correlated. Examples shown are χ^2 curves that are flat, discontinuous, non-monotonic, and inverted.

The Line-of-Sight Velocities and Velocity Dispersions

Velocity standard exposures were taken from IRS 7 before and after every program spectrum as templates for measuring the radial velocity and velocity dispersion. The templates were made by convolving each spectrum of IRS 7 with a Gaussian function with a width corresponding to velocity dispersions of 0, 25, 50, 75, 100, 125, 150, 200, 250, and 300 km s^{-1}. The spectra were then cross correlated at each velocity dispersion in the following way. The algorithm linearly interpolated the spectra to four times the pixel resolution and renormalized to the CO band depth of the velocity standard at the position of the maximum slope in the CO profile. A series of discrete offset velocities $v_1, v_2, ..., v_N$ were used to compute a correlation coefficient, $R(v_j)$, and its square, $R^2(v_j)$, about the velocity reference spectrum at $v_K = 0.0$ (k = ½ N).

$$R(v_j) = \frac{1}{N} \sum_{i=1}^{N} \frac{F_{ref}(v_i)}{F_{test}(v_i - v_j)}$$

$$R^2(v_j) = \frac{1}{N} \sum_{i=1}^{N} \left(\frac{F_{ref}(v_i)}{F_{test}(v_i - v_j)} \right)^2$$

From the correlation coefficient curves, curves of $\chi^2(v_j)$ vs. v_j were computed at each velocity dispersion, D, following the usual definition of χ^2:

$$\chi^2_D(v_j) = \frac{N\, R^2_D(v_j) - (\, R_D(v_j)\,)^2}{N-1}$$

Unfortunately the yield of successful cross correlations was not very high. Out of 162 spectra, only six from slit Position 1 gave satisfactory results (Figure 5-5). Types of failure included flat χ^2 curves, discontinuous curves, non-monotonic curves with discontinuities, and inverted curves

(Figure 5-6). One possible cause that may be hampering the procedure is the method used to renormalize the spectra. At each position of the spectrum, the slope is computed from the average of the slopes at positions within ± 5 pixels. This is perhaps too sensitive to the effects of decreased signal-to-noise as well as the diminished CO strength near the center. The velocity dispersion, σ_{RAW}, and offset velocity from IRS 7, V_{IRS7}, were determined by finding the minimum of the $\chi^2(v)$ curves in the σ_{RAW}-V_{IRS7} plane by parabolic interpolation. The slit positions and measured values of σ_{RAW}, and V_{IRS7} values are shown in Table 5-2.

Error analysis was done by a Monte Carlo simulation procedure. A template spectrum of IRS 7 was convolved with a Gaussian velocity dispersion, $\sigma_V(0)$, and duplicated 100 times at signal-to-noise ratios of 10, 20, 30,...,90,100. The synthetic spectra were cross correlated and the resulting σ_{RAW} and V_{IRS7} values were measured from the χ^2 curves in the same way as the

TABLE 5-2 :
Raw Velocity Dispersions and Relative Velocities From IRS 7

Slit Position	S/N	θ_{SGRA*} (")	σ_{RAW} (km s^{-1})	V_{IRS7} (km s^{-1})
P1-11	48	5.2	142.5	+41.0
P1-12	61	6.4	98.5	+29.8
P1-13	51	6.9	101.2	+60.7
P1-14	44	7.7	111.3	+77.7
P1-15	43	8.6	112.3	+80.3
P1-17	22	10.3	108.6	+127.8

data. For those trials that produced reliable χ^2 curves, the average and dispersion of the measured $<\sigma_V>$ and $<V_{IRS7}>$ were calculated. In general it was found that successful cross correlation systematically overestimated the velocity dipsersion and systematic velocity with errors that monotonically decreased with increasing signal-to-noise (S/N) (Figure 5-7). Below a S/N of 10, the measured velocity dispersion was ~ 190 km s^{-1} independent of the true

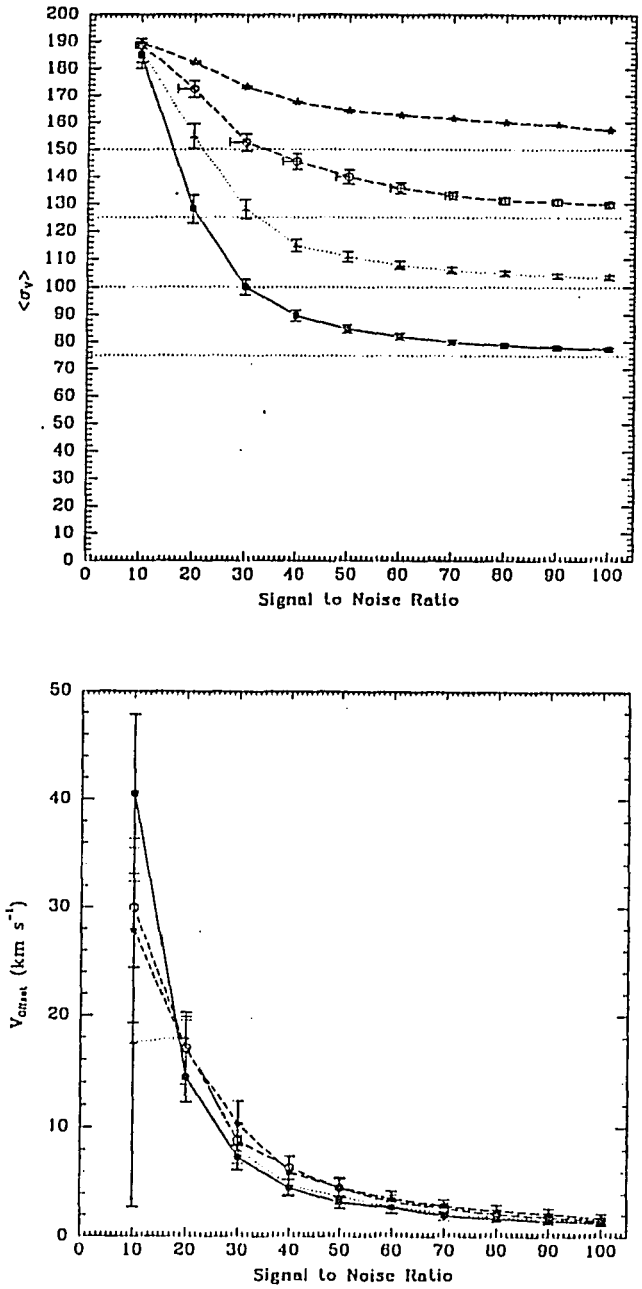

Figure 5-7: Figure 5-7a shows the mean measured velocity dispersion vs. S/N for synthetic input spectra of IRS 7 with intrinsic velocity dispersions of 75, 100, 125, and 150 km s^{-1}. In all instances the cross correlation technique overestimates the dispersion. Figure 5-7b is the mean measured systematic velocity vs. S/N for the same spectra. Generally the systematic error and its standard deviation (Figure 5-7c) depend only on the signal-to-noise ratio for S/N > 20. Figure 5-7d is the fractional error of the velocity dispersion vs. signal to noise and Figure 5-7e shows its standard deviation. Estimates of the velocity dispersion systematic errors can be reliably made for S/N > 40. The percentage yield of successful cross correlations vs. S/N is shown in 5-7f.

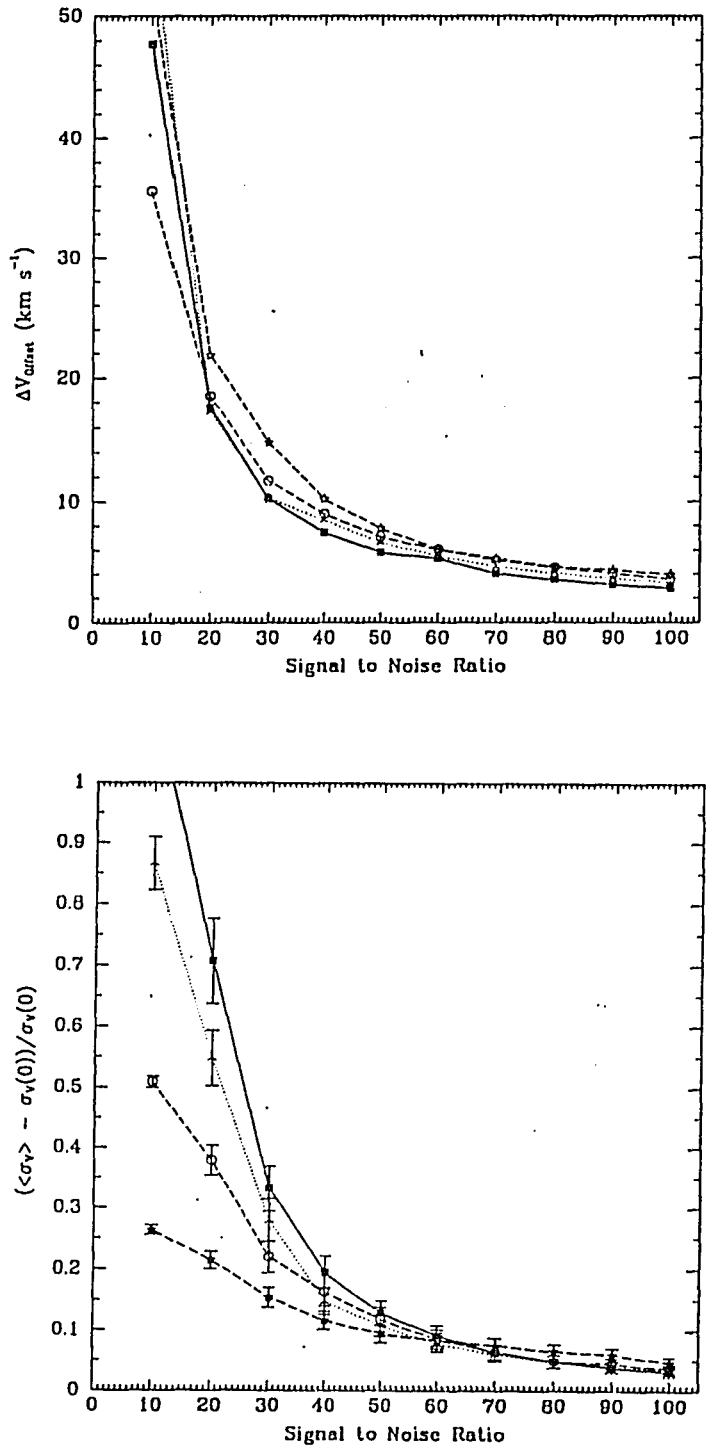

Figure 5-7: Continued.

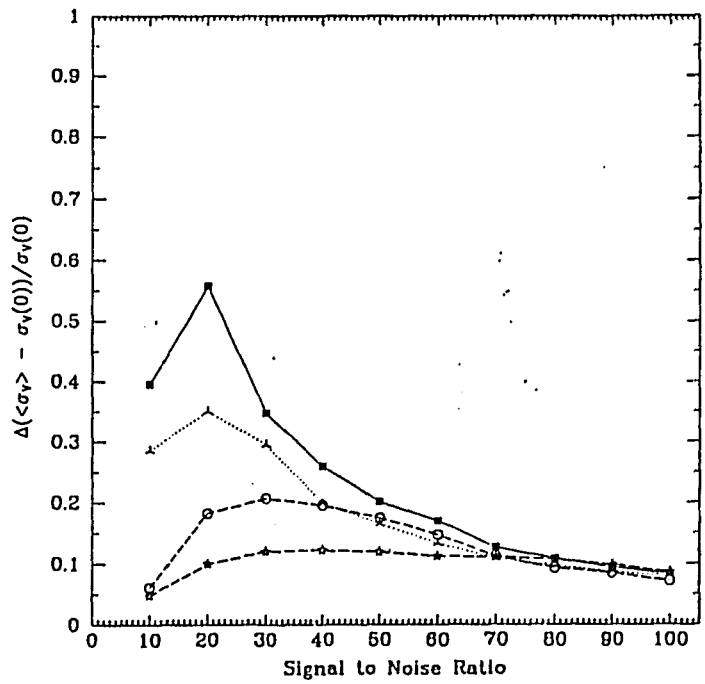

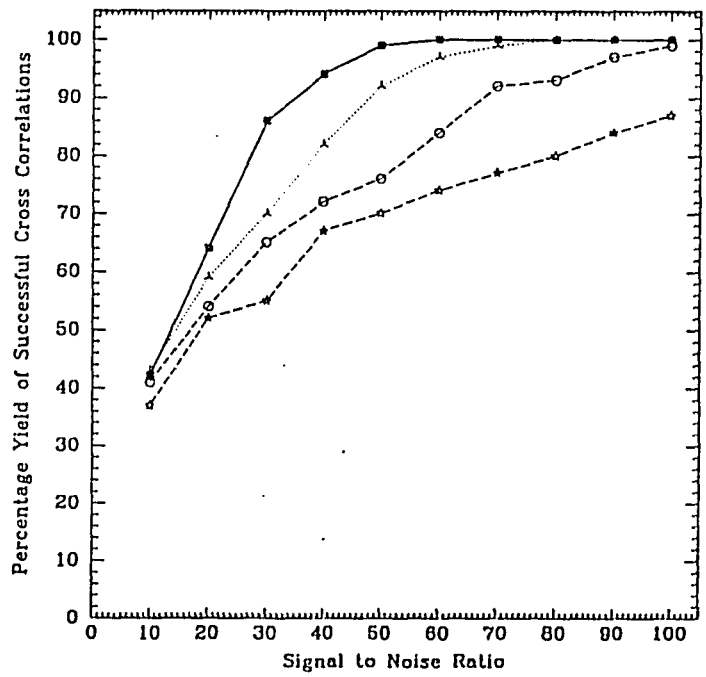

Figure 5-7: Continued.

velocity dispersion while for S/N > 40 the fractional error of the measured velocity dispersion was independent of the true velocity dispersion. Thus for sufficiently high quality spectra, a reliable correction for systematic errors could be made to the measured results. The dispersion of the fractional systematic error was a function of S/N and $\sigma_v(0)$, varying from 0.1 - 0.2 for $\sigma_v(0)$ = 75 -150 km s^{-1}. The yield rate of the cross correlation program was also an increasing function of S/N. At fixed S/N, the yield rate decreased significantly for $\sigma_v(0)$ greater than 100 km s^{-1}. Thus the failure of the program to measure the velocity dispersion can be at least partially attributed to insufficient S/N in the spectra. There is also the consideration that the intrinsic CO depth is decreasing monotonically inside 10″. The fractional error in determining the strength of the feature, ε, as a function of S/N in the continuum will go as

$$\frac{\Delta\epsilon}{\epsilon} = \frac{\sqrt{(1 - \epsilon)(2 - \epsilon)}}{\epsilon} \frac{1}{(S/N)}$$

The decreased S/N in the continua of those spectra with $r \geq 10''$ from the center, as well as the diminished intrinsic strength of the CO feature for those close to the center both have the effect of minimizing the chances for the cross correlation program to renormalize the CO band correctly to that of the template spectrum. The measured systematic velocity with respect to the template spectrum was always on the order of a few km s^{-1} with an error on the order of 5 km s^{-1} for S/N > 20 and was not a strong function of intrinsic velocity dispersion.

Table 5-3 lists the corrected velocity dispersions, V_{LSR} velocities and estimated errors for the measurements listed in Table 5-2. The corrected velocity dispersion is σ_{RAW} / (1+β). The column listing ΔV_{LSR} gives the systematic error correction and dispersion respectively. The V_{LSR} of IRS 7 was taken to be −130 km s^{-1} (McGinn *et al.* 1989).

TABLE 5-3
Velocity Dispersions and Line-of Sight Velocities Corrected For Systematic Errors

Slit Position	S/N	β	Δβ	$\Delta\sigma_{RAW}$ (km s^{-1})	$\Delta VLSR$ (km s-1)	σ_v (km s^{-1})	V_{LSR} (km s^{-1})
P1-11	48	0.13	0.05	21	-4.5/7	126 ± 19	-93 ± 7
P1-12	62	0.08	0.02	15	-2.8/6	91 ± 15	-103 ± 6
P1-13	52	0.11	0.03	17	-3.7/7	91 ± 17	-66 ± 7
P1-14	45	0.12	0.06	19	-4.3/8	99 ± 18	-56 ± 8
P1-15	44	0.12	0.06	19	-4.3/8	100 ± 18	-54 ± 8
P1-17	22	0.45	0.50	38	-14.4/7	75 ± 37	-16 ± 17

Given the relatively poor S/N of the last measurement, the data will be examined in two groups: set #1 containing all six data points in Table 5-3 and set #2 containing only the first five. The σ_v vs. r_{SgrA*} and V_{LSR} vs. r_{SgrA*} diagrams are shown in Figure 5-8. The average velocity dispersion of the sample shows a slight gradient but the average value, 98.8 ± 2.4 km s^{-1} is intermediate between the results of Rieke and Rieke (1988) at 75 km s^{-1} and McGinn *et al.* (1989) at 125 km s^{-1} for this same region. The most striking result is the V_{LSR} vs. r_{SgrA*} diagram. The positions of these velocities have small angular inclinations from the Galactic equator and agree in sign with the results of McGinn *et al.* (1989). It is reasonable to interpret them as a measurement of the Galactic rotation curve over the same range of radius. The data show the Galactic Center stellar rotation curve inside 10″ from Sgr A* has a gradient of ~16 km s^{-1} $arcsec^{-1}$. Figure 5-9 shows the velocity data plotted with the V_{LSR} values measured by McGinn *et al.* (1989) (their positive velocity data have been included by reflecting them onto the approaching side) and there is good agreement with the velocity measurements at 10.3″. Starting with a minimum velocity near 0 km s^{-1} at 10″, the curve begins to rise to at least 100 km s^{-1} at the 5″ position. Although it has an intrinsic characteristic length scale 100 times smaller, this rotation curve has similar behavior to the rotation curve of the central few

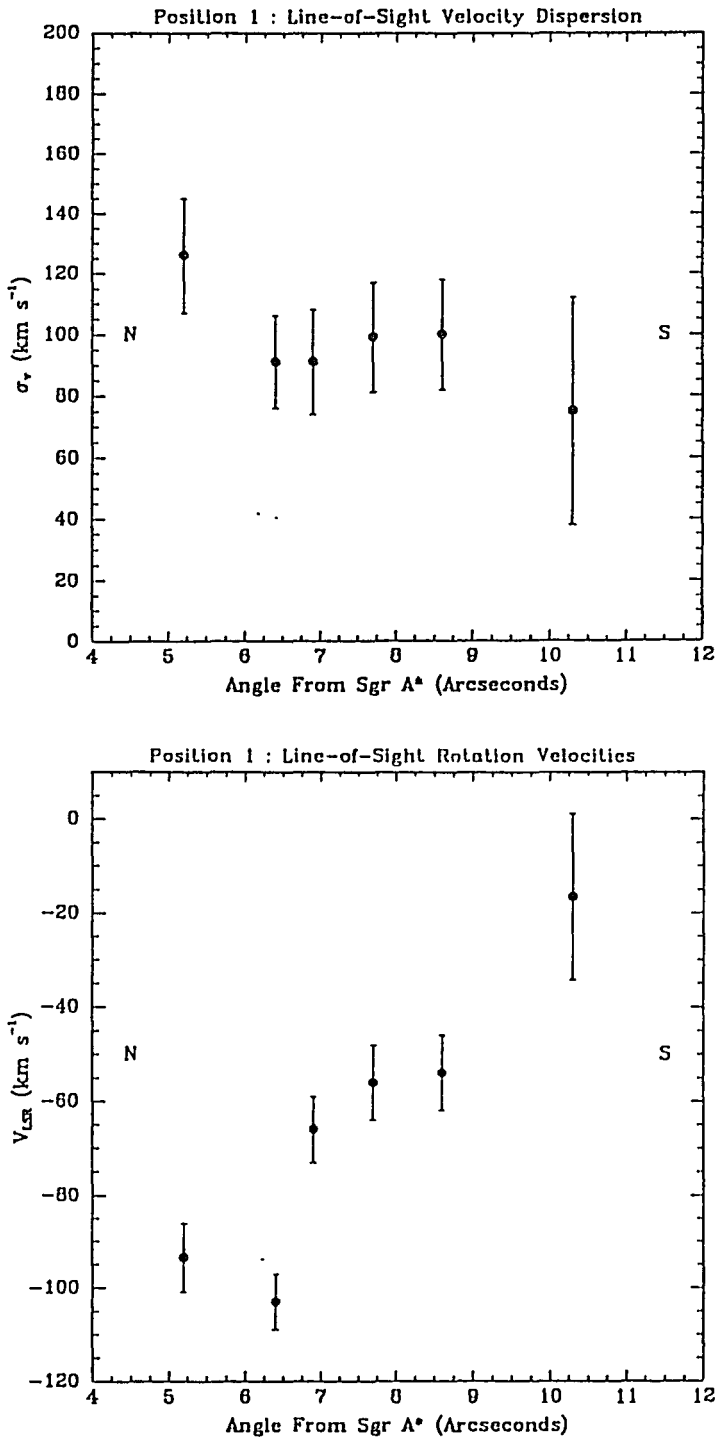

Figure 5-8: The top figure is the velocity dispersion vs. projected angle from Sgr A* for Position 1 data points. The north and south ends of the slit are indicated. The bottom figure shows the V_{LSR} vs. r_{SgrA*} curve which indicates rapidly increasing Galactic rotational velocities inside of 10″ from Sgr A*.

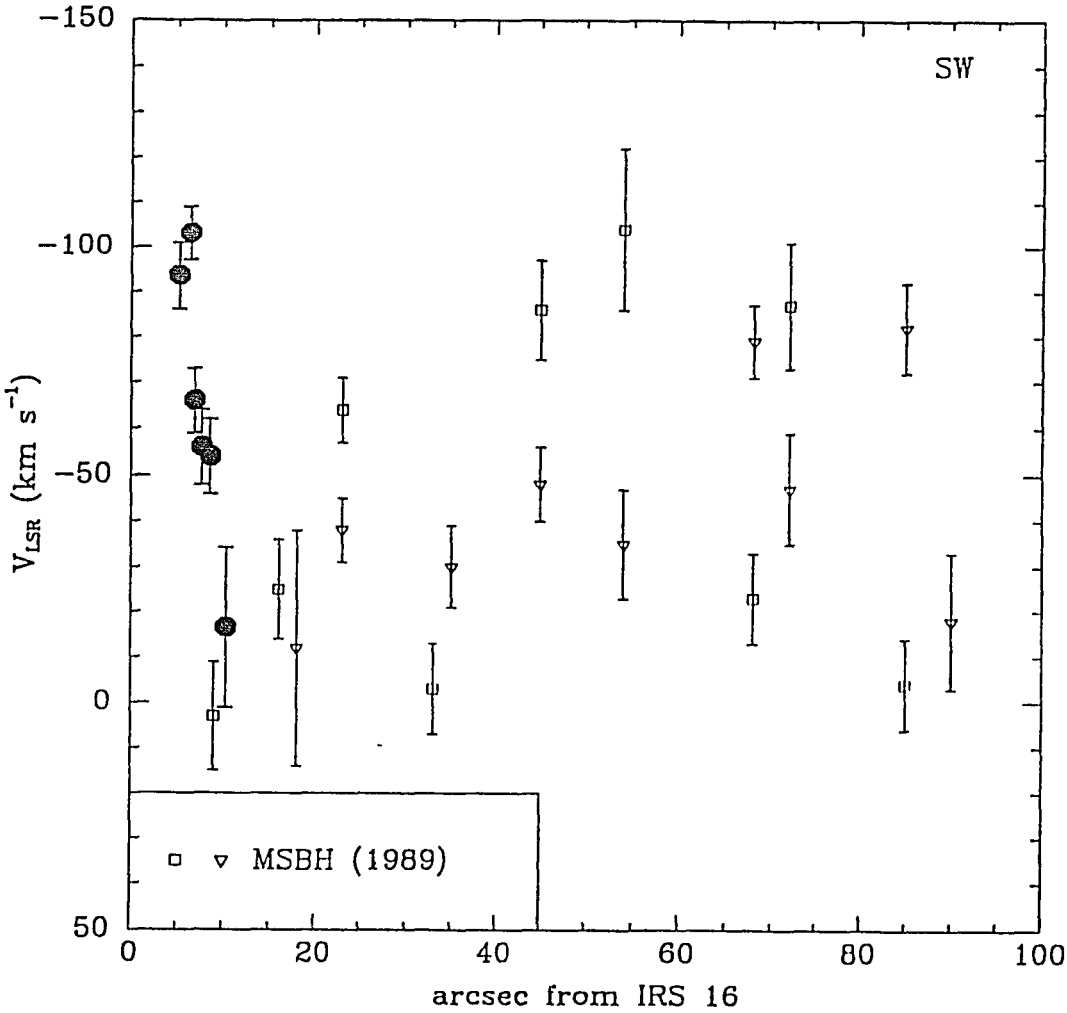

Figure 5-9: The figure shows the Galactic Center rotation curve of McGinn *et al.* (1989) from the CO absorption feature using 20″ apertures. Data points marked by (□) have approaching LSR velocities while points marked by (▽) have receeding velocites and have been reflected onto the approaching side. The filled circles are the data points from the present study. The rotation curve reaches a minimum of − 0 km s^{-1} near 10″ and then begins an abrupt rise with decreasing radius.

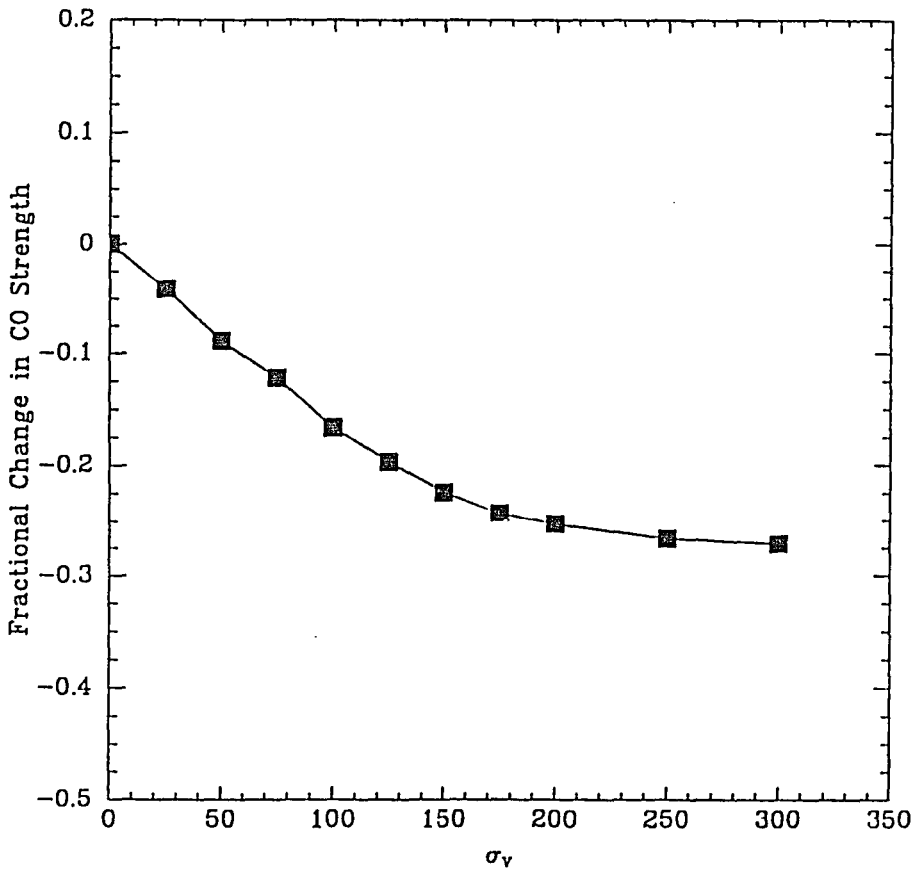

Figure 5-10: The fractional change in the intrinsic CO band depth due to velocity broadening as measured from the velocity template spectra of IRS 7. The fractional change for the measured data points at slit Position 1 is of the order of 15-20%

arcseconds of M31 at optical wavelengths (Kormendy 1988; see Figure 2).

The CO band strength is at least partially depleted by the effects of velocity broadening. The fractional change in CO strength vs. velocity dispersion was computed from the IRS 7 template spectra (Figure 5-10). In the range of the measured velocity dispersions of the data, the fractional change in the CO strength is approximately 15-20%. A nominal correction of 20% due to velocity broadening was applied to the CO band strengths that are treated below in the discussion section.

The Enclosed Mass vs. Radius

By assuming the velocity dispersion and bulk motion of the CO emission primarily originates from a region along the line-of-sight at each projected radius, the enclosed mass vs. radius may be derived by application of the first moment of the Boltzmann equation as discussed above. Here it was assumed that the velocity ellipsoid was isotropic ($\lambda = 2$) and this is partially supported by the fact that $V_{LSR}/\langle\sigma_v\rangle \sim 1$ (Kormendy and Illingworth 1982; McGinn *et al.* 1989) but complete justification can only come with isophotal information of the unresolved emission for this region which is presently not available. Since the CO absorption profile cannot be fitted properly unless R_{CORE} of the 2.2μm light distribution is smaller than ~2.5″ (see below) we will use $n(r) \propto r^{-1.8\pm0.1}$ (Becklin and Neugebauer 1968; Allen, Hyland, and Jones 1983) for the number density of 2.2μm sources, in agreement with McGinn *et al.* (1989). Two equivalent forms of the moment equation were applied to the two data sets:

$$M(r) = \frac{r\,\sigma_v^2}{G}\left(- \frac{d \ln n(r)}{d \ln r} - \frac{d \ln \sigma_v^2}{d \ln r} + \frac{V_{LSR}}{\sigma_v^2} \right)$$

$$M(r) = \frac{r\,\sigma_v^2}{G}\left(- \frac{d \ln n(r)}{d \ln r} - \frac{2r}{\sigma_v}\frac{d\sigma_v}{dr} + \frac{V_{LSR}}{\sigma_v^2} \right)$$

with the additional three case assumptions

CASE I	DATA SET #1	$d \ln \sigma_v^2 / d \ln r = -0.99 \pm 0.80$
	DATA SET #2	$d \ln \sigma_v^2 / d \ln r = -0.93 \pm 0.86$
CASE II	DATA SET #1	$d \sigma_v / dr = -5.8 \pm 6.0$ km s^{-1} arcsec^{-1}
	DATA SET #2	$d \sigma_v / dr = -5.2 \pm 7.1$ km s^{-1} arcsec^{-1}
CASE III	DATA SET #1/#2	$d \sigma_v / dr = 0$

The velocity dispersion gradients were determined by a linear least squares fit to the data. (Case III is for an isothermal sphere with no velocity dispersion gradient.) Given these assumptions, and applying the above equations to both data sets the following *M(r)* vs, *r* values are derived.

Including the velocity dispersion of the P1-17 spectrum into the estimates of the velocity dispersion gradient does not greatly affect the average enclosed mass, but it does tend to produce a more negative gradient in the M(r) values. The logarithmic velocity gradient in Case I produces higher mass estimates than the simple gradient of Case II. Assuming positional errors of ±0.5″, the major contributors to the errors of the above mass estimates are from the velocity dispersion and its gradient. Case II produced larger formal errors because the error term for the dispersion gradient depends on r^2 while in Case I this error only depends on *r*.

TABLE 5-4 : ENCLOSED MASS VS. RADIUS ESTIMATES

Slit Position	$r_{Sgr A^*}$ (″ | pc) R_0 = 6.9 kpc	ENCLOSED MASS (10^6 $M_\odot$)				
		CASE I		CASE II		CASE III
		Data Set #1	Data Set #2	Data Set #1	Data Set #2	Data Set #1/#2
P1-11	5.2 | 0.17	2.14 ± 0.78	2.11 ± 0.80	1.82 ± 0.55	1.78 ± 0.58	1.51 ± 0.39
P1-12	6.4 | 0.22	1.68 ± 0.53	1.66 ± 0.53	1.61 ± 0.49	1.57 ± 0.53	1.27 ± 0.27
P1-13	6.9 | 0.23	1.48 ± 0.60	1.45 ± 0.61	1.43 ± 0.57	1.39 ± 0.62	1.03 ± 0.32
P1-14	7.7 | 0.26	1.83 ± 0.77	1.79 ± 0.78	1.78 ± 0.75	1.72 ± 0.82	1.24 ± 0.40
P1-15	8.6 | 0.30	2.06 ± 0.87	2.02 ± 0.89	2.07 ± 0.90	2.00 ± 0.99	1.40 ± 0.45
P1-17	10.3| 0.35	1.28 ± 1.30	-	1.56 ± 1.38	-	0.83 ± 0.80
<M(r)>		1.75 ± 0.14	1.80 ± 0.12	1.71 ± 0.09	1.69 ± 0.10	1.21 ± 0.10

Discussion

Interpretations of the CO Absorption Feature

Sellgren *et al.* (1990) (SMBH) were the first to examine what changes in the unresolved population would be needed to produce the observed CO depletion. The two models they discussed with their observations will be reintroduced here and compared to the present results. Additionally, more generalized models will also be compared.

We first consider that the 2.2μm light distribution is known to depend on radius as $R^{-0.8}$, which implies a stellar number density that goes as $R^{-1.8}$. The core radius of this distribution has been the subject of some controversy with Allen *et al.* (1983) reporting a core radius of ≈ 1.0″ while Rieke and Lebofsky (1987) favored a value of ≈ 20″. In any case, the luminosity density of 2.2μm sources can be represented by:

$$F_K(r) = F_K(0) \quad ; \; r \leq R_{CORE}$$

$$F_K(r) = F_K(0) \times \left(\frac{r}{R_{CORE}}\right)^{-1.8} \quad ; \; r > R_{CORE}$$

The luminosity density of CO absorbing sources in the models presented by SMBH were:

MODEL SMBH-A

$$F_{CO}(r) = 0 \quad ; \; r \leq R_{CO}$$

$$F_{CO}(r) = F_K(r) \quad ; \; r > R_{CO}$$

MODEL SMBH-B

$$F_{CO}(r) = F_K(R_{CO}) \quad ; \; r \leq R_{CO}$$

$$F_{CO}(r) = F_K(r) \quad ; \; r > R_{CO}$$

Model A represents a situation where CO absorbing stars are completely absent inside a distance of R_{CO}. This could be due to an interface between two populations (a very unlikely situation) or the CO in the stellar photospheres is somehow being removed (by star-star collisions; photoionizations; ablation by outflowing material; etc.). Model B has a cool population extending into the core, but the number density of CO absorbing stars is constant for $r < R_{CO}$. The remaining 2.2μm emission is augmented by a hotter population, but in such a way that the total light profile still obeys the $R^{-0.8}$ law.

For clarity, the following definitions will be made:

$F_K(i)$ ≡ the continuum luminosity density at K.
$F_{CO}(i)$ ≡ the 2.3μm luminosity density.
$\mu_K(i)$ ≡ the continuum surface brightness at K.
$\mu_{CO}(i)$ ≡ the surface brightness at 2.3μm.
i = 1 will represent the stellar component with CO absorption.
i = 2 will represent the stellar component without CO absorption.

$\varepsilon \equiv$ the average CO depth/star for the $i = 1$ stars.
$r = r(x,y,z) =$ the radius from the Galactic Center.

Placing the origin of the coordinates at the Galactic Center and orienting the z-axis along the line-of-sight toward the center, the surface brightness μ at projected radius $(x^2 + y^2)^{1/2}$ and the luminosity density $F(r)$ are related by

$$\mu(x,y) \propto \int_{-R_0}^{+\infty} F(\, r(x,y,z)\,)\, dz.$$

For stars with CO absorption we take $F_{CO}(1) = (1 - \varepsilon) \times F_K(1)$, and for stars without CO absorption $F_{CO}(2) = F_K(2)$. Using these definitions, the observed CO band depth at a each position is given by

$$\varepsilon_{eff} = \frac{\mu_K - \mu_{CO}}{\mu_K}$$

$$= \frac{(\mu_K(1) - \mu_{CO}(1)) + (\mu_K(2) - \mu_{CO}(2))}{\mu_K}$$

$$= \varepsilon \frac{\mu_K(1)}{\mu_K}$$

Thus for the SMBH models, where ε is regarded as a constant for all CO absorbing stars, the observed band depth is a measure of the fractional contribution of CO absorbers to the total 2.2μm surface brightness. Neither of the SMBH models with the parameter values stated by them compare well with these observations but SMBH-A can be matched with $R_{CO} \approx 8.5''$ (Figure 5-11). Their preferred model, SMBH-A, matches $R_{CO} = 10''$ adequately but it falls away too steeply at smaller projected radii. Model SMBH-B with $R_{CO} = 15''$ does not fit the shoulder of the CO absorption curve very well, but it does make a better fit inside of 10″. SMBH were

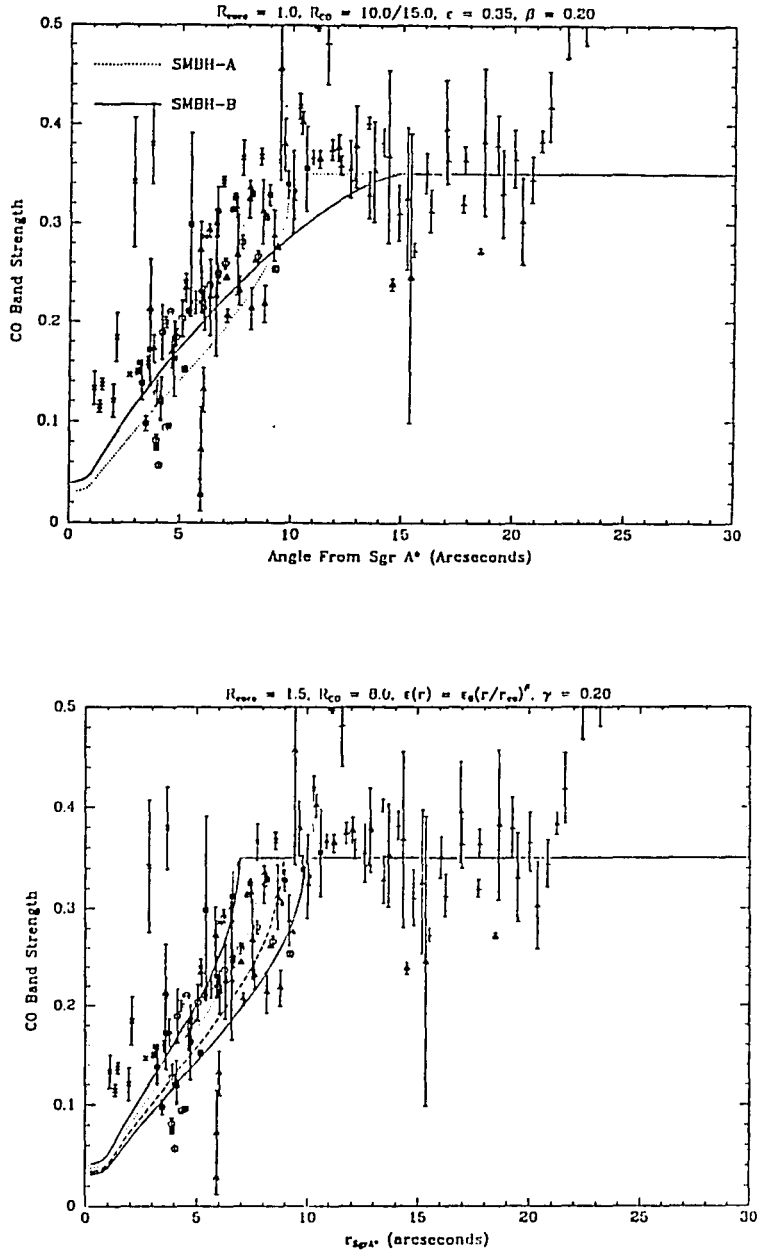

Figure 5-11: The top figure shows the observed CO absorption profile (corrected by 20% for velocity broadening effects) compared to the Sellgren *et al.* (1990) models SMBH-A ($F_{CO}(r) = 0$ for $r < 10''$) and SMBH-B ($F_{CO}(r) = F_K(15'')$ for $r < 15''$). Neither of the models give a satisfactory fit over the range of the observations. The bottom figure shows model SMBH-A with $R_{CO} = 7''$, $8''$, $9''$, and $10''$ from which an approximate fit of $8.5''$ is indicated.

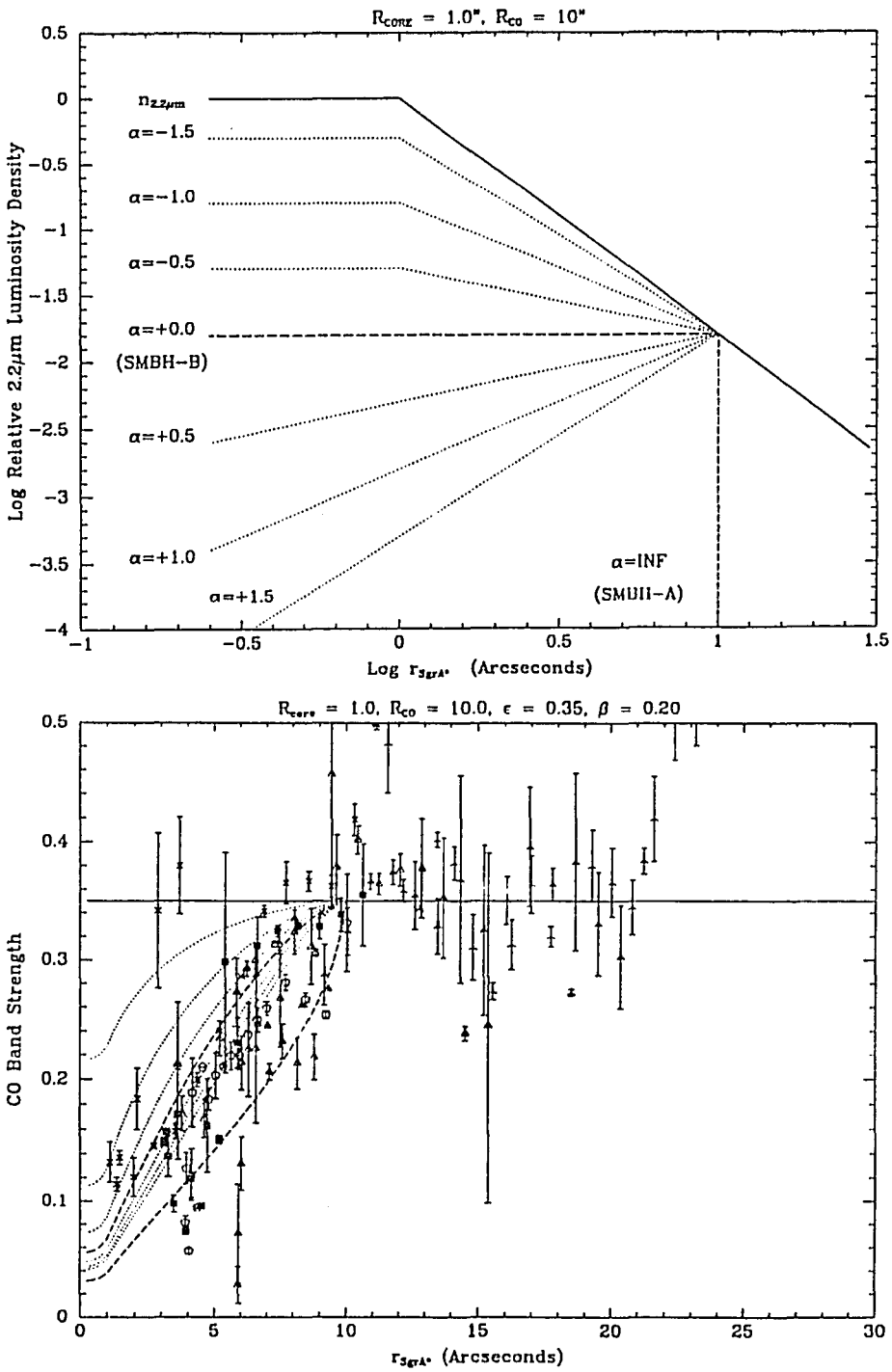

Figure 5-12: The top figure shows the distribution of the total number of 2.2μm sources and the number of CO absorbers for various values of the parameter α for R_{CO} = 10" and R_{CORE} = 1.0". The Sellgren *et al.* (1990) models "A" and "B" correspond to parameter values of α = 0 and α = ∞. The CO absorption will only be sampled at the projected radius if α > 0, otherwise the observed emission will be due to material at a true radius of R_{CO}. The bottom figure is the resulting CO absorption strength vs. r_{SgrA*} curves with a velocity broadening correction of +20% applied. The assumed intrinsic CO band strength for the population is 35% (Sellgren *et al.* 1990).

not satisfied with the interpretation of model B because of the contrived situation that would have to exist for a bluer population component to be added in such a particular way that the 2.2μm light profile would retain its $R^{-0.8}$ form into the core radius. They preferred model A, which, again, can be interpreted as the total destruction of CO in the photospheres of those stars with $r < R_{CO}$. They estimated that the ambient UV radiation field emerging from the central parsec ($\approx 10^{51}$ sec^{-1}; Becklin, Gatley, and Werner 1982) was insufficient to cause the depletion out to such a large distance but stellar collisions (Phinney 1989; see below) were not ruled out.

These models can be further extended by considering the CO luminosity density to be varying as

$$F_{CO}(r) = F_K(R_{CO}) \times \left(\frac{r}{R_{CO}}\right)^{\alpha} \quad ; \quad r \le R_{CO}$$

$$F_{CO}(r) = F_K(r) \quad ; \quad r > R_{CO}$$

where $F_K(r)$ has the same form given above. The parameter values $\alpha = \infty$, $R_{CO} = 10''$ and $\alpha = 0$, $R_{CO} = 15''$ reproduce models SMBH-A and SMBH-B respectively. Figure 5-12 shows the luminosity density for both the total 2.2μm and CO absorbing distributions for various values of α and $R_{CO} = 10''$ and the resulting CO band strength profiles compared to the observations. (For models with $\alpha < 0$ an additional constraint for $r < R_{CORE}$ is applied such that $F_{CO}(r) = F_{CO}(R_{CORE})$ so that the number density of CO absorbers will remain bounded.) The model fits are sensitive to the ratio R_{CO}/R_{CORE}, with values less than ≈ 5 giving excessive amounts of CO absorption inside of R_{CO}. One of the important results of these data is that they favors values of the 2.2μm core radius that are no greater than $\approx 2.0''$. If a two component stellar population is present, there must be a very large fraction of stars too hot for significant CO absorption near the center of the stellar distribution to adequately diminish the CO strength.

Yet another situation can be considered instead of a two-component population. The

CO band strength is a function of both luminosity class and temperature (Kleinmann and Hall 1986) so we consider the effect of gradual changes in the feature. We allow the 2.2μm light distribution to be due to a single component of stars, but instead let the parameter ε be a function of radius inside the projected distance R_{CO}.

$$\varepsilon(r) = \varepsilon(R_{CO}) \times \left(\frac{r}{R_{CO}}\right)^{\beta} \quad ; \quad r \leq R_{CO}$$

$$\varepsilon(r) = \varepsilon(R_{CO}) \quad ; \quad r > R_{CO}$$

The observed CO band strength will then be given by

$$\varepsilon_{eff} = \frac{\mu_K - \mu_{CO}}{\mu_K} = \frac{\int_{-\infty}^{+\infty} \varepsilon(r) \times F_K(r)\, dz}{\int_{-\infty}^{+\infty} F_K(r)\, dz}$$

which is the average band depth along the line-of-sight, weighted by the luminosity density. If we now examine the integrand of the numerator in the range $R_{CORE} < r < R_{CO}$ we find

$$\varepsilon(r) \times F_K(r) = \varepsilon(R_{CO}) \left(\frac{r}{R_{CO}}\right)^{\beta} \times F_K(R_{CO}) \left(\frac{r}{R_{CO}}\right)^{-1.8}$$

$$= \varepsilon(R_{CO}) \times F_K(R_{CO}) \left(\frac{r}{R_{CO}}\right)^{\beta-1.8}$$

Thus for models with a single population component and $\varepsilon = \varepsilon(r)$, a given value of β is equivalent to a SMBH model with a value of $\alpha + 1.8$.

This result has very important consequences for interpretations of the line-of-sight

velocity dispersions used in measuring the enclosed M(r). If the stellar population inside R_{CO} is consistent with model SMBH-A with of $\alpha > 0.5$-1.0, as favored by the observations, then the observed CO band depth is dominated by stars at a true radius of R_{CO} and efforts to measure the enclosed mass vs. radius cannot reliably proceed to smaller projected radii. But if the CO depletion is caused by a process that gradually affects a single population of late-type stars where $\varepsilon \propto r^{\beta}$, and $\beta < 1.8$, the effective value of α will be less than 0 and the observed line-of-sight velocity dispersion will be dominated by stars at the projected radius, even for $r < R_{CO}$. The model fits seem to favor parameter values of $\alpha >> 1$ and $R_{CO} \approx 8.5''$. By just considering the observed CO absorption profile alone, it appears that the CO absorption feature observed at *projected* radii less than R_{CO} is dominated by stars with a *true* radius of R_{CO}. If this is the true situation then it would mean the enclosed mass vs. radius measurements have not been consistently applied.

The Galactic Center Rotation Curve

The models above that attribute the observed CO feature to stars near a true radius of R_{CO} are incompatible with the turnover in the V_{LSR} vs. r_{SgrA^*} curve near *10″*. Figure 5-13 shows that the CO strength is correlated with both σ_v and V_{LSR}. The rotational velocity gradient cannot be due to a corrective 1° rotation that was applied to the data because of a tilt in the array. Even if systematic velocity errors are present, the change in the velocity gradient across 6 pixels (corresponding to the spacing of the data points examined here) would only be on the order of 1 km s^{-1} $arcsec^{-1}$.

The measurements from P1-14 and P1-15 are nearly identical in CO depth, V_{LSR}, and σ_v. The intensity profile at this position shows a slight enhancement in the emission and the CO absorption profile shows a plateau superimposed on a nearly parabolic profile (Figure 5-14). There is a faint resolved source near this position that is apparent on the high resolution K map

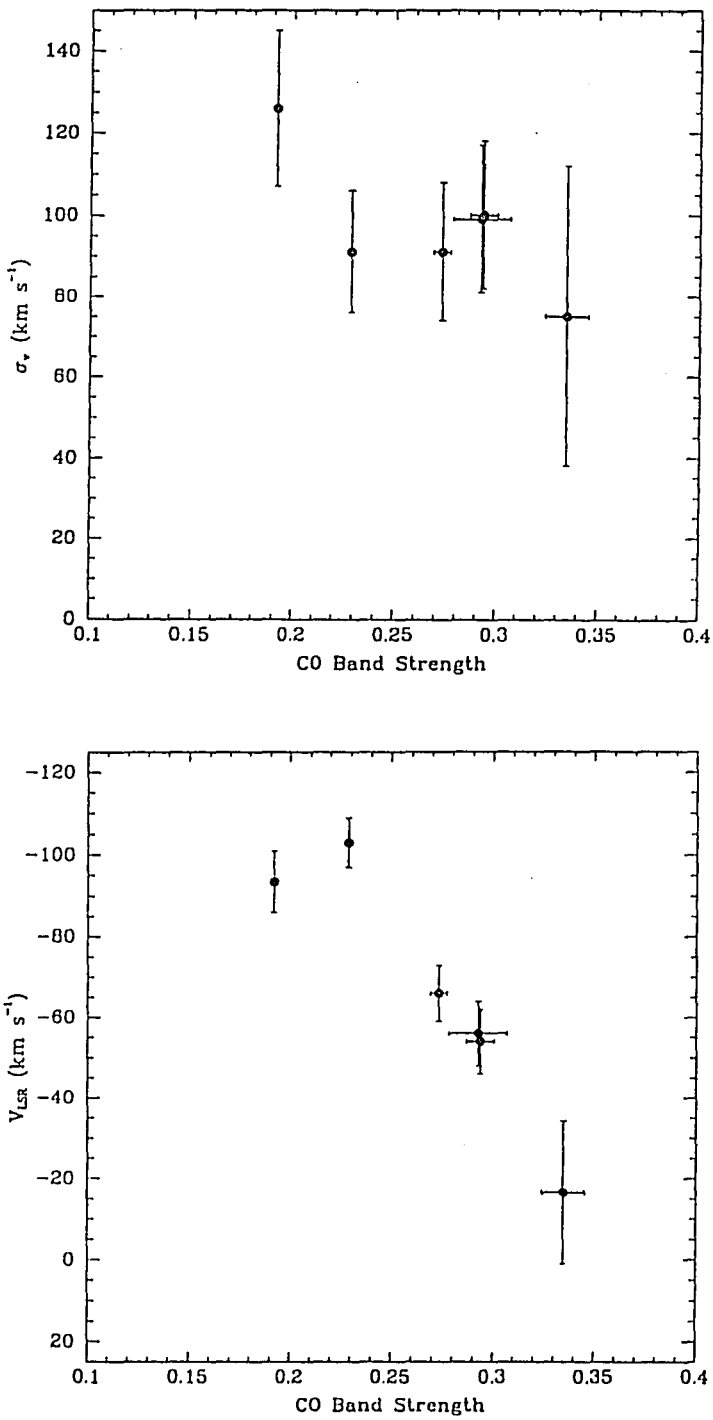

Figure 5-13: The top figure is the σ_v vs. r_{SgrA*} for the measured points at from slit P1. The bottom figure is the corresponding V_{LSR} vs. r_{SgrA*} diagram. Both plots show the CO band strength is anticorrelated with these kinematic quantities.

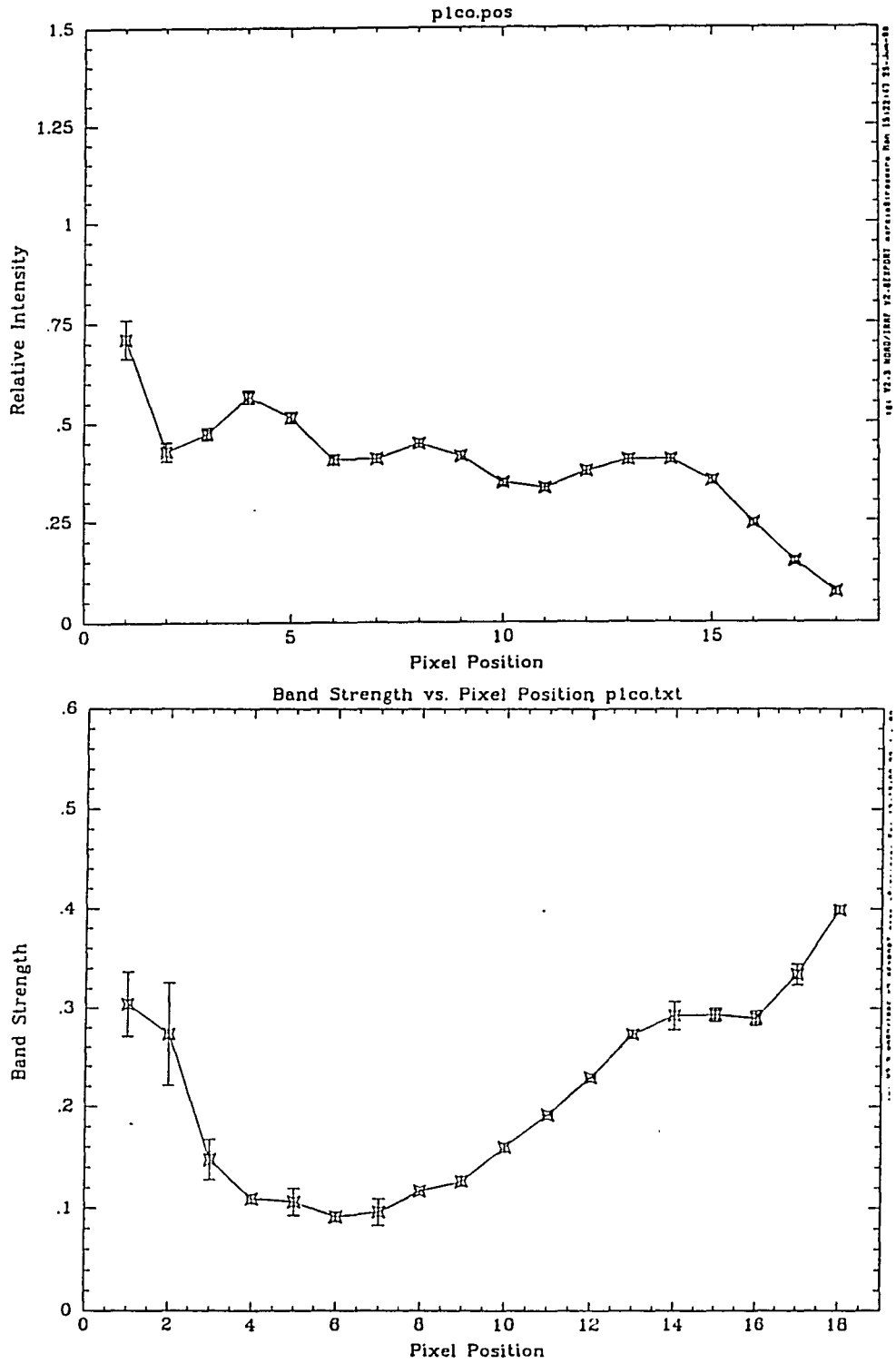

Figure 5-14: Relative Intensity and CO band strength vs. Pixel Position for slit P1. The plateau in the CO absorption for pixels 14 and 15, as well as the enhanced emission suggest these pixels are contaminated by a resolved source.

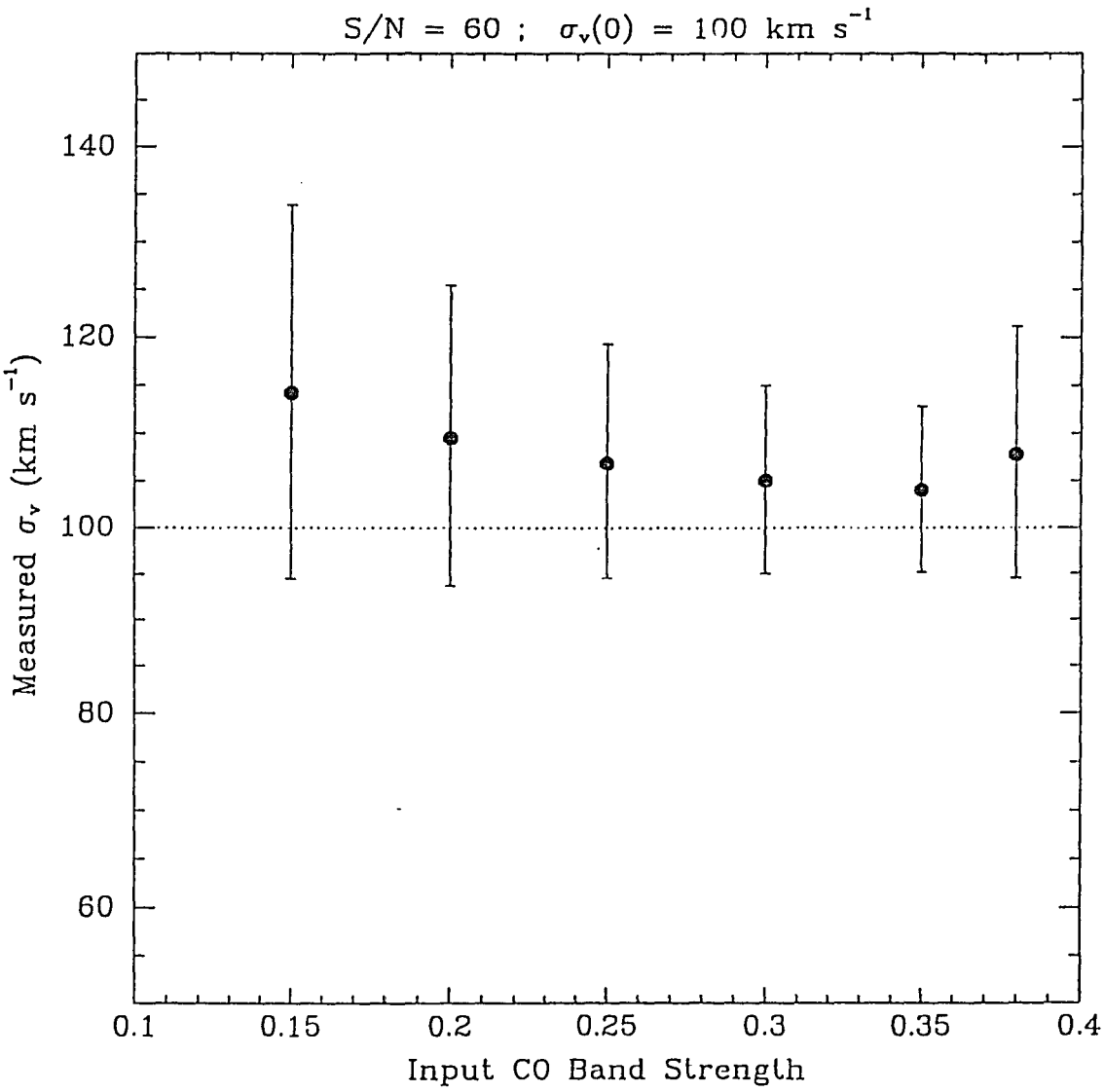

Figure 5-15: The effect of the intrinsic CO band strength on the systematic errors of the cross correlation algorithm at S/N=60 calculated from synthetic spectra made from IRS 7. The variations in the error of σ_v is from 5-10% over the range of CO band strength measured in the data. More important for the stellar rotation curve are the V_{LSR} errors which only vary by ~ 2 km s^{-1} over the range of CO depths.

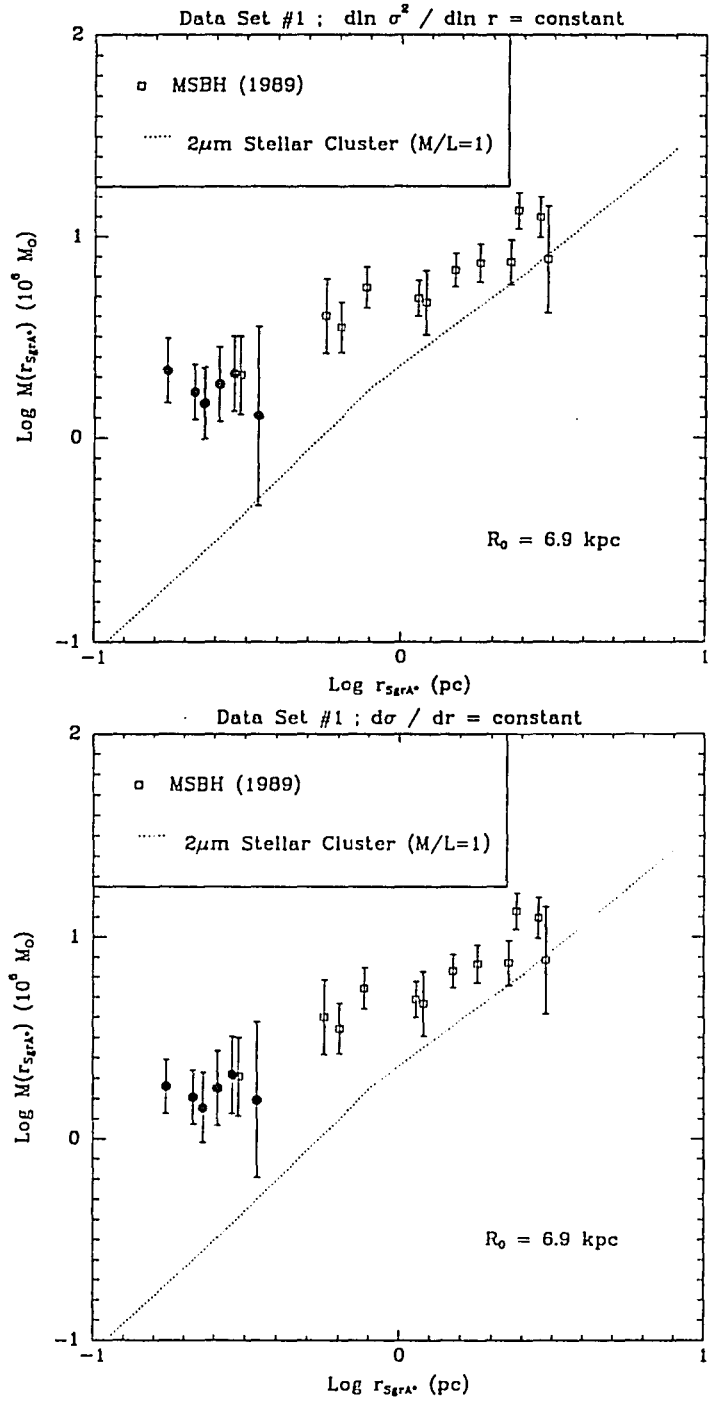

Figure 5-16: The enclosed mass vs. r_{SgrA^*} for Case I, Data Set #1 (top) and Case II, Data Set #1 (bottom). The dotted line is the predicted enclosed mass model of McGinn *et al.* (1989) (see their fig. 10) derived from the 2.2μm light distribution (Becklin and Neugebauer 1968; Matsumoto *et al.* 1982), assuming a M/L ratio of 1 $M_\odot/L_\odot$ and calibrated by the enclosed mass estimates of HI gas at 300pc (Listz and Burton 1978) and then corrected for a value of R_0 = 6.9 kpc. The open squares are the enclosed mass estimates by McGinn *et al.* (1989) made by the CO absorption velocity dispersion of the unresolved stellar emission with $r > 9''$. The results of the present study are consistent with a constant enclosed mass with a high M/L ratio.

(Rieke and Rieke, unpublished) that would then also imply a small positional error in the placement of the slit by about 0.5″. These facts would all indicate contamination by a point source. But this is perhaps not the whole explanation because the CO velocity dispersion of a single source would clearly be separable from the measured velocity dispersions of ~100 km s^{-1}. So either there are still significant contributions in the emission from the unresolved background or this is perhaps a binary or small cluster of late-type stars. Slit positions P1-12 and P1-13 have similar velocity dispersions but they have very different values of V_{LSR}. The remaining two positions show no indication of any contamination. Even with the rejection of the measurements that have possible resolved source contamination, the gradients in V_{LSR} and σ_v are still present and are perhaps better determined.

These velocity results are not due to spurious results of the cross correlation technique due to decreasine CO band strength. This is shown by simulating different CO band strengths from the template IRS 7 spectrum that are then cross correlated with the original. Figure 5-15 shows that for a test at a S/N = 60 there are no significant variations in the systematic errors due to decreasing CO strength.

If the interpretation of the SMBH models discussed above is correct, CO absorption at a true radius of R_{CO} would be expected to have a measured $V_{LSR}(\theta)$ vs. r_{SgrA*} curve that would *decrease* with decreasing separation from Sgr A* as $V_{LSR}(r) = V_{LSR}(R_{CO}) \times SIN(\pi/2 \times r_{SgrA*}/R_{CO})$ due to projection effects. If this unlikely situation were the case, then there are *large* azimuthal changes in the rotation speed of the stars and the true rotation speed is in fact much larger. Thus the velocity observations indicate that CO absorption lies mostly at the projected radius.

The velocity curve implies that CO depletion in the central 0.5 pc is due to dynamical effects on the stars orbiting inside 10″. Phinney (1989) estimated that probability for a giant-dwarf collision in the central cluster to be ~ $0.02\sigma_{80}\ r_{pc}^{-2}$ based on the expected rate of stellar collisions and the time spent in the red giant phase. Giant stars at a distance of 0.2pc would have a 97% chance for their envelopes to be stripped through a collision. The fact that CO is

still seen means that at least some remnants are able to reestablish a giant star atmosphere after collision. The rising velocity dispersion gradient with decreasing distance means that velocity broadening effects are more important at smaller radii. Incorporating this effect into the CO profile models would adjust the model predictions in the right direction to make them consistent, but this has yet to be demonstrated.

The Central Mass Distribution

The CO absorption models and the rotational velocity curves are inconsistent. The models suggest that the absorption is dominated by emission at R_{CO} which would mean that the enclosed mass estimates are inappropriate. Yet, the Galactic rotation curve clearly shows a strong gradient inconsistent with this interpretation thus the weight of evidence falls toward failure of the CO models. Given the rising velocity dispersion and rotational velocity toward the center it would seem the enclosed mass vs. radius is being measured. The enclosed mass departs very strongly from predictions made by the 2.2μm surface brightness distribution at a radius of 0.17pc by 6-7 standard deviations in dex (Figure 5-18) and the M/L ratio within R_{CO} is rapidly increasing. Table 5-5 lists the enclosed mass estimated from the 2.2μm light distribution for a model that assumes a M/L = 1 $M_\odot/L_\odot$ (McGinn *et al.* 1989). Table 5-6 lists the corresponding M/L ratios for the enclosed mass estimates listed in Table 5-3.

For all three case assumptions, the enclosed mass measurement at 8.6″ agrees with the result of McGinn *et al.* (1989) and the measurement at 5.2″ departs significantly from the predictions of the 2.2μm light distribution. It also agrees with the Rieke and Rieke (1988) radial velocity study using the projected mass method and the assumption of isotropic velocities and a dominant central mass. Lacy, Actermann, and Serabyn (1992) showed the morphology of the ionized gas structures extending to within 2″ of Sgr A* can be modelled as a linear spiral structure on circular orbits around a central mass of $(1.7 \pm 0.4)\times10^6$ $M_\odot$. The model parameters

they used in their fit indicate that 10% of the mass distribution inside of 0.17 pc is due to stars and this also agrees well with the present enclosed mass measurements and the estimated 2.2μm light distribution. Melia (1991) has modeled the total emission from Sgr A*, from the radio to gamma rays, as the result of accreting material from a 10^{-3} $M_\odot$ yr^{-1} stellar wind originating from close to IRS 16 C. The preferred range for the mass of Sgr A* from the model fits was 0.7 $\times 10^6$ $M_\odot \leq M_{SgrA^*} \leq 1.7 \times 10^6$ $M_\odot$. The results of this experiment lead to the conclusion that the stellar kinematics between 0.17-0.35 pc from Sgr A* show a very compact mass distribution of 1.7×10^6 $M_\odot$ inside a radius of 0.17 pc with a M/L ratio > 10. This is strong evidence for the presence of a massive black hole at the Galactic Center.

TABLE 5-5
2.2μm ENCLOSED MASS MODEL

Slit Position	r_{SgrA^*} (" | pc[b])	2.2μm ENCLOSED MASS[a] ($10^6 M_\odot$)
P1-11	5.2 | 0.17	0.200
P1-12	6.4 | 0.22	0.264
P1-13	6.9 | 0.23	0.293
P1-14	7.7 | 0.26	0.341
P1-15	8.6 | 0.28	0.397
P1-17	10.3| 0.35	0.509

[a]McGinn *et al.* (1989), [b]R_0 = 6.9 kpc.

TABLE 5-6
ENCLOSED MASS TO LIGHT RATIO VS. RADIUS

Slit Position	r_{SgrA^*} (" | pc)	ENCLOSED MASS TO LIGHT RATIO ($M_\odot$ / $L_\odot$)				
		CASE I		CASE II		CASE III
	R_0 = 6.9 kpc	Data Set #1	Data Set #2	Data Set #1	Data Set #2	Data Set #1/#2
P1-11	5.2 | 0.17	10.84 ± 3.90	10.56 ± 4.02	9.18 ± 2.80	9.02 ± 2.95	7.61 ± 1.95
P1-12	6.4 | 0.22	6.37 ± 2.00	6.27 ± 2.02	6.10 ± 1.86	5.97 ± 2.01	4.82 ± 1.04
P1-13	6.9 | 0.23	5.04 ± 2.05	4.95 ± 2.07	4.88 ± 1.94	4.74 ± 2.10	3.53 ± 1.08
P1-14	7.7 | 0.26	5.36 ± 2.27	5.26 ± 2.30	5.22 ± 2.20	5.06 ± 2.40	3.65 ± 1.19
P1-15	8.6 | 0.28	5.18 ± 2.20	5.10 ± 2.23	5.22 ± 2.28	5.04 ± 2.50	3.52 ± 1.13
P1-17	10.3| 0.35	2.51 ± 2.55	-	3.06 ± 2.71	-	1.63 ± 1.58

Conclusions

New measurements of 2.29μm CO absorption from the unresolved stellar emission within 30″ of Sgr A* confirms there is strong CO depletion within a distance $R_{CO} \approx 8.5''$ and in addition shows that it is highly correlated with radius. The stellar velocity dispersion begins to rise inside this distance as $\sim r^{-1/2}$ and the Galactic stellar rotation curve begins to rise rapidly from a minimum near 0 km s^{-1} at 10″ to 100 km s^{-1} at 5.2″ with a gradient of 16 km s^{-1} $arcsec^{-1}$.

The CO absorption distribution has been sufficiently determined from model comparisons to contrain the core radius of the unresolved 2.2μm light distribution to $< \sim 0.2 \times R_{CO}$, and if the average CO band strength varies as r^{β}, then β must be no larger than 1.8 if the stellar rotation and velocity dispersion are to be sampled at each projected radius. Given the velocity curve observations, this is a strong prediction on future models using stellar collision theory and/or population synthesis that attempt to explain the CO depletion. The near coincidence of R_{CO} and the radius of minimum stellar rotation suggest dynamical processes may be responsible.

The enclosed mass vs. radius derived from these measurements within 5-10″ (0.17-0.35 pc) of Sgr A* is relatively constant at $\sim (1.7 \pm 0.35) \times 10^6 M_{\odot}$ departing from mass models based on the 2.2μm light at 5.2″ by 6σ in dex. The M/L ratio of the enclosed mass increases with decreasing radius with $M/L \approx \sim 9\text{-}10\ M_{\odot}/L_{\odot}$ at 5.2″. This result agrees with the enclosed mass determinations by [NeII] ionized gas in the "mini-spiral" (Lacy *et al.* 1991), radial velocities of resolved sources with isotropic orbits (Rieke and Rieke 1988), unresolved stellar velocity dispersions with $r_{SgrA^*} > 9''$ (McGinn *et al.* 1989) and accretion models for Sgr A* (Melia 1991). Given the fact that the stars are overwhelmingly likely to be dynamically influenced only through gravity, this result is strong evidence for a massive black hole at the Galactic Center.

CHAPTER 6:

SUMMARY AND PROSPECTS FOR FUTURE RESEARCH

In the last decade, comprehensive explanations of the phenomena of the Galactic Center has been proposed by the "Central Engine" and "Starburst" models. Many of the results discussed in chapter 1 suggest that the *energetics* of this region are strongly influenced by the presence of massive stars in the central cluster. The studies presented in chapters 3 and 4 show that star formation has been recurrent in the Galactic Center and it is highly possible that the population of bright nonvariables are an extension of the late-type massive star population in the central cluster, further supporting a starburst model. However, the results of chapter 5 show that the *dynamics* of the central parsec are governed by a dark matter concentration that can most easily be interpreted as a massive black hole. Perhaps the presence of the massive stars is only a proximate explanation to the energetics and that ultimately the reason we see them is because their formation, in addition to accretion processes, is one way that energy is dissipated by infalling material. It is interesting that the results presented in this work, and by others, are the fruits of the earlier discoveries of huge structures of gas with large amounts of kinetic energy and the 10^7 $L_\odot$ of radiation from the central parsec that initiated a search for a 10^8 $M_\odot$ black hole in the nucleus. The search seems to have found a rather "puny" massive black hole only about 1% of the originally expected mass.

Future Research

Additional 2.2μm photometry of the central few parsecs is already available to establish the light curves of the Galactic Center LPVs and place further limits on the amplitudes of the nonvariables. The photometric results should be improved because of the better performance

characteristics of the NICMOS 256×256 arrays with lower read noise, larger formats, better sampling of the PSF, and more experience with performing photometric measurements in crowded fields. A map corresponding to the central region discussed here can be acquired in only 8 data frames with the NICMOS camera as opposed to 50 frame with the older 64×64 camera. If the insensitivity of the M_{BOL} vs. Period relation to metallicity holds true in the Galactic Center, then a new way of determining R_0 will be available that makes a minimum of geometric assumptions regarding the objects of interest because of their highly compact spatial distribution, although the foreground and intrinsic reddening effects will have to be carefully considered. The new 256×256 NICMOS array spectrometer will also be useful for a detailed study of metallicity and age for these AGB stars to test repeating star formation theories. Knowing the mass loss rates of these stars would contribute to understanding the formation and dynamics of the molecular ring.

The CO absorption spectra may have been limited in their results more by the cross correlation algorithm than by intrinsic noise. If a better procedure for renormalization can be found it would be possible to obtain an enclosed mass estimate to within 1.5″ (0.05pc = 0.17 Lt yr). If the enclosed mass is constant to within that distance, any hypothesis other than a massive black hole would be difficult to support. Incorporating velocity dispersion corrections to the CO band strength may make the models consistent with the fact that a rising rotation curve is observed. High resolution imaging with the NICMOS 256×256 IR camera should clear up the issue of the discrepant value of R_{CORE} for the 2.2μm light distribution. This quantity has become crucial for understanding the CO absorption strength as a function of distance. If R_{CORE} turns out to be comparable to R_{CO} then new models must be developed with quite different assumptions to reproduce the observed profiles.

The NICMOS 256×256 IR spectrometer could also be used for a more detailed study of the additional CO absorption features out to the atmospheric cutoff at 2.5μm to confirm the rotation curve results presented here. Changes in the continuum as a function of r_{SgrA^*} and the

strength of the near IR Mg and Si lines would help diagnose a changing stellar population. The onset of CO depletion occurs near the minimum velocity of the rotation curve. It would be interesting to sample the region within 2″ of the dynamical center of M31 to see if there is a corresponding effect. This would strengthen the hypothesis that the CO depletion is due to dynamical effects on the stellar photospheres.

A better understanding of the details of star-star collisions inside of R_{CO} is also needed. What fraction of the envelope remains after the collision? How important is heat dissipation subsequent to collision and how rapidly does a giant-like atmosphere become reestablished? The results of this work predict that whatever processes are at involved, the average CO bandstrength of the stellar population as a function of r_{SgrA*} must go approximately as r^{β} where $\beta \leq 1.8$ in order for material to be observed predominantly at the projected radius.

APPENDIX 1 :

ESTIMATION OF STELLAR FOREGROUND CONTAMINATION

The calculations of the estimated foreground star contamination within the observed Galactic Center field are described. Simple models of the stellar density and extinction distributions similar to the Bahcall-Soneira Galaxy model (Bahcall and Soneira 1980) are used with luminosity functions appropriate to the near infrared (e.g. Garwood and Jones 1987; Ruelas-Mayorga 1991). Small scale variations of the stellar density and extinction distributions along the line of sight (e.g. spiral arms, star clusters, molecular clouds) are neglected. The bulge and disk contributions are considered separately.

Estimate of Disk Contamination

Based on the formalism in Mihalas and Binney (1981), the space density of stars of absolute K magnitude M_K and spectral class i at a distance r from the Sun is given by $\nu(r,M_K,i)$. This function is assumed to be the product of a density function $\rho_i(r)$ and a luminosity function $\mu_i(M_K)$:

$$\nu(r,M_K,i) = \rho_i \times \mu_i = \rho_i(r) \times \mu_i(M_K) \qquad (6)$$

The luminosity function $\mu_i(M_K)$ for each spectral class, parameterized by the average absolute K magnitude $M_K(0)_i$ and dispersion σ_i, is given the exponential form:

$$\mu_i(M_K) = \frac{1}{\sqrt{2\pi\sigma_i^2}} \times \exp\left[-\frac{1}{2}\left(\frac{M_K - M_K(0)_i}{\sigma_i} \right)^2 \right]. \qquad (2)$$

The space density of each spectral class $\rho_i(r)$ was assumed to have the form

$$\rho_i(r) = \rho_{i\odot} \exp\left(\frac{r}{\alpha_\rho}\right) \quad ; \quad r < R_\circ$$
$$\rho_i(r) = \rho_{i\odot} \exp\left(\frac{R_\circ}{\alpha_\rho}\right) \exp\left(\frac{-(r - R_\circ)}{\alpha_\rho}\right) \quad ; \quad r \geq R_\circ \tag{8}$$

where $R_\circ$ is the Galactic Center distance, α_ρ is the characteristic length scale of the stellar density distribution, and $\rho_{i\odot}$ is the space density of spectral class i in the solar neighborhood. The assumed parameter values for each spectral class were taken from Garwood and Jones (1987).

A similar form is used for the distribution of the foreground extinction where $A_\lambda(r)$ is the extinction at wavelength λ for stars at a distance r from the sun:

$$A_\lambda(r) = \int_0^r a_\lambda(r)dr$$
$$a_\lambda(r) = a_{\lambda\odot} \exp\left(\frac{r}{\alpha_A}\right) \quad ; \quad r < R_\circ \tag{9}$$
$$a_\lambda(r) = a_{\lambda\odot} \exp\left(\frac{R_\circ}{\alpha_A}\right) \exp\left(\frac{-(r - R_\circ)}{\alpha_A}\right) \quad ; \quad r \geq R_\circ$$

The extinction function was normalized so that $A_V(R_\circ) = 30$ mag and with $a_{V\odot} = 1.000$ mag Kpc^{-1}. For a given value of $R_\circ$ the value of α_ρ is then fixed. We use the Galactic Center extinction curve of Rieke and Lebofsky (1985) which gives $A_K = 0.112 \times A_V$ and $A_H = 0.175 \times A_V$.

For a field of solid angle ω, the observed number of star counts $A(m_K)$ in a magnitude

bin of width Δm with apparent magnitude m_k is given by (Mihalas and Binney 1981):

$$A(m_K) = \omega \sum_{i=1}^{5} \int_0^{\infty} \rho_i(r) \left[\int_{m_k-\frac{1}{2}\Delta m}^{m_k+\frac{1}{2}\Delta m} \mu_i \left(m_k - 5 \log\left(\frac{r}{10pc}\right) - A_K(r) \right) dm_K \right] r^2 dr \quad (10)$$

and the total number of foreground stars detected $N_{TOT}(m_{lim})$ to a limiting apparent magnitude m_{lim} is

$$N_{TOT}(m_{lim}) = \omega \sum_{i=1}^{5} \int_0^{\infty} \rho_i(r) \left[\int_{-\infty}^{m_{lim}} \mu_i \left(m_k - 5 \log\left(\frac{r}{10pc}\right) - A_K(r) \right) dm_K \right] r^2 dr. \quad (11)$$

The color distribution of foreground stars is, however, most instructive. For convenience let y be the observed (H-K) color, then given a constant $(H-K)_o$ for all stars in each spectral class the contribution of the foreground stars to the observed (H-K) color distribution of bin width Δy is given by:

$$N(y) = \omega \sum_{i=1}^{5} \int_0^{\infty} \rho_i(r) \left[\int_{y-\frac{1}{2}\Delta y}^{y+\frac{1}{2}\Delta y} \delta\left(y' - (H-K)_{\alpha} - \left(\frac{a_H}{a_K} - 1\right) A_K(r) \right) dy' \right] \quad (12)$$
$$\times \left[\int_{-\infty}^{m_{lim}} \mu_i \left(m_k - 5 \log\left(\frac{r}{10pc}\right) - A_K(r) \right) dm_K \right] r^2 dr$$

The first factor in brackets represents the color distribution for the particular spectral class (approximated here as a Dirac delta function) while the second factor in brackets represents the fraction of the luminosity function at distance r above the threshold detection limit m_K. The H-K colors for each spectral class were taken from Frogel *et al.* 1978. The resulting color distribution

of foreground stars (figure A1-1) shows that most contaminants in the observed distribution are likely to have (H-K) < 1.5.

The distribution of stars along the line-of-sight to the Galactic Center is shown in figure A1-2. Nearby main sequence stars make a very small contribution at small distances. The most likely contaminants are giant branch stars at distances a few kiloparsecs out from the sun where the extinction is still minimal. Those with $(H-K)_{OBS} > 1.5$ are within 1 kpc of the Galactic Center and so would most likely be indistinguishable from our HK sample. The curve begins to rise again from the combined effects of the sampled volume along the line-of-sight increasing as r^2 and the exponentially increasing stellar density of supergiants near the Galactic Center. The luminosity function model parameters are probably being extrapolated beyond valid limits. Nevertheless supergiants within 1 kpc of the Galactic Center would be indistinguishable from our HK sample, but even disk stars would produce very little contamination.

Estimate of Bulge Contamination

Since the stellar density distribution is so sharply peaked near the nucleus, it is easier to consider the fractional distribution of stars within distance $|x - R_0|$ from the Galactic Center. In other words, we want to calculate the dispersal of stars along the line of sight using several simplifying assumptions. The surface brightness profile of 2.2μm emission implies a density distribution of $\rho \propto R^{-1.8}$ (Sanders and Lowinger 1968). We assume the extinction and the luminosity function are constant to first order and then calculate the fraction of stars, *F*, within the distance along the line of sight $|x - R_o|$ about the center for a stellar density profile of $\rho \propto R^{-1.8}$, R_o = 8 kpc, along a square solid angle of side angle θ, and core radii R_{core} = 0.1,0.6,1.0 pc.

The results (figure A1-3) show that approximately 60% of the stars in our luminosity

$$F(|x-R_0|) = \frac{\int_{-\frac{1}{2}R_0\theta}^{+\frac{1}{2}R_0\theta} dz \int_{-\frac{1}{2}R_0\theta}^{+\frac{1}{2}R_0\theta} dy \int_{-|x-R_0|}^{+|x-R_0|} \rho(\vec{R})\, dx}{\int_{-\frac{1}{2}R_0\theta}^{+\frac{1}{2}R_0\theta} dz \int_{-\frac{1}{2}R_0\theta}^{+\frac{1}{2}R_0\theta} dy \int_{-\infty}^{+\infty} \rho(\vec{R})\, dx}$$

$$\rho(\vec{R}) = \rho_{CORE}\,,\ |\vec{R}-\vec{R}_0| < R_{CORE}$$

$$\rho(\vec{R}) = \rho_{CORE}\left(\frac{|\vec{R}-\vec{R}_0|}{R_{CORE}}\right)^{(-1.8)}\,,\ |\vec{R}-\vec{R}_0| \geq \vec{R}_{CORE}$$

function are within the projected distance corresponding to the field of view (6.4 pc); 90% are within 50pc; 95% within 104 pc, independent of the core radius. The dispersion in magnitude caused by the depth effects corresponding to these distances from the center is much smaller than the photometric errors of our sample. Thus we can be confident that the luminosity function derived from the complete sample principally resides within 20pc of the Galactic Center.

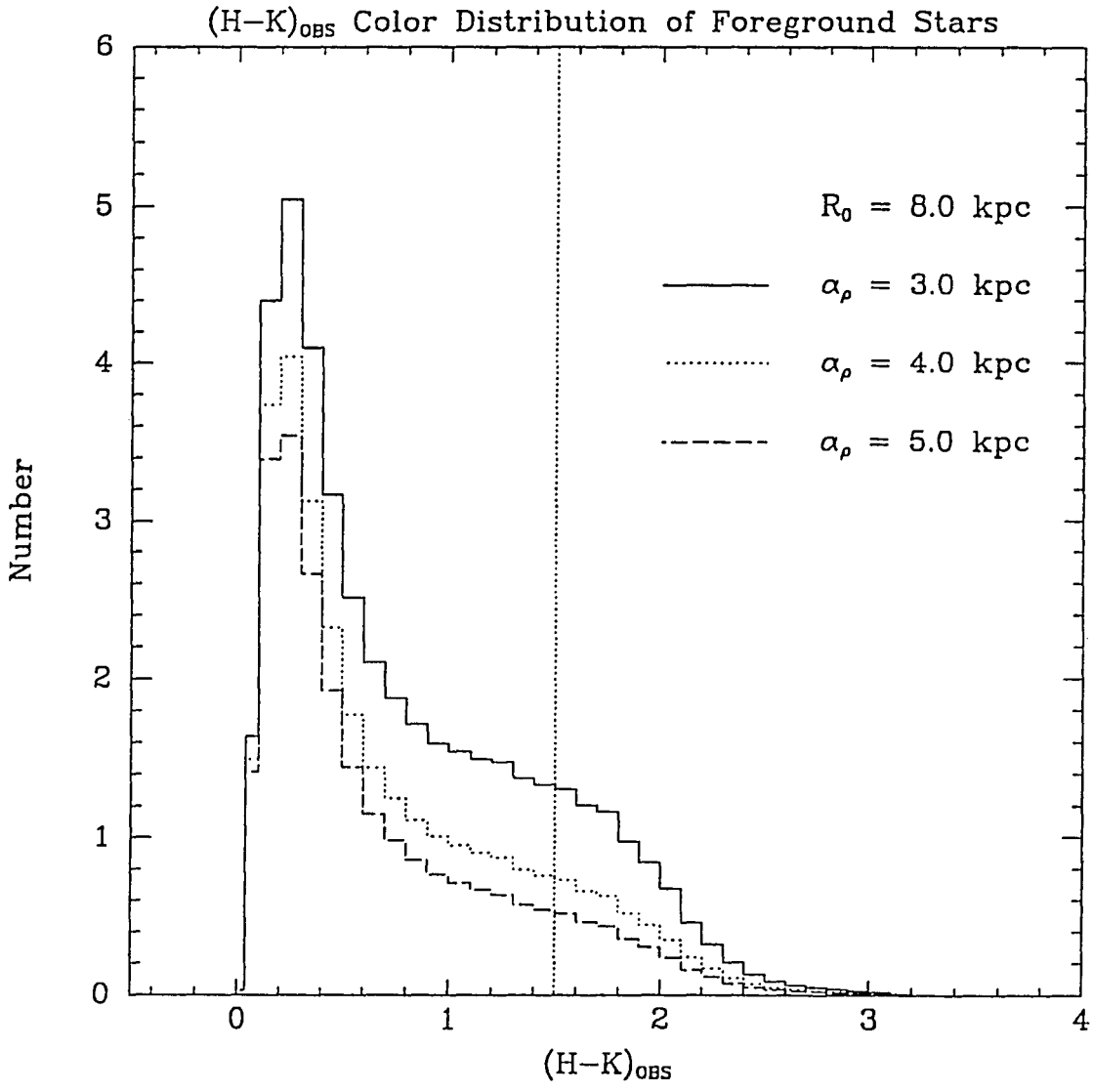

Figure A1-1 The estimated $(H\text{-}K)_{OBS}$ color distribution of foreground disk stars along the line-of-sight to the Galactic Center. The parameter α_ρ is the scale length for the exponential stellar density distribution. A vertical line at $(H\text{-}K)_{OBS} = 1.5$ shows the cutoff used to select the complete HK sample.

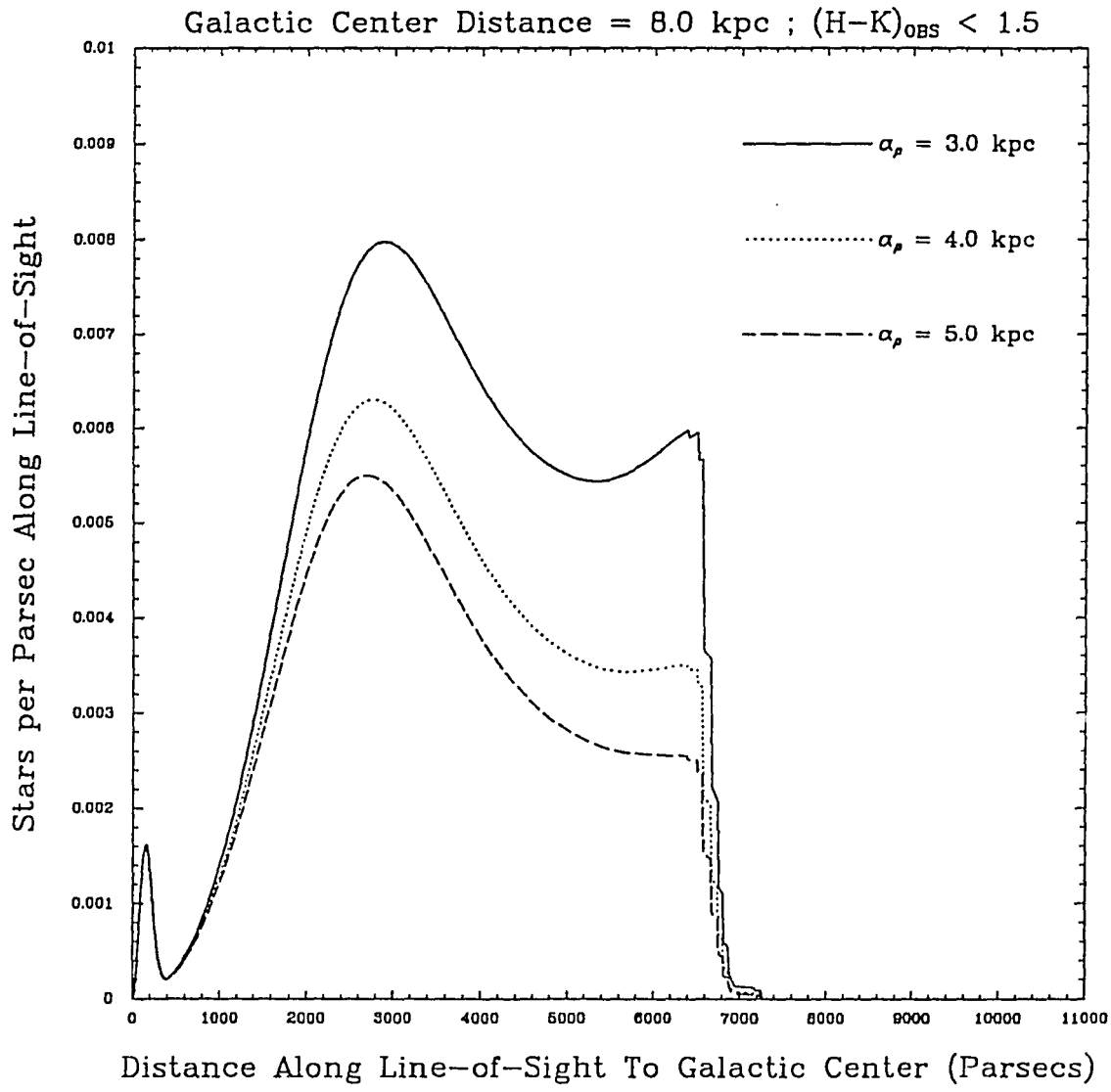

Figure A1-2 The distribution of stars along the line-of-sight to the Galactic Center. The small spike near 200pc is the small contribution make by nearby main sequence stars. The peak near 2000pc is from giant branch stars and the rise near 6000pc is from the increasing contribution of supergiants near the nucleus. The color cutoff of $(H\text{-}K)_{OBS} > 1.5$ is reflected in the sharp vertical drop near 7000pc, eliminating nearly all the stars along the line of sight.

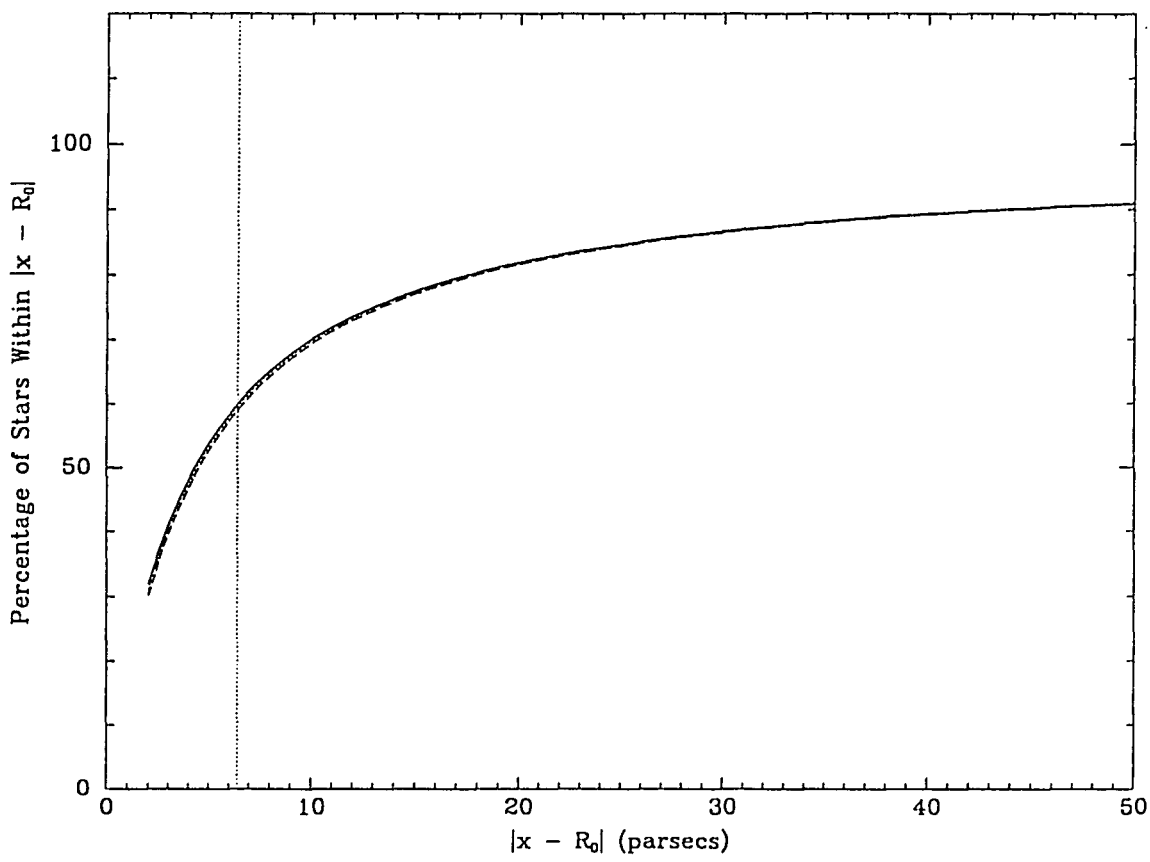

Figure A1-3 The percentage of stars within a 5′×5′ field-of-view along the line-of-sight to the Galactic Center and inside a distance of $|x-R_0|$. The Galactic Center is located at a distance R_0 from the observer and it is assumed that the extinction is uniform across the FOV. The stellar density distribution is given by $\rho \propto R^{-1.8}$ outside a core radius R_{CORE}. The three curves represent core radii of 0.1, 0.6, and 1.0pc but this has negligible effect on the fractional line-of-sight dispersion.

APPENDIX 2 :

GALACTIC CENTER HK PHOTOMETRY

The following table is a listing of the HK database of 638 stars used in the discussions of chapters 3 and 4. The column names are designated by:

ID : Star Identification Number
α_{IRS7} : Right ascension offset position from IRS 7, $17^h\ 42^m\ 29.2^s$ (1950), in arcseconds.
δ_{IRS7} : Declination offset position from IRS 7, -28° 59′ 12.9″ (1950), in arcseconds.
n_{K1} : Number of K detections in May 1987
n_{K2} : Number of K detections in September 1987
n_{K3} : Number of K detections in May 1988
n_{H3} : Number of H detections in May 1988
$<m_K>$: Average K magnitude. The photometric errors are 0.09, 0.07, 0.10, and 0.15 (H) mag respectively
$(H-K)_{OBS}$: Observed H-K color
$(H-K)_0$: Intrinsic H-K color, dereddened with the extinction curve of Rieke and Lebofsky (1985) ($A_H = 0.175 \times A_V$; $A_K = 0.112 \times A_V$) and assuming a forground visual extinction of 31.8.
Δm_K : The RMS magnitude residual between epochs. Nonvariables will have $\Delta m_K < 0.274$ at the 3σ level.
M_{BOL} : The inferred bolometric magnitude assuming a constant foreground visual extinction of 31.8 mag, a distance modulus to the Galactic Center of 14.2, and bolometric correction BC_K = 3.0.

TABLE A2-1

ID	α_{IRS7}	δ_{IRS7}	n_{K1}	n_{K2}	n_{K3}	n_{H3}	$<m_K>$	$(H-K)_{obs}$	$(H-K)_0$	Δm_K	M_{BOL}
1	-187.6	-103.8	0	2	2	2	10.383	2.283	0.280	0.157	-4.222
2	-184.5	-72.8	0	2	2	2	10.617	2.753	0.750	0.000	-3.988
3	-183.6	13.5	0	2	2	1	9.929	2.508	0.505	0.000	-4.676
4	-183.0	-24.3	0	2	2	2	9.884	2.062	0.059	0.000	-4.721
5	-182.7	-89.9	1	2	2	2	10.746	2.163	0.160	0.079	-3.859
6	-181.7	-106.7	3	2	2	2	10.088	2.014	0.011	0.152	-4.517
7	-180.7	-27.4	1	2	2	2	9.766	1.982	-0.021	0.214	-4.839
8	-180.3	-118.5	2	2	2	2	9.750	1.664	-0.339	0.107	-4.855
9	-180.2	-123.8	2	2	2	2	10.829	2.302	0.299	0.156	-3.776
10	-178.6	-20.1	2	2	2	2	10.156	1.898	-0.105	0.080	-4.449
11	-178.0	96.6	0	1	1	1	10.887	2.205	0.202	0.060	-3.718
12	-177.2	-6.7	3	2	2	2	10.883	2.389	0.386	0.099	-3.722
13	-176.9	22.0	2	2	2	2	9.245	2.847	0.844	0.395	-5.360
14	-176.8	-37.1	2	2	2	2	10.853	1.940	-0.063	0.063	-3.752
15	-176.5	34.1	2	3	3	3	10.599	3.006	1.003	0.108	-4.006

ID	α_{IRS7}	δ_{IRS7}	n_{K1}	n_{K2}	n_{K3}	n_{H3}	$<m_K>$	$(H-K)_{obs}$	$(H-K)_0$	Δm_K	M_{BOL}
16	-175.6	41.6	2	2	2	2	10.352	2.328	0.325	0.102	-4.253
17	-174.9	-163.6	1	1	1	1	10.705	1.764	-0.239	0.189	-3.900
18	-174.7	4.6	2	2	1	2	10.883	2.209	0.206	0.061	-3.722
19	-174.4	-107.3	3	2	2	2	10.468	2.201	0.198	0.105	-4.137
20	-174.3	162.9	1	1	1	1	9.412	2.028	0.025	0.135	-5.193
21	-173.7	8.0	2	2	2	2	10.686	1.725	-0.278	0.042	-3.919
22	-173.1	-167.4	1	0	1	1	10.129	2.465	0.462	0.030	-4.476
23	-173.0	131.2	2	2	2	2	10.763	2.238	0.235	0.036	-3.842
24	-172.3	46.6	2	2	2	2	10.956	2.330	0.327	0.190	-3.649
25	-171.9	72.0	2	1	2	2	10.375	1.786	-0.217	0.165	-4.230
26	-168.2	95.8	3	2	2	2	10.825	2.199	0.196	0.070	-3.780
27	-167.7	-158.0	1	1	1	1	10.529	2.867	0.864	0.100	-4.076
28	-166.1	17.9	2	1	2	2	10.766	1.850	-0.153	0.221	-3.839
29	-165.8	-91.2	2	2	2	2	10.701	1.984	-0.019	0.082	-3.904
30	-165.1	-125.2	2	2	2	2	10.435	1.509	-0.494	0.117	-4.170
31	-164.9	112.6	2	2	2	2	10.559	2.126	0.123	0.059	-4.046
32	-164.7	21.6	2	2	2	1	10.772	2.075	0.072	0.193	-3.833
33	-164.5	65.8	2	2	3	1	9.888	2.398	0.395	0.157	-4.717
34	-164.4	71.4	2	1	2	2	10.118	1.532	-0.471	0.093	-4.487
35	-164.1	53.5	2	2	2	2	10.566	2.334	0.331	0.209	-4.039
36	-161.0	109.3	2	2	2	2	10.129	1.528	-0.475	0.065	-4.476
37	-160.8	-26.8	2	2	2	2	10.771	2.293	0.290	0.100	-3.834
38	-159.9	57.8	2	2	2	2	10.622	1.721	-0.282	0.068	-3.983
39	-159.8	-128.8	2	1	2	1	9.642	1.973	-0.030	0.491	-4.963
40	-159.7	-88.5	2	2	2	2	10.616	1.706	-0.297	0.086	-3.989
41	-158.6	-18.6	2	2	2	2	10.837	2.198	0.195	0.061	-3.768
42	-158.5	-56.9	2	2	2	2	10.346	2.031	0.028	0.145	-4.259
43	-158.2	-168.9	1	0	0	1	11.252	1.703	-0.300	-1.00	-3.353
44	-157.4	23.7	2	2	2	2	10.388	2.050	0.047	0.035	-4.217
45	-157.4	-44.8	2	2	2	2	9.302	2.086	0.083	0.074	-5.303
46	-157.3	90.4	2	2	2	2	9.329	2.672	0.669	0.127	-5.276
47	-156.5	-50.3	2	2	2	2	10.315	2.197	0.194	0.064	-4.290
48	-156.5	107.8	2	2	2	2	10.769	2.008	0.005	0.131	-3.836
49	-155.4	-23.0	2	2	2	2	10.810	2.357	0.354	0.111	-3.795
50	-154.4	8.2	2	2	2	2	10.051	2.993	0.990	0.250	-4.554
51	-154.0	130.7	2	2	2	2	8.239	2.151	0.148	0.080	-6.366
52	-153.8	-71.4	2	2	2	2	10.705	1.609	-0.394	0.051	-3.900
53	-152.9	-120.5	2	2	2	2	10.853	1.503	-0.500	0.026	-3.752
54	-152.4	-132.2	2	2	2	2	10.744	1.998	-0.005	0.196	-3.861
55	-152.3	-88.2	2	2	2	2	10.242	1.585	-0.418	0.066	-4.363
56	-152.3	79.0	2	2	2	2	10.687	3.098	1.095	0.069	-3.918
57	-151.9	89.0	2	2	2	2	10.313	2.926	0.923	0.105	-4.292
58	-151.8	-63.9	2	3	2	2	9.456	1.883	-0.120	0.047	-5.149
59	-151.4	-78.2	1	2	2	1	10.546	2.536	0.533	0.199	-4.059
60	-148.1	60.0	2	2	2	2	10.087	2.022	0.019	0.060	-4.518

ID	α_{IRS7}	δ_{IRS7}	n_{K1}	n_{K2}	n_{K3}	n_{H3}	$\langle m_K \rangle$	$(H-K)_{obs}$	$(H-K)_0$	Δm_K	M_{BOL}
61	-147.8	-81.0	2	2	2	2	8.671	2.452	0.449	0.489	-5.934
62	-147.4	-27.6	2	2	2	2	10.602	2.286	0.283	0.083	-4.003
63	-147.3	-96.3	2	2	2	2	10.219	2.408	0.405	0.095	-4.386
64	-147.0	24.5	2	1	2	2	9.939	2.500	0.497	0.247	-4.666
65	-146.7	-78.2	1	2	0	1	10.593	2.580	0.577	0.155	-4.012
66	-146.7	-122.8	2	2	2	2	10.075	1.910	-0.093	0.079	-4.530
67	-146.6	111.4	2	2	2	2	9.988	2.267	0.264	0.058	-4.617
68	-146.5	-4.7	3	2	2	2	10.382	3.638	1.635	0.119	-4.223
69	-146.1	31.4	0	0	1	1	10.858	2.589	0.586	-1.00	-3.747
70	-146.0	-154.6	1	1	1	1	10.548	2.353	0.350	0.147	-4.057
71	-145.5	-39.6	3	2	2	2	9.861	1.787	-0.216	0.229	-4.744
72	-144.8	-106.3	3	2	2	2	10.290	2.787	0.784	0.207	-4.315
73	-144.3	15.5	2	2	2	2	10.564	1.824	-0.179	0.046	-4.041
74	-144.2	140.1	1	1	1	1	10.196	3.295	1.292	0.127	-4.409
75	-143.0	-109.5	2	2	2	2	10.302	2.919	0.916	0.100	-4.303
76	-142.9	-25.7	2	2	2	2	10.799	2.505	0.502	0.105	-3.806
77	-142.9	-45.6	2	3	2	1	10.911	2.538	0.535	0.161	-3.694
78	-142.2	-67.4	2	3	2	3	9.195	2.031	0.028	0.123	-5.410
79	-141.4	-30.5	2	3	2	2	10.082	2.241	0.238	0.168	-4.523
80	-141.2	133.3	1	2	2	1	10.863	2.154	0.151	0.112	-3.742
81	-139.5	21.4	2	2	2	2	10.561	2.394	0.391	0.106	-4.044
82	-138.8	40.1	2	2	2	2	10.726	2.449	0.446	0.126	-3.879
83	-138.7	-24.9	2	2	2	2	10.546	1.726	-0.277	0.103	-4.059
84	-138.3	-134.3	2	2	4	4	10.418	2.565	0.562	0.101	-4.187
85	-138.2	-167.5	1	2	2	2	8.911	2.709	0.706	0.242	-5.694
86	-138.0	-114.6	2	2	2	4	10.011	2.443	0.440	0.067	-4.594
87	-137.8	112.6	2	2	2	2	10.985	2.268	0.265	0.091	-3.620
88	-137.6	8.6	2	2	2	2	10.363	2.268	0.265	0.051	-4.242
89	-137.5	71.3	2	1	2	2	10.769	2.163	0.160	0.293	-3.836
90	-137.4	-138.6	2	2	2	3	9.595	1.931	-0.072	0.163	-5.010
91	-137.2	-127.7	2	4	4	4	10.597	2.206	0.203	0.062	-4.008
92	-136.8	28.9	3	2	2	2	9.588	1.973	-0.030	0.166	-5.017
93	-136.7	-109.1	2	4	4	4	10.842	1.705	-0.298	0.083	-3.763
94	-136.1	-159.9	1	2	2	2	10.812	1.621	-0.382	0.088	-3.793
95	-136.0	-121.8	2	4	4	4	10.970	2.415	0.412	0.103	-3.635
96	-136.0	-78.3	2	4	2	4	10.909	2.656	0.653	0.066	-3.696
97	-135.9	50.6	2	2	2	2	10.219	1.787	-0.216	0.074	-4.386
98	-134.8	-54.9	2	4	4	4	9.734	1.713	-0.290	0.043	-4.871
99	-134.6	-83.8	2	4	4	4	10.619	2.226	0.223	0.017	-3.986
100	-134.6	7.7	0	1	0	2	10.514	1.975	-0.028	-1.00	-4.091
101	-133.7	56.7	2	2	2	2	10.770	2.043	0.040	0.094	-3.835
102	-132.4	38.3	2	4	4	4	10.989	2.190	0.187	0.113	-3.616
103	-132.0	-48.1	2	3	4	4	10.636	1.890	-0.113	0.286	-3.969
104	-131.4	112.0	2	3	3	2	9.356	1.810	-0.193	0.031	-5.249
105	-131.1	139.4	1	1	1	1	8.953	1.826	-0.177	0.057	-5.652

ID	α_{IRS7}	δ_{IRS7}	n_{K1}	n_{K2}	n_{K3}	n_{H3}	$\langle m_K \rangle$	$(H-K)_{obs}$	$(H-K)_0$	Δm_K	M_{BOL}
106	-131.0	20.5	3	4	4	4	10.847	2.007	0.004	0.058	-3.758
107	-130.3	-149.5	2	2	2	2	10.478	2.462	0.459	0.027	-4.127
108	-130.3	-75.5	4	4	4	4	10.883	2.008	0.005	0.164	-3.722
109	-129.8	78.3	2	4	4	4	9.924	2.284	0.281	0.086	-4.681
110	-129.1	-164.5	2	2	2	2	10.740	2.361	0.358	0.118	-3.865
111	-129.0	-16.0	4	4	4	4	10.659	2.473	0.470	0.023	-3.946
112	-128.7	-88.0	4	4	4	4	10.951	2.127	0.124	0.076	-3.654
113	-128.7	-169.1	2	1	2	1	10.605	2.348	0.345	0.197	-4.000
114	-128.0	-67.4	4	6	4	6	10.296	2.035	0.032	0.067	-4.309
115	-127.9	136.4	2	1	3	3	10.763	2.260	0.257	0.060	-3.842
116	-126.1	51.5	4	4	4	4	10.636	1.936	-0.067	0.072	-3.969
117	-125.5	-111.6	4	4	4	4	10.322	2.024	0.021	0.068	-4.283
118	-124.2	10.0	4	4	4	4	10.325	2.884	0.881	0.242	-4.280
119	-122.2	93.1	4	4	4	4	10.252	1.890	-0.113	0.014	-4.353
120	-121.5	-165.0	2	2	2	2	10.585	2.199	0.196	0.178	-4.020
121	-121.4	-80.7	3	4	4	4	10.032	1.899	-0.104	0.108	-4.573
122	-121.3	44.3	4	4	4	1	9.945	3.449	1.446	0.615	-4.660
123	-121.1	-159.1	2	2	2	2	9.218	2.164	0.161	0.113	-5.387
124	-120.4	152.5	2	1	2	2	8.418	2.029	0.026	0.186	-6.187
125	-119.8	-75.7	4	4	4	4	9.383	3.491	1.488	0.477	-5.222
126	-119.4	75.0	4	4	4	4	10.459	2.668	0.665	0.045	-4.146
127	-117.8	93.9	4	3	4	4	10.212	1.663	-0.340	0.095	-4.393
128	-116.7	-72.5	1	2	0	4	11.002	1.921	-0.082	0.206	-3.603
129	-116.6	-53.7	4	2	2	3	9.618	1.911	-0.092	0.217	-4.987
130	-116.5	146.7	2	1	2	2	10.449	1.823	-0.180	0.201	-4.156
131	-115.3	31.0	5	1	5	5	10.094	1.518	-0.485	0.129	-4.511
132	-115.2	-6.1	5	2	2	2	10.593	3.528	1.525	0.118	-4.012
133	-114.8	93.6	3	1	4	1	10.852	1.632	-0.371	0.169	-3.753
134	-114.7	104.6	4	3	4	5	9.981	1.559	-0.444	0.045	-4.624
135	-114.5	85.7	4	2	3	4	9.623	2.043	0.040	0.237	-4.982
136	-114.3	-36.9	5	2	2	2	10.794	1.563	-0.440	0.005	-3.811
137	-114.2	-60.5	4	2	2	4	10.760	2.587	0.584	0.252	-3.845
138	-113.4	-88.0	3	2	2	2	10.028	2.562	0.559	0.108	-4.577
139	-113.0	-72.4	4	2	2	2	10.858	1.975	-0.028	0.077	-3.747
140	-112.4	113.1	4	1	2	4	10.500	1.937	-0.066	0.105	-4.105
141	-111.8	160.4	2	0	2	1	10.989	3.390	1.387	0.173	-3.616
142	-111.6	10.9	4	2	2	4	10.697	2.057	0.054	0.194	-3.908
143	-111.0	-13.4	3	2	2	2	10.931	2.021	0.018	0.155	-3.674
144	-110.5	20.6	2	2	2	4	10.780	2.016	0.013	0.075	-3.825
145	-110.3	-53.0	2	2	2	2	10.399	2.077	0.074	0.046	-4.206
146	-109.9	-108.0	2	2	2	2	10.817	2.098	0.095	0.062	-3.788
147	-109.6	-98.0	2	1	2	3	9.858	2.005	0.002	0.345	-4.747
148	-108.8	8.3	2	2	2	2	10.107	2.506	0.503	0.159	-4.498
149	-108.2	-153.8	1	1	1	1	8.832	1.776	-0.227	0.069	-5.773
150	-107.3	-134.6	2	2	2	2	9.282	1.568	-0.435	0.068	-5.323

ID	α_{IRS7}	δ_{IRS7}	n_{K1}	n_{K2}	n_{K3}	n_{H3}	$\langle m_K \rangle$	$(H-K)_{obs}$	$(H-K)_0$	Δm_K	M_{BOL}
151	-107.2	117.6	4	1	2	4	10.129	1.583	-0.420	0.161	-4.476
152	-107.0	-24.2	2	2	2	2	10.487	1.939	-0.064	0.198	-4.118
153	-105.7	-165.9	1	1	1	1	9.417	1.660	-0.343	0.142	-5.188
154	-105.5	65.0	3	2	2	2	10.487	1.728	-0.275	0.042	-4.118
155	-105.4	56.6	2	2	2	2	10.701	2.224	0.221	0.045	-3.904
156	-105.4	120.6	1	1	2	2	10.582	1.640	-0.363	0.008	-4.023
157	-105.3	41.3	2	2	2	2	10.636	2.716	0.713	0.055	-3.969
158	-105.0	-21.9	0	1	1	1	10.739	1.914	-0.089	0.127	-3.866
159	-104.0	110.9	2	1	2	2	10.001	2.132	0.129	0.035	-4.604
160	-103.6	-104.0	1	2	3	2	9.410	2.357	0.354	0.502	-5.195
161	-103.5	-96.2	2	2	2	2	10.854	2.437	0.434	0.125	-3.751
162	-103.3	-150.5	1	1	1	1	10.023	1.686	-0.317	0.114	-4.582
163	-103.2	52.8	2	2	2	2	10.726	2.427	0.424	0.133	-3.879
164	-102.9	-122.4	1	2	2	2	10.822	1.598	-0.405	0.105	-3.783
165	-102.7	-1.6	2	3	3	3	9.114	2.074	0.071	0.139	-5.491
166	-102.2	-138.3	2	1	2	1	10.233	2.181	0.178	0.077	-4.372
167	-102.1	72.1	2	2	2	2	10.682	1.910	-0.093	0.083	-3.923
168	-102.0	-125.0	2	2	2	2	10.784	2.047	0.044	0.031	-3.821
169	-101.4	-100.8	2	3	2	2	10.418	3.093	1.090	0.458	-4.187
170	-101.3	55.9	2	2	2	2	10.415	2.313	0.310	0.088	-4.190
171	-100.3	154.9	1	0	1	1	9.488	3.505	1.502	0.303	-5.117
172	-99.5	44.0	2	2	2	2	10.426	1.946	-0.057	0.141	-4.179
173	-99.2	-94.8	2	2	2	2	9.926	3.497	1.494	0.100	-4.679
174	-98.9	-159.0	1	1	1	1	10.842	1.917	-0.086	0.199	-3.763
175	-98.4	-165.9	1	1	1	1	10.282	2.429	0.426	0.152	-4.323
176	-98.0	-23.8	2	1	2	2	10.275	1.929	-0.074	0.147	-4.330
177	-97.6	95.1	2	2	2	2	10.529	3.138	1.135	0.076	-4.076
178	-97.2	-126.4	2	2	2	2	10.179	1.891	-0.112	0.027	-4.426
179	-97.0	14.4	1	1	2	1	10.186	3.101	1.098	0.117	-4.419
180	-96.6	-62.6	2	2	2	1	10.720	2.609	0.606	0.215	-3.885
181	-95.5	-35.5	2	3	3	3	10.201	2.121	0.118	0.149	-4.404
182	-95.2	-153.0	1	1	1	1	10.880	2.479	0.476	0.053	-3.725
183	-95.2	-159.1	1	1	1	1	10.589	2.409	0.406	0.298	-4.016
184	-94.9	-41.7	2	2	2	2	10.243	2.491	0.488	0.080	-4.362
185	-94.8	67.8	2	3	2	3	10.853	2.566	0.563	0.232	-3.752
186	-94.1	31.9	2	3	3	3	10.752	2.369	0.366	0.249	-3.853
187	-93.9	-32.0	2	2	2	2	10.818	2.793	0.790	0.081	-3.787
188	-93.8	-89.9	2	2	2	2	10.000	2.311	0.308	0.050	-4.605
189	-93.4	83.8	2	2	2	2	9.673	1.649	-0.354	0.134	-4.932
190	-93.3	-19.6	2	2	2	2	10.722	2.104	0.101	0.168	-3.883
191	-92.8	127.8	2	1	2	2	10.441	2.250	0.247	0.068	-4.164
192	-92.1	-81.0	2	2	2	2	8.907	2.190	0.187	0.026	-5.698
193	-91.9	161.6	1	0	1	1	9.755	2.144	0.141	0.091	-4.850
194	-91.6	3.8	2	2	2	2	9.129	2.414	0.411	0.133	-5.476
195	-91.0	60.5	1	2	0	2	10.561	2.739	0.736	0.362	-4.044

ID	α_{IRS7}	δ_{IRS7}	n_{K1}	n_{K2}	n_{K3}	n_{H3}	$<m_K>$	$(H-K)_{obs}$	$(H-K)_0$	Δm_K	M_{BOL}
196	-91.0	-113.5	2	2	2	2	8.668	1.887	-0.116	0.103	-5.937
197	-91.0	147.9	1	0	1	1	10.113	1.913	-0.090	0.028	-4.492
198	-90.6	135.7	1	0	2	2	9.980	2.122	0.119	0.017	-4.625
199	-90.1	-45.4	2	2	2	2	9.920	2.547	0.544	0.423	-4.685
200	-89.8	-49.9	2	2	2	2	10.639	1.641	-0.362	0.159	-3.966
201	-89.7	31.2	3	2	3	2	11.042	2.033	0.030	0.142	-3.563
202	-89.5	46.4	2	2	2	1	10.851	2.499	0.496	0.132	-3.754
203	-89.5	-89.7	2	2	2	2	10.843	2.043	0.040	0.104	-3.762
204	-87.7	159.5	1	0	1	1	10.636	1.961	-0.042	0.059	-3.969
205	-87.7	-11.9	2	2	2	2	10.866	2.362	0.359	0.152	-3.739
206	-87.6	61.6	2	2	2	2	9.588	2.768	0.765	0.590	-5.017
207	-87.5	5.2	1	2	2	2	10.919	1.765	-0.238	0.051	-3.686
208	-87.3	-53.4	2	2	2	2	10.346	2.005	0.002	0.009	-4.259
209	-87.2	55.5	2	2	2	2	10.659	2.121	0.118	0.049	-3.946
210	-86.1	105.8	2	1	2	2	9.924	1.875	-0.128	0.093	-4.681
211	-85.4	122.4	2	1	2	1	10.257	1.851	-0.152	0.085	-4.348
212	-84.6	-131.8	0	1	0	1	10.985	2.904	0.901	-1.00	-3.620
213	-84.5	9.5	2	2	4	2	10.939	2.117	0.114	0.083	-3.666
214	-84.3	87.1	2	2	2	2	8.284	2.012	0.009	0.167	-6.321
215	-83.6	-74.5	4	4	4	4	10.868	1.983	-0.020	0.069	-3.737
216	-83.0	80.1	2	2	3	2	10.803	1.680	-0.323	0.212	-3.802
217	-83.0	141.9	1	0	1	1	9.713	1.916	-0.087	0.070	-4.892
218	-82.7	-130.1	4	4	4	4	10.209	3.140	1.137	0.362	-4.396
219	-82.6	68.6	2	1	4	3	10.336	1.685	-0.318	0.199	-4.269
220	-82.3	24.1	2	2	4	2	10.133	2.522	0.519	0.055	-4.472
221	-82.2	13.1	2	3	4	3	10.747	2.776	0.773	0.081	-3.858
222	-82.0	-137.7	4	2	3	3	10.567	3.315	1.312	0.092	-4.038
223	-81.8	-141.5	3	2	2	2	10.560	2.289	0.286	0.111	-4.045
224	-81.5	108.2	2	1	4	2	10.831	1.946	-0.057	0.048	-3.774
225	-81.3	-44.9	3	4	4	4	10.103	2.059	0.056	0.093	-4.502
226	-80.5	-109.4	4	4	4	4	10.257	3.071	1.068	0.164	-4.348
227	-79.8	71.3	2	4	5	3	9.565	2.046	0.043	0.092	-5.040
228	-79.7	-51.7	4	4	4	4	10.745	2.330	0.327	0.103	-3.860
229	-79.2	-36.3	4	5	5	5	9.026	2.186	0.183	0.061	-5.579
230	-78.9	35.8	4	5	5	6	10.097	2.238	0.235	0.145	-4.508
231	-78.6	50.3	4	4	4	4	10.869	1.704	-0.299	0.157	-3.736
232	-78.5	21.7	4	4	4	4	10.369	2.664	0.661	0.226	-4.236
233	-78.5	-129.9	1	4	4	3	10.927	2.408	0.405	0.210	-3.678
234	-78.4	3.6	4	4	5	4	10.223	2.328	0.325	0.126	-4.382
235	-77.1	89.5	4	4	4	4	10.833	2.142	0.139	0.170	-3.772
236	-77.1	-40.2	4	1	2	2	9.821	2.138	0.135	0.090	-4.784
237	-77.0	-66.9	4	5	3	4	10.842	2.657	0.654	0.117	-3.763
238	-76.8	-120.1	4	4	4	4	10.660	1.755	-0.248	0.066	-3.945
239	-76.8	-45.5	4	4	4	4	10.015	2.114	0.111	0.053	-4.590
240	-76.4	-160.1	2	2	2	2	10.768	2.779	0.776	0.016	-3.837

ID	α_{IRS7}	δ_{IRS7}	n_{K1}	n_{K2}	n_{K3}	n_{H3}	$\langle m_K \rangle$	$(H-K)_{obs}$	$(H-K)_0$	Δm_K	M_{BOL}
241	-75.9	154.6	2	1	2	2	9.382	2.048	0.045	0.075	-5.223
242	-75.7	-95.9	4	4	4	4	10.424	2.554	0.551	0.085	-4.181
243	-75.6	-103.5	2	4	3	5	10.210	2.468	0.465	0.556	-4.395
244	-75.4	140.0	2	1	2	2	10.494	2.288	0.285	0.078	-4.111
245	-75.4	68.5	4	4	4	6	10.160	1.911	-0.092	0.035	-4.445
246	-75.0	73.6	4	4	4	4	10.595	1.947	-0.056	0.105	-4.010
247	-74.5	13.9	4	4	4	4	9.819	2.584	0.581	0.263	-4.786
248	-74.0	80.7	4	4	4	4	10.937	1.834	-0.169	0.071	-3.668
249	-73.7	-33.4	4	6	4	6	10.619	1.707	-0.296	0.026	-3.986
250	-73.6	-69.7	3	5	4	6	9.669	1.607	-0.396	0.083	-4.936
251	-73.0	-131.4	4	4	4	4	9.797	2.642	0.639	0.089	-4.808
252	-73.0	7.2	4	4	4	4	10.792	2.366	0.363	0.057	-3.813
253	-72.6	105.8	1	3	3	4	10.959	1.549	-0.454	0.224	-3.646
254	-72.3	98.0	4	4	4	4	10.882	2.131	0.128	0.019	-3.723
255	-72.0	53.8	4	4	4	4	10.656	2.309	0.306	0.089	-3.949
256	-72.0	-110.8	4	4	3	4	10.705	3.056	1.053	0.149	-3.900
257	-71.8	108.1	4	3	4	2	10.748	1.986	-0.017	0.171	-3.857
258	-71.8	143.9	2	1	2	2	10.517	2.254	0.251	0.186	-4.088
259	-70.5	19.0	4	4	4	3	10.515	2.342	0.339	0.179	-4.090
260	-70.0	126.2	4	3	4	4	10.748	2.413	0.410	0.086	-3.857
261	-69.9	26.8	4	3	3	1	10.566	2.092	0.089	0.196	-4.039
262	-69.8	-90.1	4	4	4	4	9.498	2.318	0.315	0.386	-5.107
263	-69.2	-55.0	4	4	4	4	10.624	2.441	0.438	0.009	-3.981
264	-69.2	-122.2	4	4	4	4	9.305	2.393	0.390	0.076	-5.300
265	-68.3	-84.6	3	1	4	3	10.591	2.276	0.273	0.119	-4.014
266	-67.4	-81.9	3	4	4	3	10.574	2.204	0.201	0.169	-4.031
267	-66.8	85.8	4	4	4	4	10.356	1.921	-0.082	0.175	-4.249
268	-66.6	-131.4	4	2	2	3	10.126	2.212	0.209	0.150	-4.479
269	-66.6	7.8	4	4	4	3	10.697	1.731	-0.272	0.159	-3.908
270	-66.4	-102.6	4	4	1	5	10.849	2.043	0.040	0.160	-3.756
271	-66.0	-108.1	4	0	2	3	10.649	1.583	-0.420	0.234	-3.956
272	-64.5	27.8	5	1	2	2	10.454	2.042	0.039	0.197	-4.151
273	-64.4	80.5	4	4	4	3	10.652	2.058	0.055	0.139	-3.953
274	-64.1	-115.4	4	2	2	2	10.552	2.440	0.437	0.138	-4.053
275	-62.8	-25.3	3	1	1	2	10.255	1.834	-0.169	0.130	-4.350
276	-62.5	-79.8	2	2	2	2	10.288	1.726	-0.277	0.005	-4.317
277	-61.8	95.5	4	4	4	4	10.528	2.198	0.195	0.061	-4.077
278	-60.5	44.3	4	2	2	3	10.679	2.335	0.332	0.108	-3.926
279	-60.4	99.2	5	1	2	5	10.662	1.913	-0.090	0.116	-3.943
280	-59.0	-160.0	1	1	1	1	10.828	3.413	1.410	0.250	-3.777
281	-58.9	-43.1	2	2	2	2	10.860	2.452	0.449	0.133	-3.745
282	-57.9	-90.1	2	2	2	2	10.176	2.217	0.214	0.070	-4.429
283	-57.5	-102.2	2	1	2	3	10.857	2.103	0.100	0.245	-3.748
284	-56.7	-59.3	2	2	2	2	10.825	2.209	0.206	0.248	-3.780
285	-56.7	-23.7	2	2	2	2	10.921	2.325	0.322	0.052	-3.684

ID	α_{IRS7}	δ_{IRS7}	n_{K1}	n_{K2}	n_{K3}	n_{H3}	$\langle m_K \rangle$	$(H-K)_{obs}$	$(H-K)_0$	Δm_K	M_{BOL}
286	-56.6	-94.0	0	2	2	2	10.717	2.389	0.386	0.000	-3.888
287	-56.4	65.9	2	3	2	2	10.863	2.560	0.557	0.090	-3.742
288	-56.0	-75.1	2	2	2	2	10.658	2.935	0.932	0.090	-3.947
289	-55.5	40.4	2	2	2	2	10.027	2.409	0.406	0.020	-4.578
290	-55.1	-114.0	2	2	2	2	10.554	1.945	-0.058	0.156	-4.051
291	-54.6	-146.1	1	1	1	1	9.388	2.897	0.894	0.028	-5.217
292	-54.2	3.2	0	2	1	1	11.051	2.091	0.088	0.108	-3.554
293	-54.1	-1.4	2	3	2	3	10.256	1.875	-0.128	0.195	-4.349
294	-54.1	-50.5	2	2	2	2	10.981	2.566	0.563	0.065	-3.624
295	-53.7	-29.1	2	2	2	2	9.735	2.235	0.232	0.120	-4.870
296	-53.5	168.8	0	1	1	1	10.366	2.037	0.034	0.026	-4.239
297	-53.3	-3.8	0	1	2	1	10.778	2.015	0.012	0.128	-3.827
298	-53.2	6.4	2	2	2	2	10.529	2.262	0.259	0.154	-4.076
299	-52.9	-117.4	2	2	2	2	10.906	2.911	0.908	0.255	-3.699
300	-52.8	-12.3	2	2	2	2	8.529	2.112	0.109	0.026	-6.076
301	-51.9	11.5	2	2	2	1	10.260	2.457	0.454	0.071	-4.345
302	-51.9	97.8	1	1	2	2	10.784	1.998	-0.005	0.084	-3.821
303	-51.2	146.5	1	1	1	1	10.423	2.046	0.043	0.086	-4.182
304	-51.0	-30.8	1	2	0	2	10.739	1.868	-0.135	0.292	-3.866
305	-51.0	161.7	1	1	1	1	10.063	3.174	1.171	0.441	-4.542
306	-50.0	-24.2	2	2	2	2	10.465	2.979	0.976	0.221	-4.140
307	-49.3	-17.5	0	1	1	2	10.367	2.204	0.201	0.119	-4.238
308	-49.3	-123.5	2	2	2	2	9.817	2.808	0.805	0.277	-4.788
309	-49.0	135.4	1	2	2	2	10.585	2.736	0.733	0.185	-4.020
310	-48.9	-164.1	1	1	1	1	10.669	2.871	0.868	0.112	-3.936
311	-47.4	5.6	1	2	2	2	9.683	2.013	0.010	0.315	-4.922
312	-47.4	59.4	2	2	2	2	10.979	2.468	0.465	0.134	-3.626
313	-47.3	81.4	2	2	2	2	10.984	2.336	0.333	0.101	-3.621
314	-46.2	-62.2	2	2	2	2	10.069	2.543	0.540	0.192	-4.536
315	-45.4	-1.7	2	2	2	3	10.336	2.180	0.177	0.400	-4.269
316	-45.0	-57.6	2	0	1	1	10.939	2.182	0.179	0.014	-3.666
317	-43.7	7.4	2	2	2	2	9.152	1.990	-0.013	0.153	-5.453
318	-43.4	-66.2	2	1	3	3	9.350	2.094	0.091	0.131	-5.255
319	-42.7	33.3	2	3	3	2	10.702	2.163	0.160	0.118	-3.903
320	-42.4	-142.9	1	1	1	1	9.960	2.596	0.593	0.076	-4.645
321	-42.4	-59.6	2	2	2	2	10.512	2.176	0.173	0.203	-4.093
322	-42.3	72.4	2	2	2	2	10.610	2.636	0.633	0.055	-3.995
323	-42.2	163.5	0	1	1	1	10.413	1.785	-0.218	0.026	-4.192
324	-41.9	25.4	2	2	2	2	10.743	2.305	0.302	0.065	-3.862
325	-41.8	-101.1	2	3	3	3	10.092	1.670	-0.333	0.255	-4.513
326	-41.6	-51.0	2	2	2	2	10.313	2.702	0.699	0.091	-4.292
327	-41.4	-2.0	2	2	2	3	10.015	2.193	0.190	0.176	-4.590
328	-41.3	92.2	2	2	2	2	9.019	1.975	-0.028	0.026	-5.586
329	-41.2	160.7	1	1	1	1	9.331	2.841	0.838	0.022	-5.274
330	-40.0	-34.1	2	3	3	1	10.249	2.879	0.876	0.094	-4.356

ID	α_{IRS7}	δ_{IRS7}	n_{K1}	n_{K2}	n_{K3}	n_{H3}	$\langle m_K \rangle$	$(H-K)_{obs}$	$(H-K)_0$	Δm_K	M_{BOL}
331	-39.7	-9.8	0	1	0	2	11.141	2.088	0.085	-1.00	-3.464
332	-39.7	1.2	1	3	0	1	10.765	2.252	0.249	0.416	-3.840
333	-39.3	-41.6	2	2	2	2	10.160	3.061	1.058	0.209	-4.445
334	-38.9	-107.0	3	2	2	2	9.925	1.874	-0.129	0.341	-4.680
335	-38.1	112.5	2	2	2	2	10.442	1.812	-0.191	0.109	-4.163
336	-38.0	155.5	1	1	1	1	10.505	2.719	0.716	0.121	-4.100
337	-37.9	-8.1	2	2	2	2	10.212	2.335	0.332	0.447	-4.393
338	-37.6	144.8	1	1	1	1	10.433	2.483	0.480	0.170	-4.172
339	-36.5	58.7	0	1	1	2	10.963	2.456	0.453	0.000	-3.642
340	-36.2	6.4	0	2	2	2	10.433	1.756	-0.247	0.087	-4.172
341	-36.2	-49.5	1	2	2	2	10.404	1.962	-0.041	0.160	-4.201
342	-34.9	74.3	2	2	2	2	9.862	1.876	-0.127	0.158	-4.743
343	-34.6	90.3	2	2	2	2	10.499	2.239	0.236	0.026	-4.106
344	-33.9	-146.4	1	3	2	1	10.462	3.620	1.617	0.050	-4.143
345	-33.8	-43.5	0	1	2	2	10.941	2.100	0.097	0.203	-3.664
346	-33.7	14.6	1	2	1	3	10.534	2.331	0.328	0.231	-4.071
347	-33.6	155.9	1	1	1	1	10.870	2.391	0.388	0.072	-3.735
348	-33.6	59.9	2	2	2	2	10.393	2.849	0.846	0.030	-4.212
349	-33.1	79.7	2	2	2	2	9.288	2.004	0.001	0.017	-5.317
350	-32.9	-18.4	4	2	4	3	10.228	2.849	0.846	0.217	-4.377
351	-32.4	-165.7	1	3	2	2	10.564	2.623	0.620	0.089	-4.041
352	-31.6	120.6	2	2	2	2	10.335	2.278	0.275	0.148	-4.270
353	-30.4	114.9	3	2	3	2	9.073	2.192	0.189	0.101	-5.532
354	-30.3	-51.8	3	3	3	3	10.681	2.556	0.553	0.157	-3.924
355	-29.4	2.6	4	3	4	4	10.952	2.430	0.427	0.129	-3.653
356	-28.0	-22.2	4	2	4	3	10.433	2.439	0.436	0.259	-4.172
357	-28.0	-111.6	3	4	4	4	10.746	3.350	1.347	0.094	-3.859
358	-27.5	-34.5	4	2	4	6	10.081	2.103	0.100	0.144	-4.524
359	-26.8	-161.6	1	3	2	2	10.934	2.120	0.117	0.051	-3.671
360	-26.7	-39.1	5	3	4	4	9.804	3.032	1.029	0.183	-4.801
361	-25.7	18.1	2	3	2	3	10.225	3.023	1.020	0.171	-4.380
362	-25.3	129.5	5	4	4	4	10.518	2.604	0.601	0.158	-4.087
363	-25.1	165.7	2	1	2	2	10.999	2.751	0.748	0.080	-3.606
364	-24.7	36.4	2	4	3	4	10.888	2.397	0.394	0.194	-3.717
365	-24.5	71.6	4	4	3	4	9.681	1.906	-0.097	0.035	-4.924
366	-24.0	75.9	4	4	3	4	10.288	2.188	0.185	0.057	-4.317
367	-23.7	68.1	3	5	4	4	10.145	2.032	0.029	0.103	-4.460
368	-22.6	96.8	6	4	3	4	9.807	2.407	0.404	0.115	-4.798
369	-22.6	-100.0	4	6	5	5	8.506	2.517	0.514	0.556	-6.099
370	-22.5	16.2	4	3	4	4	9.619	2.385	0.382	0.074	-4.986
371	-22.3	11.6	2	3	3	1	10.614	2.777	0.774	0.156	-3.991
372	-21.6	40.7	4	4	3	4	9.233	2.383	0.380	0.051	-5.372
373	-21.4	115.9	4	4	4	4	10.030	2.175	0.172	0.039	-4.575
374	-20.8	-143.7	1	3	2	2	10.892	3.249	1.246	0.115	-3.713
375	-20.0	-91.3	4	4	4	4	10.642	2.430	0.427	0.167	-3.963

ID	α_{IRS7}	δ_{IRS7}	n_{K1}	n_{K2}	n_{K3}	n_{H3}	$\langle m_K \rangle$	$(H-K)_{obs}$	$(H-K)_0$	Δm_K	M_{BOL}
376	-19.8	-161.9	1	3	1	2	10.607	2.234	0.231	0.143	-3.998
377	-19.1	76.8	3	4	3	4	10.153	2.102	0.099	0.049	-4.452
378	-18.9	-30.7	3	2	4	3	10.422	3.214	1.211	0.355	-4.183
379	-18.7	-22.9	2	2	3	3	10.816	2.592	0.589	0.267	-3.789
380	-18.2	24.6	4	3	4	3	10.457	2.175	0.172	0.136	-4.148
381	-17.9	73.1	4	4	3	4	9.632	1.939	-0.064	0.040	-4.973
382	-17.3	130.6	5	4	4	4	10.202	1.988	-0.015	0.080	-4.403
383	-17.0	27.6	3	2	4	3	10.673	2.424	0.421	0.287	-3.932
384	-16.4	10.1	4	3	4	4	10.023	1.869	-0.134	0.280	-4.582
385	-15.7	-76.1	2	4	2	4	9.896	2.990	0.987	0.049	-4.709
386	-15.4	18.0	4	3	4	4	10.047	2.258	0.255	0.033	-4.558
387	-15.0	158.5	3	2	2	2	10.226	2.273	0.270	0.002	-4.379
388	-14.9	23.0	2	1	2	1	11.041	2.311	0.308	0.188	-3.564
389	-14.3	121.9	4	4	4	4	10.600	1.998	-0.005	0.293	-4.005
390	-12.5	-6.7	0	1	0	3	10.376	2.479	0.476	-1.00	-4.229
391	-12.4	84.5	4	4	2	4	10.158	1.894	-0.109	0.299	-4.447
392	-12.4	105.2	4	4	3	3	10.592	1.978	-0.025	0.204	-4.013
393	-12.2	-16.2	0	2	2	2	9.943	2.388	0.385	0.558	-4.662
394	-12.0	-23.8	0	1	1	1	10.799	2.076	0.073	0.295	-3.806
395	-11.0	128.9	4	4	2	4	10.290	1.836	-0.167	0.041	-4.315
396	-10.9	77.8	4	4	0	4	10.280	1.892	-0.111	0.136	-4.325
397	-10.8	-86.4	2	2	2	2	10.533	2.736	0.733	0.190	-4.072
398	-10.4	158.4	3	2	0	2	10.774	1.602	-0.401	0.298	-3.831
399	-10.3	45.4	4	1	1	4	10.395	1.904	-0.099	0.138	-4.210
400	-10.1	19.8	3	1	2	4	9.847	2.064	0.061	0.280	-4.758
401	-9.8	93.2	4	0	1	4	10.960	2.302	0.299	0.046	-3.645
402	-9.4	113.2	4	2	2	4	8.747	2.212	0.209	0.131	-5.858
403	-8.9	-19.8	0	0	2	1	10.498	1.500	-0.503	-1.00	-4.107
404	-8.5	-33.2	2	0	2	3	9.154	2.250	0.247	0.110	-5.451
405	-8.4	-7.7	0	0	1	2	10.114	2.434	0.431	-1.00	-4.491
406	-8.3	-16.2	2	0	2	3	9.687	1.717	-0.286	0.208	-4.918
407	-8.2	17.9	0	1	2	2	10.230	2.050	0.047	0.026	-4.375
408	-8.1	7.8	2	1	2	3	8.868	2.172	0.169	0.058	-5.737
409	-8.0	162.9	2	1	1	2	10.769	1.896	-0.107	0.103	-3.836
410	-7.0	89.1	1	2	1	4	10.637	2.085	0.082	0.210	-3.968
411	-6.8	128.7	2	2	2	4	10.837	1.844	-0.159	0.091	-3.768
412	-6.2	-26.3	1	0	2	2	9.898	2.315	0.312	0.173	-4.707
413	-6.0	104.1	2	2	2	3	8.743	1.939	-0.064	0.176	-5.862
414	-6.0	0.2	1	1	2	3	9.998	2.637	0.634	0.521	-4.607
415	-5.1	-21.3	2	0	2	2	9.935	1.658	-0.345	0.112	-4.670
416	-4.9	47.0	2	2	1	2	9.309	2.081	0.078	0.085	-5.296
417	-4.8	35.6	1	2	1	2	10.955	2.861	0.858	0.233	-3.650
418	-3.4	-12.4	2	0	2	2	8.503	2.157	0.154	0.047	-6.102
419	-3.4	-31.0	2	0	2	2	8.166	1.986	-0.017	0.017	-6.439
420	-2.9	95.0	2	2	1	2	10.713	2.445	0.442	0.229	-3.892

ID	α_{IRS7}	δ_{IRS7}	n_{K1}	n_{K2}	n_{K3}	n_{H3}	$\langle m_K \rangle$	$(H-K)_{obs}$	$(H-K)_0$	Δm_K	M_{BOL}
421	-1.2	-23.9	0	0	2	2	10.952	1.715	-0.288	-1.00	-3.653
422	-1.0	-48.6	2	1	2	2	10.161	2.178	0.175	0.173	-4.444
423	-0.8	12.1	2	1	2	1	9.764	2.311	0.308	0.276	-4.841
424	-0.3	30.8	2	2	1	3	10.547	1.940	-0.063	0.189	-4.058
425	0.0	0.0	2	1	2	3	6.901	2.693	0.690	0.148	-7.704
426	0.3	-13.4	2	0	2	2	8.718	2.198	0.195	0.057	-5.887
427	0.5	94.2	2	2	1	2	10.590	1.668	-0.335	0.048	-4.015
428	0.5	154.6	2	1	1	1	9.269	2.184	0.181	0.112	-5.336
429	0.7	111.8	2	2	2	2	10.588	2.676	0.673	0.122	-4.017
430	1.0	5.4	1	1	2	2	8.904	2.325	0.322	0.133	-5.701
431	1.0	-27.1	2	0	2	2	9.931	2.550	0.547	0.068	-4.674
432	1.5	72.9	0	2	1	2	10.243	2.481	0.478	0.300	-4.362
433	1.7	42.0	2	2	1	2	9.419	2.370	0.367	0.080	-5.186
434	1.9	120.0	2	2	2	2	9.613	2.318	0.315	0.088	-4.992
435	1.9	23.4	2	1	2	2	9.759	3.502	1.499	0.083	-4.846
436	2.1	34.4	2	2	1	2	10.729	2.729	0.726	0.247	-3.876
437	2.7	-5.2	1	0	1	2	7.938	2.027	0.024	0.095	-6.667
438	3.0	75.7	2	2	1	1	10.022	2.402	0.399	0.122	-4.583
439	3.3	-16.4	1	0	2	1	9.930	2.554	0.551	0.248	-4.675
440	4.4	-23.4	2	0	2	2	10.709	2.156	0.153	0.153	-3.896
441	4.4	80.8	2	2	1	2	10.241	2.123	0.120	0.129	-4.364
442	4.6	28.1	2	1	2	2	9.630	2.259	0.256	0.156	-4.975
443	5.0	144.1	2	1	1	1	10.561	1.653	-0.350	0.047	-4.044
444	5.1	-11.7	2	0	2	2	8.550	2.291	0.288	0.033	-6.055
445	5.5	138.5	2	1	1	1	9.697	1.854	-0.149	0.117	-4.908
446	5.7	-4.5	2	0	1	1	8.171	2.493	0.490	0.098	-6.434
447	5.8	165.1	2	1	1	1	9.956	1.891	-0.112	0.098	-4.649
448	5.8	110.4	2	2	2	2	11.006	2.242	0.239	0.260	-3.599
449	6.1	121.8	2	2	2	1	10.618	1.831	-0.172	0.087	-3.987
450	6.1	160.4	2	1	1	1	10.826	3.034	1.031	0.077	-3.779
451	6.3	-58.8	2	1	2	2	9.656	1.930	-0.073	0.110	-4.949
452	6.5	98.5	3	2	1	3	10.433	2.363	0.360	0.471	-4.172
453	6.8	102.6	2	2	2	2	10.314	1.946	-0.057	0.129	-4.291
454	7.2	154.6	2	1	1	1	10.919	1.697	-0.306	0.038	-3.686
455	7.6	-1.4	0	1	2	2	9.166	2.578	0.575	0.625	-5.439
456	8.5	-23.5	2	0	2	2	10.155	2.560	0.557	0.254	-4.450
457	8.6	66.6	2	2	1	2	10.085	2.619	0.616	0.236	-4.520
458	8.7	136.6	2	1	1	1	10.426	1.773	-0.230	0.125	-4.179
459	9.4	-83.7	2	3	3	2	10.954	1.535	-0.468	0.330	-3.651
460	10.1	104.6	2	2	2	2	10.116	2.325	0.322	0.151	-4.489
461	10.2	-149.7	0	2	1	1	10.934	2.028	0.025	0.221	-3.671
462	10.2	-11.2	2	0	2	2	9.534	2.831	0.828	0.053	-5.071
463	10.6	71.0	2	2	1	1	10.410	2.847	0.844	0.143	-4.195
464	11.2	78.2	2	2	1	2	10.181	2.364	0.361	0.215	-4.424
465	12.5	-120.7	1	2	2	4	10.738	2.190	0.187	0.049	-3.867

ID	α_{IRS7}	δ_{IRS7}	n_{K1}	n_{K2}	n_{K3}	n_{H3}	$\langle m_K \rangle$	$(H-K)_{obs}$	$(H-K)_0$	Δm_K	M_{BOL}
466	12.6	-0.2	2	1	2	3	8.911	2.064	0.061	0.042	-5.694
467	13.6	17.8	2	1	2	3	10.238	2.713	0.710	0.163	-4.367
468	14.2	-24.1	2	0	2	3	8.468	2.852	0.849	0.101	-6.137
469	14.9	-16.2	2	0	2	3	9.721	2.493	0.490	0.145	-4.884
470	15.4	3.9	1	1	2	4	9.784	2.029	0.026	0.060	-4.821
471	15.7	-10.1	1	0	2	3	10.390	2.505	0.502	0.144	-4.215
472	15.8	97.3	3	2	1	2	10.081	1.675	-0.328	0.101	-4.524
473	15.8	24.6	1	1	2	1	10.539	2.891	0.888	0.538	-4.066
474	16.1	89.0	2	1	1	2	10.195	2.322	0.319	0.302	-4.410
475	16.2	-63.7	2	1	2	3	10.762	2.765	0.762	0.385	-3.843
476	16.8	13.6	2	1	2	3	10.650	2.122	0.119	0.354	-3.955
477	16.9	-0.5	2	2	2	5	9.687	2.025	0.022	0.082	-4.918
478	17.2	44.0	2	2	1	4	8.562	2.391	0.388	0.086	-6.043
479	17.8	8.2	0	1	1	4	10.360	2.168	0.165	0.110	-4.245
480	17.9	90.3	0	2	1	3	10.404	1.819	-0.184	0.300	-4.201
481	19.2	23.3	2	3	2	4	9.880	2.230	0.227	0.152	-4.725
482	19.5	58.4	2	1	1	1	9.477	2.596	0.593	0.205	-5.128
483	20.1	14.6	1	3	2	4	10.406	2.527	0.524	0.067	-4.199
484	20.2	-7.5	2	1	2	4	9.984	2.551	0.548	0.036	-4.621
485	20.3	32.3	2	4	1	1	10.568	2.522	0.519	0.038	-4.037
486	20.8	-98.5	2	2	4	4	10.931	2.252	0.249	0.126	-3.674
487	22.0	9.3	2	3	3	4	10.021	2.981	0.978	0.078	-4.584
488	22.3	17.6	2	3	3	4	9.911	3.216	1.213	0.169	-4.694
489	23.5	118.9	2	4	2	4	9.539	2.420	0.417	0.007	-5.066
490	23.7	166.5	2	1	1	2	10.998	2.017	0.014	0.142	-3.607
491	24.2	-16.0	2	0	3	1	10.934	2.358	0.355	0.352	-3.671
492	24.5	-2.4	1	3	3	2	10.322	3.206	1.203	0.200	-4.283
493	24.7	-21.5	0	1	0	3	10.960	2.792	0.789	-1.00	-3.645
494	25.1	38.5	2	4	3	4	10.297	2.155	0.152	0.129	-4.308
495	25.3	58.1	2	4	3	3	10.632	2.358	0.355	0.192	-3.973
496	25.6	85.0	2	4	3	4	10.265	1.905	-0.098	0.084	-4.340
497	26.0	-13.0	1	0	0	1	10.995	2.297	0.294	-1.00	-3.610
498	26.0	98.7	3	4	4	6	10.746	2.254	0.251	0.040	-3.859
499	26.4	-22.7	2	1	3	1	10.909	3.176	1.173	0.303	-3.696
500	26.9	46.8	2	4	3	4	9.624	2.250	0.247	0.157	-4.981
501	26.9	4.1	2	3	3	3	10.555	3.253	1.250	0.250	-4.050
502	27.5	129.7	1	4	4	4	9.136	2.105	0.102	0.007	-5.469
503	28.3	42.9	2	3	1	4	10.692	2.352	0.349	0.195	-3.913
504	28.4	21.2	4	3	3	4	10.697	2.336	0.333	0.133	-3.908
505	29.7	131.4	0	1	1	2	10.130	1.910	-0.093	0.000	-4.475
506	30.2	61.4	0	1	0	1	10.953	2.962	0.959	-1.00	-3.652
507	30.3	-85.1	2	1	4	3	10.895	2.154	0.151	0.111	-3.710
508	30.9	30.9	4	3	3	6	9.554	2.110	0.107	0.087	-5.051
509	31.0	63.9	4	5	5	4	10.401	2.819	0.816	0.246	-4.204
510	31.2	168.0	1	0	0	2	10.911	2.525	0.522	-1.00	-3.694

ID	α_{IRS7}	δ_{IRS7}	n_{K1}	n_{K2}	n_{K3}	n_{H3}	$\langle m_K \rangle$	$(H-K)_{obs}$	$(H-K)_0$	Δm_K	M_{BOL}
511	31.4	92.5	5	4	3	4	10.848	2.497	0.494	0.058	-3.757
512	31.7	43.5	4	4	2	1	10.735	2.956	0.953	0.074	-3.870
513	32.6	48.3	4	4	3	4	10.792	1.870	-0.133	0.168	-3.813
514	32.7	66.7	4	4	3	4	10.627	2.615	0.612	0.038	-3.978
515	33.7	-20.0	1	0	0	1	11.006	2.832	0.829	-1.00	-3.599
516	33.9	-62.8	2	1	4	4	9.380	1.961	-0.042	0.315	-5.225
517	34.0	-13.8	1	0	0	1	10.509	3.106	1.103	-1.00	-4.096
518	34.2	75.5	3	4	3	4	10.449	2.492	0.489	0.080	-4.156
519	34.5	128.6	4	4	4	4	9.694	1.880	-0.123	0.131	-4.911
520	34.8	24.4	4	3	3	4	8.411	2.557	0.554	0.372	-6.194
521	35.0	-121.6	0	1	2	3	9.578	2.461	0.458	0.246	-5.027
522	35.1	121.7	4	4	4	4	10.054	1.898	-0.105	0.052	-4.551
523	36.0	-68.5	0	1	1	5	10.568	1.983	-0.020	0.090	-4.037
524	36.7	141.7	3	2	2	2	10.757	2.915	0.912	0.014	-3.848
525	36.8	38.9	3	4	3	4	9.515	2.096	0.093	0.062	-5.090
526	37.1	30.5	1	4	3	4	10.766	2.439	0.436	0.161	-3.839
527	38.3	79.1	3	4	3	4	9.197	3.191	1.188	0.491	-5.408
528	39.3	-39.5	1	1	2	2	10.808	2.160	0.157	0.116	-3.797
529	39.4	-27.8	1	1	1	2	9.297	2.793	0.790	0.437	-5.308
530	39.8	9.3	2	3	1	3	8.579	2.375	0.372	0.214	-6.026
531	41.4	40.3	2	2	2	2	10.490	2.532	0.529	0.126	-4.115
532	41.5	120.8	2	4	0	4	10.982	1.644	-0.359	0.062	-3.623
533	41.6	-22.0	1	1	1	2	10.559	2.836	0.833	0.087	-4.046
534	43.5	12.1	0	2	0	1	10.602	2.446	0.443	-1.00	-4.003
535	44.0	1.6	2	2	1	2	10.384	2.013	0.010	0.127	-4.221
536	44.3	152.4	1	1	1	1	8.961	1.991	-0.012	0.219	-5.644
537	44.6	16.6	2	2	1	2	9.719	2.316	0.313	0.090	-4.886
538	44.9	37.7	2	2	2	2	10.971	2.802	0.799	0.125	-3.634
539	45.3	93.1	3	2	2	2	10.047	2.218	0.215	0.145	-4.558
540	45.6	115.8	2	2	1	2	9.636	2.906	0.903	0.106	-4.969
541	46.1	23.5	2	2	1	2	10.525	2.087	0.084	0.129	-4.080
542	47.1	73.7	2	2	2	2	10.551	2.420	0.417	0.066	-4.054
543	47.5	161.4	1	1	1	1	10.521	1.910	-0.093	0.098	-4.084
544	48.7	20.6	0	1	0	1	10.937	2.082	0.079	-1.00	-3.668
545	49.2	90.1	2	2	2	2	9.754	1.954	-0.049	0.068	-4.851
546	49.8	84.6	2	2	2	1	10.536	1.872	-0.131	0.168	-4.069
547	50.3	-10.3	1	1	1	2	10.821	2.759	0.756	0.191	-3.784
548	50.5	69.6	0	0	1	1	10.949	2.029	0.026	-1.00	-3.656
549	50.8	58.2	2	2	2	2	9.910	1.989	-0.014	0.095	-4.695
550	50.8	26.6	3	2	1	2	10.115	1.957	-0.046	0.151	-4.490
551	50.9	-68.9	0	0	2	3	10.487	2.469	0.466	-1.00	-4.118
552	51.8	22.8	1	2	1	1	10.701	2.215	0.212	0.161	-3.904
553	52.9	72.6	2	2	2	2	10.156	1.941	-0.062	0.155	-4.449
554	54.1	107.7	2	2	2	2	10.645	1.951	-0.052	0.178	-3.960
555	54.4	28.6	3	3	2	3	10.014	2.027	0.024	0.029	-4.591

ID	α_{IRS7}	δ_{IRS7}	n_{K1}	n_{K2}	n_{K3}	n_{H3}	$\langle m_K \rangle$	$(H-K)_{obs}$	$(H-K)_0$	Δm_K	M_{BOL}
556	54.6	19.5	2	2	1	2	10.305	2.132	0.129	0.078	-4.300
557	54.8	58.8	2	2	2	1	10.538	3.089	1.086	0.131	-4.067
558	55.3	125.0	2	2	2	2	9.024	1.719	-0.284	0.055	-5.581
559	55.9	111.2	2	2	2	1	10.852	2.282	0.279	0.145	-3.753
560	55.9	143.8	1	1	1	1	10.389	2.280	0.277	0.065	-4.216
561	56.1	-34.4	1	1	1	2	10.520	3.812	1.809	0.165	-4.085
562	56.3	67.8	2	2	2	2	8.223	2.613	0.610	0.149	-6.382
563	57.6	75.6	2	2	2	2	9.461	2.258	0.255	0.104	-5.144
564	57.8	87.1	2	2	2	2	10.377	2.339	0.336	0.097	-4.228
565	57.9	71.3	1	0	2	1	10.009	2.083	0.080	0.151	-4.596
566	59.1	54.4	2	1	2	2	10.434	2.154	0.151	0.133	-4.171
567	59.7	110.9	1	2	2	2	10.748	2.731	0.728	0.110	-3.857
568	60.0	22.8	2	2	1	2	9.897	3.130	1.127	0.354	-4.708
569	60.1	78.1	2	2	2	1	9.826	2.433	0.430	0.109	-4.779
570	60.4	126.6	1	1	2	2	9.082	1.798	-0.205	0.170	-5.523
571	60.4	57.4	2	2	2	2	10.217	2.427	0.424	0.195	-4.388
572	60.4	13.4	1	2	0	1	10.966	3.311	1.308	0.623	-3.639
573	61.7	119.4	2	2	2	2	10.353	1.860	-0.143	0.043	-4.252
574	61.9	-40.7	0	0	2	2	10.825	2.272	0.269	-1.00	-3.780
575	61.9	51.8	2	2	2	2	9.923	2.271	0.268	0.073	-4.682
576	62.4	45.8	2	2	2	2	10.649	2.407	0.404	0.078	-3.956
577	62.6	71.5	2	2	2	1	10.159	2.290	0.287	0.157	-4.446
578	62.9	35.6	2	2	2	2	10.668	2.356	0.353	0.116	-3.937
579	63.3	126.1	2	2	2	2	8.598	2.943	0.940	0.335	-6.007
580	63.5	-110.4	0	0	2	2	10.637	2.348	0.345	-1.00	-3.968
581	63.9	66.3	2	2	2	2	10.570	2.459	0.456	0.158	-4.035
582	64.3	62.4	2	3	3	3	9.431	2.498	0.495	0.106	-5.174
583	64.5	143.1	1	1	1	1	10.411	2.987	0.984	0.110	-4.194
584	64.6	16.6	2	2	1	2	10.166	1.798	-0.205	0.124	-4.439
585	65.7	138.6	1	1	1	1	10.891	2.403	0.400	0.061	-3.714
586	66.2	76.4	2	2	2	2	9.622	2.417	0.414	0.042	-4.983
587	66.6	-47.9	0	0	2	2	9.892	2.403	0.400	-1.00	-4.713
588	67.0	-79.1	0	0	2	2	10.322	2.566	0.563	-1.00	-4.283
589	67.4	26.4	1	1	0	1	11.157	2.011	0.008	0.028	-3.448
590	69.1	159.9	1	1	1	1	8.839	2.153	0.150	0.194	-5.766
591	69.2	37.6	2	4	2	4	9.233	2.869	0.866	0.161	-5.372
592	69.6	21.2	2	4	1	4	9.300	2.750	0.747	0.068	-5.305
593	69.8	-80.4	0	0	2	2	10.215	2.447	0.444	-1.00	-4.390
594	70.3	50.8	2	3	2	3	10.502	2.067	0.064	0.090	-4.103
595	70.5	65.7	2	5	2	6	9.916	3.308	1.305	0.121	-4.689
596	70.5	46.7	2	4	2	4	9.334	1.918	-0.085	0.142	-5.271
597	71.0	-168.8	0	0	1	1	10.367	2.350	0.347	-1.00	-4.238
598	72.4	123.0	2	4	2	4	10.482	3.413	1.410	0.231	-4.123
599	72.7	76.5	2	4	3	4	10.337	2.185	0.182	0.102	-4.268
600	73.0	85.7	2	4	3	4	10.846	2.565	0.562	0.186	-3.759

ID	α_{IRS7}	δ_{IRS7}	n_{K1}	n_{K2}	n_{K3}	n_{H3}	$<m_K>$	$(H-K)_{obs}$	$(H-K)_0$	Δm_K	M_{BOL}
601	74.3	51.9	2	3	3	4	10.226	2.596	0.593	0.317	-4.379
602	74.4	117.9	2	4	3	4	10.398	1.874	-0.129	0.052	-4.207
603	74.9	-114.6	0	0	2	2	10.362	3.505	1.502	-1.00	-4.243
604	75.2	81.0	2	4	4	4	10.389	2.246	0.243	0.089	-4.216
605	75.3	41.0	2	4	4	4	10.127	3.170	1.167	0.133	-4.478
606	76.1	88.9	2	4	4	4	10.439	2.394	0.391	0.068	-4.166
607	76.2	14.7	2	4	3	4	10.614	2.028	0.025	0.171	-3.991
608	76.3	-172.6	0	0	1	1	10.436	3.454	1.451	-1.00	-4.169
609	76.6	70.2	2	4	4	5	9.432	2.322	0.319	0.087	-5.173
610	76.7	23.1	2	4	3	2	10.100	2.814	0.811	0.174	-4.505
611	77.2	49.5	0	0	1	3	10.828	3.028	1.025	-1.00	-3.777
612	79.3	147.1	1	2	2	2	9.203	2.949	0.946	0.067	-5.402
613	81.1	-22.9	2	2	2	2	10.555	2.150	0.147	0.090	-4.050
614	81.4	-34.6	2	2	2	3	10.058	2.396	0.393	0.051	-4.547
615	81.7	108.1	2	4	4	4	10.942	2.925	0.922	0.120	-3.663
616	82.3	44.3	1	4	3	2	10.575	2.481	0.478	0.106	-4.030
617	82.4	-26.0	2	2	2	1	10.909	2.217	0.214	0.045	-3.696
618	82.5	73.0	4	4	4	1	10.737	3.374	1.371	0.206	-3.868
619	84.1	55.6	4	4	4	2	10.595	2.612	0.609	0.058	-4.010
620	84.9	-22.9	2	2	2	3	10.699	1.712	-0.291	0.098	-3.906
621	85.5	44.4	1	4	3	3	10.615	2.505	0.502	0.349	-3.990
622	87.1	99.5	4	4	5	5	10.179	1.993	-0.010	0.069	-4.426
623	87.6	130.8	2	4	2	4	10.723	2.773	0.770	0.124	-3.882
624	87.6	16.8	4	4	3	3	10.865	3.132	1.129	0.185	-3.740
625	88.4	53.8	4	4	4	4	10.841	2.692	0.689	0.167	-3.764
626	88.4	153.5	2	2	2	2	11.001	1.899	-0.104	0.028	-3.604
627	89.9	111.0	4	4	4	4	10.471	3.216	1.213	0.095	-4.134
628	90.0	46.8	4	1	4	2	10.165	2.606	0.603	0.124	-4.440
629	90.4	90.1	4	2	4	3	10.697	1.927	-0.076	0.163	-3.908
630	91.6	40.1	4	2	4	2	9.362	2.408	0.405	0.092	-5.243
631	93.4	45.3	4	2	3	2	10.252	2.099	0.096	0.159	-4.353
632	98.2	129.6	1	2	2	2	10.556	1.831	-0.172	0.170	-4.049
633	100.8	1.0	2	2	2	2	10.571	2.160	0.157	0.124	-4.034
634	102.6	76.9	2	2	2	2	9.170	1.897	-0.106	0.062	-5.435
635	103.1	-20.6	1	1	1	1	9.767	1.825	-0.178	0.059	-4.838
636	104.0	-6.7	2	1	1	1	10.973	2.133	0.130	0.087	-3.632
637	104.2	118.4	2	2	2	2	10.097	2.321	0.318	0.251	-4.508
638	105.0	1.9	2	2	2	2	10.156	2.406	0.403	0.057	-4.449
639	106.1	21.2	2	2	2	2	10.368	2.699	0.696	0.101	-4.237
640	108.3	143.2	1	1	1	1	10.879	2.012	0.009	0.109	-3.726
641	109.6	93.9	3	2	2	2	9.409	2.005	0.002	0.094	-5.196
642	111.6	159.7	1	1	1	1	9.429	2.626	0.623	0.096	-5.176
643	111.8	147.1	1	1	1	1	9.987	1.904	-0.099	0.060	-4.618
644	112.7	89.0	2	2	2	2	10.714	2.162	0.159	0.188	-3.891
645	120.4	153.4	1	1	1	1	10.902	2.045	0.042	0.037	-3.703

ID	α_{IRS7}	δ_{IRS7}	n_{K1}	n_{K2}	n_{K3}	n_{H3}	$<m_K>$	$(H-K)_{obs}$	$(H-K)_0$	Δm_K	M_{BOL}
646	120.7	-11.3	1	2	2	1	10.792	2.221	0.218	0.214	-3.813
647	122.6	90.9	2	3	3	1	10.154	4.498	2.495	0.637	-4.451
648	124.2	137.1	1	2	1	1	10.828	3.097	1.094	0.050	-3.777
649	125.8	139.2	1	2	2	1	10.753	2.687	0.684	0.074	-3.852
650	126.0	120.9	2	4	4	2	10.683	2.951	0.948	0.106	-3.922
651	127.0	62.4	1	6	5	2	10.050	2.552	0.549	0.039	-4.555
652	128.4	159.2	1	2	2	1	10.824	2.281	0.278	0.054	-3.781
653	129.0	-20.5	1	2	2	1	9.079	2.280	0.277	0.198	-5.526
654	131.6	108.8	2	4	4	2	9.094	1.996	-0.007	0.068	-5.511
655	131.8	150.1	1	2	2	1	10.190	3.064	1.061	0.201	-4.415
656	133.6	161.3	2	2	2	1	9.427	2.161	0.158	0.245	-5.178
657	133.7	46.4	3	4	4	2	10.584	2.612	0.609	0.091	-4.021
658	137.2	60.9	5	4	5	2	10.928	2.160	0.157	0.169	-3.677
659	137.2	124.0	4	4	4	2	10.227	1.934	-0.069	0.079	-4.378

TABLE A2-2
GALACTIC CENTER STARS WITH OPTICALLY DETERMINED POSITIONS

No.	Optical (1950)		Infrared (1950)		Optical-Infrared			
	RA	DEC	RA	DEC	ΔRA (")	ΔDEC (")	K (2.2μm)	(H-K)
1	17 42 32.70	-28 59 17.3	17 42 32.5	-28 59 17.3	+2.6	0.0	10.83	1.04
2	17 42 32.19	-28 58 28.4	17 42 32.1	-28 58 27.9	+1.2	-0.5	10.53	0.76
3	17 42 30.20	-29 00 19.3	17 42 30.0	-29 00 19.0	+2.6	-0.3	9.44	1.10
4	17 42 35.72	-28 58 37.6	17 42 35.5	-28 58 38.8	-2.9	+0.8	10.33	0.61
5	17 42 22.37	-29 00 11.8	17 42 22.3	-29 00 09.3	+1.0	-2.5	10.66	1.48
6	17 42 20.95	-28 59 47.7	17 42 21.1	-29 59 47.2	-2.0	+0.5	7.29	0.54
7	17 42 28.89	-29 01 11.7	17 42 28.7	-28 01 10.8	+2.5	-0.9	8.56	0.55
8	17 42 37.94	-28 57 28.1	17 42 37.8	-29 57 30.0	-1.8	+1.9	9.29	0.90
9	17 42 29.39	-29 01 49.4	17 42 29.1	-29 01 47.8	-3.8	-1.6	9.91	0.71
10	17 42 19.74	-29 01 16.6	17 42 19.8	-29 01 15.8	-0.8	-0.8	9.59	0.37

APPENDIX 3 :

GALACTIC CENTER HKL PHOTOMETRY

The following table is a listing of the HKL database of 257 stars used in the discussions of chapter 4. The column are designated by:

ID : Star Identification Number
α_{IRS7} : Right Ascension position offset from IRS 7; $17^h\ 42^m\ 29.2^s$ (1950), in arcseconds.
δ_{IRS7} : Declination offset position from IRS 7; -29° 59′ 12.9″ (1950), in arcseconds.
n_{K3} : Number of K detections in May 1988
n_{H3} : Number of H detections in May 1988
n_{L3} : Number of L detections in June 1988
$<m_K>$: Average K magnitude
Δm_K : The RMS residual K magnitude between epochs
$(H-K)_{OBS}$: Observed H-K color, $m_H - m_K(3)$
$(K-L)_{OBS}$: Observed K-L color, $m_K(3) - m_L$
$(H-K)_0$: Intrinsic H-K
$(K-L)_0$: Intrinsic K-L

All colors were dereddened by $A_V = 31.8$ mag using the extinction curve of Rieke and Lebofsky (1985).

TABLE A3-1

ID	α_{IRS7}	δ_{IRS7}	n_K	n_H	n_L	$<m_K>$	Δm_K	$(H-K)_{OBS}$	$(K-L)_{OBS}$	$(H-K)_0$	$(K-L)_0$
1	-184.5	-72.8	2	2	1	10.62	0.00	2.75	2.13	0.75	0.38
2	-183.6	13.5	2	1	1	9.93	0.00	2.51	2.03	0.51	0.28
3	-178.6	-20.1	2	2	1	10.16	0.08	1.90	1.60	-0.10	-0.14
4	-176.9	22.0	2	2	1	9.24	0.40	2.85	2.06	0.84	0.31
5	-176.5	34.1	3	3	1	10.60	0.11	3.01	2.31	1.00	0.56
6	-175.6	41.6	2	2	1	10.35	0.10	2.33	2.08	0.33	0.33
7	-174.7	4.6	1	2	1	10.88	0.06	2.21	2.32	0.21	0.57
8	-174.3	162.9	1	1	1	9.41	0.14	2.03	1.81	0.03	0.07
9	-167.7	-158.0	1	1	1	10.53	0.10	2.87	2.02	0.86	0.27
10	-165.8	-91.2	2	2	1	10.70	0.08	1.98	2.00	-0.02	0.25
11	-164.5	65.8	3	1	1	9.89	0.16	2.40	2.01	0.40	0.26
12	-160.8	-26.8	2	2	1	10.77	0.10	2.29	2.38	0.29	0.63
13	-159.8	-128.8	2	1	1	9.64	0.49	1.97	2.23	-0.03	0.48
14	-158.5	-56.9	2	2	1	10.35	0.14	2.03	1.78	0.03	0.03
15	-157.4	-44.8	2	2	2	9.30	0.07	2.09	2.07	0.08	0.32
16	-157.3	90.4	2	2	2	9.33	0.13	2.67	1.51	0.67	-0.23
17	-156.5	-50.3	2	2	2	10.31	0.06	2.20	2.00	0.19	0.25
18	-154.4	8.2	2	2	2	10.05	0.25	2.99	2.52	0.99	0.77
19	-154.0	130.7	2	2	2	8.24	0.08	2.15	2.05	0.15	0.30
20	-151.9	89.0	2	2	1	10.31	0.10	2.93	1.80	0.92	0.05
21	-151.8	-63.9	2	2	1	9.46	0.05	1.88	1.67	-0.12	-0.08

ID	α_{IRS7}	δ_{IRS7}	n_K	n_H	n_L	$<m_K>$	Δm_K	$(H-K)_{OBS}$	$(K-L)_{OBS}$	$(H-K)_0$	$(K-L)_0$
22	-148.1	60.0	2	2	2	10.09	0.06	2.02	1.95	0.02	0.20
23	-147.0	24.5	2	2	2	9.94	0.25	2.50	2.34	0.50	0.59
24	-146.6	111.4	2	2	1	9.99	0.06	2.27	1.56	0.26	-0.19
25	-146.5	-4.7	2	2	2	10.38	0.12	3.64	2.39	1.64	0.64
26	-145.5	-39.6	2	2	2	9.86	0.23	1.79	1.85	-0.22	0.10
27	-144.8	-106.3	2	2	1	10.29	0.21	2.79	2.03	0.78	0.28
28	-144.2	140.1	1	1	3	10.20	0.13	3.29	1.62	1.29	-0.13
29	-142.2	-67.4	2	3	3	9.20	0.12	2.03	1.65	0.03	-0.10
30	-141.4	-30.5	2	2	3	10.08	0.17	2.24	1.44	0.24	-0.31
31	-138.7	-24.9	2	2	1	10.55	0.10	1.73	2.01	-0.28	0.26
32	-138.3	-134.3	4	4	1	10.42	0.10	2.56	1.70	0.56	-0.05
33	-138.2	-167.5	2	2	2	8.91	0.24	2.71	1.80	0.71	0.05
34	-138.0	-114.6	2	4	2	10.01	0.07	2.44	1.52	0.44	-0.22
35	-137.8	112.6	2	2	1	10.98	0.09	2.27	3.01	0.27	1.26
36	-137.6	8.6	2	2	1	10.36	0.05	2.27	1.77	0.27	0.02
37	-137.4	-138.6	2	3	1	9.60	0.16	1.93	1.21	-0.07	-0.54
38	-136.8	28.9	2	2	2	9.59	0.17	1.97	1.58	-0.03	-0.17
39	-135.9	50.6	2	2	3	10.22	0.07	1.79	1.59	-0.22	-0.16
40	-134.8	-54.9	4	4	2	9.73	0.04	1.71	1.26	-0.29	-0.49
41	-133.7	56.7	2	2	2	10.77	0.09	2.04	2.24	0.04	0.49
42	-131.4	112.0	3	2	2	9.36	0.03	1.81	1.46	-0.19	-0.29
43	-131.1	139.4	1	1	2	8.95	0.06	1.83	1.53	-0.18	-0.22
44	-129.8	78.3	4	4	1	9.92	0.09	2.28	2.06	0.28	0.32
45	-128.0	-67.4	4	6	3	10.30	0.07	2.04	1.76	0.03	0.01
46	-124.2	10.0	4	4	2	10.32	0.24	2.88	2.28	0.88	0.53
47	-121.4	-80.7	4	4	3	10.03	0.11	1.90	1.60	-0.10	-0.15
48	-121.3	44.3	4	1	2	9.95	0.61	3.45	3.32	1.45	1.57
49	-121.1	-159.1	2	2	3	9.22	0.11	2.16	1.79	0.16	0.04
50	-120.4	152.5	2	2	3	8.42	0.19	2.03	1.94	0.03	0.19
51	-119.8	-75.7	4	4	3	9.38	0.48	3.49	2.61	1.49	0.86
52	-117.8	93.9	4	4	3	10.21	0.10	1.66	1.98	-0.34	0.23
53	-116.6	-53.7	2	3	1	9.62	0.22	1.91	1.67	-0.09	-0.08
54	-115.3	31.0	5	5	2	10.09	0.13	1.52	1.79	-0.48	0.04
55	-115.2	-6.1	2	2	1	10.59	0.12	3.53	2.65	1.52	0.91
56	-114.8	93.6	4	1	3	10.85	0.17	1.63	2.34	-0.37	0.59
57	-114.7	104.6	4	5	3	9.98	0.04	1.56	2.01	-0.44	0.27
58	-114.5	85.7	3	4	1	9.62	0.24	2.04	2.15	0.04	0.40
59	-114.2	-60.5	2	4	1	10.76	0.25	2.59	2.14	0.58	0.39
60	-113.4	-88.0	2	2	3	10.03	0.11	2.56	1.93	0.56	0.18
61	-111.8	160.4	2	1	2	10.99	0.17	3.39	2.48	1.39	0.73
62	-110.3	-53.0	2	2	2	10.40	0.05	2.08	2.11	0.07	0.36
63	-108.2	-153.8	1	1	3	8.83	0.07	1.78	1.64	-0.23	-0.11
64	-107.3	-134.6	2	2	3	9.28	0.07	1.57	1.36	-0.43	-0.39
65	-107.2	117.6	2	4	2	10.13	0.16	1.58	1.65	-0.42	-0.10
66	-105.7	-165.9	1	1	2	9.42	0.14	1.66	1.20	-0.34	-0.55

ID	α_{IRS7}	δ_{IRS7}	n_K	n_H	n_L	$\langle m_K \rangle$	Δm_K	$(H-K)_{obs}$	$(K-L)_{obs}$	$(H-K)_0$	$(K-L)_0$
67	-104.0	110.9	2	2	3	10.00	0.04	2.13	1.91	0.13	0.16
68	-103.2	52.8	2	2	1	10.73	0.13	2.43	2.15	0.42	0.40
69	-102.7	-1.6	3	3	2	9.11	0.14	2.07	1.86	0.07	0.11
70	-100.3	154.9	1	1	3	9.49	0.30	3.50	3.00	1.50	1.25
71	-99.2	-94.8	2	2	2	9.93	0.10	3.50	2.02	1.49	0.27
72	-97.6	95.1	2	2	3	10.53	0.08	3.14	1.99	1.14	0.24
73	-93.8	-89.9	2	2	2	10.00	0.05	2.31	1.68	0.31	-0.07
74	-93.4	83.8	2	2	2	9.67	0.13	1.65	1.28	-0.35	-0.47
75	-92.1	-81.0	2	2	3	8.91	0.03	2.19	1.61	0.19	-0.14
76	-91.9	161.6	1	1	2	9.76	0.09	2.14	1.37	0.14	-0.38
77	-91.6	3.8	2	2	2	9.13	0.13	2.41	1.69	0.41	-0.06
78	-91.0	60.5	3	2	2	10.56	0.36	2.74	1.99	0.74	0.24
79	-91.0	147.9	1	1	2	10.11	0.03	1.91	1.64	-0.09	-0.11
80	-90.6	135.7	2	2	3	9.98	0.02	2.12	1.70	0.12	-0.05
81	-90.1	-45.4	2	2	3	9.92	0.42	2.55	2.42	0.54	0.67
82	-87.6	61.6	2	2	2	9.59	0.59	2.77	2.08	0.77	0.33
83	-86.1	105.8	2	2	3	9.92	0.09	1.88	1.66	-0.13	-0.09
84	-85.4	122.4	2	1	3	10.26	0.09	1.85	1.85	-0.15	0.10
85	-84.3	87.1	2	2	3	8.28	0.17	2.01	1.80	0.01	0.06
86	-83.0	141.9	1	1	3	9.71	0.07	1.92	1.59	-0.09	-0.15
87	-82.7	-130.1	4	4	2	10.21	0.36	3.14	2.38	1.14	0.63
88	-82.6	68.6	4	3	2	10.34	0.20	1.69	1.92	-0.32	0.17
89	-82.3	24.1	4	2	2	10.13	0.06	2.52	1.75	0.52	0.00
90	-81.3	-44.9	4	4	1	10.10	0.09	2.06	1.56	0.06	-0.19
91	-80.5	-109.4	4	4	1	10.26	0.16	3.07	1.70	1.07	-0.05
92	-79.8	71.3	5	3	2	9.56	0.09	2.05	1.96	0.04	0.21
93	-79.2	-36.3	5	5	2	9.03	0.06	2.19	1.80	0.18	0.05
94	-78.9	35.8	5	6	3	10.10	0.14	2.24	1.87	0.23	0.12
95	-78.4	3.6	5	4	2	10.22	0.13	2.33	1.65	0.33	-0.10
96	-77.1	-40.2	2	2	2	9.82	0.09	2.14	1.65	0.14	-0.10
97	-76.8	-45.5	4	4	2	10.02	0.05	2.11	1.53	0.11	-0.21
98	-75.9	154.6	2	2	1	9.38	0.07	2.05	1.70	0.04	-0.05
99	-75.6	-103.5	3	5	2	10.21	0.56	2.47	2.27	0.47	0.52
100	-75.4	68.5	4	6	1	10.16	0.04	1.91	1.70	-0.09	-0.05
101	-74.5	13.9	4	4	2	9.82	0.26	2.58	1.85	0.58	0.10
102	-73.6	-69.7	4	6	3	9.67	0.08	1.61	2.16	-0.40	0.41
103	-73.0	-131.4	4	4	3	9.80	0.09	2.64	1.55	0.64	-0.20
104	-71.8	143.9	2	2	2	10.52	0.19	2.25	2.22	0.25	0.47
105	-70.0	126.2	4	4	2	10.75	0.09	2.41	2.25	0.41	0.51
106	-69.8	-90.1	4	4	2	9.50	0.39	2.32	2.01	0.32	0.26
107	-69.2	-55.0	4	4	1	10.62	0.01	2.44	1.99	0.44	0.24
108	-69.2	-122.2	4	4	2	9.30	0.08	2.39	1.58	0.39	-0.17
109	-66.8	85.8	4	4	3	10.36	0.17	1.92	2.07	-0.08	0.32
110	-66.6	-131.4	2	3	1	10.13	0.15	2.21	1.73	0.21	-0.01
111	-60.5	44.3	2	3	3	10.68	0.11	2.33	2.05	0.33	0.30

ID	α_{IRS7}	δ_{IRS7}	n_K	n_H	n_L	$\langle m_K \rangle$	Δm_K	$(H-K)_{OBS}$	$(K-L)_{OBS}$	$(H-K)_0$	$(K-L)_0$
112	-57.9	-90.1	2	2	1	10.18	0.07	2.22	1.57	0.21	-0.18
113	-55.5	40.4	2	2	3	10.03	0.02	2.41	2.06	0.41	0.31
114	-54.6	-146.1	1	1	3	9.39	0.03	2.90	1.84	0.89	0.09
115	-54.1	-1.4	2	3	2	10.26	0.20	1.88	1.96	-0.13	0.21
116	-53.7	-29.1	2	2	3	9.73	0.12	2.23	1.51	0.23	-0.24
117	-52.8	-12.3	2	2	1	8.53	0.03	2.11	1.64	0.11	-0.11
118	-51.9	11.5	2	1	2	10.26	0.07	2.46	2.03	0.45	0.28
119	-51.2	146.5	1	1	1	10.42	0.09	2.05	2.48	0.04	0.73
120	-51.0	-30.8	3	2	2	10.74	0.29	1.87	2.43	-0.14	0.68
121	-51.0	161.7	1	1	3	10.06	0.44	3.17	2.76	1.17	1.01
122	-49.3	-17.5	1	2	1	10.37	0.12	2.20	2.26	0.20	0.51
123	-49.0	135.4	2	2	3	10.59	0.18	2.74	1.83	0.73	0.08
124	-43.7	7.4	2	2	2	9.15	0.15	1.99	1.33	-0.01	-0.42
125	-42.4	-142.9	1	1	1	9.96	0.08	2.60	1.32	0.59	-0.43
126	-42.3	72.4	2	2	2	10.61	0.06	2.64	1.88	0.63	0.13
127	-41.6	-51.0	2	2	1	10.31	0.09	2.70	1.95	0.70	0.20
128	-41.4	-2.0	2	3	2	10.02	0.18	2.19	1.82	0.19	0.07
129	-41.3	92.2	2	2	2	9.02	0.03	1.98	1.44	-0.03	-0.31
130	-41.2	160.7	1	1	2	9.33	0.02	2.84	2.25	0.84	0.50
131	-40.0	-34.1	3	1	2	10.25	0.09	2.88	2.04	0.88	0.29
132	-38.9	-107.0	2	2	2	9.93	0.34	1.87	1.47	-0.13	-0.28
133	-38.0	155.5	1	1	1	10.51	0.12	2.72	2.11	0.72	0.36
134	-37.6	144.8	1	1	1	10.43	0.17	2.48	2.33	0.48	0.58
135	-33.6	155.9	1	1	1	10.87	0.07	2.39	2.17	0.39	0.42
136	-33.1	79.7	2	2	1	9.29	0.02	2.00	1.78	0.00	0.03
137	-32.9	-18.4	4	3	1	10.23	0.22	2.85	2.08	0.85	0.33
138	-31.6	120.6	2	2	3	10.34	0.15	2.28	1.65	0.28	-0.10
139	-30.4	114.9	3	2	3	9.07	0.10	2.19	1.75	0.19	0.01
140	-27.5	-34.5	4	6	2	10.08	0.14	2.10	1.83	0.10	0.08
141	-26.7	-39.1	4	4	2	9.80	0.18	3.03	1.95	1.03	0.20
142	-25.7	18.1	2	3	2	10.22	0.17	3.02	1.82	1.02	0.08
143	-25.3	129.5	4	4	1	10.52	0.16	2.60	1.87	0.60	0.12
144	-24.7	36.4	3	4	2	10.89	0.19	2.40	2.50	0.39	0.75
145	-24.5	71.6	3	4	2	9.68	0.04	1.91	1.66	-0.10	-0.09
146	-24.0	75.9	3	4	2	10.29	0.06	2.19	1.59	0.18	-0.15
147	-23.7	68.1	4	4	2	10.14	0.10	2.03	1.95	0.03	0.20
148	-22.6	96.8	3	4	2	9.81	0.12	2.41	1.63	0.40	-0.12
149	-22.6	-100.0	5	5	3	8.51	0.56	2.52	2.52	0.51	0.77
150	-22.5	16.2	4	4	2	9.62	0.07	2.38	2.20	0.38	0.45
151	-21.6	40.7	3	4	3	9.23	0.05	2.38	1.83	0.38	0.08
152	-21.4	115.9	4	4	2	10.03	0.04	2.17	1.41	0.17	-0.34
153	-19.1	76.8	3	4	3	10.15	0.05	2.10	1.65	0.10	-0.10
154	-18.9	-30.7	4	3	3	10.42	0.35	3.21	2.84	1.21	1.09
155	-17.9	73.1	3	4	3	9.63	0.04	1.94	1.16	-0.06	-0.59
156	-17.3	130.6	4	4	3	10.20	0.08	1.99	2.22	-0.01	0.47

ID	α_{IRS7}	δ_{IRS7}	n_K	n_H	n_L	$\langle m_K \rangle$	Δm_K	$(H-K)_{OBS}$	$(K-L)_{OBS}$	$(H-K)_0$	$(K-L)_0$
157	-17.0	27.6	4	3	3	10.67	0.29	2.42	2.50	0.42	0.75
158	-15.7	-76.1	2	4	3	9.90	0.05	2.99	1.87	0.99	0.12
159	-15.4	18.0	4	4	2	10.05	0.03	2.26	1.75	0.26	0.00
160	-15.0	158.5	2	2	1	10.23	0.00	2.27	1.64	0.27	-0.11
161	-12.4	84.5	2	4	2	10.16	0.30	1.89	1.80	-0.11	0.05
162	-12.4	105.2	3	3	2	10.59	0.20	1.98	2.25	-0.03	0.50
163	-12.2	-16.2	2	2	2	9.94	0.56	2.39	2.04	0.39	0.29
164	-10.9	77.8	8	4	3	10.28	0.14	1.89	2.44	-0.11	0.69
165	-10.3	45.4	1	4	2	10.39	0.14	1.90	1.79	-0.10	0.05
166	-10.1	19.8	2	4	1	9.85	0.28	2.06	1.75	0.06	0.00
167	-9.8	93.2	1	4	1	10.96	0.05	2.30	2.34	0.30	0.59
168	-9.4	113.2	2	4	3	8.75	0.13	2.21	1.92	0.21	0.17
169	-8.3	-16.2	2	3	1	9.69	0.21	1.72	1.49	-0.29	-0.26
170	-8.1	7.8	2	3	2	8.87	0.06	2.17	2.06	0.17	0.31
171	-6.8	128.7	2	4	2	10.84	0.09	1.84	2.22	-0.16	0.47
172	-6.0	104.1	2	3	2	8.74	0.18	1.94	1.83	-0.06	0.09
173	-5.1	-21.3	2	2	2	9.94	0.11	1.66	1.52	-0.34	-0.23
174	-4.9	47.0	1	2	2	9.31	0.09	2.08	1.66	0.08	-0.09
175	-2.9	95.0	1	2	3	10.71	0.23	2.44	2.22	0.44	0.47
176	-1.0	-48.6	2	2	2	10.16	0.17	2.18	1.56	0.17	-0.19
177	-0.8	12.1	2	1	1	9.76	0.28	2.31	1.83	0.31	0.08
178	0.5	94.2	1	2	1	10.59	0.05	1.67	1.92	-0.34	0.17
179	0.5	154.6	1	1	3	9.27	0.11	2.18	1.62	0.18	-0.13
180	1.0	5.4	2	2	3	8.90	0.13	2.33	1.45	0.32	-0.30
181	1.7	42.0	1	2	3	9.42	0.08	2.37	1.64	0.37	-0.11
182	1.9	120.0	2	2	3	9.61	0.09	2.32	1.98	0.32	0.23
183	1.9	23.4	2	2	3	9.76	0.08	3.50	3.81	1.50	2.06
184	2.1	34.4	1	2	2	10.73	0.25	2.73	2.57	0.73	0.82
185	3.0	75.7	1	1	3	10.02	0.12	2.40	1.79	0.40	0.04
186	3.3	-16.4	2	1	2	9.93	0.25	2.55	2.18	0.55	0.43
187	4.6	28.1	2	2	1	9.63	0.16	2.26	1.97	0.26	0.22
188	5.5	138.5	1	1	2	9.70	0.12	1.85	1.46	-0.15	-0.29
189	6.3	-58.8	2	2	3	9.66	0.11	1.93	1.13	-0.07	-0.62
190	6.5	98.5	1	3	1	10.43	0.47	2.36	1.36	0.36	-0.39
191	6.8	102.6	2	2	2	10.31	0.13	1.95	1.57	-0.06	-0.18
192	8.6	66.6	1	2	3	10.09	0.24	2.62	1.45	0.62	-0.30
193	10.1	104.6	2	2	2	10.12	0.15	2.33	1.60	0.32	-0.15
194	10.2	-11.2	2	2	3	9.53	0.05	2.83	1.87	0.83	0.12
195	11.2	78.2	1	2	2	10.18	0.21	2.36	1.45	0.36	-0.30
196	12.6	-0.2	2	3	3	8.91	0.04	2.06	1.43	0.06	-0.32
197	13.6	17.8	2	3	1	10.24	0.16	2.71	2.09	0.71	0.34
198	14.9	-16.2	2	3	3	9.72	0.14	2.49	1.28	0.49	-0.47
199	15.8	97.3	1	2	2	10.08	0.10	1.68	1.76	-0.33	0.01
200	16.1	89.0	1	2	2	10.20	0.30	2.32	1.98	0.32	0.23
201	16.9	-0.5	2	5	1	9.69	0.08	2.02	1.62	0.02	-0.13

ID	α_{IRS7}	δ_{IRS7}	n_K	n_H	n_L	$\langle m_K \rangle$	Δm_K	$(H-K)_{OBS}$	$(K-L)_{OBS}$	$(H-K)_0$	$(K-L)_0$
202	17.2	44.0	1	4	3	8.56	0.09	2.39	1.68	0.39	-0.07
203	20.2	-7.5	2	4	1	9.98	0.04	2.55	1.63	0.55	-0.12
204	22.3	17.6	3	4	3	9.91	0.17	3.22	1.93	1.21	0.18
205	23.5	118.9	2	4	3	9.54	0.01	2.42	1.91	0.42	0.16
206	24.2	-16.0	3	1	1	10.93	0.35	2.36	2.13	0.35	0.38
207	25.1	38.5	3	4	2	10.30	0.13	2.15	1.52	0.15	-0.23
208	25.6	85.0	3	4	2	10.27	0.08	1.91	1.79	-0.10	0.04
209	26.9	46.8	3	4	3	9.62	0.16	2.25	1.30	0.25	-0.45
210	27.5	129.7	4	4	1	9.14	0.01	2.10	1.44	0.10	-0.31
211	30.9	30.9	3	6	2	9.55	0.09	2.11	3.10	0.11	1.35
212	31.0	63.9	5	4	3	10.40	0.25	2.82	2.92	0.82	1.17
213	31.2	168.0	1	2	1	10.91	-1.00	2.52	2.62	0.52	0.87
214	32.7	66.7	3	4	1	10.63	0.04	2.62	2.22	0.61	0.47
215	33.9	-62.8	4	4	2	9.38	0.32	1.96	1.52	-0.04	-0.23
216	34.5	128.6	4	4	2	9.69	0.13	1.88	1.23	-0.12	-0.52
217	36.8	38.9	3	4	3	9.52	0.06	2.10	1.33	0.09	-0.42
218	38.3	79.1	3	4	3	9.20	0.49	3.19	2.99	1.19	1.24
219	39.3	-39.5	2	2	1	10.81	0.12	2.16	2.35	0.16	0.60
220	39.4	-27.8	1	2	2	9.30	0.44	2.79	2.04	0.79	0.29
221	39.8	9.3	1	3	2	8.58	0.21	2.38	2.01	0.37	0.26
222	44.3	152.4	1	1	3	8.96	0.22	1.99	1.82	-0.01	0.07
223	44.6	16.6	1	2	2	9.72	0.09	2.32	1.63	0.31	-0.12
224	45.3	93.1	2	2	3	10.05	0.14	2.22	1.50	0.21	-0.24
225	45.6	115.8	1	2	2	9.64	0.11	2.91	1.90	0.90	0.15
226	49.2	90.1	2	2	3	9.75	0.07	1.95	1.21	-0.05	-0.54
227	54.4	28.6	2	3	2	10.01	0.03	2.03	1.64	0.02	-0.11
228	55.3	125.0	2	2	1	9.02	0.06	1.72	1.66	-0.28	-0.09
229	56.3	67.8	2	2	2	8.22	0.15	2.61	1.48	0.61	-0.27
230	57.6	75.6	2	2	3	9.46	0.10	2.26	1.41	0.26	-0.34
231	57.8	87.1	2	2	1	10.38	0.10	2.34	1.67	0.34	-0.07
232	60.0	22.8	1	2	3	9.90	0.35	3.13	2.23	1.13	0.48
233	60.1	78.1	2	1	3	9.83	0.11	2.43	1.32	0.43	-0.43
234	61.9	51.8	2	2	2	9.92	0.07	2.27	1.24	0.27	-0.51
235	63.3	126.1	2	2	1	8.60	0.34	2.94	2.30	0.94	0.55
236	64.3	62.4	3	3	2	9.43	0.11	2.50	1.54	0.49	-0.21
237	69.1	159.9	1	1	3	8.84	0.19	2.15	1.71	0.15	-0.04
238	69.2	37.6	2	4	3	9.23	0.16	2.87	1.16	0.87	-0.59
239	69.6	21.2	1	4	3	9.30	0.07	2.75	1.57	0.75	-0.18
240	70.5	65.7	2	6	3	9.92	0.12	3.31	1.28	1.30	-0.47
241	74.3	51.9	3	4	1	10.23	0.32	2.60	1.51	0.59	-0.24
242	75.3	41.0	4	4	3	10.13	0.13	3.17	1.54	1.17	-0.21
243	76.6	70.2	4	5	3	9.43	0.09	2.32	1.23	0.32	-0.52
244	76.7	23.1	3	2	2	10.10	0.17	2.81	1.53	0.81	-0.22
245	79.3	147.1	2	2	3	9.20	0.07	2.95	1.44	0.95	-0.31
246	81.1	-22.9	2	2	2	10.55	0.09	2.15	2.12	0.15	0.37

ID	α_{IRS7}	δ_{IRS7}	n_K	n_H	n_L	$<m_K>$	Δm_K	$(H-K)_{OBS}$	$(K-L)_{OBS}$	$(H-K)_0$	$(K-L)_0$
247	81.4	-34.6	2	3	3	10.06	0.05	2.40	1.70	0.39	-0.05
248	84.1	55.6	4	2	2	10.60	0.06	2.61	1.91	0.61	0.16
249	90.0	46.8	4	2	3	10.16	0.12	2.61	1.74	0.60	-0.01
250	91.6	40.1	4	2	3	9.36	0.09	2.41	1.71	0.41	-0.04
251	93.4	45.3	3	2	3	10.25	0.16	2.10	2.03	0.10	0.28
252	102.6	76.9	2	2	3	9.17	0.06	1.90	1.44	-0.11	-0.31
253	103.1	-20.6	1	1	2	9.77	0.06	1.82	1.46	-0.18	-0.29
254	104.2	118.4	2	2	1	10.10	0.25	2.32	1.19	0.32	-0.56
255	105.0	1.9	2	2	2	10.16	0.06	2.41	1.53	0.40	-0.22
256	109.6	93.9	2	2	3	9.41	0.09	2.00	1.19	0.00	-0.56
257	111.6	159.7	1	1	3	9.43	0.10	2.63	1.56	0.62	-0.19
258	122.6	90.9	3	1	3	10.15	0.64	4.50	3.78	2.50	2.03

LIST OF REFERENCES

Aaronson, M. and Mould J. 1982, *Ap.J.Suppl.*, **48**, 161

Aitken, D.K., Roche, P.F., Bailey, J.A., Briggs, G.P., Hough, J.H. and Thomas, J.A. 1986, *MNRAS*, **218**, 363

Allen, D.A., Hyland, A.R. and Jones, T.J. 1983, *MNRAS*, **204**, 1145

Allen, D.A. and Sanders, R.H. 1986, *Nature*, **319**, 191

Allen, D.A., Hyland, A.R. and Hillier, D.J. 1990, *MNRAS*, **244**, 706

Backer, D.C. (ed.) 1987, *The Galactic Center* (AIP Conf. Proc. No. 155), AIP

Bahcall, J.N. and Soneira, R.M. 1980, *Ap.J.Suppl.*, **44**, 77

Bahcall, J.N. and Tremaine, S. 1981, *Ap.J.*, **244**, 805

Balick, B. and Brown, R.L. 1974, *Ap.J.*, **194**, 265

Bally, J., Stark, A.A., Wilson, R.W., and Henkel, C. 1987, *Ap.J.Suppl.*, **65**, 13

Bally, J., Stark, A.A., Wilson, R.W., and Henkel, C. 1988, *Ap.J.*, **324**, 223

Baud, B., Habing, H.J., Matthews, H.E. and Winnberg, A. 1981, *A.A.*, **95**, 156

Becklin, E.E., Dinerstein, H., Gatley, I., Werner, M.W., and Jones, B. 1987, in *The Galactic Center* (AIP Conf. Proc. No. 155), D.C. Backer (ed.), (NY:AIP), 162

Becklin, E.E., Gatley, I. and Werner, M.W. 1982, *Ap.J.*, **258**, 135

Becklin, E. E., Matthews, K., Neugebauer, G., and Willner, S. P. 1978, Ap.J., **220**, 831.

Becklin, E. E., and Neugebauer, G. 1968, *Ap.J.*, **151**, 145.

Becklin, E.E. and Neugebauer, G. 1975, *Ap.J.*, **200**, L71

Binney, J. Gerhard, O.E., Stark, A.A., Bally, J. and Uchida, K.I. 1991, *MNRAS*, **252**, 210

Blanco, V. M. 1988, *A.J.*, **95**, 1400

Blanco, V.M. and Blanco, B.M. 1988, *Mem. Soc. Astr. Italiana*, **56**, 15

Blanco, V. M. and Terndrup D.M. 1989, *A.J.*, **98**(3), 843

Blöcker, T. and Schönberner, D. 1991, *A.A.*, **244**, L43

Bowen, G.H. and Wilson, L.A. 1991, *Ap.J.*, **375**, L53

Brinks, E. 1984, Ph.D. thesis, University of Leiden

Brown, R.L. and Liszt, H.S. 1984, *Ann.Rev.Astron.Astrophys.*, **22**, 223

Catchpole, R.M., Glass, I.S., and Whitelock, P. 1989, *The Center of the Galaxy* (IAU Symp. No. 136), M. Morris (ed.), Kluwer, 75

Charlot, S. and Bruzual A, G. 1991, *Ap.J.*, **367**, 126

Crane, P.C., Dickel, J.R. and Cowan, J.J. 1992, *Ap.J.*, **390**, L9

Davies, R.L., Frogel, J.A. and Terndrup, D.M. 1991, *A.J.*, **102**, 1729

Depoy, D.L. and Sharp, N.A. 1991, *A.J.*, **101** (4), 1324

de Vaucouleurs, G. and Pence W. D. 1978, *A.J.*, **83**, 1163.

Downes, D., Maxwell, A. and Meeks, M.L. 1966, *Ap.J.*, **146**, 653

Dressler, A. and Richstone, D.O. 1988, *Ap.J.*, **324**, 701

Eckart, A., Genzel, R., Krabbe, A., Hofmann, R., van der Werf, P.P., and Drapatz, S.S. 1992, *Nature*, **355**, 526

Elias, J. H., Frogel, J. A., and Humphreys, R. M. 1985, *Ap.J.Suppl.*, **57**, 91.

Elias, J. H., Frogel, J. A., Matthews, K., and Neugebauer, G. 1982, *A.J.*, **87**, 1029.

Elston, R. and Silva, D.R. 1992, *A.J.*, preprint

Ekers, R.D., van Gorkom, J.H., Schwarz, U.J., and Goss, W.M. 1983, *A.A.*, **122**, 143

Feast, M.W. 1986, *Light on Dark Matter*, F.P. Israel (ed.), Reidel, 339

Feast, M.W., Robertson, B.S.C., Catchpole, R.M., Lloyd Evans, T., Glass, I.S., and Carter, B.S., 1982, *MNRAS*, **201**, 439

Feast, M.W., and Whitelock, P.A., 1987, *Late Stages of Stellar Evolution*, Kwok, S. and Pottasch, B.R. (eds.), 33

Forest, W.J., Shure, M.A., Pipher, J.L., and Woodward, C.E. 1987, in *The Galactic Center* (AIP Conf. Proc. No. 155), D.C. Backer (ed.), (NY:AIP), 153

Freedman, W.L. 1992, *A.J.*, preprint

Frenk, C.S. and White, S.D.M. 1982, *MNRAS*, **198**, 173

Frogel, J. A., Persson, S. E., Aaronson, M., and Matthews, K. 1978, *Ap.J.*, **220**, 75

Frogel, J. A., and Whitford, A. E. 1987, *Ap.J.*, **320**, 199

Frogel, J.A. and Elias, J.H. 1988, *Ap.J.*, **324**, 823

Frogel, J. A., Terndrup, D. M., Blanco, V. M., and Whitford, A. E. 1990, *Ap.J.*, **353**, 494

Garwood, R., and Jones, T. J. 1987, *Pub.A.S.P.*, **99**, 453

Gatley, I. 1982, in *The Galactic Center* (AIP Conf. Proc. No. 83), G.R. Riegler and R.L. Blanford (eds.), (NY:AIP), 25

Gatley, I., Jones, T.J., Hyland, A.R., Beattie, D.H., and Lee, T.J. 1984, *MNRAS*, **210**, 565

Gatley, I., Jones, T.J., Hyland, A.R., Wade, R., Geballe, T.R. and Krisciunas, K.L. 1986, *MNRAS*, **222**, 299

Gatley, I. 1987, in *The Galactic Center* (AIP Conf. Proc. No. 155), D.C. Backer (ed.), (NY:AIP), 8

Gatley, I. 1989, in *The Center of the Galaxy* (IAU Symp. No. 136), M. Morris (ed.), 645

Gatley, I., Becklin, E.E., Werner, M.W., and Wynn-Williams, C.G. 1977, *Ap.J.*, **216**, 277

Geballe, T.R., Krisciunas, K., Lee, T.J., Gatley, I., Wade, R., Duncan, W.D., Garden, R., Becklin, E.E. 1984, *Ap.J.*, **284**, 118

Geballe, T.R., Wade, R., Krisciunas, K., Gatley, I., and Bird, M.C. 1987, *Ap.J.*, **320**, 562

Geballe, T.R., Krisciunas, K., Bailey, J.A., and Wade, R. 1991, *Ap.J.*, **370**, L73

Genzel, I., Watson, D.M., Crawford, M.K. and Townes, C.H. 1985, *Ap.J.*, **297**, 766

Genzel, I. and Townes, C.H. 1987, *Ann.Rev.Astron.Astrophys.*, **25**, 377

Glass, I.S., Catchpole, R.M., and Whitelock, P.A. 1987, *MNRAS*, **227**, 373

Glass, I.S., and Feast, I.S., 1982, *MNRAS*, **198**, 199

Gordon, M. A., and Burton, W. B. 1976, *Ap.J.*, **208**, 346.

Hall, D.N.B., Kleimann, S.G. and Scoville, N.Z., 1982, *Ap.J.*, **262**, L53

Harmon, R. and Gilmore, G. 1988, *MNRAS*, **235**, 1025

Hartwick, F.D.A. and Sargent, W.L.W. 1978, *Ap.J.*, **221**, 512

Heisler, J., Tremaine, S., and Bahcall, J.N. 1985, *Ap.J.*, **298**, 8

Hinkle, K.H., Hall, D.N.B., and Ridgeway, S.T. 1982, *Ap.J.*, **252**, 697

Kerr, F.J. and Lynden-Bell, D. 1986, *MNRAS*, **221**, 1023

King, I.R. *et al.*, 1992, *Ap.J.*, **397**, L35

Kleinmann, S.G. and Hall, D.N.B. 1986, *Ap.J.Suppl.*, **62**, 501

Kormendy, J. 1988, *Ap.J.*, **325**, 128

Kormendy, J. and Illingworth, G. 1982, *Ap.J.*, **256**, 460

Krabbe, A., Genzel, R. Drapatz, S. and Rotaciul, V. 1991, *Ap.J.*, **382**, L19

Lacy, J.H., Townes, C.H., Geballe, T.R. and Hollenbach, D.J. 1980, *Ap.J.*, **241**, 132

Lacy, J.H., Townes, C.H. and Hollenbach, D.J. 1982, *Ap.J.*, **262**, 120

Lacy, J.H. 1989, *The Center of the Galaxy* (IAU Symp. No. 136), M. Morris (ed.), Kluwer, 493

Lacy, J.H., Achtermann, J.M., and Serabyn, E. 1991, *Ap.J.Lett.*, **380**, L71

Lebofsky, M.J., Rieke, G.H., Deshpande, M.R. and Kemp, J.C. 1982, *Ap.J.*, **263**, 672

Lebofsky, M. J., Rieke, G. H., and Tokunaga, A. T. 1982, Ap.J., **263**, 736.

Lester, D. F., Bregman, J. D., Witteborn, F. C., Rank, D. M., and Dinerstein, H. L. 1981, Ap.J., **248**, 524.

Light, E.S., Danielson, R.E. and Schwarzschild, M. 1974, *Ap.J.*, **194**, 257

Lindqvist, M., Winnberg, A., Habing, H.J., and Matthews, H.E. 1992a, *A.A.Suppl.*, **92**, 43

Lindqvist, M., Habinng, H.J., and Winnberg, A. 1992b, *A.A.*, **259**, 118

Litszt, H.S. and Burton, W.B. 1978, *Ap.J.*, **226**, 790

Litszt, H.S. van der Hulst, J.M., Burton, W.B. and Ondrechen, M.P. 1983, *A.A.*, **126**, 341

Lo, K.Y. 1982, in *The Galactic Center* (AIP Conf. Proc. No. 83), G.R. Riegler and R.D. Blanford (eds.), (NY:AIP), 1

Lo, K.Y. 1987, in *The Galactic Center* (AIP Conf. Proc. No. 155), D.C. Backer (ed.),

(NY:AIP), 30

Lo, K.Y. 1989, in *The Center of the Galaxy* (IAU Symp. No. 136), M. Morris (ed.), Kluwer, 527

Lo, K.Y. and Claussen, M.J. 1983, *Nature*, **306**, 647

Loose, H.H., Krügel, E., and Tutukov, A., 1982, *A.A.*, **105**, 342

Low, F.J., Kleinmann, D.E., Forbes, F.F. and Auman, H.H. 1969, *Ap.J.*, **157**, L97

Lugten, J.B., Harris, A.I., Stacey, G.H., Genzel, R., and Townes, C.H. 1987, *The Galactic Center* (AIP Conf. Proc. No. 155), D. Backer (ed.), AIP, 118

Lynden-Bell, D. and Rees, M.J. 1971, *MNRAS*, **152**, 461

Maeder, A., and Meynet, G. 1988, *A.A.Suppl.*, **76**, 411

Maeder, A., and Meynet, G. 1989, *A.A.*, **210**, 155

Matsumoto, T., Hayakawa, S., Koizumi, H. *et al.* 1982, *The Galactic Center* (AIP Conf. Proc. No. 83), G.R. Reigler and R.D. Blandford (eds.), AIP, 48

McGinn, M. T., Sellgren, K., Becklin, E. E., and Hall, D.N.B. 1989, *Ap.J.*, **338**, 824.

Melia, F. 1992, *Ap.J.*, 338, L25

Mihalas, D., and Binney, J. J. 1981, *Galactic Astronomy*, 2nd edition, (San Francisco : Freeman).

Miller, G.E. and Scalo, J.M. 1974, *Ap.J.Suppl.*, **41**, 513

Mould, J. and Aronson, M. 1980, *Ap.J.*, **240**, 464

Morris, M. (ed.) 1989, *The Center of the Galaxy*, (IAU Symp. No. 136), Kluwer Academic Publishers

Neugebauer, G., Becklin, E. E., Beckwith, S., Matthews, K., and Wynn-Williams, C. G. 1976. *Ap.J.Lett.*, **205**, L139.

Oort, J.H. and Rougoor, G.W. 1960, *MNRAS*, **121**, 171

Oort, J.H. 1977, *Ann.Rev.Astron.Astrophys.*, **15**, 295

Paczynski, B. 1970, Acta Astron., 20, 47

Pedlar, A., Anantharamaiah, K.R., Ekers, R.D., Goss, W.M. van Gorkom, J.H. and

Schwarz, U.J. 1989, *Ap.J.* **342**, 769

Phinney, E.S. 1989, *The Center of the Galaxy*, (IAU Symposium No. 136.), M. Morris (ed.), Kluwer, 543

Reid, M.J., Schneps, M.H., Moran, J.M., Gwinn, C.R., Genzel, R., Downes, D., and Ronnang, B. 1986, *IAU Symp. No. 115, Star Formation*, M. Peimbert and J. Jagaku (eds.), Reidel

Reid, M.J. 1989, *The Center of the Galaxy* (IAU Symp. No. 136), M.Morris (ed.), Kluwer, 37

Reid, N., Glass, I.S., and Catchpole, R.M., 1988, *MNRAS*, **232**, 57

Rich, R.M. 1988, *A.J.*, **95**, 828

Rich, R.M. and Mould, J.R. 1991, *A.J.*, **101**, 1286

Riegler, G.R. and Blanford, R.D. (eds.) 1982, *The Galactic Center*, (AIP Conf. Proc. No. 83), AIP

Rieke, G.H., and Lebofsky, M.J. 1978, *Ap.J.Lett.*, **220**, L38

Rieke, G.H., and Lebofsky, M.J. 1985, *Ap.J.*, **288**, 618.

Rieke, G.H., and Lebofsky, M.J. 1987, *The Galactic Center*, AIP Conf. Proc. No. 155, D. Backer (ed.), 91

Rieke, G.H. and Lebofsky, M.J., 1988, *Ap.J.*, 330, L33

Rieke, G. H., and Rieke, M. J. 1988, *Ap.J.Lett.*, **330**, L33.

Rieke, G.H., Rieke, M.J. and Paul, A.E. 1989, *Ap.J.*, **336**, 752

Rieke, G. H., Telesco, C. M., and Harper, D. A. 1978, *Ap.J.*, **220**, 556.

Rieke, M. J. 1987, in *Nearly Normal Galaxies*, ed. S. M. Faber, (New York : Springer-Verlag), p. 90.

Rieke, M. J. 1988, in *Galactic and Extragalactic Star Formation*, eds. R. E. Pudrtiz amd M. Fich, (Dordrecht : Kluwer), p. 345.

Ruelas-Mayorga, R.A. 1991, *Rev. Mexicana Astron. Astrof.*, **22**, 27

Sandage, A.R., Becklin, E.E. and Neugebauer, G. 1969, *Ap.J.*, **157**, 55

Sanders, R. and Lowinger, T. 1968, *A.J.*, **77**, 292

Sellgren, K., Hall, D. N. B., Kleinmann, S. G., and Scoville, N. Z. 1987, *Ap.J.*, **371**, 881.

Sellgren, K., McGinn, M.T., Becklin, E. E., and Hall, D.N.B. 1990, *Ap.J.*, **359**, 112.

Serabyn, E., Lacy, J.H., Townes, C.H., and Bharat, R. 1988, *Ap.J.*, **326**, 171

Smith, L.F., Biermann, P. and Mezger, P.G. 1978, *A.A.*, **66**, 65

Sofue, Y. 1989, *The Center of the Galaxy* (IAU Symp. No. 136), M. Morris (ed.), Kluwer, 213

Soifer, B.T., Rice, W.L., Mould, J.R., Gillet, F.C., Rowan Robinson, M. and Habing, H.T. 1986, *Ap.J.*, **304**, 651

Spitzer, L. 1978, *Physical Processes in the Interstellar Medium*, Wiley and Sons

Stacy, J.G., Dame, T.M. and Thaddeus, P. 1989, *20th International Cosmic Ray Conference*, **1**, 117

Stark, A.A., Ortwin, O.E., Gerhard, O.E, Binney, J. and Bally, J. 1991, *MNRAS*, **248**, 14p

Stetson, P. B. 1987, *Pub.A.S.P.*, **99**, 191.

Sweigart, A. V., and Gross, P.G. 1978, *Ap.J.Suppl.*, **36**, 405

Sunyaev, R., Churazov, E., Gilfanov, M., Pavinsky, M., Grebenev, S., Babalyan, G., Dekhanav, I., Yamburenko, N., Bouchet, L., Niel, M., Roques, J.P., Mandrou, P., Goldwurun, A., Gordier, B., Laurent, Ph., and Paul, J. 1991, *A.A.*, **247**, L29

Telesco, C.M. 1977, Ph.D. thesis, University of Chicago.

Terndrup, D.M. 1988, *A.J.*, **96**, 884

Terndrup, D. M., Frogel, J. A., and Whitford, A. E. 1991, *Ap.J.*, **378**, 742

Tonry, J.L. 1987, *Ap.J.*, **322**, 632

Treffers, R.R., Fink, U., Larson, H.P. and Gautier, T.N. III 1976, *Ap.J.*, **209**, L115

Wardle, M. and Yusef-Zadeh, F. 1992, *Nature*, preprint

Whitelock, P.A., Feast, M. and Catchpole, R.M. 1991, *MNRAS*, **248**, 276

Winnberg, A., Baud, B., Matthews, H.E., Habing, H.J., and Olnon, F.M. 1985, *Ap.J.Lett.*, **291**, L45

Wollman, E.R., Smith, H.A., and Larson, H.P. 1982, *Ap.J.*, **258**, 506

Wood, P.R. and Bessell, M.S. 1983, *Ap.J.*, **265**, 748

Wood, P.R., Bessell, M.S., and Fox, M.W. 1983, *Ap.J.*, **272**, 99

Wright, M.C.H., Genzel, R. Güsten, R., and Jaffe, D.J. 1987, *The Galactic Center* (AIP Conf. Proc. No. 155), D. Backer (ed.), AIP, 133

Wynn-Williams, C.G. and Becklin, E.E. 1974, *Pub.A.S.P.*, **86**, 5

Yusef-Zadeh, F. and Melia, F. 1992, *Ap.J.*, **385**, L41

Yusef-Zadeh, F. and Morris, M. 1991, *Ap.J.*, **371**, L59